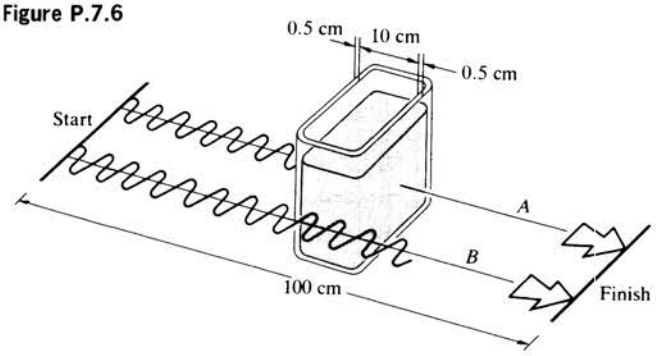
(b) How many waves span the gap when a glass plate 5 cm thick ($n = 1.5$) is inserted in the path?
(c) Determine the *OPD* between the two situations.
(d) Verify that Λ/λ_0 corresponds to the difference between the solutions to (a) and (b) above.

7.6* Determine the optical path difference for the two waves *A* and *B*, both having vacuum wavelengths of 500 nm, depicted in Fig. P.7.6; the glass ($n = 1.52$) tank is filled with water ($n = 1.33$). If the waves start out in-phase and all the above numbers are exact, find their relative phase difference at the finishing line.

Figure P.7.6



7.7* Using Eqs. (7.9), (7.10), and (7.11), show that the resultant of the two waves

$$E_1 = E_{01} \sin [\omega t - k(x + \Delta x)]$$

and

$$E_2 = E_{01} \sin (\omega t - kx)$$

is

$$E = 2E_{01} \cos\left(\frac{k\,\Delta x}{2}\right) \sin\left[\omega t - k\left(x + \frac{\Delta x}{2}\right)\right] \qquad [7.17]$$

7.8 Add the two waves of Problem 7.7 directly to find Eq. (7.17).

7.9 Use the complex representation to find the resultant $E = E_1 + E_2$, where

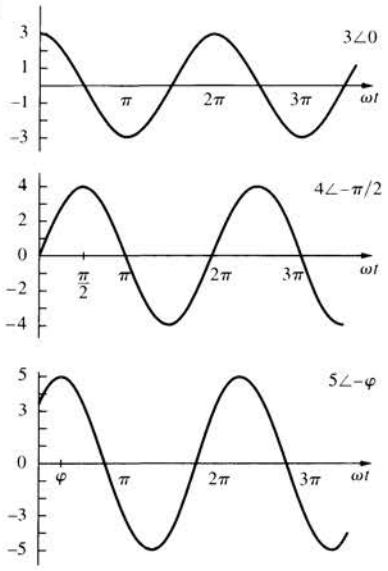
$$E_1 = E_0 \cos (kx + \omega t) \quad \text{and} \quad E_2 = -E_0 \cos (kx - \omega t)$$

Describe the composite wave.

7.10* Consider the functions $E_1 = 3 \cos \omega t$ and $E_2 = 4 \sin \omega t$. First prove that $E_2 = 4 \cos (\omega t - \pi/2)$. Then, using phasors and referring to Fig. P.7.10, show that $E_3 = E_1 + E_2 = 5 \cos (\omega t - \varphi)$; determine φ. Discuss the values of E_3 wherever either $E_1 = 0$ or $E_2 = 0$. Does E_3 lead or lag E_1? Explain.

7.11 The electric field of a standing electromagnetic plane wave is

Figure P.7.10



given by

$$E(x, t) = 2E_0 \sin kx \cos \omega t \qquad [7.30]$$

Derive an expression for $B(x, t)$. (You might want to take another look at Section 3.2.) Make a sketch of the standing wave.

7.12* Considering Wiener's experiment (Fig. 7.14) in monochromatic light of wavelength 550 nm, if the film plane is angled at 1.0° to the reflecting surface, determine the number of bright bands per centimeter that will appear on it.

7.13* Microwaves of frequency 10^{10} Hz are beamed directly at a metal reflector. Neglecting the refractive index of air, determine the spacing between successive nodes in the resulting standing-wave pattern.

7.14* A standing wave is given by

$$E = 100 \sin \tfrac{2}{3}\pi x \cos 5\pi t$$

Determine two waves that can be superimposed to generate it.

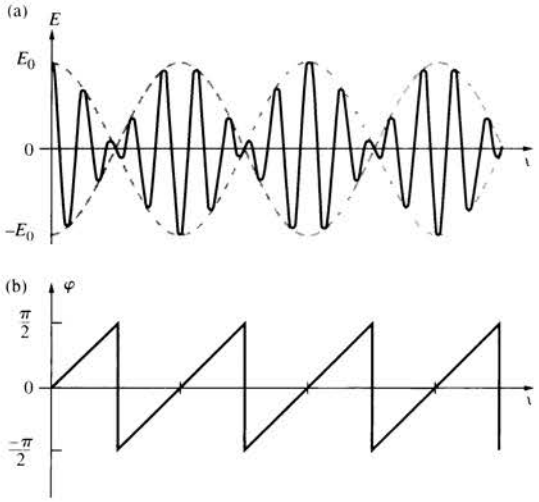
7.15* Imagine that we strike two tuning forks, one with a frequency of 340 Hz, the other 342 Hz. What will we hear?

7.16* Use the phasor method, described in conjunction with Fig. 7.17, to explain how two equal-amplitude waves of sightly different frequencies generate the beat pattern shown in Fig. 7.16 or Fig. P.7.16*a*. The curve in Fig. P.7.16*b* is a sketch of the phase of the resultant measured with respect to one of the constituent waves.

Giesecke+Devrient GmbH,
Giesecke+Devrient Currency Technology GmbH,
and Papierfabrik Louisenthal GmbH. - Ex. 1027

Explain its main features. When is it zero and why? When does the phase change abruptly and why?

Figure P.7.16



7.17* As we've seen, Eq. (7.33) describes the beat pattern. Let's now derive a different version of that expression assuming that the two overlapping equal-amplitude cosine waves have angular spatial frequencies of $k_c + \Delta k$ and $k_c - \Delta k$, and angular temporal frequencies of $\omega_c + \Delta\omega$ and $\omega_c - \Delta\omega$, respectively. Here k_c and ω_c correspond to the central frequencies. Show that the resultant wave is then

$$E = 2E_{01} \cos(\Delta k x - \Delta\omega t) \cos(k_c x - \omega_c t)$$

Explain how each term relates back to

$$E = 2E_{01} \cos(k_m x - \omega_m t) \cos(\bar{k}x - \bar{\omega}t) \qquad [7.33]$$

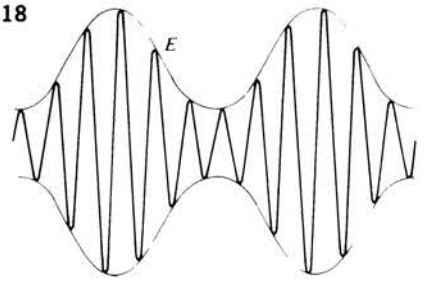
Prove that the speed of the envelope, which is the wavelength of the envelope divided by the period of the envelope, equals the group velocity, namely, $\Delta\omega/\Delta k$.

7.18 Figure P.7.18 shows a carrier of frequency ω_c being amplitude-modulated by a sine wave of frequency ω_m, that is,

$$E = E_0(1 + a \cos \omega_m t) \cos \omega_c t$$

Show that this is equivalent to the superposition of three waves of frequencies ω_c, $\omega_c + \omega_m$, and $\omega_c - \omega_m$. When a number of modulating frequencies are present, we write E as a Fourier series and sum over all values of ω_m. The terms $\omega_c + \omega_m$ constitute what is called the *upper sideband*, and all the $\omega_c - \omega_m$ terms form the *lower sideband*. What bandwidth would you need in order to transmit the complete audible range?

Figure P.7.18



7.19 Given the dispersion relation $\omega = ak^2$, compute both the phase and group velocities.

7.20* Using the relation $1/v_g = d\kappa/d\nu$, prove that

$$\frac{1}{v_g} = \frac{1}{v} - \frac{\nu}{v^2}\frac{dv}{d\nu}$$

7.21* In the case of lightwaves, show that

$$\frac{1}{v_g} = \frac{n}{c} + \frac{\nu}{c}\frac{dn}{d\nu}$$

7.22 The speed of propagation of a surface wave in a liquid of depth much greater than λ is given by

$$v = \sqrt{\frac{g\lambda}{2\pi} + \frac{2\pi\Upsilon}{\rho\lambda}}$$

where g = acceleration of gravity, λ = wavelength, ρ = density, Υ = surface tension. Compute the group velocity of a pulse in the long wavelength limit (these are called *gravity waves*).

7.23* Show that the group velocity can be written as

$$v_g = v - \lambda\frac{dv}{d\lambda}$$

7.24 Show that the group velocity can be written as

$$v_g = \frac{c}{n + \omega(dn/d\omega)}$$

7.25* With the previous problem in mind prove that

$$n_g = n(\nu) + \nu\frac{dn(\nu)}{d\nu}$$

Giesecke+Devrient GmbH,
Giesecke+Devrient Currency Technology GmbH,
and Papierfabrik Louisenthal GmbH. - Ex. 1027

7.26* Determine the group velocity of waves when the phase velocity varies inversely with wavelength.

7.27* Show that the group velocity can be written as

$$v_g = \frac{c}{n} + \frac{\lambda c}{n^2}\frac{dn}{d\lambda}$$

7.28* For a wave propagating in a periodic structure for which $\omega(k) = 2\omega_0 \sin(k\ell/2)$, determine both the phase and group velocities. Write the former as a sinc function.

7.29* An ionized gas or plasma is a dispersive medium for EM-waves. Given that the dispersion equation is

$$\omega^2 = \omega_p{}^2 + c^2k^2$$

where ω_p is the constant plasma frequency, determine expressions for both the phase and group velocities and show that $vv_g = c^2$.

7.30 Using the dispersion equation,

$$n^2(\omega) = 1 + \frac{Nq_e^2}{\epsilon_0 m_e}\sum_j \left(\frac{f_j}{\omega_{0j}^2 - \omega^2}\right) \qquad [3.71]$$

show that the group velocity is given by

$$v_g = \frac{c}{1 + Nq_e^2/\epsilon_0 m_e \omega^2 2}$$

for high-frequency electromagnetic waves (e.g., X-rays). Keep in mind that since f_j are the weighting factors, $\sum_j f_j = 1$. What is the phase velocity? Show that $vv_g \approx c^2$.

7.31* Analytically determine the resultant when the two functions $E_1 = 2E_0 \cos \omega t$ and $E_2 = \frac{1}{2}E_0 \sin 2\omega t$ are superimposed. Draw E_1, E_2, and $E = E_1 + E_2$. Is the resultant periodic; if so, what is its period in terms of ω?

7.32 Show that

$$\int_0^\lambda \sin akx \cos bkx\, dx = 0 \qquad [7.44]$$

$$\int_0^\lambda \cos akx \cos bkx\, dx = \frac{\lambda}{2}\delta_{ab} \qquad [7.45]$$

$$\int_0^\lambda \sin akx \sin bkx\, dx = \frac{\lambda}{2}\delta_{ab} \qquad [7.46]$$

where $a \neq 0$, $b \neq 0$, and a and b are positive integers.

7.33 Compute the Fourier series components for the periodic function shown in Fig. 7.20.

7.34* Given the function $f(x) = A \cos(\pi x/L)$, determine its Fourier series.

7.35* Take the function $f(\theta) = \theta^2$ in the interval $0 < \theta < 2\pi$ and assume it repeats itself with a period of 2π. Now show that the Fourier expansion of that function is

$$f(x) = \frac{4\pi^2}{3} + \sum_{m=1}^{\infty}\left(\frac{4}{m^2}\cos m\theta - \frac{4\pi}{m}\sin m\theta\right)$$

7.36* Show that the Fourier series representation of the function $f(\theta) = |\sin\theta|$ is

$$f(\theta) = \frac{2}{\pi} - \frac{4}{\pi}\sum_{m=1}^{\infty}\frac{\cos 2m\theta}{4m^2 - 1}$$

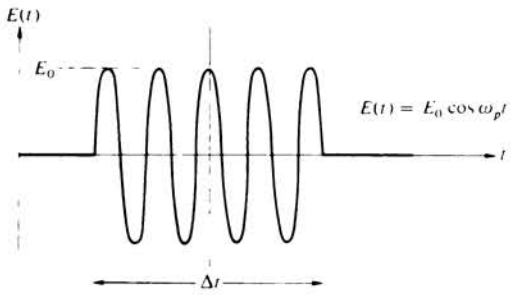
7.37 Change the upper limit of Eq. (7.59) from ∞ to a and evaluate the integral. Leave the answer in terms of the so-called *sine integral*:

$$\mathrm{Si}(z) = \int_0^z \mathrm{sinc}\, w\, dw$$

which is a function whose values are commonly tabulated.

7.38 Write an expression for the transform $A(\omega)$ of the harmonic pulse of Fig. P.7.38. Check that sinc u is 50% or greater for values of u *roughly* less than $\pi/2$. With that in mind, show that $\Delta\nu\, \Delta t \approx 1$, where $\Delta\nu$ is the bandwidth of the transform at half its maximum amplitude. Verify that $\Delta\nu\, \Delta t \approx 1$ at half the maximum value of the power spectrum as well. The purpose here is to get some sense of the kind of approximations used in the discussion.

Figure P.7.38



7.39 Derive an expression for the coherence length (in vacuum) of a wavetrain that has a frequency bandwidth $\Delta\nu$; express your answer in terms of the *linewidth* $\Delta\lambda_0$ and the mean wavelength $\bar{\lambda}_0$ of the train.

7.40 Consider a photon in the visible region of the spectrum emitted

Giesecke+Devrient GmbH,
Giesecke+Devrient Currency Technology GmbH,
and Papierfabrik Louisenthal GmbH. - Ex. 1027

during an atomic transition of about 10^{-8} s. How long is the wave packet? Keeping in mind the results of the previous problem (if you've done it), estimate the linewidth of the packet ($\bar{\lambda}_0 = 500$ nm). What can you say about its monochromaticity, as indicated by the frequency stability?

7.41 The first* experiment directly measuring the bandwidth of a laser (in this case a continuous-wave $Pb_{0.88}Sn_{0.12}Te$ diode laser) was carried out in 1969. The laser, operating at $\lambda_0 = 10\,600$ nm, was heterodyned with a CO_2 laser, and bandwidths as narrow as 54 kHz were observed. Compute the corresponding frequency stability and coherence length for the lead-tin-telluride laser.

7.42* A magnetic-field technique for stabilizing a He–Ne laser to 2 parts in 10^{10} has been patented. At 632.8 nm, what would be the coherence length of a laser with such a frequency stability?

*D. Hinkley and C. Freed, *Phys. Rev. Letters* **23**, 277 (1969).

7.43 Imagine that we chop a continuous laserbeam (assumed to be monochromatic at $\lambda_0 = 632.8$ nm) into 0.1-ns pulses, using some sort of shutter. Compute the resultant linewidth $\Delta\lambda$, bandwidth, and coherence length. Find the bandwidth and linewidth that would result if we could chop at 10^{15} Hz.

7.44* Suppose that we have a filter with a pass band of 1.0 Å centered at 600 nm, and we illuminate it with sunlight. Compute the coherence length of the emerging wave.

7.45* A filter passes light with a mean wavelength of $\bar{\lambda}_0 = 500$ nm. If the emerging wavetrains are roughly $20\bar{\lambda}_0$ long, what is the frequency bandwidth of the exiting light?

7.46* Suppose we spread white light out into a fan of wavelengths by means of a diffraction grating and then pass a small select region of that spectrum out through a slit. Because of the width of the slit, a band of wavelengths 1.2 nm wide centered on 500 nm emerges. Determine the frequency bandwidth and the coherence length of this light.

Giesecke+Devrient GmbH,
Giesecke+Devrient Currency Technology GmbH,
and Papierfabrik Louisenthal GmbH. - Ex. 1027

8 Polarization

8.1 The Nature of Polarized Light

It has already been established that light may be treated as a transverse electromagnetic wave. Thus far we have considered only **linearly polarized** or **plane-polarized** light, that is, light for which the orientation of the electric field is constant, although its magnitude and sign vary in time (Fig. 3.14). In that case, the electric field or optical disturbance resides in what is known as the **plane-of-vibration**. That fixed plane contains both $\vec{\mathbf{E}}$ and $\vec{\mathbf{k}}$, the electric field vector and the propagation vector in the direction of motion.

Imagine two harmonic, linearly polarized lightwaves of the same frequency, moving through the same region of space, in the same direction. If their electric field vectors are colinear, the superimposing disturbances will simply combine to form a resultant linearly polarized wave. Its amplitude and phase will be examined in detail, under a diversity of conditions, in the next chapter, when we consider the phenomenon of interference. On the other hand, if the two lightwaves are such that their respective electric-field directions are mutually perpendicular, the resultant wave may or may not be linearly polarized. The exact form the light takes (i.e., its *state of polarization*) and how we can observe it, produce it, change it, and make use of it is the concern of this chapter.

8.1.1 Linear Polarization

The two orthogonal optical disturbances that were considered above can be represented as

$$\vec{\mathbf{E}}_x(z, t) = \hat{\mathbf{i}} E_{0x} \cos (kz - \omega t) \tag{8.1}$$

and

$$\vec{\mathbf{E}}_y(z, t) = \hat{\mathbf{j}} E_{0y} \cos (kz - \omega t + \varepsilon) \tag{8.2}$$

where ε is the relative phase difference between the waves, both of which are traveling in the z-direction. Keep in mind from the start that because the phase is in the form $(kz - \omega t)$, the addition of a *positive* ε means that the cosine function in Eq. (8.2) will not attain the same value as the cosine in Eq. (8.1) until a later time (ε/ω). Accordingly, E_y lags E_x by $\varepsilon > 0$. Of course, if ε is a negative quantity, E_y leads E_x by $\varepsilon < 0$. The resultant optical disturbance is the vector sum of these two perpendicular waves:

$$\vec{\mathbf{E}}(z, t) = \vec{\mathbf{E}}_x(z, t) + \vec{\mathbf{E}}_y(z, t) \tag{8.3}$$

If ε is zero or an integral multiple of $\pm 2\pi$, the waves are said



Many animals can see variations in polarization just as we see variations in color. The pygmy octopus is one such creature. The varying pattern of polarized light reflected from its surface suggests it might be "communicating" with other pygmy octopuses, the way birds display color. (Photo courtesy Thomas W. Cronin and Nadav Shashar, University of Maryland.)

Giesecke+Devrient GmbH,
Giesecke+Devrient Currency Technology GmbH,
and Papierfabrik Louisenthal GmbH. - Ex. 1027

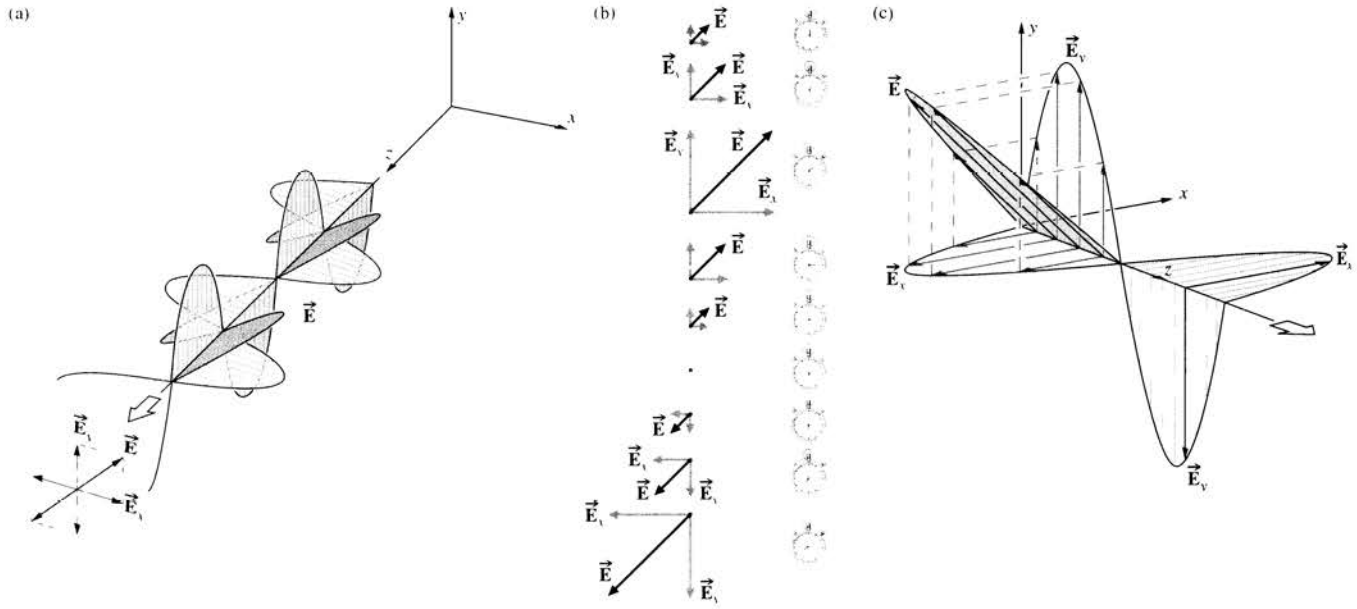


Figure 8.1 Linear light. (*a*) The *E*-field linearly polarized in the first and third quadrants. (*b*) That same oscillating field seen head on. (*c*) Light linearly polarized in the second and fourth quadrants.

to be in-phase. In that case Eq. (8.3) becomes

$$\vec{\mathbf{E}} = (\hat{\mathbf{i}}E_{0x} + \hat{\mathbf{j}}E_{0y}) \cos(kz - \omega t) \tag{8.4}$$

The resultant wave has a fixed amplitude equal to $(\hat{\mathbf{i}}E_{0x} + \hat{\mathbf{j}}E_{0y})$; in other words, it too is linearly polarized (Fig. 8.1). The waves advance toward a plane of observation where the fields are to be measured. There one sees a single resultant $\vec{\mathbf{E}}$ oscillating, along a tilted line, cosinusoidally in time (Fig. 8.1*b*). The $\vec{\mathbf{E}}$-field progresses through one complete oscillatory cycle as the wave advances along the z-axis through one wavelength. This process can be carried out equally well in reverse; that is, we can resolve any plane-polarized wave into two orthogonal components.

Suppose now that ε is an odd integer multiple of $\pm\pi$. The two waves are 180° out-of-phase, and

$$\vec{\mathbf{E}} = (\hat{\mathbf{i}}E_{0x} - \hat{\mathbf{j}}E_{0y}) \cos(kz - \omega t) \tag{8.5}$$

This wave is again linearly polarized, but the plane-of-vibration has been rotated (and not necessarily by 90°) from that of the previous condition, as indicated in Fig. 8.2.

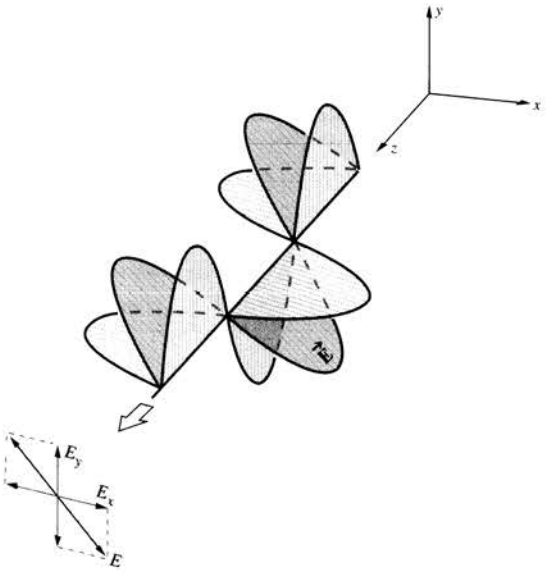


Figure 8.2 Linear light oscillating in the second and fourth quadrants.

Giesecke+Devrient GmbH,
Giesecke+Devrient Currency Technology GmbH,
and Papierfabrik Louisenthal GmbH. - Ex. 1027

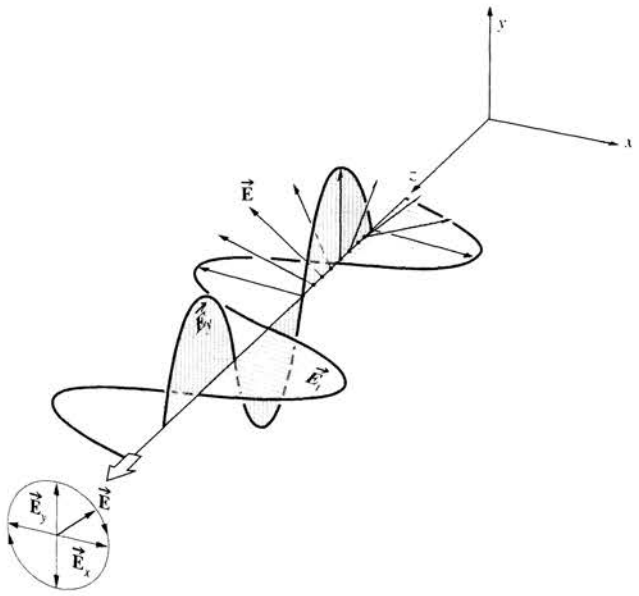


Figure 8.3 Right-circular light. (*a*) Here the electric field, which has a constant amplitude, rotates clockwise with the same frequency with which it oscillates. (*b*) Two perpendicular antennas radiating with a 90° phase difference produce circularly polarized electromagnetic waves.

8.1.2 Circular Polarization

Another case of particular interest arises when both constituent waves have equal amplitudes (i.e., $E_{0x} = E_{0y} = E_0$), and in addition, their relative phase difference $\varepsilon = -\pi/2 + 2m\pi$, where $m = 0, \pm 1, \pm 2, \ldots$. In other words, $\varepsilon = -\pi/2$ or any value increased or decreased from $-\pi/2$ by whole-number multiples of 2π. Accordingly

$$\vec{\mathbf{E}}_x(z, t) = \hat{\mathbf{i}} E_0 \cos(kz - \omega t) \tag{8.6}$$

and

$$\vec{\mathbf{E}}_y(z, t) = \hat{\mathbf{j}} E_0 \sin(kz - \omega t) \tag{8.7}$$

The consequent wave is

$$\vec{\mathbf{E}} = E_0[\hat{\mathbf{i}} \cos(kz - \omega t) + \hat{\mathbf{j}} \sin(kz - \omega t)] \tag{8.8}$$

(Fig. 8.3). Notice that now the scalar amplitude of $\vec{\mathbf{E}}$, that is, $(\vec{\mathbf{E}} \cdot \vec{\mathbf{E}})^{1/2} = E_0$, is a constant. But the direction of $\vec{\mathbf{E}}$ is time-varying, and it's not restricted, as before, to a single plane. Figure 8.4 depicts what is happening at some arbitrary point z_0 on the axis. At $t = 0$, $\vec{\mathbf{E}}$ lies along the reference axis in Fig. 8.4*a*, and so

$$\vec{\mathbf{E}}_x = \hat{\mathbf{i}} E_0 \cos kz_0 \quad \text{and} \quad \vec{\mathbf{E}}_y = \hat{\mathbf{j}} E_0 \sin kz_0$$

At a later time, $t = kz_0/\omega$, $\vec{\mathbf{E}}_x = \hat{\mathbf{i}} E_0$, $\vec{\mathbf{E}}_y = 0$, and $\vec{\mathbf{E}}$ is along the x-axis. The resultant electric-field vector $\vec{\mathbf{E}}$ is rotating *clockwise* at an angular frequency of ω, as seen by an observ-

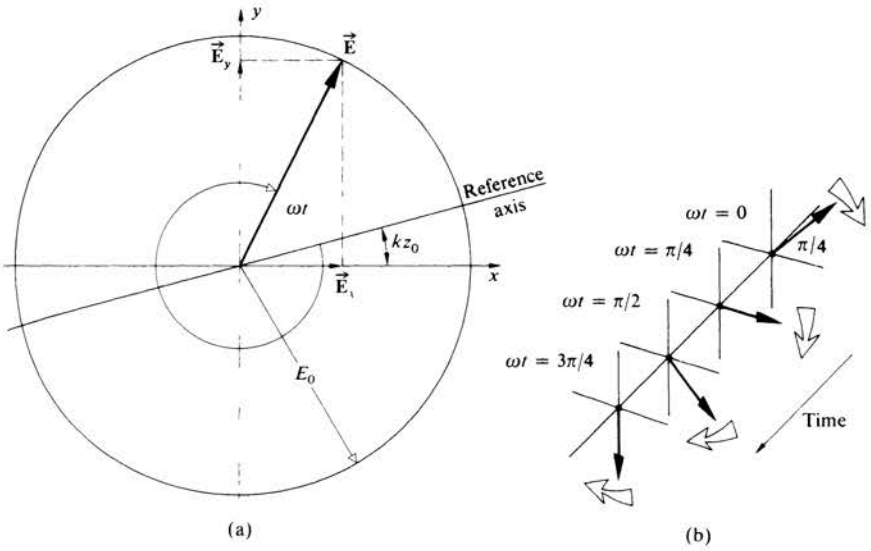


Figure 8.4 Rotation of the electric vector in a right-circular wave. Note that the rotation rate is ω and $kz = \pi/4$.

Giesecke+Devrient GmbH,
Giesecke+Devrient Currency Technology GmbH,
and Papierfabrik Louisenthal GmbH. - Ex. 1027

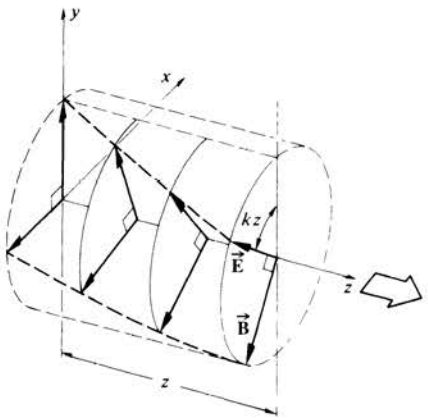


Figure 8.5 Right-circular light. Looking down the z-axis toward the origin, we see the electric field vector rotates clockwise as the wave advances toward the observer.

er toward whom the wave is moving (i.e., looking back at the source). Such a wave is **right-circularly polarized** (Fig. 8.5), and one generally simply refers to it as *right-circular light*. The $\vec{\mathbf{E}}$-vector makes one complete rotation as the wave advances through one wavelength. In comparison, if $\varepsilon = \pi/2$, $5\pi/2$, $9\pi/2$, and so on (i.e., $\varepsilon = \pi/2 + 2m\pi$, where $m = 0$, ± 1, ± 2, ± 3,...), then

$$\vec{\mathbf{E}} = E_0[\hat{\mathbf{i}} \cos(kz - \omega t) - \hat{\mathbf{j}} \sin(kz - \omega t)] \qquad (8.9)$$

The amplitude is unaffected, but $\mathbf{E}$ now rotates *counterclockwise*, and the wave is **left-circularly polarized**.

A linearly polarized wave can be synthesized from two oppositely polarized circular waves of equal amplitude. In particular, if we add the right-circular wave of Eq. (8.8) to the left-circular wave of Eq. (8.9), we get

$$\vec{\mathbf{E}} = 2E_0\hat{\mathbf{i}} \cos(kz - \omega t) \qquad (8.10)$$

which has a constant amplitude vector of $2E_0\hat{\mathbf{i}}$ and is therefore linearly polarized.

8.1.3 Elliptical Polarization

As far as the mathematical description is concerned, both linear and circular light may be considered to be special cases of **elliptically polarized** light, or more simply *elliptical light*. This means that, in general, the resultant electric-field vector $\vec{\mathbf{E}}$ will rotate, and change its magnitude, as well. In such cases the endpoint of $\vec{\mathbf{E}}$ will trace out an ellipse, in a fixed-space perpendicular to $\vec{\mathbf{k}}$, as the wave sweeps by. We can see this better by actually writing an expression for the curve traversed by the tip of $\vec{\mathbf{E}}$. To that end, recall that

$$E_y = E_{0y} \cos(kz - \omega t) \qquad (8.11)$$

and

$$E_x = E_{0x} \cos(kz - \omega t + \varepsilon) \qquad (8.12)$$

The equation of the curve we are looking for should not be a function of either position or time; in other words, we should be able to get rid of the $(kz - \omega t)$ dependence. Expand the expression for E_x into

$$E_x/E_{0x} = \cos(kz - \omega t) \cos\varepsilon - \sin(kz - \omega t) \sin\varepsilon$$

and combine it with E_y/E_{0y} to yield

$$\frac{E_x}{E_{0x}} - \frac{E_y}{E_{0y}} \cos\varepsilon = -\sin(kz - \omega t) \sin\varepsilon \qquad (8.13)$$

It follows from Eq. (8.11) that

$$\sin(kz - \omega t) = [1 - (E_y/E_{0y})^2]^{1/2}$$

so Eq. (8.13) leads to

$$\left(\frac{E_x}{E_{0x}} - \frac{E_y}{E_{0y}} \cos\varepsilon\right)^2 = \left[1 - \left(\frac{E_y}{E_{0y}}\right)^2\right] \sin^2\varepsilon$$

Finally, on rearranging terms, we have

$$\left(\frac{E_x}{E_{0x}}\right)^2 + \left(\frac{E_y}{E_{0y}}\right)^2 - 2\left(\frac{E_x}{E_{0x}}\right)\left(\frac{E_y}{E_{0y}}\right) \cos\varepsilon = \sin^2\varepsilon \qquad (8.14)$$

This is the equation of an ellipse making an angle α with the (E_x, E_y)-coordinate system (Fig. 8.6) such that

$$\tan 2\alpha = \frac{2E_{0x}E_{0y} \cos\varepsilon}{E^2_{0x} - E^2_{0y}} \qquad (8.15)$$

Equation (8.14) might be a bit more recognizable if the principal axes of the ellipse were aligned with the coordinate axes, that is, $\alpha = 0$ or equivalently $\varepsilon = \pm\pi/2$, $\pm 3\pi/2$, $\pm 5\pi/2$, ..., in which case we have the familiar form

$$\frac{E_x^2}{E_{0x}^2} + \frac{E_y^2}{E_{0y}^2} = 1 \qquad (8.16)$$

Furthermore, if $E_{0x} = E_{0y} = E_0$, this can be reduced to

$$E_x^2 + E_y^2 = E_0^2 \qquad (8.17)$$

Giesecke+Devrient GmbH,
Giesecke+Devrient Currency Technology GmbH,
and Papierfabrik Louisenthal GmbH. - Ex. 1027

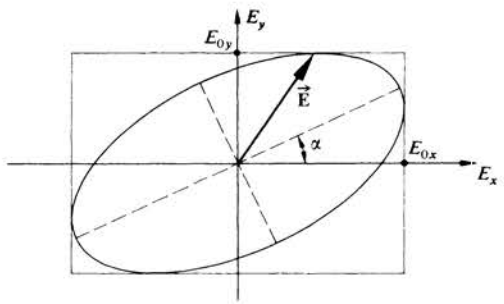


Figure 8.6 Elliptical light. The endpoint of the electric field vector sweeps out an ellipse as it rotates once around.

which, in agreement with our previous results, is a circle. If ε is an even multiple of π, Eq. (8.14) yields

$$E_y = \frac{E_{0y}}{E_{0x}} E_x \tag{8.18}$$

and similarly for odd multiples of π,

$$E_y = -\frac{E_{0y}}{E_{0x}} E_x \tag{8.19}$$

These are both straight lines having slopes of $\pm E_{0y}/E_{0x}$; in other words, we have linear light.

Figure 8.7 diagrammatically summarizes most of these conclusions. This very important diagram is labeled across the bottom "E_x leads E_y by: 0, $\pi/4$, $\pi/2$, $3\pi/4$,...," where these are the positive values of ε to be used in Eq. (8.2). The same set of curves will occur if "E_y leads E_x by: 2π, $7\pi/4$, $3\pi/2$, $5\pi/4$,...," and that happens when ε equals -2π, $-7\pi/4$, $-3\pi/2$, $-5\pi/4$, and so forth. Figure 8.7*b* illustrates how E_x leading E_y by $\pi/2$ is equivalent to E_y leading E_x by $3\pi/2$ (where the sum of these two angles equals 2π). This will be of continuing concern as we go on to shift the relative phases of the two orthogonal components making up the wave.

We are now in a position to refer to a particular lightwave in terms of its specific **state of polarization**. We shall say that linearly polarized or plane-polarized light is in a $\mathscr{P}$-state, and right- or left-circular light is in an $\mathscr{R}$- or $\mathscr{L}$-*state*, respectively. Similarly, the condition of elliptical polarization corresponds to an $\mathscr{E}$-*state*. We've already seen that a $\mathscr{P}$-state can be represented as a superposition of $\mathscr{R}$- and $\mathscr{L}$-states [Eg. (8.10)], and the same is true for an $\mathscr{E}$-state. In this case, as shown in Fig. 8.8, the amplitudes of the two circular waves are different. (An analytical treatment is left for Problem 8.3.)

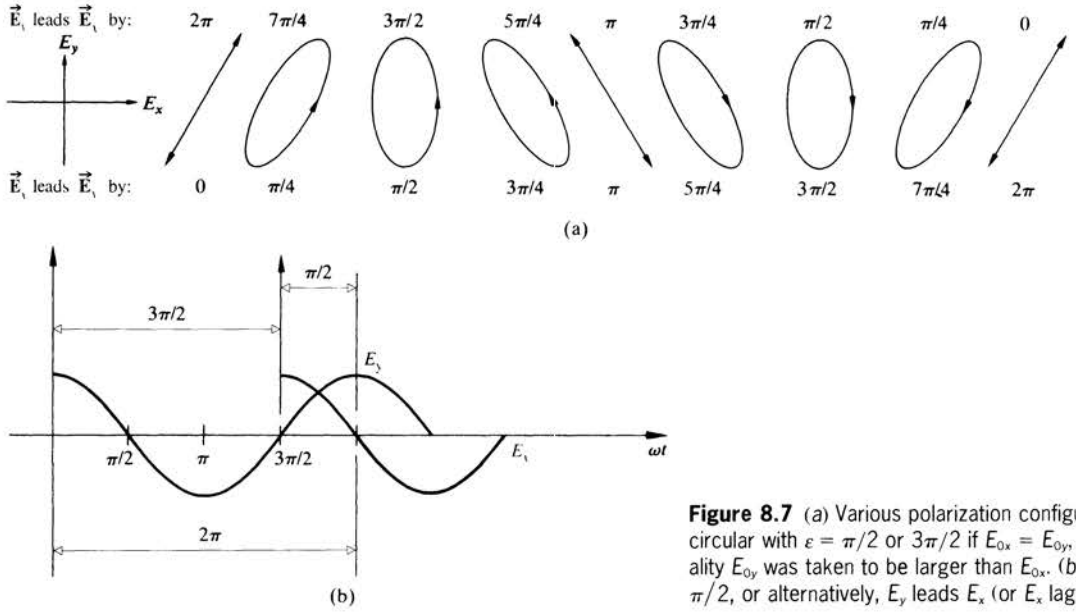


Figure 8.7 (*a*) Various polarization configurations. The light would be circular with $\varepsilon = \pi/2$ or $3\pi/2$ if $E_{0x} = E_{0y}$, but here for the sake of generality E_{0y} was taken to be larger than E_{0x}. (*b*) E_x leads E_y (or E_y lags E_x) by $\pi/2$, or alternatively, E_y leads E_x (or E_x lags E_y) by $3\pi/2$.

Giesecke+Devrient GmbH,
Giesecke+Devrient Currency Technology GmbH,
and Papierfabrik Louisenthal GmbH. - Ex. 1027

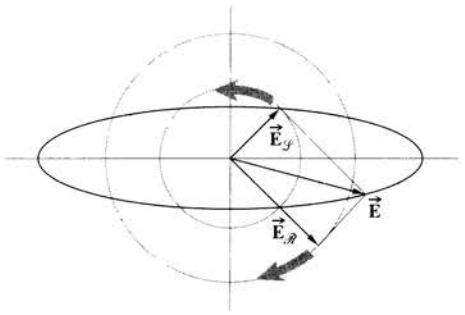


Figure 8.8 Elliptical light as the superposition of an $\mathscr{R}$- and $\mathscr{L}$-state.

8.1.4 Natural Light

An ordinary light source consists of a very large number of randomly oriented atomic emitters. Each excited atom radiates a polarized wavetrain for roughly 10^{-8} s. All emissions having the same frequency will combine to form a single resultant polarized wave, which persists for no longer than 10^{-8} s. New wavetrains are constantly emitted, and the overall polarization changes in a completely unpredictable fashion. If these changes take place at so rapid a rate as to render any single resultant polarization state indiscernible, the wave is referred to as **natural light**. It is also known as *unpolarized light*, but this is a misnomer, since in actuality the light is composed of a rapidly varying succession of the different polarization states. *Randomly polarized* is probably a better way to speak of it.

We can mathematically represent natural light in terms of two arbitrary, *incoherent*, orthogonal, linearly polarized waves of equal amplitude (i.e., waves for which the relative phase difference varies rapidly and randomly).

Keep in mind that an idealized monochromatic plane wave must be depicted as an infinite wavetrain. If this disturbance is resolved into two orthogonal components perpendicular to the direction of propagation, they, in turn, must have the same frequency, be infinite in extent, and therefore be mutually coherent (i.e., ε = constant). In other words, ***a perfectly monochromatic plane wave is always polarized***. In fact, Eqs. (8.1) and (8.2) are just the Cartesian components of a transverse ($E_z = 0$) harmonic plane wave.

Whether natural in origin or artificial, light is generally neither completely polarized nor completely unpolarized; both cases are extremes. More often, the electric-field vector varies in a way that is neither totally regular nor totally irregular, and such an optical disturbance is **partially polarized**. One useful way of describing this behavior is to envision it as the result of the superposition of specific amounts of natural and polarized light.

8.1.5 Angular Momentum and the Photon Picture

We have already seen that an electromagnetic wave impinging on an object can impart both energy and linear momentum to that body. Moreover, if the incident plane wave is circularly polarized, we can expect electrons within the material to be set into circular motion in response to the force generated by the rotating $\vec{\mathbf{E}}$-field. Alternatively, we might picture the field as being composed of two orthogonal $\mathscr{P}$-states that are 90° out-of-phase. These simultaneously drive the electron in two perpendicular directions with a $\pi/2$ phase difference. The resulting motion is again circular. In effect, the torque exerted by the $\vec{\mathbf{B}}$-field averages to zero over an orbit, and the $\vec{\mathbf{E}}$-field drives the electron with an angular velocity ω equal to the frequency of the electromagnetic wave. Angular momentum will thus be imparted by the wave to the substance in which the electrons are imbedded and to which they are bound. We can treat the problem rather simply without actually going into the details of the dynamics. The power delivered to the system is the energy transferred per unit time, $d\mathscr{E}/dt$. Furthermore, the power generated by a torque Γ acting on a rotating body is just $\omega\Gamma$ (which is analogous to vF for linear motion), so

$$\frac{d\mathscr{E}}{dt} = \omega\Gamma \tag{8.20}$$

Since the torque is equal to the time rate-of-change of the angular momentum L, it follows that on the average

$$\frac{d\mathscr{E}}{dt} = \omega\frac{dL}{dt} \tag{8.21}$$

A charge that absorbs a quantity of energy $\mathscr{E}$ from the incident circular wave will simultaneously absorb an amount of angular momentum L such that

$$L = \frac{\mathscr{E}}{\omega} \tag{8.22}$$

If the incident wave is in an $\mathscr{R}$-state, its $\vec{\mathbf{E}}$-vector rotates clockwise, looking toward the source. This is the direction in which a positive charge in the absorbing medium would rotate, and

Giesecke+Devrient GmbH,
Giesecke+Devrient Currency Technology GmbH,
and Papierfabrik Louisenthal GmbH. - Ex. 1027

the angular momentum vector is therefore taken to point in the direction opposite to the propagation direction,* as shown in Fig. 8.9.

According to the quantum-mechanical description, an electromagnetic wave transfers energy in quantized packets or photons such that $\mathscr{E} = h\nu$. Thus $\mathscr{E} = \hbar\omega$ (where $\hbar \equiv h/2\pi$), and the *intrinsic* or *spin* angular momentum of a photon is either $-\hbar$ or $+\hbar$, where the signs indicate right- or left-handedness, respectively. Notice that *the angular momentum of a photon is completely independent of its energy*. Whenever a charged particle emits or absorbs electromagnetic radiation, along with changes in its energy and linear momentum, it will undergo a change of $\pm\hbar$ in its angular momentum.†

The energy transferred to a target by an incident monochromatic electromagnetic wave can be envisaged as being transported in the form of a stream of identical photons. We can anticipate a corresponding quantized transport of angular momentum. A purely left-circularly polarized plane wave will impart angular momentum to the target as if all the constituent photons in the beam had their spins aligned in the direction of propagation. Changing the light to right circular reverses the spin orientation of the photons, as well as the torque exerted by them on the target. In 1935, using an extremely sensitive torsion pendulum, Richard A. Beth was actually able to perform such measurements.*

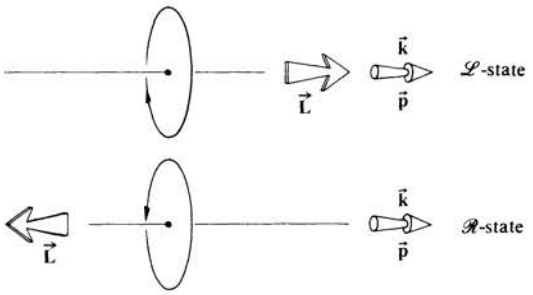


Figure 8.9 Angular momentum of a photon.

Thus far we've had no difficulty in describing purely right- and left-circular light in the photon picture; but what is linearly or elliptically polarized light? Classically, light in a $\mathscr{P}$-state can be synthesized by the coherent superposition of equal amounts of light in $\mathscr{R}$- and $\mathscr{L}$-states (with an appropriate phase difference). Any single photon whose angular momentum is somehow measured will be found to have its spin either totally parallel or antiparallel to $\vec{\mathbf{k}}$. A beam of linear light will interact with matter as if it were composed, at that instant, of equal numbers of right- and left-handed photons. There is a subtle point that has to be made here. We cannot say that the beam is actually made up of precisely equal amounts of well-defined right- and left-handed photons; the photons are all identical. Rather, each individual photon exists in either spin state with equal likelihood. If we measured the angular momentum of the constituent photons, $-\hbar$ would result as often as $+\hbar$. This is all we can observe. We are not privy to what the photon is doing before the measurement (if indeed it exists before the measurement). As a whole, a linearly polarized light beam will impart no total angular momentum to a target.

In contrast, if each photon does not occupy both spin states with the same probability, one angular momentum, say $+\hbar$, will be found to occur somewhat more often than the other, $-\hbar$. In this instance, a net positive angular momentum will therefore be imparted to the target. The result *en masse* is elliptically polarized light, that is, a superposition of unequal amounts of $\mathscr{R}$- and $\mathscr{L}$-light bearing a particular phase relationship.

8.2 Polarizers

Now that we have some idea of what polarized light is, the next logical step is to develop an understanding of the techniques used to generate, change, and manipulate it to fit our needs. An optical device whose input is natural light and

*This choice of terminology is admittedly a bit awkward. Yet its use in Optics is fairly well established, even though it is completely antithetic to the more reasonable convention adopted in elementary particle physics.

†As a rather important yet simple example, consider the hydrogen atom. It is composed of a proton and an electron, each having a spin of $\hbar/2$. The atom has slightly more energy when the spins of both particles are in the same direction. It is possible, however, that once in a very long time, roughly 10^7 years, one of the spins will flip over and be antiparallel to the other. The change in angular momentum of the atom is then $\hbar$, and this is imparted to an emitted photon which carries off the slight excess in energy as well. This is the origin of the 21-cm microwave emission, which is so significant in radio astronomy.

*Richard A. Beth, "Mechanical Detection and Measurement of the Angular Momentum of Light," *Phys. Rev.* **50**, 115 (1936).

Giesecke+Devrient GmbH,
Giesecke+Devrient Currency Technology GmbH,
and Papierfabrik Louisenthal GmbH. - Ex. 1027

whose output is some form of polarized light is a **polarizer**. For example, recall that one possible representation of unpolarized light is the superposition of two equal-amplitude, incoherent, orthogonal $\mathcal{P}$-states. An instrument that separates these two components, discarding one and passing on the other, is known as a *linear polarizer*. Depending on the form of the output, we could also have *circular* or *elliptical polarizers*. All these devices vary in effectiveness down to what might be called leaky or *partial* polarizers.

Polarizers come in many different configurations, but they are all based on one of four fundamental physical mechanisms: *dichroism*, or selective absorption; *reflection*; *scattering*; and *birefringence*, or double refraction. There is, however, one underlying property that they all share: *there must be some form of asymmetry associated with the process.* This is certainly understandable, since the polarizer must somehow select a particular polarization state and discard all others. In truth, the asymmetry may be a subtle one related to the incident or viewing angle, but usually it is an obvious anisotropy in the material of the polarizer itself.

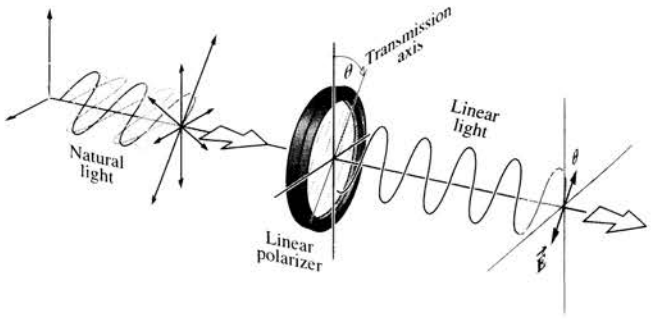


Figure 8.10 Natural light incident on a linear polarizer tilted at an angle θ with respect to the vertical.

8.2.1 Malus's Law

One matter needs to be settled before we go on: how do we determine experimentally whether or not a device is actually a linear polarizer?

By definition, if natural light is incident on an ideal linear polarizer, as in Fig. 8.10, only light in a $\mathcal{P}$-state will be transmitted. That $\mathcal{P}$-state will have an orientation parallel to a specific direction called the **transmission axis** of the polarizer. Only the component of the optical field parallel to the transmission axis will pass through the device essentially unaffected. If the polarizer in Fig 8.10 is rotated about the z-axis, the reading of the detector (e.g., a photocell) will be unchanged because of the complete symmetry of unpolarized light. Keep in mind that we are dealing with waves, but because of the very high frequency of light, our detector will measure only the incident irradiance. Since the irradiance is proportional to the square of the amplitude of the electric field [Eq. (3.44)], we need only concern ourselves with that amplitude.

Now suppose that we introduce a second identical ideal linear polarizer, or **analyzer**, whose transmission axis is vertical (Fig. 8.11). If the amplitude of the electric field transmitted by the first polarizer is E_{01}, only its component, $E_{01}\cos\theta$, parallel to the transmission axis of the analyzer will be passed on to the detector (assuming no absorption). According to Eq. (3.44), the irradiance reaching the detector is then given by

$$I(\theta) = \frac{c\epsilon_0}{2} E_{01}^2 \cos^2\theta \tag{8.23}$$

The maximum irradiance, $I(0) = c\epsilon_0 E_{01}^2/2 = I_1$, occurs when the angle θ between the transmission axes of the analyzer and polar-

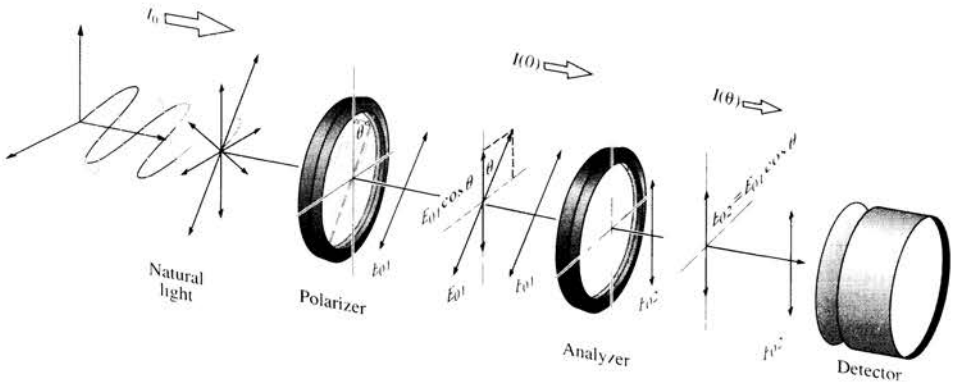


Figure 8.11 A linear polarizer and analyzer—Malus's Law. Natural light of irradiance I_0 is incident on a linear polarizer tilted at an angle θ with respect to the vertical. The irradiance leaving the first linear polarizer is $I_1 = I(0)$. The irradiance leaving the second linear polarizer (which makes an angle θ with the first) is $I(\theta)$.

Giesecke+Devrient GmbH,
Giesecke+Devrient Currency Technology GmbH,
and Papierfabrik Louisenthal GmbH. - Ex. 1027

izer is zero. Equation (8.23) can be rewritten as

$$I(\theta) = I(0)\cos^2\theta \qquad (8.24)$$

This is known as **Malus's Law**, having first been published in 1809 by Étienne Malus, military engineer and captain in the army of Napoleon.

Keep in mind that $I(0)$ is the irradiance arriving on the analyzer. Thus, if 1000 W/m^2 of natural light impinges on the first linear polarizer in Fig. 8.11, assuming that polarizer is ideal, it will pass 500 W/m^2 of linear light on to the analyzer; that's $I(0)$. Depending on θ, we can use Eq. (8.24) to calculate the transmitted irradiance $I(\theta)$. Alternatively, suppose the incident beam is 1000 W/m^2 of linear light parallel to the transmission axis of the first polarized. In that case $I(0) = 1000$ W/m^2.

Observe that $I(90°) = 0$. This arises from the fact that the electric field that passed through the polarizer is perpendicular to the transmission axis of the analyzer (the two devices so arranged are said to be *crossed*). The field is therefore parallel to what is called the *extinction axis* of the analyzer and has no component along the transmission axis. We can use the setup of Fig. 8.11 along with Malus's Law to determine whether a particular device is a linear polarizer.

As we'll see presently, the most common kind of linear polarizer used today is the Polaroid filter. And although you certainly can confirm Malus's Law with two ordinary Polaroids, you'll have to be careful to use light in the range from ≈450 nm to ≈650 nm. Ordinary Polaroids are not very good at polarizing IR.

8.3 Dichroism

In its broadest sense, the term **dichroism** refers to the selective absorption of one of the two orthogonal $\mathcal{P}$-state components of an incident beam. The dichroic polarizer itself is physically anisotropic, producing a strong asymmetric or preferential absorption of one field component while being essentially transparent to the other.

8.3.1 The Wire-Grid Polarizer

The simplest device of this sort is a grid of parallel conducting wires, as shown in Fig. 8.12. Imagine that an unpolarized electromagnetic wave impinges on the grid from the right. The electric field can be resolved into the usual two orthogonal components, in this case, one chosen to be parallel to the wires and the other perpendicular to them. The y-component of the field drives the conduction electrons along the length of each wire, thus generating a current. The electrons in turn collide with lattice atoms, imparting energy to them and thereby heating the wires (joule heat). In this manner energy is transferred from the field to the grid. In addition, electrons accelerating along the y-axis radiate in both the forward and backward directions. As should be expected, the incident wave tends to be canceled by the wave reradiated in the forward direction, resulting in little or no transmission of the y-component of the field. The radiation propagating in the backward direction simply appears as a reflected wave. In contrast, the electrons are not free to move very far in the x-direction, and the corresponding field component of the wave is essentially unaltered as it propagates through the grid. ***The transmission axis of the grid is perpendicular to the wires***. It is a common error to assume naively that the y-component of the field somehow slips through the spaces between the wires.

One can easily confirm our conclusions using microwaves and a grid made of ordinary electrical wire. It is not so easy a matter, however, to fabricate a grid that will polarize light, but it has been done! In 1960 George R. Bird and Maxfield Parrish, Jr., constructed a grid having an incredible 2160 wires per mm.* Their feat was accomplished by evaporating a stream of gold (or at other times aluminum) atoms at nearly grazing incidence onto a plastic diffraction grating replica (see Section 10.2.7). The metal accumulated along the edges of each step in the grating to form thin microscopic "wires" whose width and spacing were less than one wavelength across.

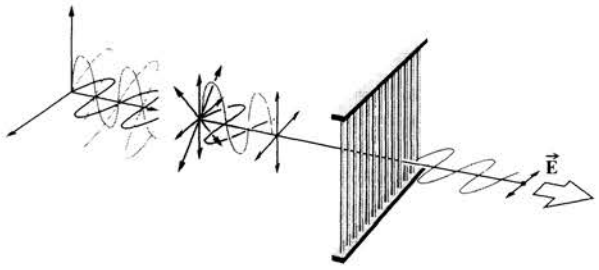


Figure 8.12 A wire-grid polarizer. The grid eliminates the vertical component (i.e., the one parallel to the wires) of the E-field and passes the horizontal component.

*G. R. Bird and M. Parrish, Jr., "The Wire Grid as a Near-Infrared Polarizer," *J. Opt. Soc. Am.* **50**, 886 (1960).

Giesecke+Devrient GmbH,
Giesecke+Devrient Currency Technology GmbH,
and Papierfabrik Louisenthal GmbH. - Ex. 1027

Although the wire grid is useful, particularly in the infrared, it is mentioned here more for pedagogical than practical reasons. The underlying principle is shared by other, more common, dichroic polarizers.

8.3.2 Dichroic Crystals

Certain materials are inherently dichroic because of an anisotropy in their respective crystalline structures. Probably the best known of these is the naturally occurring mineral *tourmaline*, a semiprecious stone often used in jewelry. Actually there are several tourmalines, which are boron silicates of differing chemical composition [e.g., $NaFe_3B_3Al_6Si_6O_{27}(OH)_4$]. For this substance there is a specific direction within the crystal known as the principal or *optic* axis, which is determined by its atomic configuration. The electric-field component of an incident lightwave that is perpendicular to the principal axis is strongly absorbed by the sample. The thicker the crystal, the more complete the absorption (Fig. 8.13). A plate cut from a tourmaline crystal parallel to its principal axis and several millimeters thick will serve as a linear polarizer. In this instance the crystal's principal axis becomes the polarizer's transmission axis. But the usefulness of tourmaline is rather limited by the fact that its crystals are comparatively small. Moreover, even the transmitted light suffers a certain amount of absorption. To complicate matters, this undesirable absorption is strongly wavelength dependent, and the specimen will therefore be colored. A tourmaline crystal held up to natural white light might appear green (they come in other colors as well) when viewed normal to the principal axis and nearly black when viewed along that axis, where all the $\vec{\mathbf{E}}$-fields are perpendicular to it (ergo the term dichroic, meaning *two colors*).

There are several other substances that display similar characteristics. A crystal of the mineral hypersthene, a ferromagnesium silicate, might look green under white light polarized in one direction and pink for a different polarization direction.

We can get a qualitative picture of the mechanism that gives rise to crystal dichroism by considering the microscopic structure of the sample. (You might want to take another look at Section 3.5.) Recall that the atoms within a crystal are strongly bound together by short-range forces to form a periodic lattice. The electrons, which are responsible for the optical properties, can be envisioned as elastically tied to their respective equilibrium positions. Electrons associated with a given atom are also under the influence of the surrounding nearby atoms, which themselves may not be symmetrically distributed. As a result, the elastic binding forces on the electrons will be different in different directions. Consequently, their response to the harmonic electric field of an incident electromagnetic wave will vary with the direction of $\vec{\mathbf{E}}$. If in addition to being anisotropic the material is absorbing, a detailed analysis would have to include an orientation-dependent conductivity. Currents will exist, and energy from the wave will be converted into joule heat. The attenuation, in addition to varying in direction, may be dependent on frequency as well. This means that if the incoming white light is in a $\mathscr{P}$-state, the crystal will appear colored, and the color will

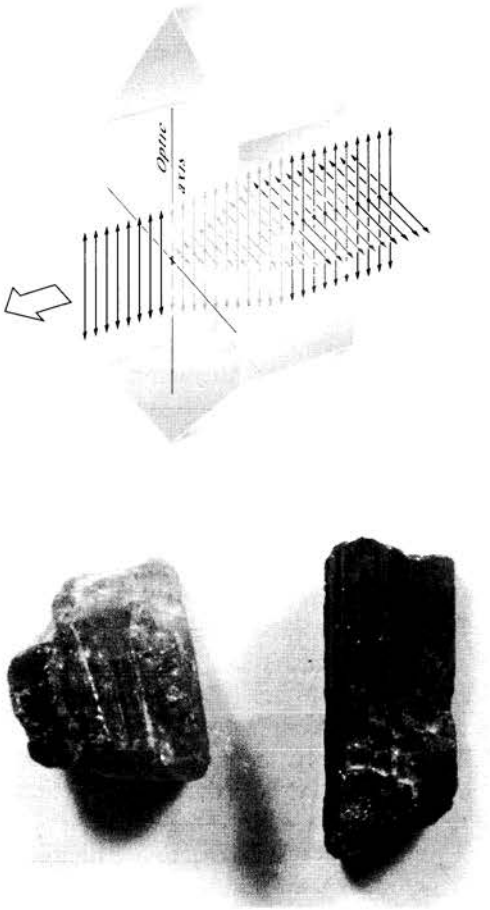


Figure 8.13 A dichroic crystal. The *E*-field parallel to the optic axis is transmitted without any diminution. The naturally occurring ridges evident in the photograph of the tourmaline crystals correspond to the optic axis. (Photo by E.H.)

Giesecke+Devrient GmbH,
Giesecke+Devrient Currency Technology GmbH,
and Papierfabrik Louisenthal GmbH. - Ex. 1027

depend on the orientation of $\vec{E}$. Substances that display two or even three different colors are said to be dichroic or trichroic, respectively.*

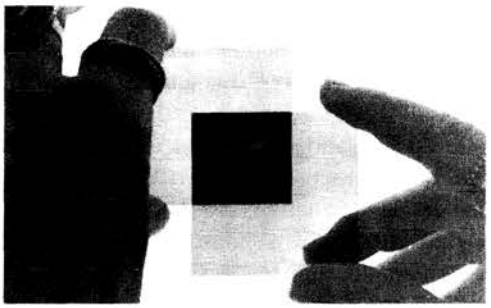
8.3.3 Polaroid

In 1928 Edwin Herbert Land, then a 19-year-old undergraduate at Harvard College, invented the first dichroic sheet polarizer, known commercially as *Polaroid J-sheet*. It incorporated a synthetic dichroic substance called *herapathite*, or *quinine sulfate periodide*.† Land's own retrospective account of his early work is rather informative and makes fascinating reading. It is particularly interesting to follow the sometimes whimsical origins of what is now, no doubt, the most widely used group of polarizers. The following is an excerpt from Land's remarks:

> In the literature there are a few pertinent high spots in the development of polarizers, particularly the work of William Bird Herapath, a physician in Bristol, England, whose pupil, a Mr. Phelps, had found that when he dropped iodine into the urine of a dog that had been fed quinine, little scintillating green crystals formed in the reaction liquid. Phelps went to his teacher, and Herapath then did something which I [Land] think was curious under the circumstances; he looked at the crystals under a microscope and noticed that in some places they were light where they overlapped and in some places they were dark. He was shrewd enough to recognize that here was a remarkable phenomenon, a new polarizing material [now known as herapathite]....
>
> Herapath's work caught the attention of Sir David Brewster, who was working in those happy days on the kaleidoscope.... Brewster, who invented the kaleidoscope, wrote a book about it, and in that book he mentioned that he would like to use herapathite crystals for the eyepiece. When I was reading this book, back in 1926 and 1927, I came across his reference to these remarkable crystals, and that started my interest in herapathite.

*More will be said about these processes later on when we consider birefringence. Suffice it to say now that for crystals classified as *uniaxial* there are two distinct directions, and therefore two colors may be displayed by *absorbing* specimens. In *biaxial* crystals there are three distinct directions and the possibility of three colors.

†E. H. Land, "Some Aspects of the Development of Sheet Polarizers," *J. Opt. Soc. Am.* **41**, 957 (1951).



A pair of crossed polaroids. Each polaroid appears gray because it absorbs roughly half the incident light. (Photo by E.H.)

Land's initial approach to creating a new form of linear polarizer was to grind herapathite into millions of submicroscopic crystals, which were naturally needle-shaped. Their small size lessened the problem of the scattering of light. In his earliest experiments, the crystals were aligned nearly parallel to each other by means of magnetic or electric fields. Later, Land found that they would be mechanically aligned when a viscous colloidal suspension of the herapathite needles was extruded through a long narrow slit. The resulting *J*-sheet was effectively a large flat dichroic crystal. The individual submicroscopic crystals still scattered light a bit, and as a result, *J*-sheet was somewhat hazy.

In 1938 Land invented *H-sheet*, which is now probably the most widely used linear polarizer. It does not contain dichroic crystals but is instead a molecular analogue of the wire grid. A sheet of clear polyvinyl alcohol is heated and stretched in a given direction, its long hydrocarbon molecules becoming aligned in the process. The sheet is then dipped into an ink solution rich in iodine. The iodine impregnates the plastic and attaches to the straight long-chain polymeric molecules, effectively forming a chain of its own. The conduction electrons associated with the iodine can move along the chains as if they were long thin wires. The component of $\vec{E}$ in an incident wave that is parallel to the molecules drives the electrons, does work on them, and is strongly absorbed. The transmission axis of the polarizer is therefore perpendicular to the direction in which the film was stretched.

Each separate miniscule dichroic entity is known as a *dichromophore*. In *H*-sheet the dichromophores are of molecular dimensions, so scattering represents no problem. *H*-sheet is a very effective polarizer across the entire visible spectrum, but is somewhat less so at the blue end. When a bright white light is viewed through a pair of crossed *H*-sheet Polaroids the

Giesecke+Devrient GmbH,
Giesecke+Devrient Currency Technology GmbH,
and Papierfabrik Louisenthal GmbH. - Ex. 1027

extinction color will be a deep blue as a result of this leakage. *HN*-50 would be the designation of a hypothetical, ideal *H*-sheet having a *neutral color* (*N*) and transmitting 50% of the incident natural light while absorbing the other 50%, which is the undesired polarization component. In practice, however, about 4% of the incoming light will be reflected back at each surface (antireflection coatings are not generally used), leaving about 92%. Half of this is presumably absorbed, and thus we might contemplate an *HN*-46 Polaroid. Actually, large quantities of *HN*-38, *HN*-32, and *HN*-22, each differing by the amount of iodine present, are produced commercially and are readily available (Problem 8.10).

Many other forms of Polaroid have been developed.* *K-sheet*, which is humidity- and heat-resistant, has as its dichromophore the straight-chain hydrocarbon polyvinylene. A combination of the ingredients of *H*- and *K*-sheets leads to *HR-sheet*, a near-infrared polarizer. And there are commercially available dichroic sheet linear polarizers that function in the ultraviolet from ≈300 nm to ≈400 nm.

Remember that sheet dichroic polarizers are designed for a specific wavelength range. A pair of crossed sheet linear polarizers intended to block the visible will leak substantially below ≈450 nm and above ≈650 nm.

Polaroid vectograph is a commercial material at one time designed to be incorporated in a process for making three-dimensional photographs. The stuff never was successful at its intended purpose, but it can be used to produce some rather thought-provoking, if not mystifying, demonstrations. Vectograph film is a water-clear plastic laminate of two sheets of polyvinyl alcohol arranged so that their stretch directions are at right angles to each other. In this form there are no conduction electrons available, and the film is not a polarizer. Using an iodine solution, imagine that we draw an *X* on one side of the film and a *Y* overlapping it on the other. Under natural illumination the light passing through the *X* will be in a $\mathscr{P}$-state perpendicular to the $\mathscr{P}$-state light coming from the *Y*. In other words, the painted regions form two crossed polarizers. They will be seen superimposed on each other. Now, if the vectograph is viewed through a linear polarizer that can be rotated, either the *X*, the *Y*, or both will be seen. Obviously, more imaginative drawings can be made. (One need only remember to make the one on the far side backward.)

*See *Polarized Light: Production and Use*, by Shurcliff, or its more readable little brother, *Polarized Light*, by Shurcliff and Ballard.

8.4 Birefringence

Many crystalline substances (i.e., solids whose atoms are arranged in some sort of regular repetitive array) are *optically anisotropic*. Their optical properties are not the same in all directions within any given sample. The dichroic crystals of the previous section are but one special subgroup. We saw there that if the crystal's lattice atoms were not completely symmetrically arrayed, the binding forces on the electrons would be anisotropic. Earlier, in Fig. 3.38*b* we represented the isotropic oscillator using the simple mechanical model of a spherical charged shell bound by identical springs to a fixed point. This was fine for *optically isotropic* substances (amorphous solids, such as glass and plastic, are usually, but not always, isotropic). Figure 8.14 shows another charged shell, this one bound by springs of differing stiffness (i.e., having different spring constants). An electron that is displaced from equilibrium along a direction parallel to one set of "springs" will evidently oscillate with a different characteristic frequency than it would were it displaced in some other direction.

As was pointed out previously, light propagates through a transparent substance by exciting the atoms within the medium. The electrons are driven by the $\vec{E}$-field, and they reradiate; these secondary wavelets recombine, and the resultant refracted wave moves on. The speed of the wave, and therefore the index of refraction, is determined by the difference between the frequency of the $\vec{E}$-field and the natural frequency of the

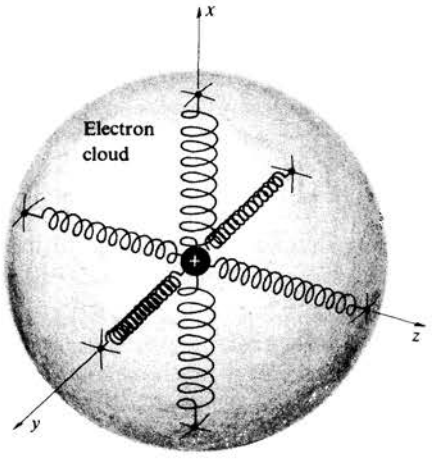


Figure 8.14 Mechanical model depicting a negatively charged shell bound to a positive nucleus by pairs of springs having different stiffness.

Giesecke+Devrient GmbH,
Giesecke+Devrient Currency Technology GmbH,
and Papierfabrik Louisenthal GmbH. - Ex. 1027

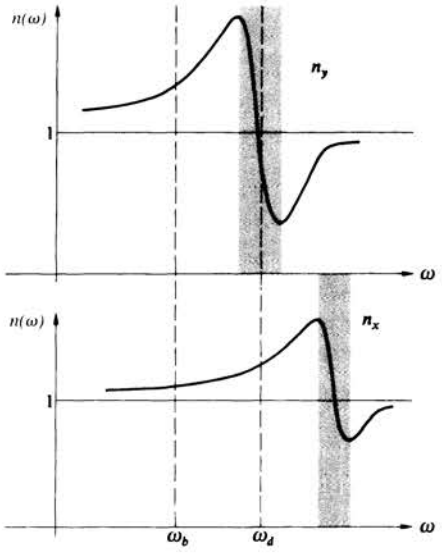


Figure 8.15 Refractive index versus frequency along two axes in a crystal. Regions where $dn/d\omega < 0$ correspond to absorption bands.

atoms. *An anisotropy in the binding force will be manifest in an anisotropy in the refractive index.* For example, if $\mathcal{P}$-state light was to move through some hypothetical crystal so that it encountered electrons that could be represented by Fig. 8.14, its speed would be governed by the orientation of $\vec{\mathbf{E}}$. If $\vec{\mathbf{E}}$ was parallel to the stiff springs, that is, in a direction of strong binding, here along the x-axis, the electron's natural frequency would be high (proportional to the square root of the spring constant). In contrast, with $\vec{\mathbf{E}}$ along the y-axis, where the binding force is weaker, the natural frequency would be somewhat lower. Keeping in mind our earlier discussion of dispersion and the $n(\omega)$ curve of Fig. 3.41, the appropriate indices of refraction might look like those in Fig. 8.15. A material of this sort, which displays two different indices of refraction, is said to be **birefringent**.*

If the crystal is such that the frequency of the incident light appears in the vicinity of ω_d, in Fig. 8.15, it resides in the absorption band of $n_y(\omega)$. A crystal so illuminated will be strongly absorbing for one polarization direction (y) and transparent for the other (x). A birefringent material that absorbs one of the orthogonal $\mathcal{P}$-states, passing on the other, is *dichroic*. Furthermore, suppose that the crystal symmetry is such that the binding forces in the y- and z-directions are identical; in other words, each of these springs has the same natural frequency and they are equally lossy. The x-axis now defines the direction of the **optic axis**. Inasmuch as a crystal can be represented by an array of these oriented anisotropic charged oscillators, ***the optic axis is actually a direction and not merely a single line***. The model works rather nicely for dichroic crystals, since if light was to propagate along the optic axis ($\vec{\mathbf{E}}$ in the yz-plane), it would be strongly absorbed, and if it moved normal to that axis, it would emerge linearly polarized.

Often the natural frequencies of birefringent crystals are above the optical range, and they appear colorless. This is represented by Fig. 8.15 where the incident light is now considered to have frequencies in the region of ω_b. Two different indices are apparent, but absorption for either polarization is negligible. Equation (3.71) shows that $n(\omega)$ varies inversely with the natural frequency. This means that a large effective spring constant (i.e., strong binding) corresponds to a low polarizability, a low dielectric constant, and a low refractive index.

We will construct, if only pictorially, a linear polarizer utilizing birefringence by causing the two orthogonal $\mathcal{P}$-states to follow different paths and separate. Even more fascinating things can be done with birefringent crystals, as we shall see later.

8.4.1 Calcite

Let's spend a moment relating the above ideas to a typical birefringent crystal, calcite. Calcite or calcium carbonate ($CaCO_3$) is a common naturally occurring substance. Both marble and limestone are made up of many small calcite crystals bonded together. Of particular interest are the beautiful large single crystals, which, although they are becoming rare, can still be found, particularly in India, Mexico, and South Africa. Calcite is the most common material for making linear polarizers for use with high-power lasers.

Figure 8.16 shows the distribution of carbon, calcium, and oxygen within the calcite structure; Fig. 8.17 is a view from above, looking down along what has, in anticipation, been labeled the optic axis in Fig. 8.16. Each CO_3 group forms a triangular cluster whose plane is perpendicular to the optic axis. If Fig. 8.17 is rotated about a line normal to and passing

*The word *refringence* used to be used instead of our present-day term *refraction*. It comes from the Latin *refractus* by way of an etymological route beginning with *frangere*, meaning to break.

Giesecke+Devrient GmbH,
Giesecke+Devrient Currency Technology GmbH,
and Papierfabrik Louisenthal GmbH. - Ex. 1027

through the center of any one of the carbonate groups, the same exact configuration of atoms would appear three times during each revolution. The direction designated as the optic axis corresponds to a special crystallographic orientation, in that it is an axis of 3-*fold symmetry*. The large birefringence displayed by calcite arises from the fact that the carbonate groups are all in planes normal to the optic axis. The behavior of their electrons, or rather the mutual interaction of the induced oxygen dipoles, is markedly different when $\vec{\mathbf{E}}$ is either in or normal to those planes (Problem 8.25). In any event the asymmetry is clear enough.

Calcite samples can readily be split, forming smooth surfaces known as ***cleavage planes***. The crystal is essentially made to come apart between specific planes of atoms where the interatomic bonding is relatively weak. All cleavage planes in calcite (Fig. 8.17) are normal to three different directions. As a crystal grows, atoms are added layer upon layer, following the same pattern. But more raw material may be available to the growth process on one side than on another, resulting in a crystal with an externally complicated shape. Even so, the cleavage planes are dependent on the atomic configuration, and if one cuts a sample so that each surface is a cleavage plane, its form will be related to the basic arrangement of its atoms. Such a specimen is referred to as a **cleavage form**. In the case of calcite it is a rhombohedron, with each face a parallelogram whose angles are 78° 5′ and 101° 55′ (Fig. 8.18).

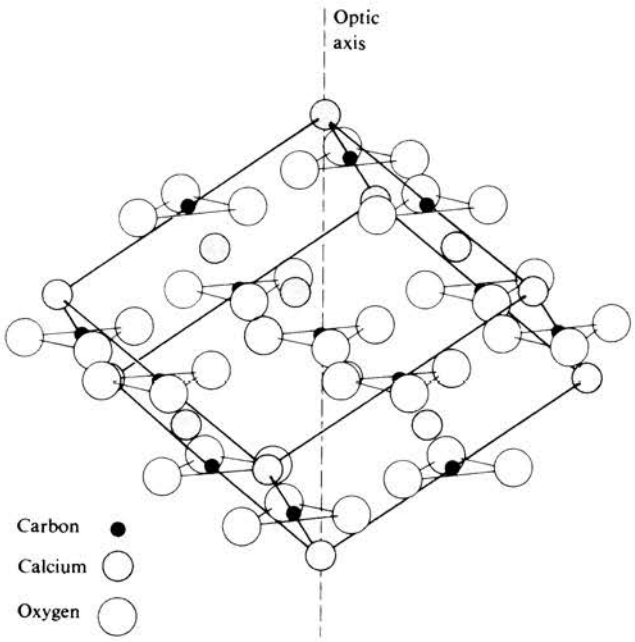


Figure 8.16 Arrangement of atoms in calcite.

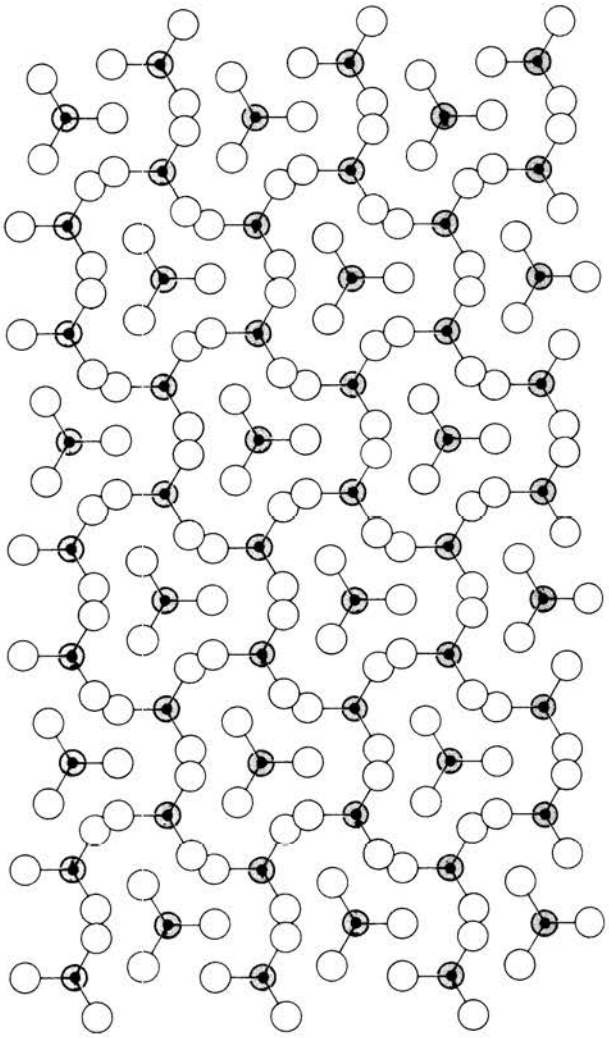


Figure 8.17 Atomic arrangement for calcite looking down the optical axis.

There are only two *blunt corners* where the surface planes meet to form three obtuse angles. A line passing through the vertex of either of the blunt corners, oriented so that it makes equal angles with each face (45.5°) and each edge (63.8°), is clearly an axis of 3-fold symmetry. (This would be a bit more obvious if we cut the rhomb to have edges of equal length.)

Giesecke+Devrient GmbH,
Giesecke+Devrient Currency Technology GmbH,
and Papierfabrik Louisenthal GmbH. - Ex. 1027

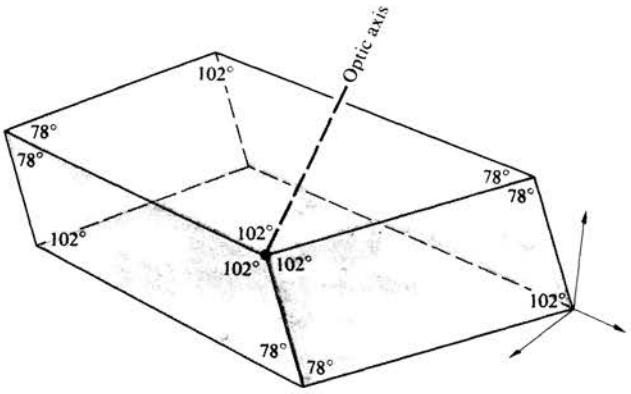


Figure 8.18 Calcite cleavage form.

Evidently, such a line must correspond to the optic axis. Whatever the natural shape of a particular calcite specimen, you need only find a blunt corner and you have the optic axis.

In 1669 Erasmus Bartholinus (1625–1692), doctor of medicine and professor of mathematics at the University of Copenhagen (and incidentally, the father-in-law of Ole Römer, the man who in 1679 first measured the speed of light), came upon a new and remarkable optical phenomenon in calcite, which he called double refraction. Calcite had been discovered not long before, near Eskifjordur in Iceland, and was then known as ***Iceland spar***. In the words of Bartholinus:*

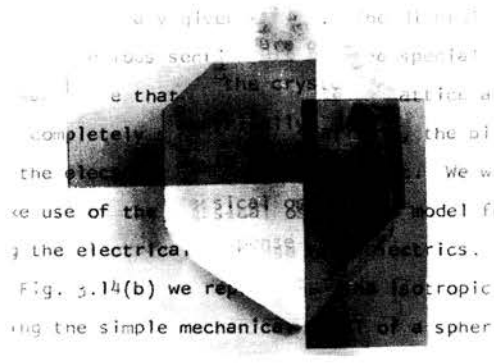
> Greatly prized by all men is the diamond, and many are the joys which similar treasures bring, such as precious stones and pearls... but he, who, on the other hand, prefers the knowledge of unusual phenomena to these delights, he will, I hope, have no less joy in a new sort of body, namely, a transparent crystal, recently brought to us from Iceland, which perhaps is one of the greatest wonders that nature has produced....
>
> As my investigation of this crystal proceeded there showed itself a wonderful and extraordinary phenomenon: objects which are looked at through the crystal do not show, as in the case of other transparent bodies, a single refracted image, but they appear double.

The double image referred to by Bartholinus is quite evident in the accompanying photograph. If we send a narrow beam of natural light into a calcite crystal normal to a cleavage plane, it will split and emerge as two parallel beams. To see the same effect quite simply, we need only place a black dot on a piece of paper and then cover it with a calcite rhomb. The image will now consist of two gray dots (black where they overlap). Rotating the crystal will cause one of the dots to remain stationary while the other appears to move in a circle about it, following the motion of the crystal. The rays forming the fixed dot, which is the one invariably closer to the upper blunt corner, behave as if they had merely passed through a plate of glass. In accord with a suggestion made by Bartholinus, they are known as the **ordinary rays**, or *o-rays*. The rays coming from the other dot, which behave in such an unusual fashion, are known as the **extraordinary rays**, or *e-rays*. If the crystal is examined through an analyzer, it will be found that the ordinary and extraordinary images are linearly polarized (see photo). Moreover, the two emerging $\mathcal{P}$-states are orthogonal.

*W. F. Magie, *A Source Book in Physics*.



Double image formed by a calcite crystal (not cleavage form). (Photo by E.H.)



A calcite crystal (blunt corner on the bottom). The transmission axes of the two polarizers are parallel to their short edges. Where the image is doubled the lower, undeflected one is the ordinary image. Take a long look: there's a lot in this one. (Photo by E.H.)

Giesecke+Devrient GmbH,
Giesecke+Devrient Currency Technology GmbH,
and Papierfabrik Louisenthal GmbH. - Ex. 1027

Any number of planes can be drawn through the rhomb so as to contain the optic axis, and these are all called **principal planes**. More specifically, if the principal plane is also normal to a pair of opposite surfaces of the cleavage form, it slices the crystal across a **principal section**. Evidently, three of these pass through any one point; each is a parallelogram having angles of 109° and 71°. Figure 8.19 is a diagrammatic representation of an initially unpolarized beam traversing a principal section of a calcite rhomb. The filled-in circles and arrows drawn along the rays indicate that the *o*-ray has its electric-field vector normal to the principal section, and the field of the *e*-ray is parallel to the principal section.

To simplify matters a bit, let $\vec{\mathbf{E}}$ in the incident plane wave be linearly polarized perpendicular to the optic axis, as shown in Fig. 8.20. The wave strikes the surface of the crystal, thereupon driving electrons into oscillation, and they in turn reradiate secondary wavelets. The wavelets superimpose and recombine to form the refracted wave, and the process is repeated over and over again until the wave emerges from the crystal. This represents a cogent physical argument for applying the ideas of scattering via Huygens's Principle. Huygens himself, though without benefit of electromagnetic theory, used his construction to explain many aspects of double refraction in calcite as long ago as 1690. It should be made clear from the outset, however, that his treatment is incomplete,* in which form it is appealingly, though deceptively, simple.

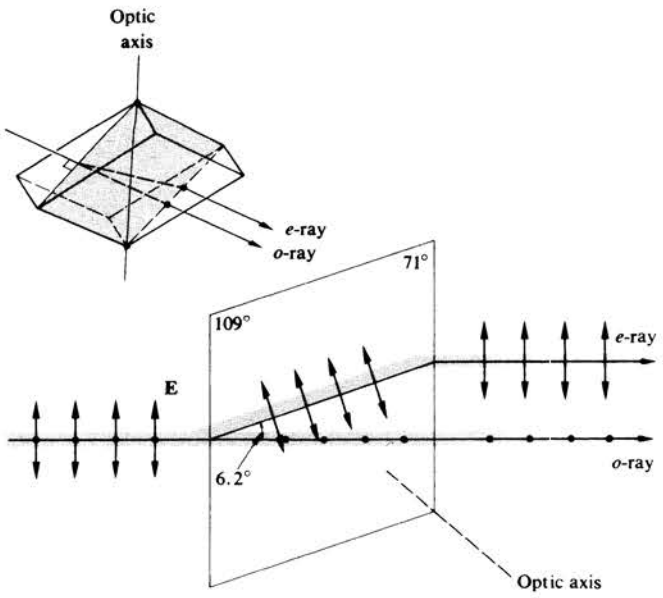


Figure 8.19 A light beam with two orthogonal field components traversing a calcite principal section.

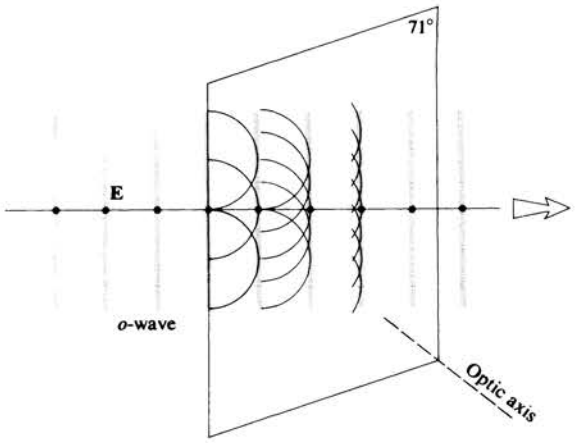


Figure 8.20 An incident plane wave polarized perpendicular to the principal section.

Inasmuch as the $\vec{\mathbf{E}}$-field is perpendicular to the optic axis, one assumes that the wavefront stimulates countless atoms on the surface, which then act as sources of spherical wavelets, all of which are in-phase. Presumably, as long as the *field of the wavelets is everywhere normal to the optic axis*, they will expand into the crystal in all directions with a speed $v_\perp$, as they would in an isotropic medium. (Keep in mind that the speed is a function of frequency.) Since the *o*-wave displays no anomalous behavior, this assumption seems reasonable. The envelope of the wavelets is essentially a portion of a plane wave, which in turn stimulates a distribution of secondary atomic point sources. The process continues, and the wave moves straight across the crystal.

In contrast, consider the incident wave in Fig. 8.21 whose $\vec{\mathbf{E}}$-field is parallel to the principal section. Notice that $\vec{\mathbf{E}}$ now has a component normal to the optic axis, as well as a component parallel to it. Since the medium is birefringent, light of a given frequency polarized parallel to the optic axis propagates with a speed $v_\parallel$, where $v_\parallel \neq v_\perp$. In particular for calcite and sodium yellow light ($\lambda = 589$ nm), $1.486v_\parallel = 1.658v_\perp = c$. What kind of Huygens's wavelets can we expect

*A. Sommerfeld, *Optics*, p. 148.

Giesecke+Devrient GmbH,
Giesecke+Devrient Currency Technology GmbH,
and Papierfabrik Louisenthal GmbH. - Ex. 1027

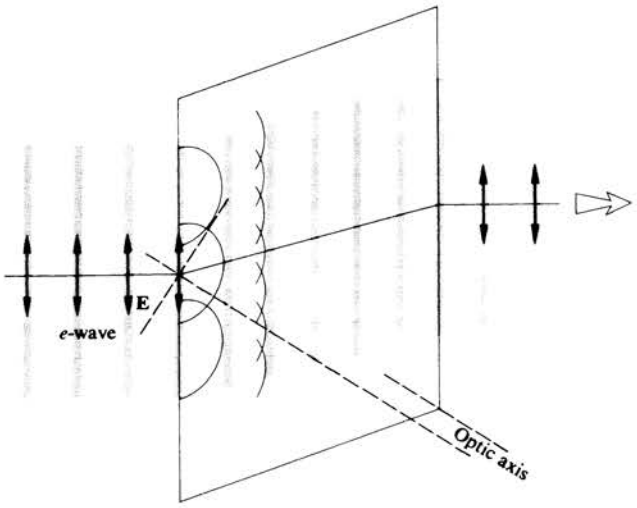


Figure 8.21 An incident plane wave polarized parallel to the principal section.

now? At the risk of oversimplifying matters, we represent each *e*-wavelet, for the moment at least, as a small sphere (Fig. 8.22). But $v_{\parallel} > v_{\perp}$, so that the wavelet will elongate in all directions normal to the optic axis. We therefore speculate, as Huygens did, that the secondary wavelets associated with the *e*-wave are ellipsoids of revolution about the optic axis. The envelope of all the ellipsoidal wavelets is essentially a portion of a plane wave parallel to the incident wave. This plane wave, however, will evidently undergo a sidewise displacement in traversing the crystal. The beam moves in a direction parallel to the lines connecting the origin of each wavelet and the point

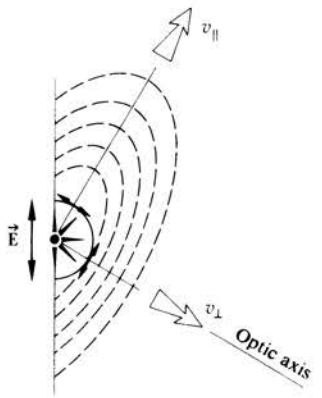


Figure 8.22 Wavelets within calcite.

of tangency with the planar envelope. This is known as the ***ray direction*** *and corresponds to the direction in which energy propagates. Clearly, in an anisotropic crystal the direction of the ray is not normal to the wavefront.*

If the incident beam is natural light, the two situations depicted in Figs. 8.20 and 8.21 will exist simultaneously, with the result that the beam will split into two orthogonal linearly polarized beams (Fig. 8.19). You can actually see the two diverging beams within a crystal by using a properly oriented narrow laserbeam ($\vec{E}$ neither normal nor parallel to the principal plane, which is usually the case). Light will scatter off internal flaws, making its path fairly visible.

The electromagnetic description of what is happening is rather complicated but well worth examining at this point, even if only superficially. Recall from Chapter 3 that the incident $\vec{E}$-field will polarize the dielectric; that is, it will shift the distribution of charges, thereby creating electric dipoles. The field within the dielectric is thus altered by the inclusion of an induced field, and one is led to introduce a new quantity, the *displacement* $\vec{D}$ (see Appendix 1). In isotropic media $\vec{D}$ is related to $\vec{E}$ by a scalar quantity, and the two are therefore always parallel. In anisotropic crystals $\vec{D}$ and $\vec{E}$ are related by a tensor and are not always parallel. If we now apply Maxwell's Equations to the problem of a wave moving through such a medium, we find that the fields vibrating within the wavefront are $\vec{D}$ and $\vec{B}$ and not, as before, $\vec{E}$ and $\vec{B}$. The propagation vector $\vec{k}$, which is normal to the surfaces of constant phase, is now perpendicular to $\vec{D}$ rather than $\vec{E}$. In fact, $\vec{D}$, $\vec{E}$, and $\vec{k}$ are all coplanar. The *ray direction* corresponds to the direction of the Poynting vector $\vec{S} = v^2\epsilon\vec{E}\times\vec{B}$, which is generally different from that of $\vec{k}$. Because of the manner in which the atoms are distributed, $\vec{E}$ and $\vec{D}$ will, however, be colinear when they are both either parallel or perpendicular to the optic axis.* This means that the *o*-wavelet will encounter an effectively isotropic medium and thus be spherical, having $\vec{S}$ and $\vec{k}$ colinear. In contrast, the *e*-wavelets will have $\vec{S}$ and $\vec{k}$, or equivalently $\vec{E}$ and $\vec{D}$, parallel only in directions along or normal to the optic axis. At all other points on the wavelet it is $\vec{D}$

*In the oscillator model, the general case corresponds to the situation in which $\vec{E}$ is not parallel to any of the spring directions. The field will drive the charge, but its resultant motion will not be in the direction of $\vec{E}$ because of the anisotropy of the binding forces. The charge will be displaced most, for a given force component, in the direction of weakest restraint. The induced field will thus not have the same orientation as $\vec{E}$.

Giesecke+Devrient GmbH,
Giesecke+Devrient Currency Technology GmbH,
and Papierfabrik Louisenthal GmbH. - Ex. 1027

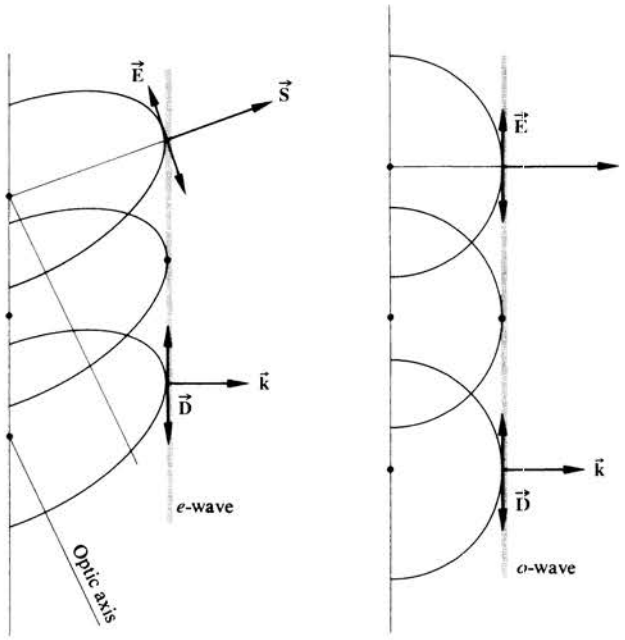


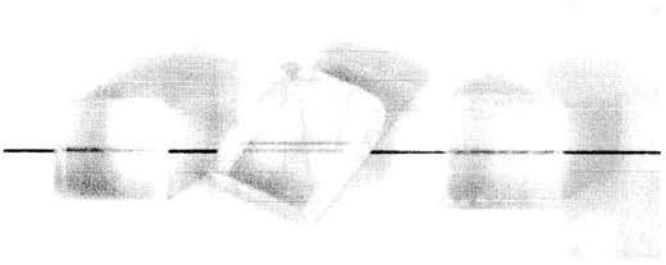
Figure 8.23 Orientations of the $\vec{E}$-, $\vec{D}$-, $\vec{S}$-, and $\vec{k}$-vectors.

that is tangent to the ellipsoid, and therefore it is always $\vec{D}$ that ends up in the envelope or composite planar wavefront within the crystal (Fig. 8.23).

8.4.2 Birefringent Crystals

Cubic crystals, such as sodium chloride (i.e., comrnon salt), have their atoms arranged in a relatively simple and highly symmetric form. (There are *four* 3-fold symmetry axes, each running from one corner to an opposite corner, unlike calcite, which has one such axis.) Light emanating from a point source within such a crystal will propagate uniformly in all directions as a spherical wave. As with amorphous solids, there will be no preferred directions in the material. It will have a single index of refraction and be *optically isotropic* (see photo). In that case all the springs in the oscillator model will evidently be identical.

Crystals belonging to the *hexagonal*, *tetragonal*, and *trigonal* systems have their atoms arranged so that light propagating in some general direction will encounter an asymmetric structure. Such substances are optically anisotropic and birefringent. The optic axis corresponds to



Crystals of potassium chloride, calcium carbonate (calcite), and sodium chloride (table salt). Only the calcite produces a double image. It's because of this that calcite is said to be birefringent. (Photo by E.H.)

a direction about which the atoms are arranged symmetrically. Crystals like these, for which there is only one such direction, are known as ***uniaxial***.

A point source of natural light embedded within one of these specimens gives rise to spherical *o*-wavelets and ellipsoidal *e*-wavelets. It is the orientation of the field with respect to the optic axis that determines the speeds with which these wavelets expand. The $\vec{E}$*-field of the o-wave is everywhere normal to the optic axis*, so it moves at a speed $v_\perp$ in all directions. Similarly, the *e*-wave has a speed $v_\perp$ only in the direction of the optic axis (Fig. 8.22), along which it is always tangent to the *o*-wave. Normal to this direction, $\vec{E}$ *is parallel to the optic axis*, and that portion of the wavelet expands at a speed $v_\parallel$ (Fig. 8.24). Uniaxial materials have two principal indices of refraction, $n_o \equiv c/v_\perp$ and $n_e \equiv c/v_\parallel$ (Problem 8.36) as indicated in Table 8.1.

The difference $\Delta n = (n_e - n_o)$ is a measure of the birefringence, and it's often called the **birefringence**. In calcite $v_\parallel > v_\perp$, $(n_e - n_o)$ is -0.172, and it is *negative uniaxial*. In comparison, there are other crystals, such as quartz (crystallized silicon dioxide) and ice, for which $v_\perp > v_\parallel$. Consequently, the ellipsoidal *e*-wavelets are enclosed within the spherical *o*-wavelets, as shown in Fig. 8.25. (Quartz is optically active and therefore actually a bit more complicated.) In that case, $(n_e - n_o)$ is positive, and the crystal is *positive uniaxial*.

The remaining crystallographic systems, namely orthorhombic, monoclinic, and triclinic, have two optic axes and are said to be biaxial. Such substances, for example, mica $[KH_2Al_3(SiO_4)_3]$, have three different principal indices of refraction. Each set of springs in the oscillator model would then be different. The birefringence of biaxial crystals is measured as the numerical difference between the largest and smallest of these indices.

Giesecke+Devrient GmbH,
Giesecke+Devrient Currency Technology GmbH,
and Papierfabrik Louisenthal GmbH. - Ex. 1027

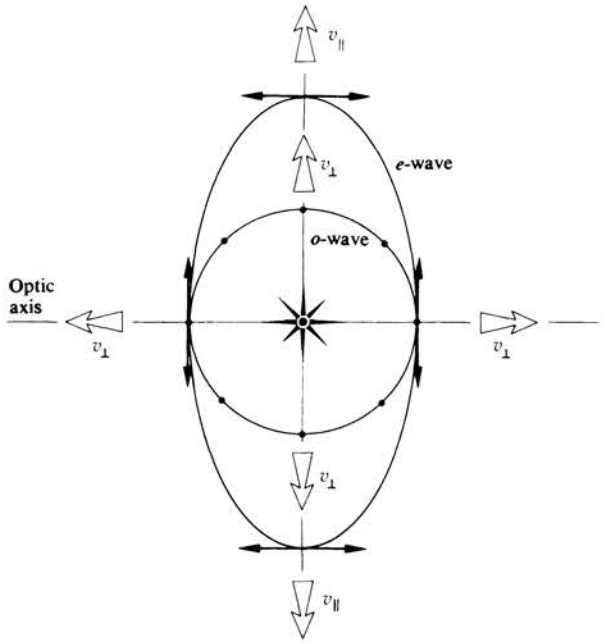


Figure 8.24 Wavelets in a negative uniaxial crystal. The arrows and dots represent the $\vec{E}$-fields of the extraordinary and ordinary waves, respectively. The $\vec{E}$-field of the *o*-wave is everywhere perpendicular to the optic axis.

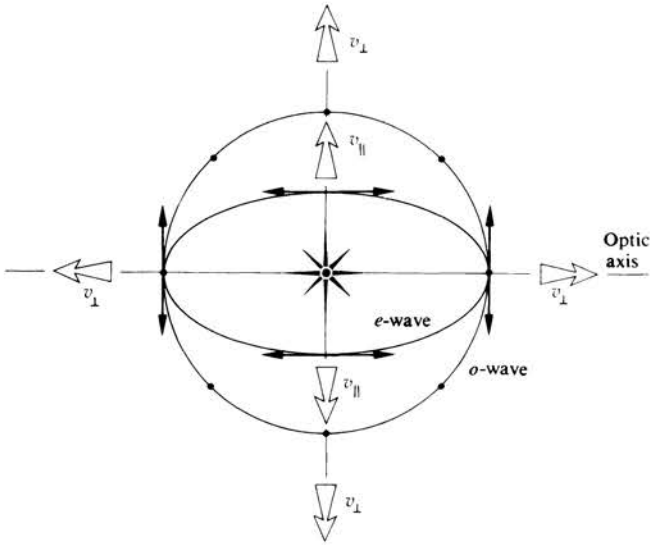


Figure 8.25 Wavelets in a positive uniaxial crystal. The arrows and dots represent the $\vec{E}$-fields of the extraordinary and ordinary waves, respectively. The $\vec{E}$-field of the *o*-wave is everywhere perpendicular to the optic axis.

8.4.3 Birefringent Polarizers

It will now be an easy matter, at least conceptually, to make some sort of linear birefringent polarizer. Any number of schemes for separating the *o*- and *e*-waves have been employed, all of them relying on the fact that $n_e \neq n_o$.

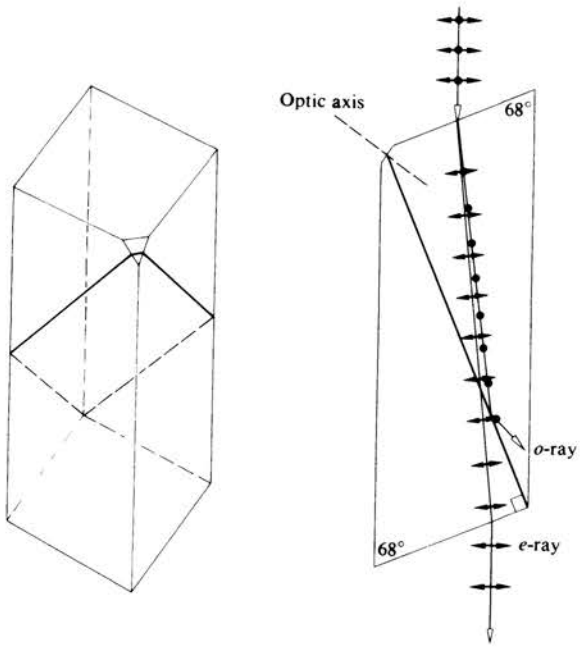
The most renowned birefringent polarizer was introduced in 1828 by the Scottish physicist William Nicol (1768–1851). The *Nicol prism* is now mainly of historical interest, having long been superseded by other, more effective polarizers. Putting it rather succinctly, the device is made by first grinding and polishing the ends (from 71° to 68°; see Fig. 8.20) of a suitably long, narrow calcite rhombohedron; after cutting the rhomb diagonally, the two pieces are polished and cemented back together with Canada balsam (Fig. 8.26). The balsam cement is transparent and has an index of 1.55 almost midway between n_e and n_o. The incident beam enters the "prism." The *o*- and *e*-rays are refracted; they separate and strike the balsam layer. The critical angle at the calcite–balsam interface for the *o*-ray is about 69° (Problem 8.38). The *o*-ray (entering within a narrow cone of roughly 28°) will be totally internally reflected and thereafter absorbed by a layer of black paint on the sides of the rhomb. The *e*-ray emerges laterally displaced but otherwise essentially unscathed, at least in the optical region of the spectrum. (Canada balsam absorbs in the ultraviolet.)

The *Glan–Foucault polarizer* (Fig. 8.27) is constructed of nothing other than calcite, which is transparent from roughly 5000 nm in the infrared to about 230 nm in the ultraviolet. It therefore can be used over a broad spectral range. The incoming ray strikes the surface normally, and $\vec{E}$ can be resolved into components that are either completely parallel or perpendicular to the optic axis. The two rays traverse the first calcite sec-

TABLE 8.1 Refractive Indices of Some Uniaxial Birefringent Crystals (λ_0 = 589.3 nm)

Crystal	n_o	n_e
Tourmaline	1.669	1.638
Calcite	1.6584	1.4864
Quartz	1.5443	1.5534
Sodium nitrate	1.5854	1.3369
Ice	1.309	1.313
Rutile (TiO_2)	2.616	2.903

Giesecke+Devrient GmbH,
Giesecke+Devrient Currency Technology GmbH,
and Papierfabrik Louisenthal GmbH. - Ex. 1027



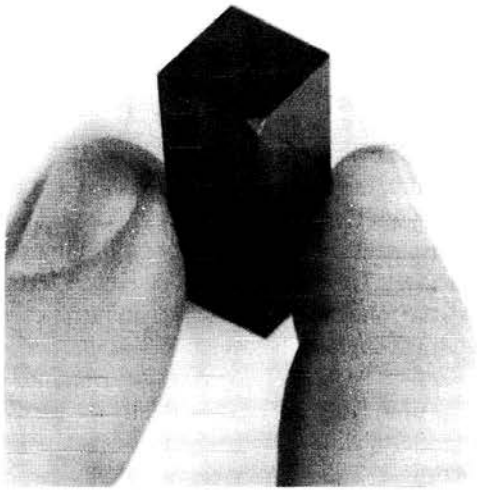


Figure 8.26 The Nicol prism. The little flat on the blunt corner locates the optic axis. (Photo by E.H.)

tion without any deviation. (We'll come back to this point later on when we talk about retarders.) If the angle-of-incidence on the calcite–air interface is θ, one need only arrange things so that $n_e < 1/\sin\theta < n_o$, in order for the o-ray, and not the e-ray, to be totally internally reflected. If the two prisms are now cemented together (glycerine or mineral oil are used in the ultraviolet) and the interface angle is changed appropriately, the device is known as a *Glan–Thompson polarizer*. Its field of view is roughly 30°, in comparison to about 10° for the Glan–Foucault, or *Glan–Air*, as it is often called. The latter, however, has the advantage of being able to handle the considerably higher power levels often encountered with lasers. For example, whereas the maximum irradiance for a Glan–Thompson could be about 1 W/cm^2 (continuous wave as opposed to pulsed), a typical Glan–Air might have an upper limit of 100 W/cm^2 (continuous wave). The difference is due to deterioration of the interface cement (and the absorbing paint, if it's used).

The *Wollaston* prism is a polarizing beamsplitter because it passes both orthogonally polarized components. It can be made of calcite or quartz in the form indicated in Fig. 8.28. The two component rays separate at the diagonal interface. There, the e-ray becomes an o-ray, changing its index accordingly. In calcite $n_e < n_o$, and the emerging o-ray is bent toward the normal. Similarly, the o-ray, whose field is initially perpendicular to the optic axis, becomes an e-ray in the right-hand section. This time, in calcite the e-ray is bent away from the normal to the interface (see Problem 8.39). The deviation angle between the two emerging beams is determined by the prism's wedge angle, θ. Prisms providing deviations ranging from about 15° to roughly 45° are available commercially. They can be purchased cemented (e.g., with castor oil or glycerine) or not cemented at all (i.e., optically contacted), depending on the frequency and power requirements.

8.5 Scattering and Polarization

Sunlight streaming into the atmosphere from one direction is scattered in all directions by the air molecules (see Section 4.2). Without an atmosphere, the daytime sky would be as black as the void of space, a point well made in the Apollo lunar photographs. You would then see only light that shone directly at you. With an atmosphere, the red end of the spectrum is, for the most part, undeviated, whereas the blue or high-frequency end is substantially scattered. This high-frequency scattered light reaches the observer from many directions, making the entire sky appear bright and blue (Fig. 8.29).

The smoke rising from the end of a lighted cigarette is made up of particles that are smaller than the wavelength of light, making it appear blue when seen against a dark background. In contrast, exhaled smoke contains relatively large

Giesecke+Devrient GmbH,
Giesecke+Devrient Currency Technology GmbH,
and Papierfabrik Louisenthal GmbH. - Ex. 1027

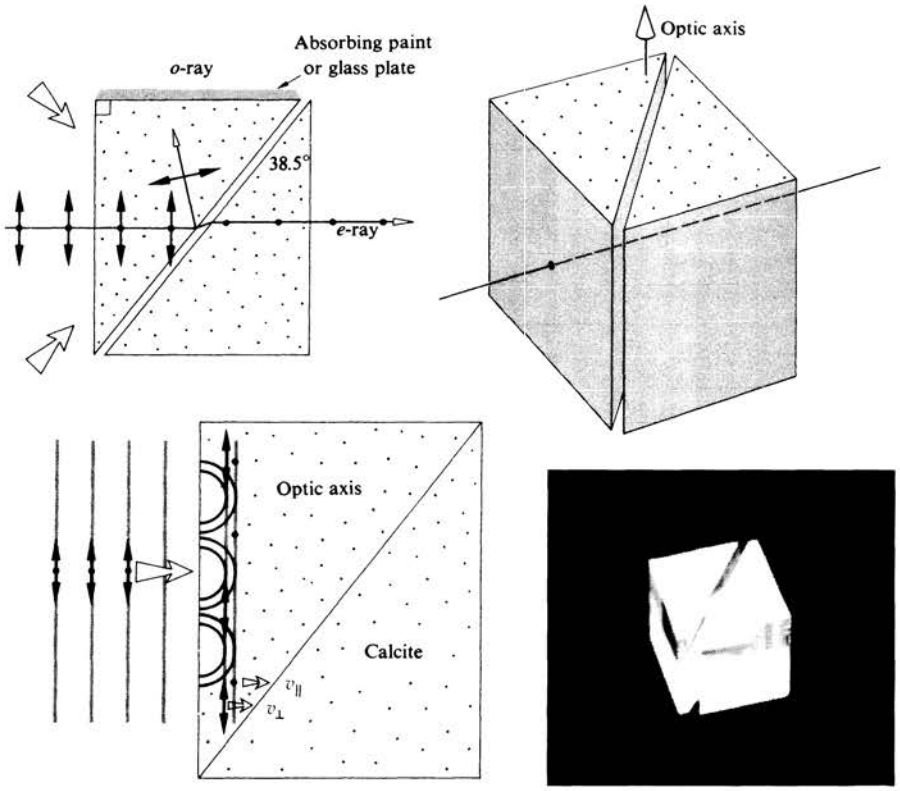


Figure 8.27 The Glan–Foucault prism.
(Photo by E.H.)

water droplets and appears white. Each droplet is larger than the constituent wavelengths of light and thus contains so many oscillators that it is able to sustain the ordinary processes of reflection and refraction. These effects are not preferential to any one frequency component in the incident white light.

The light reflected and refracted several times by a droplet and then finally returned to the observer is therefore also white. This accounts for the whiteness of small grains of salt and sugar, fog, clouds, paper, powders, ground glass, and, more ominously, the typical pallid, polluted city sky.

Particles that are approximately the size of a wavelength (remember that atoms are roughly a fraction of a nanometer across) scatter light in a very distinctive way. A large distribution of such equally sized particles can give rise to a whole range of transmitted colors. In 1883 the volcanic island Krakatoa, located in the Sunda Strait west of Java, blew apart in a fantastic conflagration. Great quantities of fine volcanic dust were spewed high into the atmosphere and drifted over vast regions of the Earth. For a few years afterward the Sun and Moon repeatedly appeared green or blue, and sunrises and sunsets were abnormally colored.

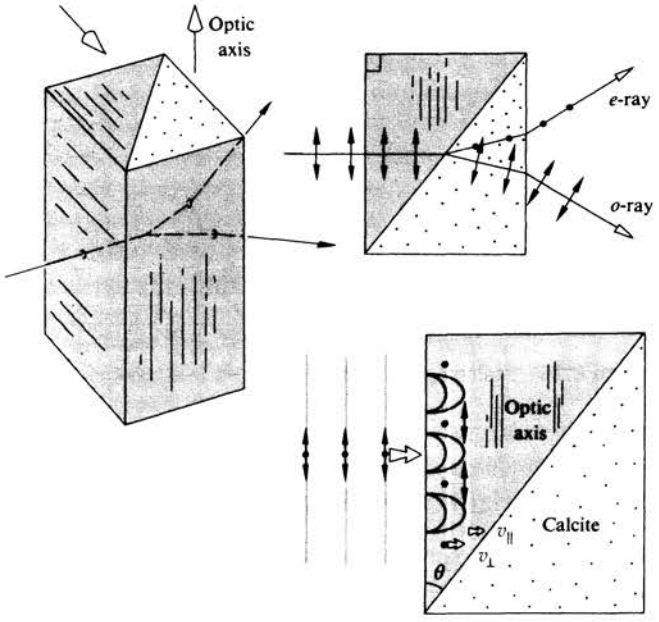


Figure 8.28 The Wollaston prism.

Giesecke+Devrient GmbH,
Giesecke+Devrient Currency Technology GmbH,
and Papierfabrik Louisenthal GmbH. - Ex. 1027



A half-Earth hanging in the black Moon sky. (Photo courtesy of NASA)

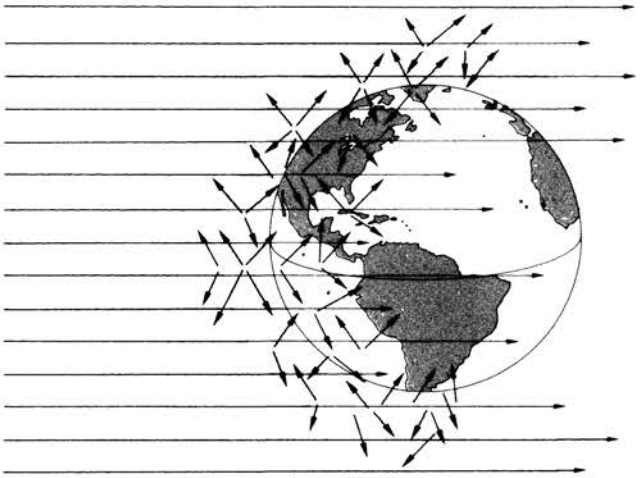


Figure 8.29 Scattering of sky light.

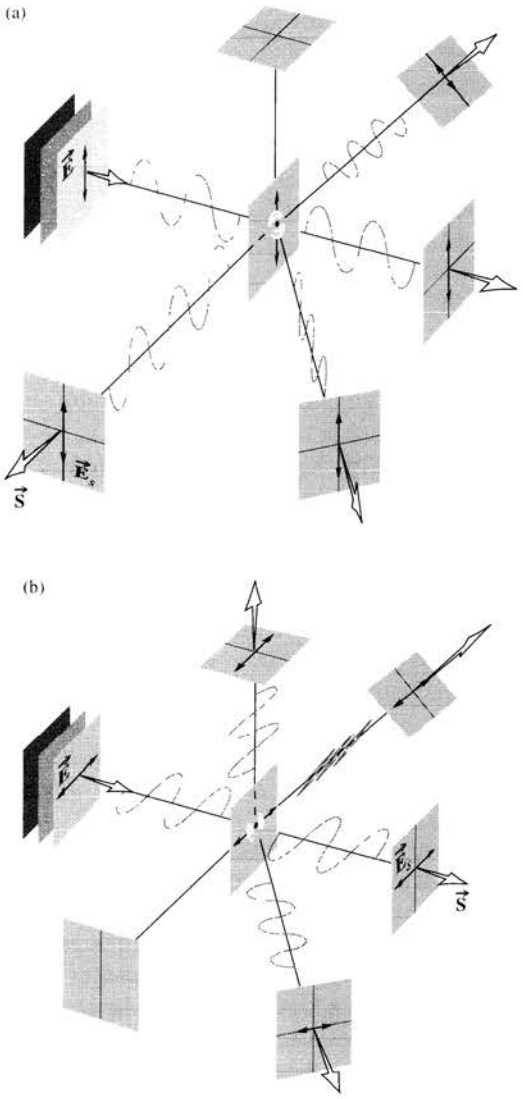


Figure 8.30 Scattering of polarized light by a molecule.

8.5.1 Polarization by Scattering

Imagine a linearly polarized plane wave incident on an air molecule, as pictured in Fig. 8.30. The orientation of the electric field of the scattered radiation (i.e., $\vec{\mathbf{E}}_s$) follows the dipole pattern such that $\vec{\mathbf{E}}_s$, the Poynting vector $\vec{\mathbf{S}}$, and the oscillating dipole are all coplanar (Fig. 3.31). The vibrations induced in the atom are parallel to the $\vec{\mathbf{E}}$-field of the incoming lightwave and so are perpendicular to the propagation direction. Observe once again that the dipole does not radiate in the direction of its axis. Now if the incident wave is unpolarized, it can be represented by two orthogonal, incoherent $\mathscr{P}$-states, in which case

Giesecke+Devrient GmbH,
Giesecke+Devrient Currency Technology GmbH,
and Papierfabrik Louisenthal GmbH. - Ex. 1027

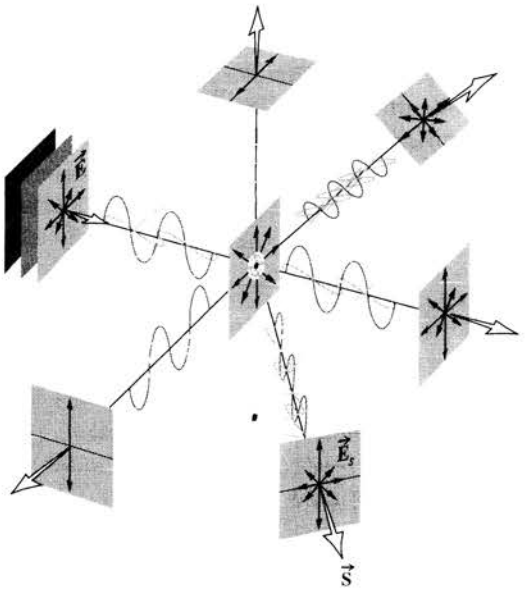
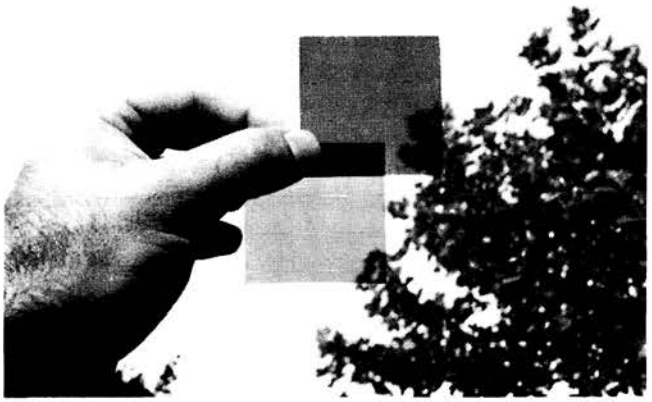


Figure 8.31 Scattering of unpolarized light by a molecule.



A pair of crossed polarizers. The upper polaroid is noticeably darker than the lower one, indicating the partial polarization of sky light. (Photo by E.H.)



A piece of waxed paper between crossed polarizers. (Photo by E.H.)

the scattered light (Fig. 8.31) is equivalent to a superposition of the conditions shown in Fig. 8.30, *a* and *b*. Evidently, the scattered light in the forward direction is completely unpolarized; off that axis it is partially polarized, becoming increasingly more polarized as the angle increases. When the direction of observation is normal to the primary beam, the light is completely linearly polarized.

You can easily verify these conclusions with a piece of Polaroid. Locate the Sun and then examine a region of the sky at roughly 90° to the solar rays. That portion of the sky will be partially polarized normal to the rays (see photo). It's not completely polarized mainly because of molecular anisotropies, the presence of large particles in the air, and the depolarizing effects of multiple scattering. The latter condition can be illustrated by placing a piece of waxed paper between crossed Polaroids (see photo). Because the light undergoes a good deal of scattering and multiple reflections within the waxed paper, a given oscillator may "see" the superposition of many essentially unrelated $\vec{E}$-fields. The resulting emission is almost completely depolarized.

As a final experiment, put a few drops of milk in a glass of water and illuminate it (perpendicular to its axis) using a bright flashlight. The solution will appear bluish white in scattered light and orange in direct light, indicating that the operative mechanism is Rayleigh Scattering. The scattered light will also be partially polarized.

Using very much the same ideas, Charles Glover Barkla (1877–1944) in 1906 established the transverse wave nature of X-ray radiation by showing that it could be polarized in certain directions as a result of scattering off matter.

Giesecke+Devrient GmbH,
Giesecke+Devrient Currency Technology GmbH,
and Papierfabrik Louisenthal GmbH. - Ex. 1027

8.6 Polarization by Reflection

One of the most common sources of polarized light is the ubiquitous process of reflection from dielectric media. The glare spread across a window pane, a sheet of paper, or a balding head, the sheen on the surface of a telephone, a billiard ball, or a book jacket are all generally partially polarized.

The effect was first studied by Étienne Malus in 1808. The Paris Academy had offered a prize for a mathematical theory of double refraction, and Malus undertook a study of the problem. He was standing at the window of his house in the Rue d'Enfer one evening, examining a calcite crystal. The Sun was setting, and its image reflected toward him from the windows of the Luxembourg Palace not far away. He held up the crystal and looked through it at the Sun's reflection. To his astonishment, he saw one of the double images disappear as he rotated the calcite. After the Sun had set, he continued to verify his observations into the night, using candlelight reflected from the surfaces of water and glass.* The significance of birefringence and the actual nature of polarized light were first becoming clear. At that time no satisfactory explanation of polarization existed within the context of the wave theory. During the next 13 years the work of many people, principally Thomas Young and Augustin Fresnel, finally led to the representation of light as some sort of transverse vibration. (Keep in mind that all this predates the electromagnetic theory of light by roughly 40 years.)

The electron-oscillator model provides a remarkably simple picture of what happens when light is polarized on reflection. Unfortunately, it's not a complete description, since it does not account for the behavior of magnetic nonconducting materials.† Nonetheless, consider an incoming plane wave linearly polarized so that its $\vec{\mathbf{E}}$-field is perpendicular to the plane of incidence (Fig. 8.32). The wave is refracted at the interface, entering the medium at some transmission angle θ_t. Its electric field drives the bound electrons, in this case normal to the plane-of-incidence, and they in turn reradiate. A portion of that reemitted energy appears in the form of a reflected wave. It should be clear then from the geometry and the dipole radiation pattern that both the reflected and refracted waves must also be in $\mathcal{P}$-states normal to the incident plane.* In contradistinction, if the incoming $\vec{\mathbf{E}}$-field is in the incident plane, the electron-oscillators near the surface will vibrate under the influence of the refracted wave, as shown in Fig. 8.32*b*. Observe that a rather interesting thing is happening to the reflected wave. Its flux density is now relatively low because the reflected ray direction makes a small angle θ with the dipole axis. If we could arrange things so that $\theta = 0$, or equivalently $\theta_r + \theta_t = 90°$, the reflected wave would vanish entirely. *Under those circumstances, for an incoming unpolarized wave made up of two incoherent orthogonal $\mathcal{P}$-states, only the component polarized normal to the incident plane and therefore parallel to the surface will be reflected.* The particular angle-of-incidence for which this situation occurs is designated by θ_p and referred to as the **polarization angle** or **Brewster's angle**, whereupon $\theta_p + \theta_t = 90°$. Hence, from Snell's Law

$$n_i \sin \theta_p = n_t \sin \theta_t$$

and the fact that $\theta_t = 90° - \theta_p$, it follows that

$$n_i \sin \theta_p = n_t \cos \theta_p$$

and

$$\tan \theta_p = n_t/n_i \tag{8.25}$$

This is known as **Brewster's Law** after the man who discovered it empirically, Sir David Brewster (1781–1868), professor of physics at St. Andrews University and, of course, inventor of the kaleidoscope.

When the incident beam is in air $n_i = 1$, and if the transmitting medium is glass, in which case $n_t \approx 1.5$, the polarization angle is $\approx 56°$. Similarly, if an unpolarized beam strikes the surface of a pond ($n_t \approx 1.33$ for H_2O) at an angle of 53°, the reflected beam will be completely polarized with its $\vec{\mathbf{E}}$-field perpendicular to the plane-of-incidence or, if you like, parallel to the water's surface (see photo on page 350). This suggests a rather handy way to locate the transmission axis of an unmarked polarizer; one just needs a piece of glass or a pond.

*Try it with a candle flame and a piece of glass. Hold the glass at $\theta_p \approx 56°$ for the most pronounced effect. At near glancing incidence both of the images will be bright, and neither will vanish as you rotate the crystal—Malus apparently lucked out at a good angle to the palace window.

† W. T. Doyle, "Scattering Approach to Fresnel's Equations and Brewster's Law," *Am. J. Phys.* **53**, 463 (1985).

*The angle of reflection is determined by the scattering array, as discussed in Section 10.2.7. The scattered wavelets in general combine constructively in only one direction, yielding a reflected ray at an angle equal to that of the incident ray.

Giesecke+Devrient GmbH,
Giesecke+Devrient Currency Technology GmbH,
and Papierfabrik Louisenthal GmbH. - Ex. 1027

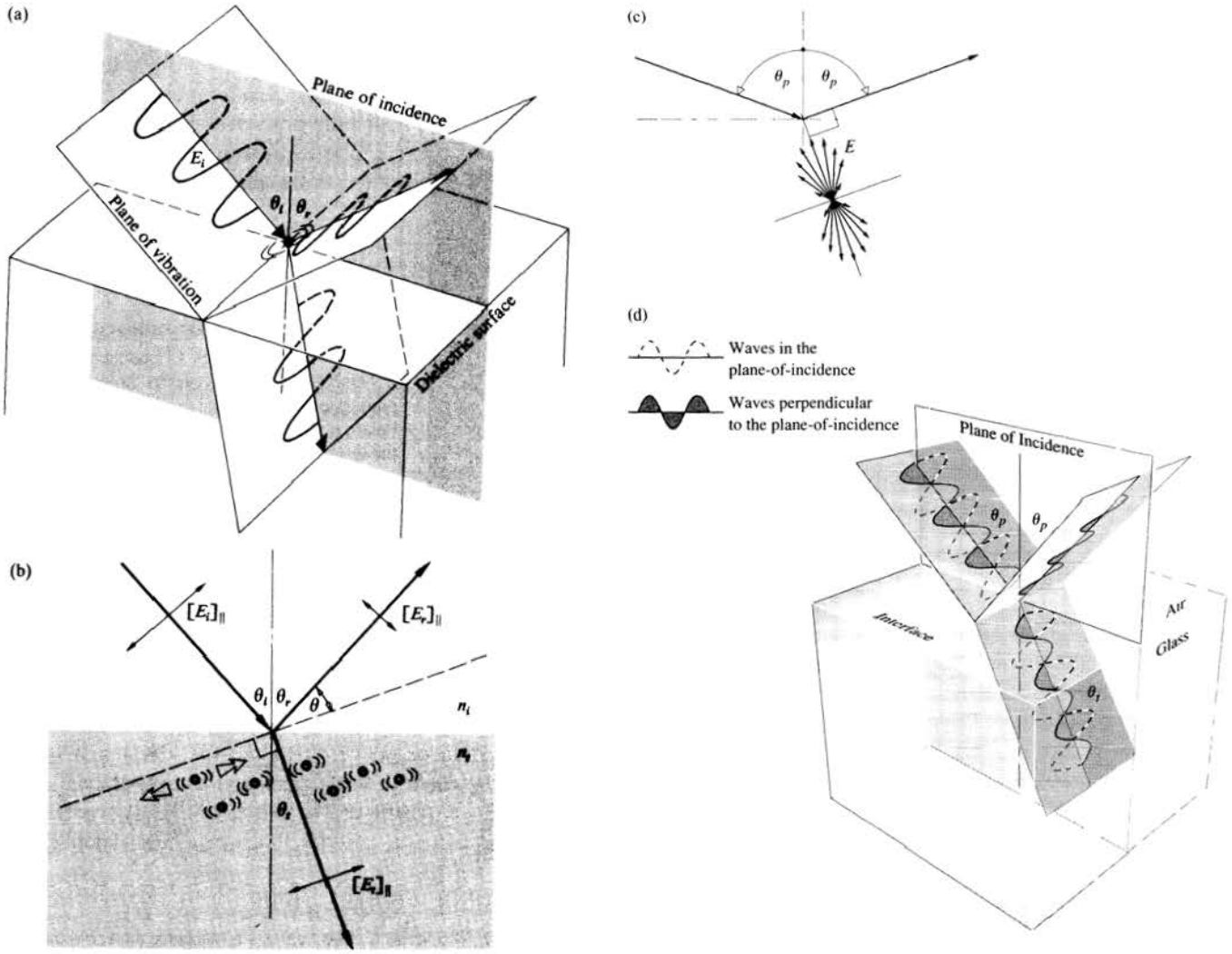
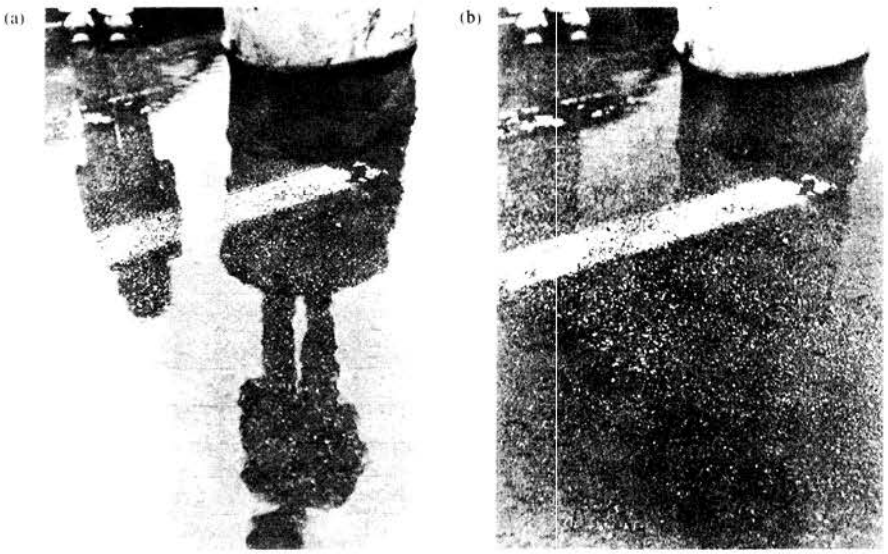


Figure 8.32 (*a*) A wave reflecting and refracting at an interface. (*b*) Electron-oscillators and Brewster's Law. (*c*) The dipole radiation pattern. (*d*) The polarization of light that occurs on reflection from a dielectric, such as glass, water, or plastic. At θ_p, the reflected beam is a $\mathcal{P}$-state perpendicular to the plane-of-incidence. The transmitted beam is strong in $\mathcal{P}$-state light parallel to the plane-of-incidence and weak in $\mathcal{P}$-state light perpendicular to the plane-of-incidence—it's partially polarized.

The problem immediately encountered in utilizing this phenomenon to construct an effective polarizer lies in the fact that the reflected beam, although completely polarized, is weak, and the transmitted beam, although strong, is only partially polarized. One scheme, illustrated in Fig. 8.33, is often referred to as a ***pile-of-plates polarizer***. It was invented by Dominique F. J. Arago in 1812. Devices of this kind can be fabricated with glass plates in the visible, silver chloride plates in the infrared, and quartz or vycor in the ultraviolet. It's an easy matter to construct a crude arrangement of this sort with a dozen or so microscope slides. (The beautiful colors that may appear when the slides are in contact are discussed in the next chapter.)

The beamsplitter cube uses the same idea to create two

Giesecke+Devrient GmbH,
Giesecke+Devrient Currency Technology GmbH,
and Papierfabrik Louisenthal GmbH. - Ex. 1027



Light reflecting off a puddle is partially polarized. (*a*) When viewed through a Polaroid filter whose transmission axis is parallel to the ground, the glare is passed and visible. (*b*) When the Polaroid's transmission axis is perpendicular to the water's surface, most of the glare vanishes. (Photo courtesy Martin Seymour.)

orthogonal linearly polarized beams that are conveniently separated by 90° (Fig. 8.34). The diagonal face of one of the two prisms is coated with multiple layers of different transparent dielectric films. Because there's little or no absorption, the device is well suited for laserbeam applications where you would want a high damage threshold and low transmitted wavefront distortion.

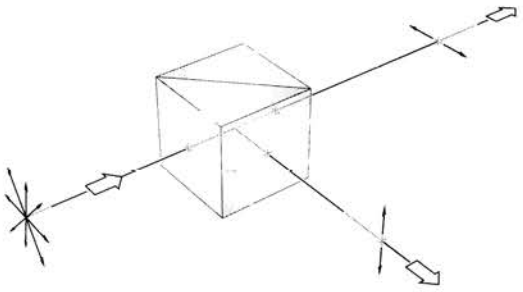


Figure 8.34 A polarizing cube contains a mutilayer dielectric thin film structure on its diagonal face. Reflection from that structure polarizes the incident light, much as would a pile-of-plates.

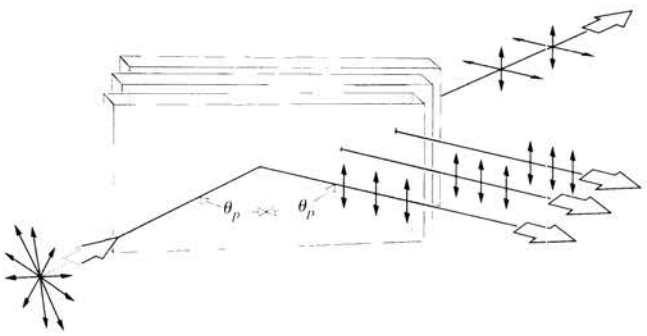


Figure 8.33 The pile-of-plates polarizer.

8.6.1 An Application of the Fresnel Equations

In Section 4.6.2 we obtained a set of formulas known as the Fresnel Equations, which describe the effects of an incoming electromagnetic plane wave falling on the interface between two different dielectric media. These equations relate the reflected and transmitted field amplitudes to the incident amplitude by way of the angles-of-incidence θ_i and transmission θ_t. For linear light having its $\vec{\mathbf{E}}$-field parallel to the plane-

Giesecke+Devrient GmbH,
Giesecke+Devrient Currency Technology GmbH,
and Papierfabrik Louisenthal GmbH. - Ex. 1027

of-incidence, we defined the *amplitude reflection coefficient* as $r_\parallel \equiv [E_{0r}/E_{0i}]_\parallel$, that is, the ratio of the reflected to incident electric-field *amplitudes*. Similarly, when the electric field is normal to the incident plane, we have $r_\perp \equiv [E_{0r}/E_{0t}]_\perp$. The corresponding irradiance ratio (the incident and reflected beams have the same cross-sectional area) is known as the *reflectance*, and since irradiance is proportional to the square of the amplitude of the field,

$$R_\parallel = r_\parallel^2 = [E_{0r}/E_{0i}]_\parallel^2 \quad \text{and} \quad R_\perp = r_\perp^2 = [E_{0r}/E_{0t}]_\perp^2$$

Squaring the appropriate Fresnel Equations yields

$$R_\parallel = \frac{\tan^2(\theta_i - \theta_t)}{\tan^2(\theta_i + \theta_t)} \tag{8.26}$$

and

$$R_\perp = \frac{\sin^2(\theta_i - \theta_t)}{\sin^2(\theta_i + \theta_t)} \tag{8.27}$$

Whereas $R_\perp$ can never be zero, $R_\parallel$ is indeed zero when the denominator is infinite, that is, when $\theta_i + \theta_t = 90°$. The reflectance, for linear light with $\vec{\mathbf{E}}$ parallel to the plane-of-incidence, thereupon vanishes; $E_{r\parallel} = 0$ and the beam is completely transmitted. This is the essence of Brewster's Law.

If the incoming light is unpolarized, we can represent it by two now familiar orthogonal, incoherent, equal-amplitude $\mathscr{P}$-states. Incidentally, the fact that they are equal in amplitude means that the amount of energy in one of these two polarization states is the same as that in the other (i.e., $I_{i\parallel} = I_{i\perp} = I_i/2$), which is quite reasonable. Thus

$$I_{r\parallel} = I_{r\parallel} I_i / 2 I_{i\parallel} = R_\parallel I_i / 2$$

and in the same way $I_{r\perp} = R_\perp I_i/2$. The reflectance in natural light, $R = I_r/I_i$, is therefore given by

$$R = \frac{I_{r\parallel} + I_{r\perp}}{I_i} = \tfrac{1}{2}(R_\parallel + R_\perp) \tag{8.28}$$

Figure 8.35 is a plot of Eqs. (8.26), (8.27), and (8.28) for the particular case when $n_i = 1$ and $n_t = 1.5$. The middle curve, which corresponds to incident natural light, shows that only about 7.5% of the incoming light is reflected when $\theta_i = \theta_p$. The transmitted light is then evidently partially polarized. When $\theta_i \neq \theta_p$ both the transmitted and reflected waves are partially polarized.

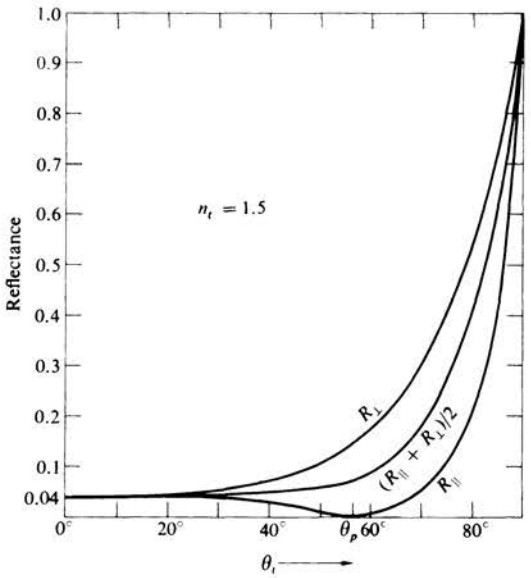


Figure 8.35 Reflectance versus incident angle.

It is often desirable to make use of the concept of the **degree of polarization** V, defined as

$$V = \frac{I_p}{I_p + I_n} \tag{8.29}$$

in which I_p and I_n are the constituent flux densities of polarized and "unpolarized" or natural light. For example, if $I_p = 4$ W/m^2 and $I_n = 6$ W/m^2, then $V = 40\%$ and the beam is partially polarized. With "unpolarized" light $I_p = 0$ and obviously $V = 0$, whereas at the opposite extreme, if $I_n = 0$, $V = 1$ and the light is completely polarized; thus $0 \leq V \leq 1$. One frequently deals with partially polarized, linear, quasimonochromatic light. In that case, if we rotate an analyzer in the beam, there will be an orientation at which the transmitted irradiance is maximum ($I_{\max}$), and perpendicular to this, a direction where it is minimum ($I_{\min}$). Clearly $I_p = I_{\max} - I_{\min}$, and so

$$V = \frac{I_{\max} - I_{\min}}{I_{\max} + I_{\min}} \tag{8.30}$$

Note that V is actually a property of the beam, which may be partially or even completely polarized before encountering any sort of polarizer.

Giesecke+Devrient GmbH,
Giesecke+Devrient Currency Technology GmbH,
and Papierfabrik Louisenthal GmbH. - Ex. 1027

8.7 Retarders

We now consider a class of optical elements known as **retarders**, which serve to change the polarization of an incident wave. In principle, the operation of a retarder is quite simple. One of the two constituent coherent $\mathcal{P}$-states is somehow caused to have its phase lag behind that of the other by a predetermined amount. Upon emerging from the retarder, the relative phase of the two components is different than it was initially, and thus the polarization state is different as well. Once we have developed the concept of the retarder, it will be possible to convert any given polarization state into any other and in so doing create circular and elliptic polarizers as well.

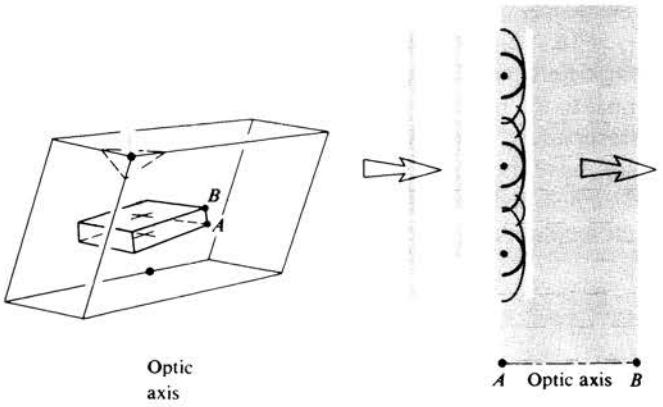


Figure 8.36 A calcite plate cut perpendicular to the optic axis.

8.7.1 Wave Plates and Rhombs

Recall that a plane monochromatic wave incident on a uniaxial crystal, such as calcite, is generally divided in two, emerging as an ordinary and an extraordinary beam. In contrast, we can cut and polish a calcite crystal so that its optic axis will be normal to both the front and back surfaces (Fig. 8.36). A normally incident plane wave can only have its $\vec{\mathbf{E}}$-field perpendicular to the optic axis. The secondary spherical and ellipsoidal wavelets will be tangent to each other in the direction of the optic axis. The *o*- and *e*-waves, which are envelopes of these wavelets, will be coincident, and a single undeflected plane wave will pass through the crystal; there are no relative phase shifts and no double images.*

Now suppose that the direction of the optic axis is arranged to be parallel to the front and back surfaces, as shown in Fig. 8.37. If the $\vec{\mathbf{E}}$-field of an incident monochromatic plane wave has components parallel and perpendicular to the optic axis, two separate plane waves will propagate through the crystal. Since $v_{\parallel} > v_{\perp}$, $n_o > n_e$, and the *e*-wave will move across the specimen more rapidly than the *o*-wave. After traversing a plate of thickness d, the resultant electromagnetic wave is the superposition of the *e*- and *o*-waves, which now have a relative phase difference of $\Delta\varphi$. Keep in mind that these are harmonic waves of the same frequency whose $\vec{\mathbf{E}}$-fields are orthogonal.

*If you have a calcite rhomb, find the blunt corner and orient the crystal until you are looking along the direction of the optic axis through one of the faces. The two images will converge until they completely overlap.

The relative optical path length difference is given by

$$\Lambda = d(|n_o - n_e|) \tag{8.31}$$

and since $\Delta\varphi = k_0\Lambda$, the phase difference, in radians, is

$$\Delta\varphi = \frac{2\pi}{\lambda_0} d(|n_o - n_e|) \tag{8.32}$$

where λ_0, as always, is the wavelength in vacuum. (The form containing the absolute value of the index difference is the most general statement.) The state of polarization of the emergent light evidently depends on the amplitudes of the incoming orthogonal field components and of course on $\Delta\varphi$.

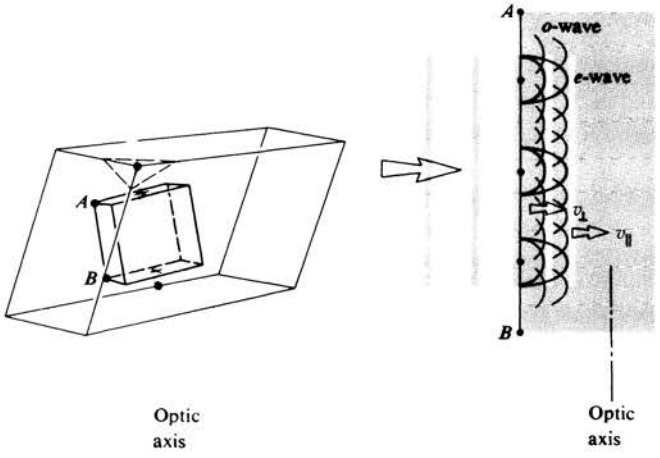


Figure 8.37 A calcite plate cut parallel to the optic axis.

Giesecke+Devrient GmbH,
Giesecke+Devrient Currency Technology GmbH,
and Papierfabrik Louisenthal GmbH. - Ex. 1027

The Full-Wave Plate

If $\Delta\varphi$ is equal to 2π, the ***relative retardation*** is one wavelength; the *e*- and *o*-waves are back in-phase, and there is no observable effect on the polarization of the incident monochromatic beam. When the *relative retardation* $\Delta\varphi$, which is also known as the **retardance**, is 360° the device is called a **full-wave plate** or **full-wave retarder**. (This does not mean that $d = \lambda$.) In general, the quantity $|n_o - n_e|$ in Eq. (8.32) changes little over the optical range, so that $\Delta\varphi$ varies effectively as $1/\lambda_0$. Evidently, a full-wave plate can function only in the manner discussed for a particular wavelength, and retarders of this sort are thus said to be *chromatic*. If such a device is placed at some arbitrary orientation between crossed linear polarizers, all the light entering it (in this case let it be white light) will be linear. Only the one wavelength that satisfies Eq. (8.32) will pass through the retarder unaffected, thereafter to be absorbed in the analyzer. All other wavelengths will undergo some retardance and will accordingly emerge from the wave plate as various forms of elliptical light. Some portion of this light will proceed through the analyzer, finally emerging as the complementary color to that which was extinguished. It is a common error to assume that a full-wave plate behaves as if it were isotropic at all frequencies; it obviously doesn't.

Recall that in calcite, the wave whose $\vec{\mathbf{E}}$-field vibrations are parallel to the optic axis travels fastest, that is, $v_\parallel > v_\perp$. The direction of the optic axis in a *negative* uniaxial retarder is therefore often referred to as the **fast axis**, and the direction perpendicular to it is the **slow axis**. For *positive* uniaxial crystals, such as quartz, these principal axes are reversed, with the slow axis corresponding to the optic axis.

The full-wave retarder is often used to eliminate inadvertent changes in the polarization state of light passing through an optical system. For example, linear light reflected from a metal-surfaced mirror will have phase shifts introduced that cause it to emerge as elliptical light. This can be corrected by passing the beam through a full-wave plate that has been tilted slightly about either its fast or slow axis.

The Half-Wave Plate

A retardation plate that introduces a relative phase difference of π radians or 180° between the *o*- and *e*-waves is known as a **half-wave plate** or **half-wave retarded**. Suppose that the plane-of-vibration of an incoming beam of linear light makes some arbitrary angle θ with the fast axis, as shown in Fig. 8.38. In a negative material the *e*-wave will have a higher speed (same ν) and a longer wavelength than the *o*-wave. When the waves emerge from the plate, there will be a relative phase shift of $\lambda_0/2$ (that is, $2\pi/2$ radians), with the effect that $\vec{\mathbf{E}}$ will have rotated through 2θ (Fig. 8.39). In fact, half-wave retarders are sometimes called polarization rotators for just that reason. Going back to Fig. 8.7, it should be evident that a half-wave plate will similarly flip elliptical light. In addition, it will invert the handedness of circular or elliptical light, changing right to left and vice versa.

As the *e*- and *o*-waves progress through any retardation plate, their relative phase difference $\Delta\varphi$ increases, and the state of polarization of the wave therefore gradually changes from one point in the plate to the next. Figure 8.7 can be envisioned as a sampling of a few of these states at one instant in time taken at different locations. Evidently, if the thickness of

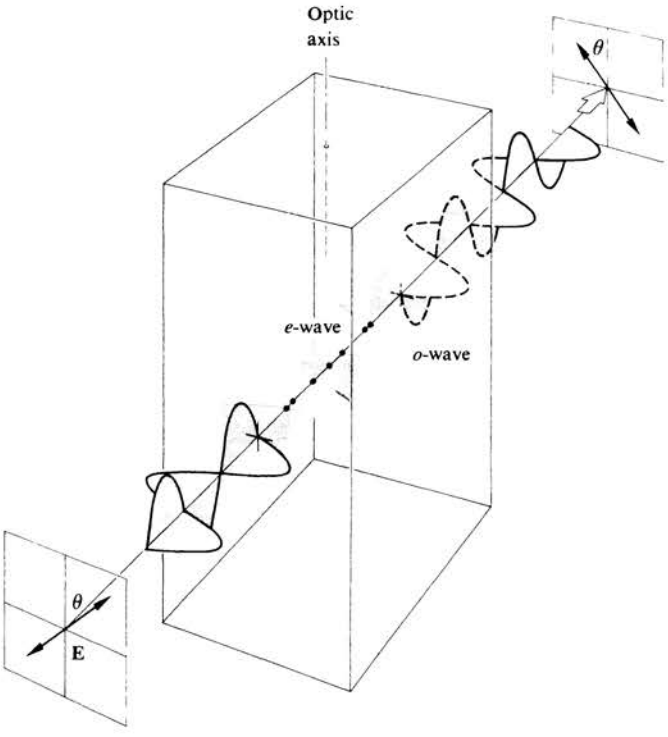


Figure 8.38 A half-wave plate showing how a net phase shift accumulates with the retarder.

Giesecke+Devrient GmbH,
Giesecke+Devrient Currency Technology GmbH,
and Papierfabrik Louisenthal GmbH. - Ex. 1027

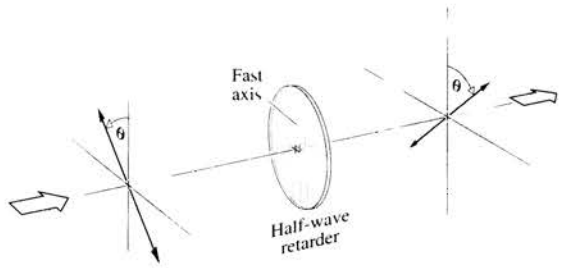


Figure 8.39 A half-wave plate rotates light initially linearly polarized at an angle θ through a total angle of 2θ. Here light was incident oscillating in the first and third quadrants, and it emerged oscillating in the second and fourth quadrants.

the material is such that

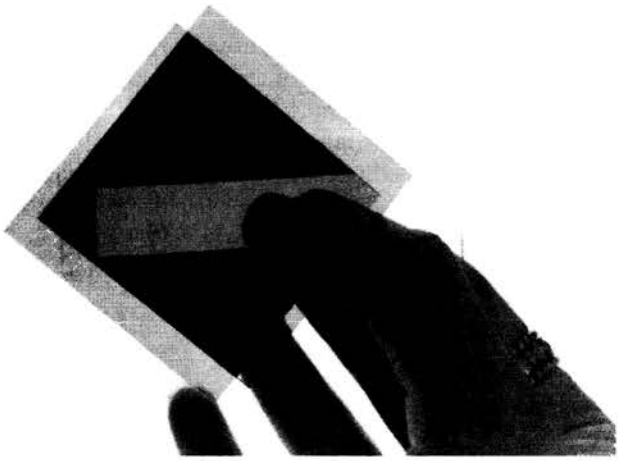
$$d(|n_o - n_e|) = (2m + 1)\lambda_0/2$$

where $m = 0, 1, 2, \ldots$, it will function as a half-wave plate ($\Delta\varphi = \pi, 3\pi, 5\pi$, etc.).

Although its behavior is simple to visualize, calcite is not often used to make retardation plates. It is brittle and difficult to handle in thin slices, but more than that, its birefringence, the difference between n_e and n_o, is a bit too large for convenience. On the other hand, quartz with its much smaller birefringence is frequently used, but it has no natural cleavage planes and must be cut, ground, and polished, making it rather expensive. The biaxial crystal mica is used most often. Several forms of mica serve the purpose admirably, for example, fluorophlogopite, biotite, or muscovite. The most commonly occurring variety is the pale brown muscovite. It is very easily cleaved into strong, flexible, and exceedingly thin large-area sections. Moreover, its two principal axes are almost exactly parallel to the cleavage planes. Along those axes the indices are about 1.599 and 1.594 for sodium light, and although these numbers vary slightly from one sample to the next, their difference is fairly constant. The minimum thickness of a mica half-wave plate is about 60 microns. Crystalline quartz, single crystal magnesium fluoride (for the IR range from 3000 nm to about 6000 nm), and cadmium sulfide (for the IR range from 6000 nm to about 12,000 nm) are also widely used for wave plates.

Retarders are also made from sheets of polyvinyl alcohol that have been stretched so as to align their long-chain organic molecules. Because of the evident anisotropy, electrons in the material do not experience the same binding forces along and perpendicular to the direction of these molecules. Substances of this sort are therefore permanently birefringent, even though they are not crystalline.

A rather nice half-wave plate can be made by just attaching a strip of old-fashioned glossy cellophane tape over the surface of a microscope slide. (Not all varieties work—the best is LePage's "Transparent Tape.") The fast axis, that is, the vibration direction of the faster of the two waves, corresponds to the transverse direction across the tape's width, and the slow axis is along its length. During its manufacture, cellophane (which is made from regenerated cellulose extracted from cotton or wood pulp) is formed into sheets, and in the process its molecules become aligned, leaving it birefringent. If you put your half-wave plate between crossed linear polarizers, it will show no effect when its principal axes coincide with those of the polarizers. If, however, it is set at 45° with respect to the polarizer, the $\vec{\mathbf{E}}$-field emerging from the tape will be flipped 90° and will be parallel to the transmission axis of the analyzer. Light will pass through the region covered by the tape as if it were a hole cut in the black background of the crossed polarizers (see photo). A piece of cellophane wrapping will generally also function as a half-wave plate. See if you can determine the orientation of each of its principal axes using the tape retarder and crossed Polaroids. (Notice the fine parallel ridges on the sheet cellophane.)



A hand holding a piece of Scotch tape stuck to a microscope slide between two crossed polaroids. (Photo by E.H.)

Giesecke+Devrient GmbH,
Giesecke+Devrient Currency Technology GmbH,
and Papierfabrik Louisenthal GmbH. - Ex. 1027

The Quarter-Wave Plate

The **quarter-wave plate** is an optical element that introduces a relative phase shift of $\Delta\varphi = \pi/2$ between the constituent orthogonal *o*- and *e*-components of a wave. It follows once again from Fig. 8.7 that a phase shift of 90° will convert linear to elliptical light (or circular light) and vice versa. It should be apparent that linear light incident parallel to either principal axis will be unaffected by any sort of retardation plate. You can't have a *relative* phase difference without having two components. With incident *natural* light, the two constituent $\mathcal{P}$-states are incoherent; that is, their relative phase difference changes randomly and rapidly. The introduction of an additional constant phase shift by any form of retarder will still result in a random phase difference and thus have no noticeable effect. When linear light at 45° to either principal axis is incident on a quarter-wave plate, its *o*- and *e*-components have equal amplitudes. Under these special circumstances, a 90° phase shift converts the wave into circular light (Fig. 8.40). Similarly, an incoming circular beam will emerge linearly polarized.

Quarter-wave plates are also usually made of quartz, mica, or organic polymeric plastic. In any case, the thickness of the birefringent material must satisfy the expression

$$d(|n_o - n_e|) = (4m + 1)\lambda_0/4$$

You can make a crude quarter-wave plate using household plastic food wrap, the thin stretchy stuff that comes on rolls. Like cellophane, it has ridges running in the long direction, which coincides with a principal axis. Overlap about a half dozen layers, being careful to keep the ridges parallel. Position the plastic at 45° to the axes of a polarizer and examine it through a rotating analyzer. Keep adding one layer at a time until the irradiance stays roughly constant as the analyzer turns; at that point you will have circular light and a quarter-wave plate. This is easier said than done in white light, but it's well worth trying.

Commercial wave plates are generally designated by their ***linear retardation***, which might be, for example, 140 nm for a quarter-wave plate. This simply means that the device has a 90° retardance only for green light of wavelength 560 nm (i.e., 4×140). The linear retardation is usually not given quite that precisely; 140 ± 20 nm is more realistic. The retardation of a wave plate can be increased or decreased from its specified value by tilting it somewhat. If the plate is rotated about its fast axis, the retardation will increase, whereas a rotation about the slow axis has the opposite effect. In this way a wave plate can be tuned to a specific frequency in a region about its nominal value.

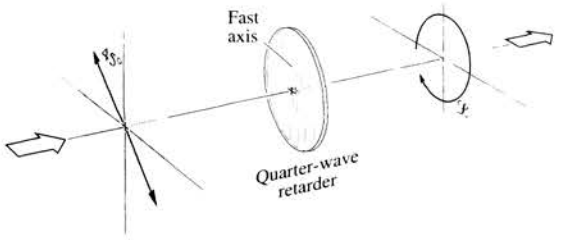


Figure 8.40 A quarter-wave plate transforms light initially linearly polarized at an angle 45° (oscillating in the first and third quadrants) into left circular light (rotating counterclockwise looking toward the source).

Retarders (Wave Plates)—Some General Considerations

A retarder can be one of three general types: zero-order, multiple-order, or compound zero-order. A **zero-order retarder** has the minimum thickness necessary to produce the required phase difference. For example, consider a quartz quarter-wave plate with a birefringence of only 0.009 2 at 550 nm. Equation (8.32) with $\Delta\varphi = \pi/2$ tells us that a zero-order quarter-wave retarder will be only 15 μm thick, and therefore will be rather fragile and difficult to fabricate. It does, however, have a large angular field-of-view.

A **multiple-order retarder** would have a thickness that corresponded to a whole number of 2π phase shifts plus the desired $\Delta\varphi$, whether that's 2π, π, or $\pi/2$. These devices are easier to make and less expensive, but they tend to be very sensitive to wavelength, incident angle, and temperature, and have a narrow field-of-view.

By combining two multiple-order retarders whose retardance difference yields the desired value of $\Delta\varphi$, we arrive at the **compound zero-order** wave plate. That's accomplished by aligning the fast axis of one with the slow axis of the other. This compensates for temperature variations that tend to cancel, but it, too, has a narrow field-of-view.

Birefringent polymers have a small birefringence and so can conveniently be made into zero-order retarders. They have a wide field-of-view and can be made with large apertures.

Giesecke+Devrient GmbH,
Giesecke+Devrient Currency Technology GmbH,
and Papierfabrik Louisenthal GmbH. - Ex. 1027

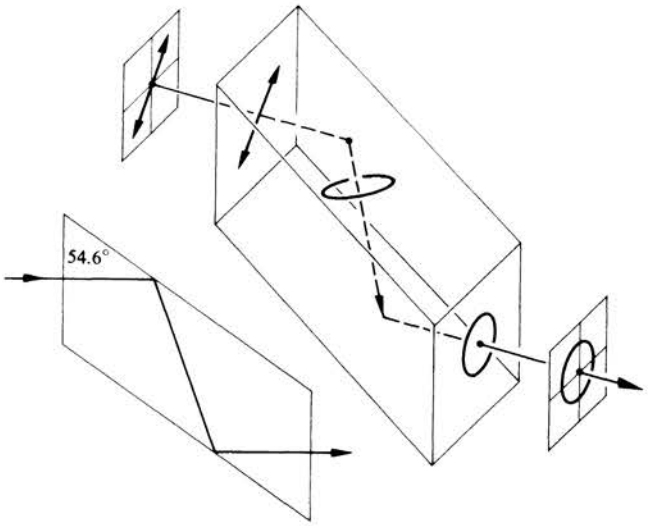


Figure 8.41 The Fresnel rhomb.

The Fresnel Rhomb

We saw in Chapter 4 that the process of total internal reflection introduced a relative phase difference between the two orthogonal field components. The components parallel and perpendicular to the plane-of-incidence were shifted in phase with respect to each other. In glass ($n = 1.51$) a shift of 45° accompanies internal reflection at the particular incident angle of 54.6° (Fig. 4.44*e*). The Fresnel rhomb shown in Fig. 8.41 utilizes this effect by causing the beam to be internally reflected twice, thereby imparting a 90° relative phase shift to its components. If the incoming plane wave is linearly polarized at 45° to the plane-of-incidence, the field components $[E_i]_\parallel$ and $[E_i]_\perp$ will initially be equal. After the first reflection, the wave within the glass will be elliptically polarized. After the second reflection, it will be circular. Since the retardance is almost independent of frequency over a large range, the rhomb is essentially an *achromatic* 90° retarder. By combining two rhombs end-to-end, we can produce $\lambda_0/2$ retardation over a broad wavelength band (≈2000 nm). The Mooney rhomb ($n = 1.65$) shown in Fig. 8.42 is similar in principle, although its operating characteristics are different in some respects.

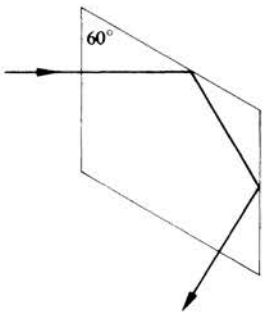


Figure 8.42 The Mooney rhomb.

8.7.2 Compensators and Variable Retarders

A **compensator** *is an optical device that is capable of impressing a controllable retardance on a wave.* Unlike a wave plate where $\Delta\varphi$ is fixed, the relative phase difference arising from a compensator can be varied continuously. Of the many different kinds of compensators, we shall consider only two of those that are used most widely. The **Babinet compensator**, depicted in Fig. 8.43, consists of two independent calcite, or more commonly quartz, wedges whose optic axes are indicated by the lines and dots in the figure. A ray passing vertically downward through the device at some arbitrary point will traverse a thickness of d_1 in the upper wedge and d_2 in the lower one. The relative phase difference imparted to the wave by the first crystal is $2\pi d_1(|n_o - n_e|)/\lambda_0$, and that of the second crystal is $-2\pi d_2(|n_o - n_e|)/\lambda_0$. As in the Wollaston prism, which this system closely resembles but which has larger angles and is much thicker, the *o*- and *e*-rays in the upper wedge become the *e*- and *o*-rays, respectively, in the bottom wedge.

The compensator is thin (the wedge angle is typically about 2.5°), and thus the separation of the rays is negligible. The

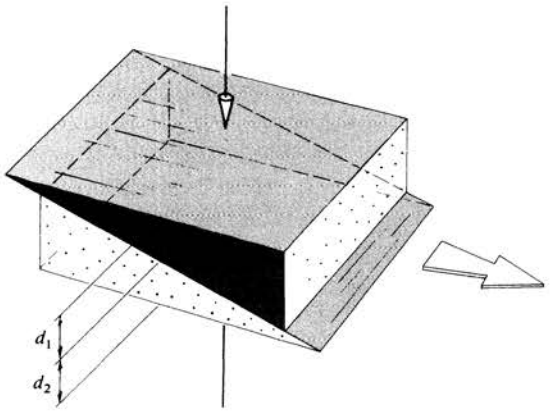


Figure 8.43 The Babinet compensator.

Giesecke+Devrient GmbH,
Giesecke+Devrient Currency Technology GmbH,
and Papierfabrik Louisenthal GmbH. - Ex. 1027

total phase difference, or retardance, is then

$$\Delta\varphi = \frac{2\pi}{\lambda_0}(d_1 - d_2)(|n_o - n_e|) \tag{8.33}$$

If the compensator is made of calcite, the e-wave leads the o-wave in the upper wedge, and therefore if $d_1 > d_2$, $\Delta\varphi$ corresponds to the total angle by which the e-component leads the o-component. The converse is true for a quartz compensator; in other words, if $d_1 > d_2$, $\Delta\varphi$ is the angle by which the o-wave leads the e-wave. At the center, where $d_1 = d_2$, the effect of one wedge is exactly canceled by the other, and $\Delta\varphi = 0$ for all wavelengths. The retardation will vary from point to point over the surface, being constant in narrow regions running the width of the compensator along which the wedge thicknesses are themselves constant. If light enters by way of a slit parallel to one of these regions and if we then move either wedge horizontally with a micrometer screw, we can get any desired $\Delta\varphi$ to emerge.

When the Babinet is positioned at 45° between crossed polarizers, a series of parallel, equally spaced, dark extinction fringes will appear across the width of the compensator. These mark the positions where the device acts as if it was a full-wave plate. In white light the fringes will be colored, with the exception of the black central band ($\Delta\varphi = 0$). The retardance of an unknown plate can be found by placing it on the compensator and examining the fringe shift it produces. Because the fringes are narrow and difficult to "read" electronically, the Babinet has become less popular than it once was. It can be modified to produce a uniform retardation over its surface by merely rotating the top wedge 180° about the vertical, so that its thin edge rests on the thin edge of the lower wedge. This configuration will, however, slightly deviate the beam.

Another variation of the Babinet, which has the advantage of producing a uniform retardance over its surface and no beam deviation, is the **Soleil compensator** shown in Fig. 8.44. Generally made of quartz (although MgF_2 and CdS are used in the infrared), it consists of two wedges and one plane-parallel slab whose optic axes are oriented as indicated. The quantity d_1 corresponds to the total thickness of both wedges, which is constant for any setting of the positioning micrometer screw.

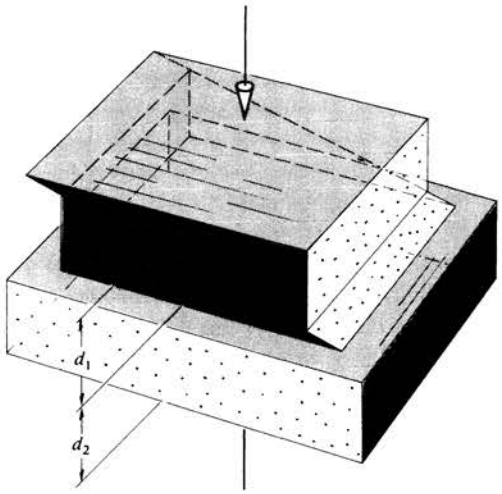


Figure 8.44 The Soleil compensator.

8.8 Circular Polarizers

Earlier we concluded that linear light whose $\vec{\mathbf{E}}$-field is at 45° to the principal axes of a quarter-wave plate will emerge from that plate circularly polarized. Any series combination of an appropriately oriented linear polarizer and a 90° retarder will therefore perform as a **circular polarizer**. The two elements function completely independently, and whereas one might be birefringent, the other could be of the reflection type. The handedness of the emergent circular light depends on whether the transmission axis of the linear polarizer is at +45° or −45° to the fast axis of the retarder. Either circular state, $\mathscr{L}$ or $\mathscr{R}$, can be generated quite easily. In fact, if the linear polarizer is situated between two retarders, one oriented at +45° and the other at −45°, the combination will be "ambidextrous." In short, it will yield an $\mathscr{R}$-state for light entering from one side and an $\mathscr{L}$-state when the input is on the other side.

CP-HN is the commercial designation for a popular one-piece circular polarizer. It is a laminate of an *HN* Polaroid and a stretched polyvinyl alcohol 90° retarder. The *input side* of such an arrangement is evidently the face of the linear polarizer. If the beam is incident on the *output side* (i.e., on the retarder), it will thereafter pass through the *H*-sheet and can only emerge linearly polarized.

A circular polarizer can be used as an analyzer to determine the handedness of a wave that is already known to be circular. To see how this might be done, imagine that we have the four elements labeled *A*, *B*, *C*, and *D* in Fig. 8.45. The first two, *A* and *B*, taken together form a circular polarizer, as do *C* and *D*. The precise handedness of these polarizers is unimportant now, as long as they are both the same, which is tantamount to saying that the fast axes of the retarders are parallel. Linear light coming from *A* receives a 90° retardance from B, at

Giesecke+Devrient GmbH,
Giesecke+Devrient Currency Technology GmbH,
and Papierfabrik Louisenthal GmbH. - Ex. 1027

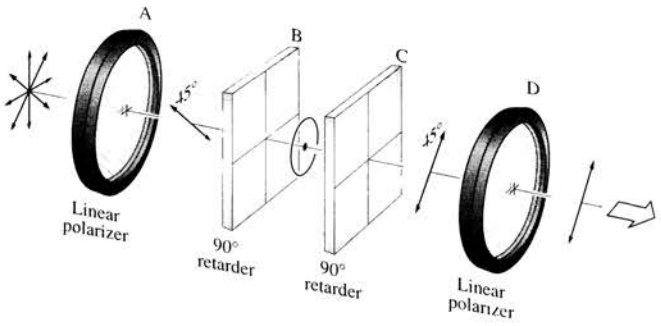


Figure 8.45 Two linear polarizers and two quarter-wave plates.

which point it is circular. As it passes through C, another 90° retardance is added on, resulting once more in a linearly polarized wave. In effect, B and C together form a half-wave plate, which merely flips the linear light from A through a spatial angle of 2θ, in this case 90°. Since the linear wave from C is parallel to the transmission axis of D, it passes through it and out of the system.

In this simple process we've actually proved something that is rather subtle. If the circular polarizers $A + B$ and $C + D$ are both left-handed, we've shown that *left-circular light entering a left-circular polarizer from the output side will be transmitted.* Furthermore, it should be apparent, at least after some thought, that right-circular light will produce a $\mathscr{P}$-state perpendicular to the transmission axis of D and so will be absorbed. The converse is true as well; that is, *of the two circular forms, only light in an $\mathscr{R}$-state will pass through a right-circular polarizer having entered from the output side.*



A crumpled piece of cellophane placed between two crossed Polaroids shows a rainbow of colors. Depending on its thickness and the frequency of the light, the cellophane rotates the E-field by different amounts. Rotating either one of the Polaroids will shift the colors to their complements.

8.9 Polarization of Polychromatic Light

8.9.1 Bandwidth and Coherence Time of a Polychromatic Wave

By its very nature purely monochromatic light, which is of course not a physical reality, must be polarized. The two orthogonal components of such a wave have the same frequency, and each has a constant amplitude. If the amplitude of either sinusoidal component varied, it would be equivalent to the presence of other additional frequencies in the Fourier-analyzed spectrum. Moreover, the two components have a constant relative phase difference; that is, they are coherent. A monochromatic disturbance is an infinite wavetrain whose properties have been fixed for all time; whether it is in an $\mathscr{R}$-, $\mathscr{L}$-, $\mathscr{P}$-, or $\mathscr{E}$-state, the wave is completely polarized.

Actual light sources are polychromatic; they emit radiant energy having a range of frequencies. Let's now examine what happens on a submicroscopic scale, paying particular attention to the polarization state of the emitted wave. Envision an electron-oscillator that has been excited into vibration (possibly by a collision) and thereupon radiates. Depending on its precise motion, the oscillator will emit some form of polarized light.

As in Section 7.4.3, we picture the radiant energy from a single atom as a wavetrain having a finite spatial extent Δl_c. Assume for the moment that its polarization state is essentially constant for a duration of the order of the coherence time Δt_c (which, as you recall, corresponds to the temporal extent of the wavetrain, i.e., $\Delta l_c/c$). A typical source generally consists of a large collection of such radiating atoms, which can be envisioned as oscillating with different phases at some dominant frequency $\bar{\nu}$. Suppose then that we examine the light coming from a very small region of the source, such that the emitted rays arriving at a point of observation are essentially parallel. During a time that is short in comparison with the average coherence time, the amplitudes and phases of the wavetrains from the individual atoms will be essentially constant. This means that if we were to look toward the source in some direction, we would, at least for an instant, "see" a coherent superposition of the waves emitted in that direction. We would "see" a resultant wave having a given polarization state. That state would only last for an interval less than the coherence time before it changed, but even so it would correspond to a great many oscillations at the frequency $\bar{\nu}$. Clearly, if the bandwidth $\Delta\nu$ is broad, the coherence time ($\Delta t_c \approx 1/\Delta\nu$)

Giesecke+Devrient GmbH,
Giesecke+Devrient Currency Technology GmbH,
and Papierfabrik Louisenthal GmbH. - Ex. 1027

will be small, and any polarization state will be short-lived. Evidently *the concepts of polarization and coherence are related in a fundamental way.*

Now consider a wave whose bandwidth is very small in comparison with its mean frequency, a quasimonochromatic wave. It can be represented by two orthogonal harmonic $\mathscr{P}$-states, as in Eqs. (8.1) and (8.2), but here the amplitudes and initial phase angles are functions of time. Furthermore, the frequency and propagation number correspond to the mean values of the spectrum present in the wave, namely, $\bar{\omega}$ and $\bar{k}$. Thus

$$\vec{\mathbf{E}}_x(t) = \hat{\mathbf{i}}E_{0x}(t)\cos\left[\bar{k}z - \bar{\omega}t + \varepsilon_x(t)\right] \qquad (8.34a)$$

and

$$\vec{\mathbf{E}}_y(t) = \hat{\mathbf{j}}E_{0y}(t)\cos\left[\bar{k}z - \bar{\omega}t + \varepsilon_y(t)\right] \qquad (8.34b)$$

The polarization state, and accordingly $E_{0x}(t)$, $E_{0y}(t)$, $\varepsilon_x(t)$, and $\varepsilon_y(t)$, will vary slowly, remaining essentially constant over a large number of oscillations. Keep in mind that the narrow bandwidth implies a relatively large coherence time. If we watch the wave during a much longer interval, the amplitudes and phase angles will vary somehow, either independently or in some correlated fashion. If the variations are completely uncorrelated, the polarization state will remain constant only for an interval that is small compared to the coherence time. In other words, the ellipse describing the polarization state may change shape, orientation, and handedness. Since, speaking practically, no existing detector could discern any one particular state lasting for so short a time, we would conclude that the wave was unpolarized.

Antithetically, if the ratio $E_{0x}(t)/E_{0y}(t)$ was constant even though both terms varied, and if $\varepsilon = \varepsilon_y(t) - \varepsilon_x(t)$ was constant as well, the wave would be polarized. Here the necessity for correlation among these different functions is obvious. Yet we can actually impress these conditions on the wave by merely passing it through a polarizer, thereby removing any undesired constituents. The time interval over which the wave thereafter maintains its polarization state is no longer dependent on the bandwidth because the wave's components have been appropriately correlated. The light could be polychromatic (even white), yet completely polarized. It will behave very much like the idealized monochromatic waves treated in Section 8.1.

Between the two extremes of completely polarized and unpolarized light is the condition of partial polarization. In fact, it can be shown that any quasimonochromatic wave can be represented as the sum of a polarized and an unpolarized wave, where the two are independent and either may be zero.

8.9.2 Interference Colors

Insert a crumpled sheet of cellophane between two Polaroids illuminated by white light. Alternatively, take an ordinary plastic bag (polyethylene), which shows nothing special between crossed Polaroids, and stretch it. That will align its molecules, making it birefringent. Now crumple it up and examine it again. The resulting pattern will be a profusion of multicolored regions, which vary in hue as either Polaroid rotates. These **interference colors** arise from the wavelength dependence of the retardation. The usual variegated nature of the patterns is due to local variations in thickness, birefringence, or both.

The appearance of interference colors is commonplace and can easily be observed in any number of substances. For example, the effect can be seen with a piece of multilayered mica, a chip of ice, a stretched plastic bag, or finely crushed particles of an ordinary white (quartz) pebble. To appreciate how the phenomenon occurs, examine Fig. 8.46. A narrow beam of monochromatic linear light is schematically shown passing through some small region of a birefringent plate Σ. Over that area the birefringence and thickness are both assumed to be constant. The transmitted light is generally elliptical. Equivalently, envision the light emerging from Σ as composed of two orthogonal linear waves (i.e., the x- and y-components of the total $\vec{\mathbf{E}}$-field), which have a relative phase difference $\Delta\varphi$, determined by Eq. (8.32). Only the components of these two disturbances, which are in the direction of the transmission axis of the analyzer, will pass through it and on to the observer.

Now these components, which also have a phase difference of $\Delta\varphi$, are coplanar and can thus interfere. When $\Delta\varphi = \pi, 3\pi,$

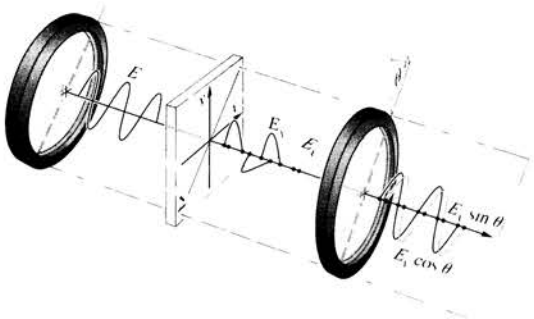


Figure 8.46 The origin of interference colors.

Giesecke+Devrient GmbH,
Giesecke+Devrient Currency Technology GmbH,
and Papierfabrik Louisenthal GmbH. - Ex. 1027

$5\pi,\ldots$, they are completely out-of-phase and tend to cancel each other. When $\Delta\varphi = 0, 2\pi, 4\pi,\ldots$, the waves are in-phase and reinforce each other. Suppose then that the retardance arising at some point P_1 on Σ for blue light ($\lambda_0 = 435$ nm) is 4π. In that case blue will be strongly transmitted. It follows from Eq. (8.32) that $\lambda_0\Delta\varphi = 2\pi d(|n_o - n_e|)$ is essentially a constant determined by the thickness and the birefringence. At the point in question, therefore, $\lambda_0\Delta\varphi = 1740\pi$ for all wavelengths. If we now change to incident yellow light ($\lambda_0 = 580$ nm), $\Delta\varphi \approx 3\pi$ and the light from P_1 is completely canceled. Under white-light illumination that particular point on Σ will seem as if it had removed yellow completely, passing on all the other colors, but none as strongly as blue. Another way of saying this is that the blue light emerging from the region about P_1 is linear ($\Delta\varphi = 4\pi$) and parallel to the analyzer's transmission axis. In contrast, the yellow light is linear ($\Delta\varphi = 3\pi$) and along the extinction axis; the other colors are elliptical. The region about P_1 behaves like a half-wave plate for yellow and full-wave plate for blue. If the analyzer were rotated 90°, the yellow would be transmitted, and the blue extinguished.

By definition two colors are said to be complementary when their combination yields white light. Thus when the analyzer is rotated through 90° it will alternately transmit or absorb complementary colors. In much the same way there might be a point P_2 somewhere else on Σ where $\Delta\varphi = 4\pi$ for red ($\lambda_0 = 650$ nm). Then, $\lambda_0\Delta\varphi = 2600\pi$, whereupon bluish-green light ($\lambda_0 = 520$ nm) will have a retardance of 5π and be extinguished. Clearly, if the retardance varies from one region to the next over the specimen, so too will the color of the light transmitted by the analyzer.

8.10 Optical Activity

The manner in which light interacts with material substances can yield a great deal of valuable information about their molecular structures. The process to be examined next, although of specific interest in the study of Optics, has had and is continuing to have far-reaching effects in the sciences of chemistry and biology.

In 1811 the French physicist Dominique F. J. Arago first observed the rather fascinating phenomenon now known as **optical activity**. It was then that he discovered that the plane of vibration of a beam of linear light underwent a continuous rotation as it propagated along the optic axis of a quartz plate (Fig. 8.47). At about the same time Jean Baptiste Biot

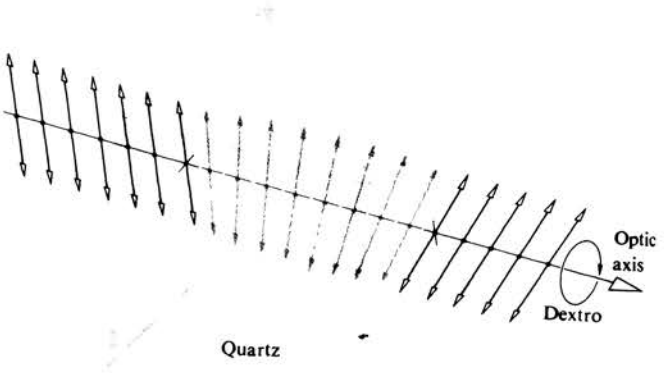


Figure 8.47 Optical activity displayed by quartz.

(1774–1862) saw this same effect while using both the vaporous and liquid forms of various natural substances like turpentine. Any material that causes the $\vec{\mathbf{E}}$-field of an incident linear plane wave to appear to rotate is said to be *optically active*. Moreover, as Biot found, one must distinguish between right- and left-handed rotation. If while looking in the direction of the source, the plane-of-vibration appears to have revolved clockwise, the substance is referred to as *dextrorotatory*, or *d-rotatory* (from the Latin *dextro*, meaning right). Alternatively, if $\vec{\mathbf{E}}$ appears to have been displaced counterclockwise, the material is *levorotatory*, or *l-rotatory* (from the Latin *levo*, meaning left).

In 1822 the English astronomer Sir John F. W. Herschel (1792–1871) recognized that *d*-rotatory and *l*-rotatory behavior in quartz actually corresponded to two different crystallographic structures. Although the molecules are identical (SiO_2), crystal quartz can be either right- or left-handed, depending on the arrangement of those molecules. As shown in Fig. 8.48, the external appearances of these two forms are the same in all respects, except that one is the mirror image of the other; they are said to be *enantiomorphs* of each other. All transparent enantiomorphic substances are optically active. Furthermore, molten quartz and *fused* quartz, neither of which is crystalline, are not optically active. Evidently, in quartz optical activity is associated with the structural distribution of the molecules as a whole. There are many substances, both organic and inorganic (e.g., benzil and $NaBrO_3$, respectively), which, like quartz, exhibit optical activity only in crystal form. In contrast, many naturally occurring organic compounds,

Giesecke+Devrient GmbH,
Giesecke+Devrient Currency Technology GmbH,
and Papierfabrik Louisenthal GmbH. - Ex. 1027

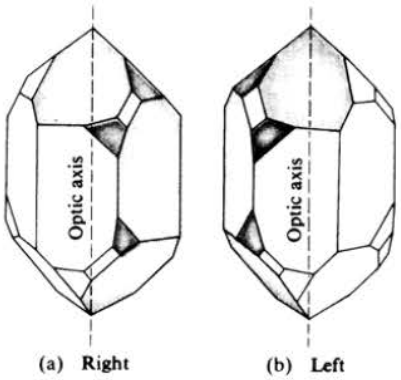


Figure 8.48 Right- and left-handed quartz crystals.

such as sugar, tartaric acid, and turpentine, are optically active in solution or in the liquid state. Here the *rotatory power*, as it is often referred to, is evidently an attribute of the individual molecules. There are also more complicated substances for which optical activity is associated with both the molecules themselves and their arrangement within the various crystals. An example is rubidium tartrate. A *d*-rotatory solution of that compound will change to *l-rotatory* when crystallized.

In 1825 Fresnel, without addressing the actual mechanism involved, proposed a simple phenomenological description of optical activity. Since the incident linear wave can be represented as a superposition of $\mathscr{R}$- and $\mathscr{L}$-states, he suggested that these two forms of circular light propagate at different speeds. An active material shows *circular birefringence*; that is, it possesses two indices of refraction, one for $\mathscr{R}$-states ($n_{\mathscr{R}}$) and one for $\mathscr{L}$-states ($n_{\mathscr{L}}$). In traversing an optically active specimen, the two circular waves would get out-of-phase, and the resultant linear wave would appear to have rotated. We can see how this is possible analytically by returning to Eqs. (8.8) and (8.9), which described monochromatic right- and left-circular light propagating in the z-direction. It was seen in Eq. (8.10) that the sum of these two waves is indeed linearly polarized. We now alter these expressions slightly in order to remove the factor of two in the amplitude of Eq. (8.10), in which case

$$\vec{\mathbf{E}}_{\mathscr{R}} = \frac{E_0}{2}[\hat{\mathbf{i}} \cos(k_{\mathscr{R}} z - \omega t) + \hat{\mathbf{j}} \sin(k_{\mathscr{R}} z - \omega t)] \quad (8.35a)$$

and

$$\vec{\mathbf{E}}_{\mathscr{L}} = \frac{E_0}{2}[\hat{\mathbf{i}} \cos(k_{\mathscr{L}} z - \omega t) - \hat{\mathbf{j}} \sin(k_{\mathscr{L}} z - \omega t)] \quad (8.35b)$$

represent the right- and left-handed constituent waves. Since ω is constant, $k_{\mathscr{R}} = k_0 n_{\mathscr{R}}$ and $k_{\mathscr{L}} = k_0 n_{\mathscr{L}}$. The resultant disturbance is given by $\vec{\mathbf{E}} = \vec{\mathbf{E}}_{\mathscr{R}} + \vec{\mathbf{E}}_{\mathscr{L}}$, and after a bit of trigonometric manipulation, it becomes

$$\vec{\mathbf{E}} = E_0 \cos[(k_{\mathscr{R}} + k_{\mathscr{L}})z/2 - \omega t][\hat{\mathbf{i}} \cos(k_{\mathscr{R}} - k_{\mathscr{L}})z/2 + \hat{\mathbf{j}} \sin(k_{\mathscr{R}} - k_{\mathscr{L}})z/2] \quad (8.36)$$

At the position where the wave enters the medium ($z = 0$) it is linearly polarized along the x-axis, as shown in Fig. 8.49; that is,

$$\vec{\mathbf{E}} = E_0 \hat{\mathbf{i}} \cos \omega t \quad (8.37)$$

Notice that at any point along the path, the two components have the same time dependence and are therefore in-phase. This just means that anywhere along the z-axis the resultant is linearly polarized (Fig. 8.50), although its orientation is certainly a function of z. Moreover, if $n_{\mathscr{R}} > n_{\mathscr{L}}$ or equivalently $k_{\mathscr{R}} > k_{\mathscr{L}}$, $\vec{\mathbf{E}}$ will rotate counterclockwise, whereas if $k_{\mathscr{L}} > k_{\mathscr{R}}$, the rotation is clockwise (looking toward the source). Traditionally, the angle β through which $\vec{\mathbf{E}}$ rotates is defined as positive

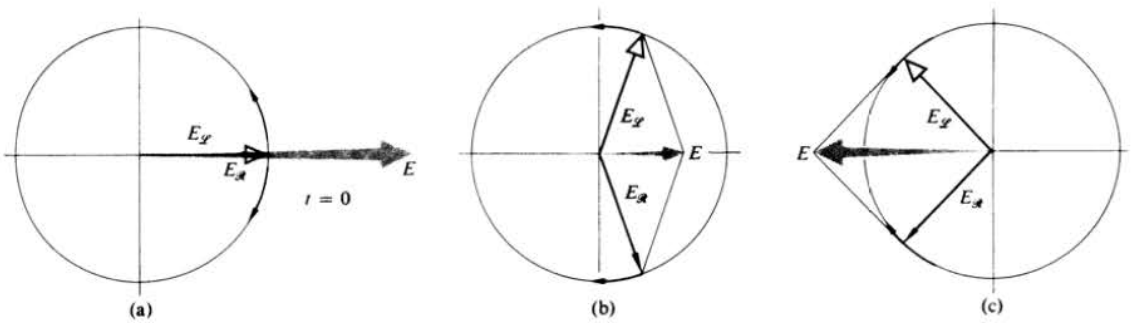


Figure 8.49 The superposition of an $\mathscr{R}$- and an $\mathscr{L}$-state at $z = 0$.

Giesecke+Devrient GmbH,
Giesecke+Devrient Currency Technology GmbH,
and Papierfabrik Louisenthal GmbH. - Ex. 1027

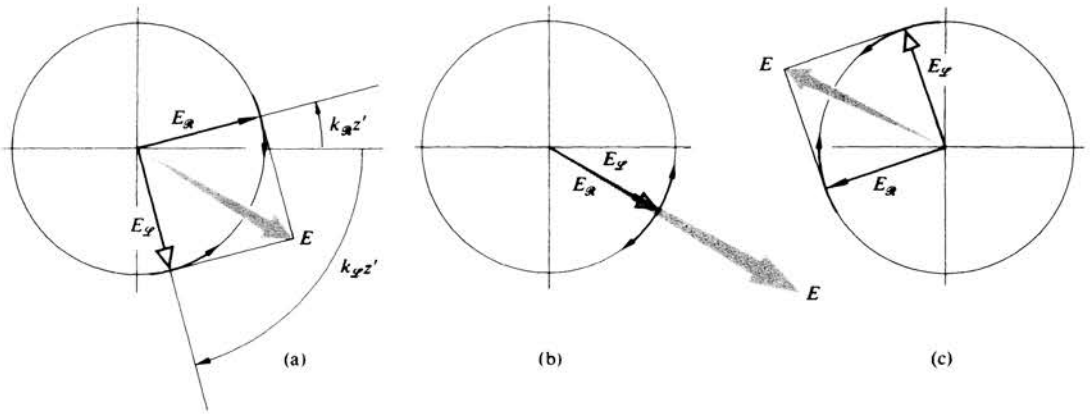


Figure 8.50 The superposition of an $\mathscr{R}$- and an $\mathscr{L}$-state at $z = z'$ ($k_{\mathscr{L}} > k_{\mathscr{R}}$).

when it is clockwise. Keeping this sign convention in mind, it should be clear from Eq. (8.36) that the field at point z makes an angle of $\beta = -(k_{\mathscr{R}} - k_{\mathscr{L}})z/2$ with respect to its original orientation. If the medium has a thickness d, the angle through which the plane-of-vibration rotates is then

$$\beta = \frac{\pi d}{\lambda_0}(n_{\mathscr{L}} - n_{\mathscr{R}}) \tag{8.38}$$

where $n_{\mathscr{L}} > n_{\mathscr{R}}$ is *d-rotatory* and $n_{\mathscr{R}} > n_{\mathscr{L}}$ is *l-rotatory* (Fig. 8.51).

Fresnel was actually able to separate the constituent $\mathscr{R}$- and $\mathscr{L}$-states of a linear beam using the composite prism of Fig. 8.52. It consists of a number of right- and left-handed quartz segments cut with their optic axes as shown. The $\mathscr{R}$-state propagates more rapidly in the first prism than in the second and is thus refracted toward the normal to the oblique boundary. The opposite is true for the $\mathscr{L}$-state, and the two circular waves increase in angular separation at each interface.

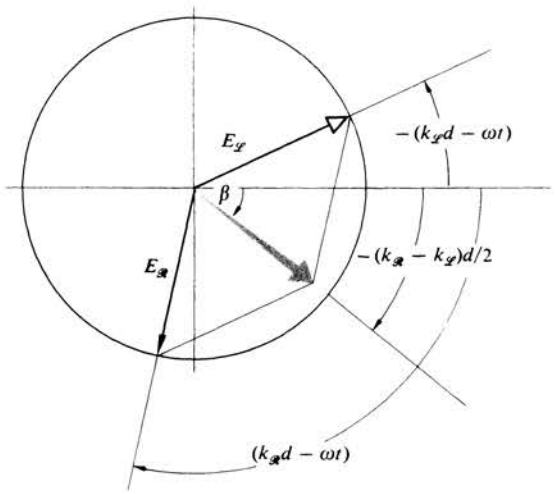


Figure 8.51 The superposition of an $\mathscr{R}$- and an $\mathscr{L}$-state at $z = d$ ($k_{\mathscr{L}} > k_{\mathscr{R}}$, $\lambda_{\mathscr{L}} < \lambda_{\mathscr{R}}$, and $v_{\mathscr{L}} < v_{\mathscr{R}}$).

In sodium light the *specific rotatory power*, which is defined as β/d, is found to be 21.7°/mm for quartz. It follows that $|n_{\mathscr{L}} - n_{\mathscr{R}}| = 7.1 \times 10^{-5}$ for light propagating along the optic axis. In that particular direction ordinary double refraction vanishes. However, with the incident light propagating normal to the optic axis (as is frequently the case in polarizing prisms, wave plates, and compensators), quartz behaves like any optically inactive, positive, uniaxial crystal. There are other birefringent, optically active crystals, both uniaxial and biaxial, such as cinnabar, HgS ($n_o = 2.854$, $n_e = 3.201$), which has a rotatory power of 32.5°/mm. In contrast, the substance $NaClO_3$ is optically active (3.1°/mm) but not birefringent. The rotatory power of liquids, in comparison, is so relatively small that it is usually specified in terms of 10-cm path lengths; for example, in the case of turpentine ($C_{10}H_6$) it is only −37°/10 cm (10°C with $\lambda_0 = 589.3$ nm). The rotatory power of solutions varies with the concentration. This fact is particularly helpful in determining, for example, the amount of sugar present in a urine sample or a commercial sugar syrup.

You can observe optical activity rather easily using colorless corn syrup, the kind available in any grocery store. You won't need much of it, since β/d is roughly +30°/inch. Put about an inch of syrup in a glass container between crossed Polaroids and illuminate it with a flashlight. The beautiful col-

Giesecke+Devrient GmbH,
Giesecke+Devrient Currency Technology GmbH,
and Papierfabrik Louisenthal GmbH. - Ex. 1027

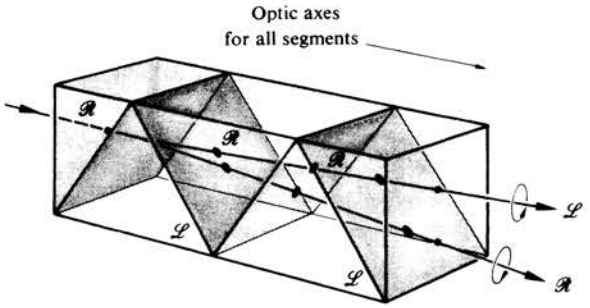


Figure 8.52 The Fresnel composite prism.

ors that appear as the analyzer is rotated arise from the fact that β is a function of λ_0, an effect known as *rotatory dispersion*. Using a filter to get roughly monochromatic light, you can readily determine the rotatory power of the syrup.*

The first great scientific contribution made by Louis Pasteur (1822–1895) came in 1848 and was associated with his doctoral research. He showed that racemic acid, which is an optically inactive form of tartaric acid, is actually composed of a mixture containing equal quantities of right- and left-handed constituents. Substances of this sort, which have the same molecular formulas but differ somehow in structure, are called *isomers*. He was able to crystallize racemic acid and then separate the two different types of mirror-image crystals (enantiomorphs) that resulted. When dissolved separately in water, they formed *d*-rotatory and *l*-rotatory solutions. This implied the existence of molecules that, although chemically the same, were themselves mirror images of each other; such molecules are now known as optical *stereoisomers*. These ideas were the basis for the development of the stereochemistry of organic and inorganic compounds, where one is concerned with the three-dimensional spatial distribution of atoms within a given molecule.

8.10.1 A Useful Model

The phenomenon of optical activity is extremely complicated, and although it can be treated in terms of classical Electromagnetic Theory, it actually requires a quantum-mechanical solution.† Despite this, we will consider a simplified model, which will yield a qualitative, yet plausible, description of the process. Recall that we represented an optically isotropic medium by a homogeneous distribution of isotropic electron-oscillators that vibrated parallel to the $\vec{\mathbf{E}}$-field of an incident wave. An optically anisotropic medium was similarly depicted as a distribution of anisotropic oscillators that vibrated at some angle to the driving $\vec{\mathbf{E}}$-field. We now imagine that the electrons in optically active substances are constrained to move along twisting paths that, for simplicity, are assumed to be helical. Such a molecule is pictured much as if it were a conducting helix. The silicon and oxygen atoms in a quartz crystal are known to be arranged in either right- or left-handed spirals about the optic axis, as indicated in Fig. 8.53. In the present representation this crystal would correspond to a parallel array of helices. In comparison, an active sugar solution would be analogous to a distribution of randomly oriented helices, each having the same handedness.*

In quartz we might anticipate that the incoming wave would interact differently with the specimen, depending on whether it "saw" right- or left-handed helices. Thus we could expect different indices for the $\mathscr{R}$- and $\mathscr{L}$-components of the wave. The detailed treatment of the process that leads to circular birefringence in crystals is by no means simple, but at least the necessary asymmetry is evident. How, then, can a random array of helices, corresponding to a solution, produce optical activity? Let us examine one such molecule in this simplified representation, for example, one whose axis happens to be parallel to the harmonic $\vec{\mathbf{E}}$-field of the electromagnetic wave. That field will drive charges up and down along the length of the molecule, effectively producing a time-varying electric dipole moment $\not{\mu}(t)$, parallel to the axis. In addition,

*A gelatin filter works well, but a piece of colored cellophane will also do nicely. Just remember that the cellophane will act as a wave plate (see Section 8.7.1), so don't put it between the polaroids unless you align its principal axes appropriately.

†The review article "Optical Activity and Molecular Dissymmetry," by S. F. Mason, *Contemp. Phys.* **9**, 239 (1968), contains a fairly extensive list of references for further reading.

*In addition to these solid and liquid states, there is a third classification of substances, which is useful because of its remarkable optical properties. It is known as the *mesomorphic* or *liquid crystal* state. Liquid crystals are organic compounds that can flow and yet maintain their characteristic molecular orientations. In particular, *cholesteric* liquid crystals have a helical structure and therefore exhibit extremely large rotatory powers, of the order of 40000°/mm. The pitch of the screw-like molecular arrangement is considerably smaller than that of quartz.

Giesecke+Devrient GmbH,
Giesecke+Devrient Currency Technology GmbH,
and Papierfabrik Louisenthal GmbH. - Ex. 1027

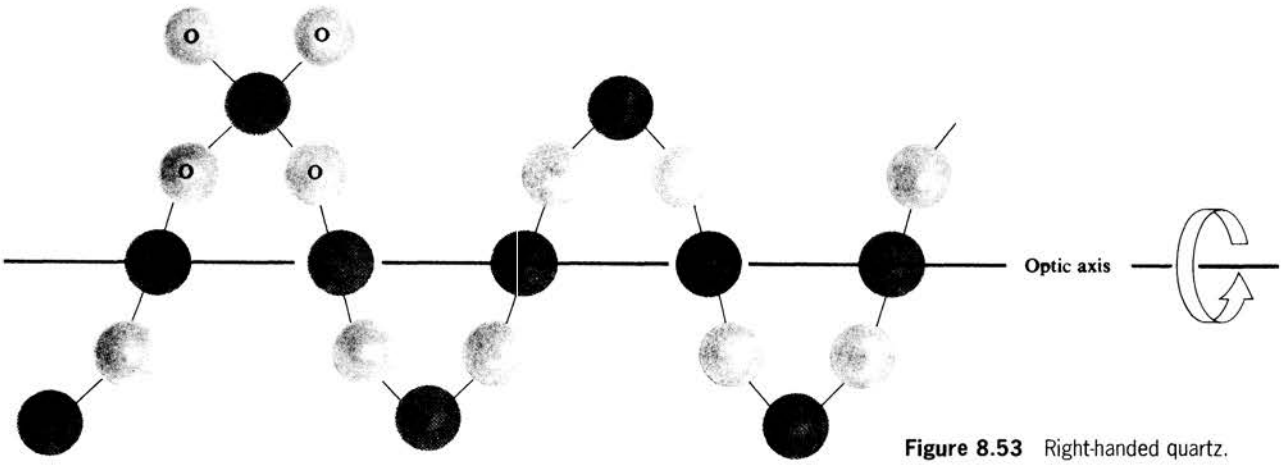


Figure 8.53 Right-handed quartz.

we now have a current associated with the spiraling motion of the electrons. This in turn generates an oscillating magnetic dipole moment $\boldsymbol{m}(t)$, which is also along the helix axis (Fig. 8.54). In contrast, if the molecule was parallel to the $\vec{\mathbf{B}}$-field of the wave, there would be a time-varying flux and thus an induced electron current circulating around the molecule. This would again yield oscillating axial electric and magnetic dipole moments. In either case $\boldsymbol{p}(t)$ and $\boldsymbol{m}(t)$ *will be parallel or antiparallel to each other, depending on the sense of the particular molecular helix*. Clearly, energy has been removed from the field, and both oscillating dipoles will scatter (i.e., reradiate) electromagnetic waves. The electric field $\vec{\mathbf{E}}_p$ emitted in a given direction by an electric dipole is perpendicular to the electric field $\vec{\mathbf{E}}_m$ emitted by a magnetic dipole. The sum of these, which is the resultant field $\vec{\mathbf{E}}_s$ scattered by a helix, will not be parallel to the incident field $\vec{\mathbf{E}}_i$ along the direction of propagation. (The same is of course true for the magnetic fields.) The plane-of-vibration of the resultant transmitted light ($\vec{\mathbf{E}}_s + \vec{\mathbf{E}}_i$) will thus be rotated in a direction determined by the sense of the helix. The amount of the rotation will vary with the orientation of each molecule, but it will always be in the same direction for helices of the same sense.

Although this discussion of optically active molecules as helical conductors is admittedly superficial, the analogy is well worth keeping in mind. In fact, if we direct a linear 3-cm microwave beam onto a box filled with a large number of identical copper helices (e.g., 1 cm long by 0.5 cm in diameter

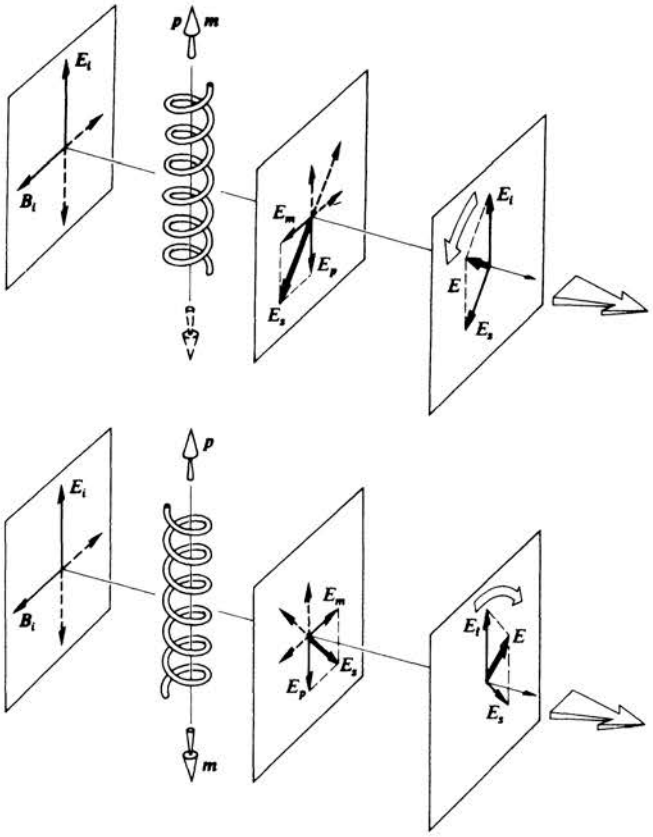


Figure 8.54 The radiation from helical molecules.

Giesecke+Devrient GmbH,
Giesecke+Devrient Currency Technology GmbH,
and Papierfabrik Louisenthal GmbH. - Ex. 1027

and insulated from each other), the transmitted wave will undergo a rotation of its plane-of-vibration.*

8.10.2 Optically Active Biological Substances

Among the most fascinating observations associated with optical activity are those in biology. Whenever organic molecules are synthesized in the laboratory, an equal number of *d*- and *l*-isomers are produced, with the effect that the compound is optically inactive. One might then expect that if they exist at all, equal amounts of *d*- and *l*-optical stereoisomers will be found in natural organic substances. This is by no means the case. Natural sugar (sucrose, $C_{12}H_{22}O_{11}$), no matter where it is grown, whether extracted from sugar cane or sugar beets, is always *d*-rotatory. Moreover, the simple sugar dextrose or *d*-glucose ($C_6H_{12}O_6$), which as its name implies is *d*-rotatory, is the most important carbohydrate in human metabolism. Evidently, living things can somehow distinguish between optical isomers.

All proteins are fabricated of compounds known as *amino acids*. These in turn are combinations of carbon, hydrogen, oxygen, and nitrogen. There are twenty-odd amino acids, and all of them (with the exception of the simplest one, glycine, which is not enantiomorphic) are generally *l*-rotatory. This means that if we break up a protein molecule, whether it comes from an egg or an eggplant, a beetle or a Beatle, the constituent amino acids will be *l*-rotatory. One important exception is the group of antibiotics, such as penicillin, which do contain some dextro amino acids. In fact, this may well account for the toxic effect penicillin has on bacteria.

It is intriguing to speculate about the possible origins of life on this and other planets. For example, did life on Earth originally consist of both mirror-image forms? Five amino acids were found in a meteorite that fell in Victoria, Australia, on September 28, 1969, and analysis has revealed the existence of roughly equal amounts of the optically right- and left-handed forms. This is in marked contrast to the overwhelming predominance of the left-handed form found in terrestrial rocks. The implications are many and marvelous.†

*I. Tinoco and M. P. Freeman, "The Optical Activity of Oriented Copper Helices," *J. Phys. Chem.* **61**, 1196 (1957).

†See *Physics Today*, Feb. 1971, p. 17, for additional discussion and references for further reading.

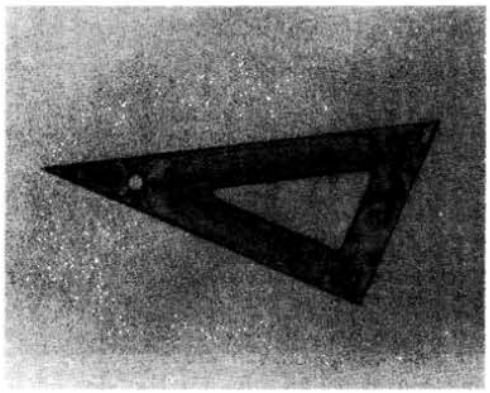
8.11 Induced Optical Effects—Optical Modulators

A number of different physical effects involving polarized light all share the single common feature of somehow being externally induced. In these instances, one exerts an external influence (e.g., a mechanical force, a magnetic or electric field) on the optical medium, thereby changing the manner in which it transmits light.

8.11.1 Photoelasticity

In 1816 Sir David Brewster discovered that normally transparent isotropic substances could be made optically anisotropic by the application of mechanical stress. The phenomenon is known as *mechanical birefringence*, **photoelasticity**, or *stress birefringence*. Under compression or tension, the material takes on the properties of a negative or positive uniaxial crystal, respectively. In either case, the effective optic axis is in the direction of the stress, and the induced birefringence is proportional to the stress. If the stress is not uniform over the sample, neither is the birefringence or the retardance imposed on a transmitted wave [Eq. (8.32)].

Photoelasticity serves as the basis of a technique for studying the stresses in both transparent and opaque mechanical structures (see photo). Improperly annealed or carelessly mounted glass, whether serving as an automobile windshield or a telescope lens, will develop internal stresses that can easily be detected. Information concerning the surface strain on opaque objects can be obtained by bonding photoelastic coat-



A clear plastic triangle between polaroids. (Photo by E. H.)

Giesecke+Devrient GmbH,
Giesecke+Devrient Currency Technology GmbH,
and Papierfabrik Louisenthal GmbH. - Ex. 1027

ings to the parts under study. More commonly, a transparent scale model of the part is made out of a material *optically sensitive to stress*, such as epoxy, glyptol, or modified polyester resins. The model is then subjected to the forces that the actual component would experience in use. Since the birefringence varies from point to point over the surface of the model, when it is placed between crossed polarizers, a complicated variegated fringe pattern will reveal the internal stresses. Examine almost any piece of clear plastic or even a block of unflavored gelatin between two Polaroids; try stressing it further and watch the pattern change accordingly (see photos).

The retardance at any point on the sample is proportional to the *principal stress difference*; that is, $(\sigma_1 - \sigma_2)$, where the sigmas are the orthogonal principal stresses. For example, if the sample were a plate under vertical tension, σ_1 would be the maximum principal stress in the vertical direction and σ_2 would be the minimum principal stress, in this case zero, horizontally. In more complicated situations, the principal stresses, as well as their differences, will vary from one region to the next. Under white-light illumination, the loci of all points on the specimen for which $(\sigma_1 - \sigma_2)$ is constant are known as *isochromatic regions*, and each such region corresponds to a particular color. Superimposed on these colored fringes will be a separate system of black bands. At any point where the $\vec{\mathbf{E}}$-field of the incident linear light is parallel to either local principal stress axis, the wave will pass through the sample unaffected, regardless of wavelength. With crossed polarizers, that light will be absorbed by the analyzer, yielding a black region known as an *isoclinic* band (Problem 8.49). In addition to being beautiful to look at, the fringes also provide both a qualitative map of the stress pattern and a basis for quantitative calculations.

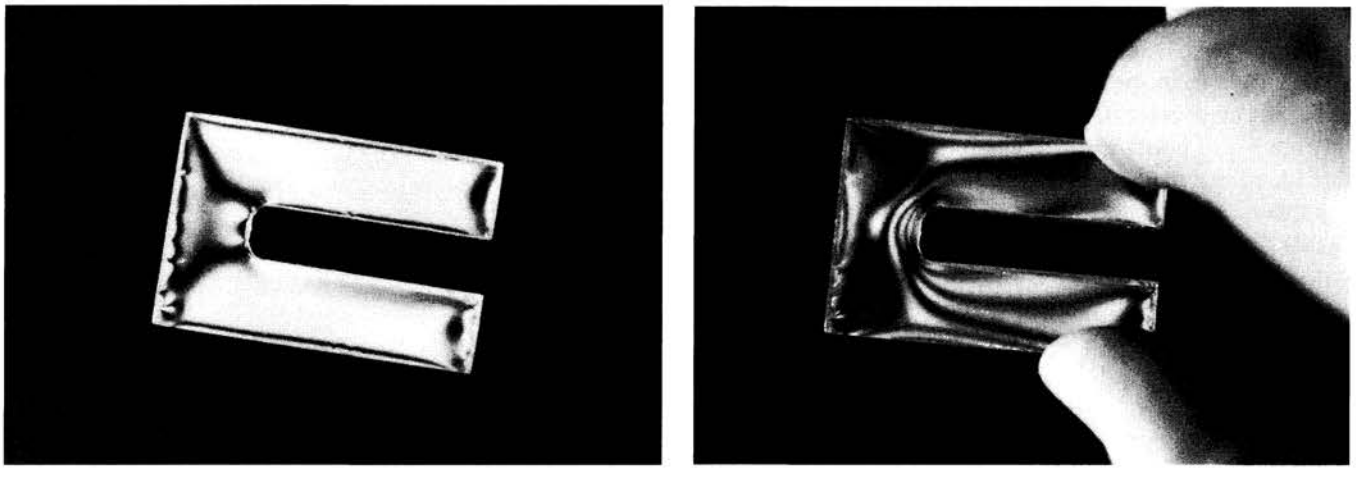
8.11.2 The Faraday Effect

Michael Faraday in 1845 discovered that the manner in which light propagated through a material medium could be influenced by the application of an external magnetic field. In particular, he found that the plane-of-vibration of linear light incident on a piece of glass rotated when a strong magnetic field was applied in the propagation direction. The **Faraday Effect** was one of the earliest indications of the interrelationship between electromagnetism and light. Although it is reminiscent of optical activity, there is an important distinction.

The angle β (measured in minutes of arc) through which the plane-of-vibration rotates is given by the empirically determined expression

$$\beta = \mathcal{V}Bd \tag{8.39}$$

where B is the static magnetic flux density (usually in gauss), d is the length of medium traversed (in cm), and $\mathcal{V}$ is a factor of proportionality known as the ***Verdet constant***. The Verdet constant for a particular medium varies with both frequency



(a) (b)

(a) A permanently stressed piece of clear plastic between crossed Polaroids. (b) The fringe pattern changes with the application of a force. (Photo by E.H.)

Giesecke+Devrient GmbH,
Giesecke+Devrient Currency Technology GmbH,
and Papierfabrik Louisenthal GmbH. - Ex. 1027

(dropping off rapidly as ν decreases) and temperature. It is roughly of the order of 10^{-5} min of arc gauss^{-1} cm^{-1} for gases and 10^{-2} min of arc gauss^{-1} cm^{-1} for solids and liquids (see Table 8.2). You can get a better feeling for the meaning of these numbers by imagining, for example, a 1-cm-long sample of H_2O in the moderately large field of 10^4 gauss. (The Earth's field is about one half gauss.) In that particular case, a rotation of 2° 11′ would result since $\mathcal{V} = 0.0131$.

By convention, *a positive Verdet constant corresponds to a (diamagnetic) material for which the Faraday Effect is l-rotatory when the light moves parallel to the applied* $\vec{\mathbf{B}}$*-field and d-rotatory when it propagates antiparallel to* $\vec{\mathbf{B}}$. No such reversal of handedness occurs in the case of natural optical activity. For a convenient mnemonic, imagine the $\vec{\mathbf{B}}$-field to be generated by a solenoidal coil wound about the sample. The plane-of-vibration, when $\mathcal{V}$ is positive, rotates in the same direction as the current in the coil, regardless of the beam's propagation direction along its axis. Consequently, the effect can be amplified by reflecting the light back and forth a few times through the sample.

The theoretical treatment of the Faraday Effect involves the quantum-mechanical theory of dispersion, including the effects of $\vec{\mathbf{B}}$ on the atomic or molecular energy levels. It will suffice here merely to outline the limited classical argument for nonmagnetic materials.

Suppose the incident light to be circular and monochromatic. An elastically bound electron will take on a steady-state circular orbit being driven by the rotating $\vec{\mathbf{E}}$-field of the wave. (The effect of the wave's $\vec{\mathbf{B}}$-field is negligible.) The introduction of a large constant applied magnetic field perpendicular to the plane of the orbit will result in a radial force F_M on the electron. That force can point either toward or away from the circle's center, depending on the handedness of the light and the direction of the constant $\vec{\mathbf{B}}$-field. The total radial force (F_M plus the elastic restoring force) can therefore have two different values, and so too can the radius of the orbit. Consequently, for a given magnetic field there will be two possible values of the electric dipole moment, the polarization, and the permittivity, as well as two values of the index of refraction, $n_{\mathscr{R}}$ and $n_{\mathscr{L}}$. The discussion can then proceed in precisely the same fashion as that of Fresnel's treatment of optical activity. As before, one speaks of two normal modes of propagation of electromagnetic waves through the medium, the $\mathscr{R}$- and $\mathscr{L}$-states.

For ferromagnetic substances things are somewhat more complicated. In the case of a magnetized material β is proportional to the component of the magnetization in the direction of propagation rather than the component of the applied dc field.

There are a number of practical applications of the Faraday Effect. It can be used to analyze mixtures of hydrocarbons, since each constituent has a characteristic magnetic rotation. When utilized in spectroscopic studies, it yields information about the properties of energy states above the ground level. Interestingly, the Faraday Effect has been used to make optical modulators. An infrared version, constructed by R. C. LeCraw, utilized the synthetic magnetic crystal yttrium–iron garnet (YIG), to which has been added a quantity of gallium. YIG has a structure similar to that of natural gem garnets. The device is depicted schematically in Fig. 8.55. A linear infrared laserbeam enters the crystal from the left. A transverse dc magnetic field saturates the magnetization of the YIG crystal in that direction. The total magnetization vector (arising from the constant field and the field of the coil) can vary in direction, being tilted toward the axis of the crystal by an amount proportional to the modulating current in the coil. Since the Faraday rotation depends on the axial component of the magnetization, the coil current controls β. The analyzer then converts this polarization modulation to amplitude modulation by way of Malus's Law [Eq. (8.24)]. In short, the signal to be transmitted is introduced across the coil as a modulating voltage, and the emerging laserbeam carries that information in the form of amplitude variations.

There are actually several other magneto-optic effects. We shall consider only two of these, and rather succinctly at that. The *Voigt* and *Cotton–Mouton Effects* both arise when a constant magnetic field is applied to a transparent medium per-

TABLE 8.2 Verdet Constants for Some Selected Substances

Material	Temperature (°C)	$\mathcal{V}$ (min of arc gauss^{-1} cm^{-1})
Light flint glass	18	0.0317
Water	20	0.0131
NaCl	16	0.0359
Quartz	20	0.0166
$NH_4Fe(SO_4)_2.12H_2O$	26	−0.00058
Air*	0	6.27×10^{-6}
CO_2*	0	9.39×10^{-6}

*λ = 578 nm and 760 mm Hg.

More extensive listings are given in the usual handbooks.

Giesecke+Devrient GmbH,
Giesecke+Devrient Currency Technology GmbH,
and Papierfabrik Louisenthal GmbH. - Ex. 1027

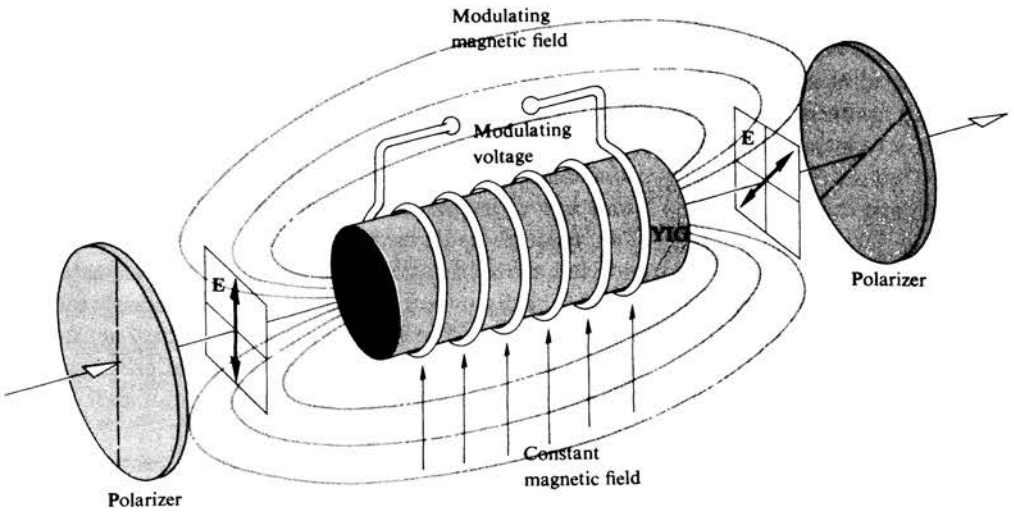


Figure 8.55 A Faraday Effect modulator.

pendicular to the direction of propagation of the incident light beam. The former occurs in vapors, whereas the latter, which is considerably stronger, occurs in liquids. In either case the medium displays birefringence similar to that of a uniaxial crystal whose optic axis is in the direction of the dc magnetic field, that is, normal to the light beam [Eq. (8.32)]. The two indices of refraction now correspond to the situations in which the plane-of-vibration of the wave is either normal or parallel to the constant magnetic field. Their difference Δn (i.e., the birefringence) is proportional to the square of the applied magnetic field. It arises in liquids from an aligning of the optically and magnetically anisotropic molecules of the medium with that field. If the incoming light propagates at some angle to the static field other than 0 or $\pi/2$, the Faraday and Cotton–Mouton Effects occur concurrently, with the former generally being much the larger of the two. The Cotton–Mouton is the magnetic analogue of the Kerr (electro-optic) Effect, to be considered next.

8.11.3 The Kerr and Pockels Effects

The first electro-optic effect was discovered by the Scottish physicist John Kerr (1824–1907) in 1875. He found that an isotropic transparent substance becomes birefringent when placed in an electric field $\vec{\mathbf{E}}$. The medium takes on the characteristics of a uniaxial crystal whose optic axis corresponds to the direction of the applied field. The two indices, $n_{\parallel}$ and $n_{\perp}$, are associated with the two orientations of the plane-of-vibration of the wave, namely, parallel and perpendicular to the applied electric field, respectively. Their difference, Δn, is the birefringence, and it is found to be

$$\Delta n = \lambda_0 K E^2 \tag{8.40}$$

where K is the ***Kerr constant***. When K is positive, as it most often is, Δn, which can be thought of as $n_e - n_o$, is positive, and the substance behaves like a positive uniaxial crystal. Values of the Kerr constant (Table 8.3) are often listed in electrostatic units, so that one must remember to enter E in Eq. (8.40) in statvolts per cm (one statvolt $\approx$ 300 V). Observe that, as with the Cotton–Mouton Effect, *the Kerr Effect is proportional to the square of the field and is often referred to as the quadratic electro-optic effect*. The phenomenon in liquids is attributed to a partial alignment of anisotropic molecules by the $\vec{\mathbf{E}}$-field. In solids the situation is considerably more complicated.

Figure 8.56 depicts an arrangement known as a Kerr shutter or optical modulator. It consists of a glass cell containing two electrodes, which is filled with a polar liquid. This *Kerr cell*, as it is called, is positioned between crossed linear polarizers whose transmission axes are at $\pm 45°$ to the applied $\vec{\mathbf{E}}$-field. With zero voltage across the plates, no light will be transmitted; the shutter is closed. The application of a modulating voltage generates a field, causing the cell to function as a variable wave plate and thus opening the shutter proportionately. The great value of such a device lies in the fact that it can respond effectively to frequencies roughly as high as 10^{10} Hz. Kerr cells, usually containing nitrobenzene or carbon

Giesecke+Devrient GmbH,
Giesecke+Devrient Currency Technology GmbH,
and Papierfabrik Louisenthal GmbH. - Ex. 1027

TABLE 8.3 Kerr Constants for Some Selected Liquids (20°C, $\lambda_0 = 589.3$ nm)

	Substance	K (in units of 10^{-7} cm statvolt^{-2})
Benzene	C_6H_6	0.6
Carbon disulfide	CS_2	3.2
Chloroform	$CHCl_3$	−3.5
Water	H_2O	4.7
Nitrotoluene	$C_5H_7NO_2$	123
Nitrobenzene	$C_6H_5NO_2$	220

disulfide, have been used for a number of years in a variety of applications. They serve as shutters in high-speed photography and as light-beam choppers to replace rotating toothed wheels. As such, they have been utilized in measurements of the speed of light. Kerr cells are also used as Q-switches in pulsed laser systems.

If the plates functioning as the electrodes have an effective length of ℓ cm and are separated by a distance d, the retardation is given by

$$\Delta\varphi = 2\pi K \ell V^2/d^2 \tag{8.41}$$

where V is the applied voltage. Thus a nitrobenzene cell in which d is one cm and ℓ is several cm will require a rather large voltage, roughly 3×10^4 V, in order to respond as a half-wave plate. This is a characteristic quantity known as the *half-wave voltage*, $V_{\lambda/2}$. Another drawback is that nitrobenzene is both poisonous and explosive. Transparent solid substances, such as the mixed crystal potassium tantalate niobate ($KTa_{0.65}Nb_{0.35}O_3$), KTN for short, or barium titanate ($BaTiO_3$), which show a Kerr Effect, are therefore of interest as electro-optical modulators.

There is another very important electro-optical effect known as the *Pockels Effect*, after the German physicist Friedrich Carl Alwin Pockels (1865–1913), who studied it extensively in 1893. It is a linear electro-optical effect, inasmuch as the induced birefringence is proportional to the first power of the applied $\vec{\mathbf{E}}$-field and therefore the applied voltage. The Pockels Effect exists only in certain crystals that lack a center of symmetry—in other words, crystals having no central point through which every atom can be reflected into an identical atom. There are 32 crystal symmetry classes, 20 of which may show the Pockels Effect. Incidentally, these same 20 classes are also piezoelectric. Thus, many crystals and all liquids are excluded from displaying a linear electro-optic effect.

The first practical Pockels cell, which could perform as a shutter or modulator, was not made until the 1940s, when suitable crystals were finally developed. The operating principle for such a device is one we've already discussed. In brief, the birefringence is varied electronically by means of a controlled applied electric field. The retardance can be altered as desired, thereby changing the state of polarization of the incident linear wave. In this way, the system functions as a polarization modulator. Early devices were made of ammonium dihydrogen phosphate ($NH_4H_2PO_4$), or ADP, and potassium dihydrogen phosphate (KH_2PO_4), known as KDP; both are still in use. A great improvement was provided by the introduction of single crystals of potassium dideuterium phosphate (KD_2PO_4), or KD*P, which yields the same retardation with voltages less than half of those needed for KDP. This process of infusing crystals with deuterium is accomplished by growing them in a solution of heavy water. Cells made with KD*P or CD*A (cesium dideuterium arsenate) have been produced commercially for some time.

A *Pockels cell* is simply an appropriate noncentrosymmetric, oriented, single crystal immersed in a controllable electric field. Such devices can usually be operated at fairly low voltages (roughly 5 to 10 times less than that of an equivalent Kerr cell); they are linear, and of course there is no problem with toxic liquids. The response time of KDP is quite short, typically less than 10 ns, and it can modulate a light beam at up to about 25 GHz (i.e., 25×10^9 Hz).

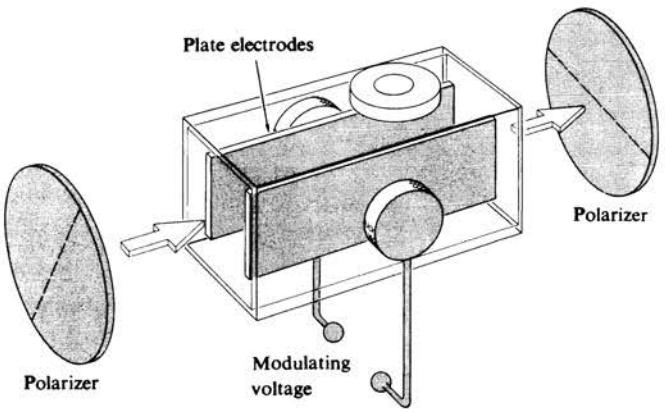


Figure 8.56 A Kerr cell.

Giesecke+Devrient GmbH,
Giesecke+Devrient Currency Technology GmbH,
and Papierfabrik Louisenthal GmbH. - Ex. 1027

There are two common cell configurations, referred to as *transverse* and *longitudinal*, depending on whether the applied $\vec{\mathbf{E}}$-field is perpendicular or parallel to the direction of propagation, respectively. The longitudinal type is illustrated, in its most basic form, in Fig. 8.57. Since the beam traverses the electrodes, these are usually made of transparent metal-oxide coatings (e.g., SnO, InO, or CdO), thin metal films, grids, or rings. The crystal itself is generally uniaxial in the absence of an applied field, and it is aligned such that its optic axis is along the beam's propagation direction. For such an arrangement the retardance is given by

$$\Delta\varphi = 2\pi n_o^3 r_{63} V/\lambda_0 \tag{8.42}$$

where r_{63} is the *electro-optic constant* in m/V, n_o is the *ordinary* index of refraction, V is the potential difference in volts, and λ_0 is the vacuum wavelength in meters.* Since the crystals are anisotropic, their properties vary in different directions, and they must be described by a group of terms referred to collectively as the second-rank electro-optic tensor r_{ij}. Fortunately, we need only concern ourselves here with one of its components, namely, r_{63}, values of which are given in Table 8.4. The half-wave voltage corresponds to a value of $\Delta\varphi = \pi$, in which case

$$\Delta\varphi = \pi \frac{V}{V_{\lambda/2}} \tag{8.43}$$

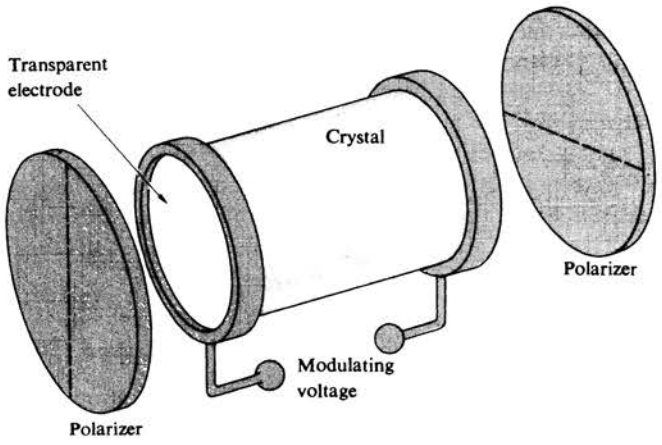


Figure 8.57 A Pockels cell.

*This expression, along with the appropriate one for the transverse mode, is derived rather nicely in A. Yariv, *Quantum Electronics*. Even so, the treatment is sophisticated and not recommended for casual reading.

TABLE 8.4 Electro-optic Constants (Room Temperature, $\lambda_0 = 546.1$ nm)

Material	r_{63} (units of 10^{-12} m/V)	n_o (approx.)	$V_{\lambda/2}$ (in kV)
ADP ($NH_4H_2PO_4$)	8.5	1.52	9.2
KDP (KH_2PO_4)	10.6	1.51	7.6
KDA (KH_2AsO_4)	~13.0	1.57	~6.2
KD*P (KD_2PO_4)	~23.3	1.52	~3.4

and from Eq. (8.42)

$$V_{\lambda/2} = \frac{\lambda_0}{2n_o^3 r_{63}} \tag{8.44}$$

As an example, for KDP, $r_{63} = 10.6 \times 10^{-12}$ m/V, $n_o = 1.51$, and we obtain $V_{\lambda/2} \approx 7.6 \times 10^3$ V at $\lambda_0 = 546.1$ nm.

Pockels cells have been used as ultra-fast shutters, Q-switches for lasers, and dc to 30-GHz light modulators.*

8.12 Liquid Crystals

In 1888 the Austrian botanist Friedrich Reintzer observed that cholesteryl benzoate seemed to have two distinct transition points, one at which the crystal changed into a cloudy liquid and another where it became transparent. Known today as **liquid crystal**, he had discovered a new phase of matter that possessed physical properties between those of ordinary liquids and solids. Liquid crystals (LCs) have long cigar-shaped molecules that can move about, and consequently, like ordinary liquids, they lack positional order. Nonetheless, like crystals, their molecules strongly interact to sustain a large-scale orientational order. There are three types of liquid crystal distinguished by the ways in which their molecules align. We'll focus on the **nematic** variety where the molecules tend to be more or less parallel, even though their positions are fairly random (Fig. 8.58).

To prepare a ***parallel nematic cell***, we first coat one face of each of two pieces of flat glass with a transparent electrically conducting metallic film, such as indium tin oxide (which has maximum transmission from 450 to 1800 nm). These two win-

*The reader interested in light modulation in general should consult D. F. Nelson, "The Modulation of Laser Light," *Scientific American* (June 1968). Also see Chapter 14, Vol. II of *Handbook of Optics* (1995).

Giesecke+Devrient GmbH,
Giesecke+Devrient Currency Technology GmbH,
and Papierfabrik Louisenthal GmbH. - Ex. 1027

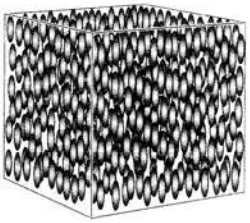


Figure 8.58 The long cigar-shaped molecules of a nematic liquid crystal align themselves in a random but parallel formation.

dows will also serve as the electrodes, between which we'll place the liquid crystal and across which we'll apply a controlling voltage. We want the LC molecules in contact with the windows to be oriented in a direction that is both parallel to the glass and to each other. To accomplish that, it's necessary to create a template of parallel ridges along which the LC molecules can align. There are several ways to do that, the simplest being to just carefully rub the indium tin oxide surface (or a thin dielectric layer covering it), thereby producing parallel microgrooves.

When the thin space (from just a few microns up to about 10 μm) between two such prepared glass windows is filled with nematic LC, the molecules in contact with the microgrooves anchor themselves parallel to the ridges. The LC molecules then essentially drag each other into alignment, and soon the entire liquid is similarly oriented (Fig. 8.59*a*). The direction in which the molecules of a liquid crystal are aligned is known as the ***director***.

Because of their elongated shape and ordered orientation, the liquid crystal molecules behave *en masse* as an anisotropic dielectric, one that's positive uniaxial birefringent. The long axis of the molecules defines the direction of the extraordinary index or slow axis. A ray of light linearly polarized parallel to the LC director will be an extraordinary ray and will experience an ongoing phase change as it traverses the cell. By contrast, a ray linearly polarized at 45° to the director will suffer a retardance $\Delta\varphi$ just as if it had passed through a birefringent crystal.

The Liquid Crystal Variable Retarder

Now suppose we apply a voltage (V) across the cell (Fig. 8.59*b*), thereby creating an electric field perpendicular to the glass windows. Electric dipoles are either present or induced, and the LC molecules experience torques that cause them to try to rotate into alignment with the field. As the voltage increases the molecules (except for those anchored to the inner surfaces of the windows), more and more turn toward the direction of the field, decreasing the birefringence, $\Delta n = (n_e - n_o)$, and the retardance $\Delta\varphi$ as well. Since the birefringence (usually from 0.1 to 0.3) is a function of the voltage, temperature (decreasing about 0.4% per °C increase), and wavelength (decreasing as λ_0 increases)

$$\Delta\varphi(V,T,\lambda_0) = \frac{2\pi}{\lambda_0} d\Delta n(V,T,\lambda_0)$$

Maximum retardance (typically $\approx\lambda_0/2$) obtains when the applied voltage is zero. The retardance when V is large (say, 20 V) is a minimum of around 30 nm (or zero, when a compensator is used to cancel the residual retardance of the anchored layers).

When the incident light is polarized parallel to the slow axis, the device can be used as a voltage-controlled ***phase modulator***. It can change the phase delay the light will experience in traversing the cell. Alternatively, when the light has components parallel and perpendicular to the slow axis, the LC cell functions as a ***continuously variable retarder*** over a broad range of frequencies. By placing the cell between crossed polarizers (at ±45°), it becomes a voltage-controlled ***irradiance modulator***.

The Liquid Crystal Display

Imagine that one of the windows of the parallel LC cell in Fig. 8.59*a* is now rotated 90° in its own plane. This drags around the nematic liquid so that its molecular layers spiral a quarter of a turn about the twist axis normal to the windows

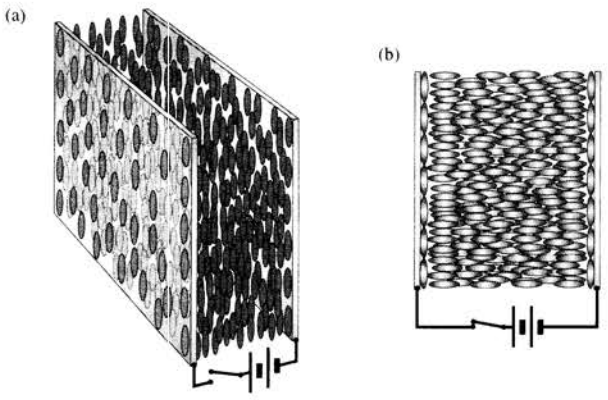


Figure 8.59 (*a*) A nematic liquid crystal between two transparent electrodes. The long molecules align parallel to a set of microgrooves on the inside faces of the two electrodes. (*b*) When a voltage is applied, the molecules rotate into alignment with the field.

Giesecke+Devrient GmbH,
Giesecke+Devrient Currency Technology GmbH,
and Papierfabrik Louisenthal GmbH. - Ex. 1027

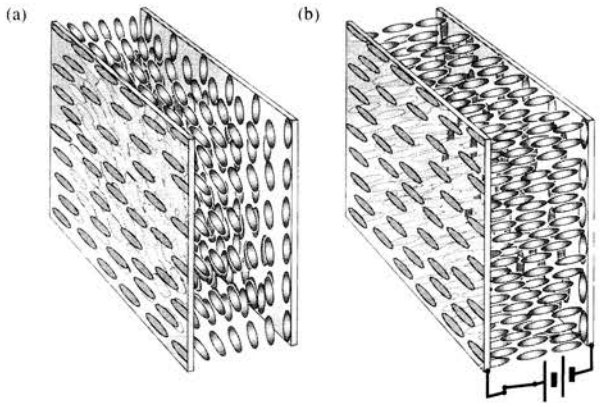


Figure 8.60 (*a*) A twisted nematic cell. The LC molecules are aligned horizontally on the left window and vertically on the right window, and they gradually twist (plane upon plane) from one to the other. (*b*) When a voltage is applied across the cell, the molecules align with the electric field.

(much like putting a deck of cards between your two hands and fanning it around). The result is a so-called **twisted nematic cell** (Fig. 8.60*a*). The molecules are aligned vertically on one window, and gradually they're rotated, layer upon layer, until they are horizontal on the other window. The cell will rotate the plane of polarization as if it were an optically active medium.* For example, a beam of linear light traveling normal to the entrance window and polarized parallel to the anchored molecules in Fig. 8.60*a*, that is horizontally, will be rotated through 90° and emerge vertically polarized.

Upon putting a voltage across the cell, an electric field parallel to the twist axis is set up throughout the liquid crystal. Consequently, the LC molecules (except for those anchored to the windows) turn into alignment with the field (Fig. 8.60*b*). The twisted structure of the cell vanishes, and it loses its ability to rotate the plane of polarization of incident light. When the E-field is removed, the cell reverts back to its twisted configuration and can again rotate light. If the cell is now placed between crossed linear polarizers (Fig. 8.61), it becomes a ***voltage-controlled switch*** that can transmit or absorb an incident beam of light.

The simplest liquid crystal display (LCD), the kind found in digital watches, clocks, cameras, calculators, and so forth, is illuminated by ambient light. Therein lies its principlal virtue: it consumes very little electrical power because it isn't self-luminous.

To make an LCD, we just put a flat mirror beyond the last polarizer on the right in Fig. 8.61. Ambient light enters from the left and is immediately linearly polarized, in this case horizontally. With no voltage on the electrodes the light emerges from the twisted LC cell oscillating vertically. It passes through the second polarizer—unaffected by it—strikes the mirror, and reflects off to the left still oscillating vertically. It then retraces its path back through the LC cell, from which it exits traveling to the left, horizontally polarized. Looking into the first polarizer, we see a relatively bright field of emerging light.

When a voltage is applied across the cell, the liquid crystal reorients itself and loses its ability to rotate the plane of polarization. Horizontal light enters and leaves the cell, only to be completely absorbed by the second polarizer; the entrance window is now black, and no light emerges.

By properly configuring the front transparent electrode, the black nonreflecting region can be confined to the shape of a number or letter, or anything you like. Usually the numbers on your calculator are produced using seven small bar electrodes (Fig. 8.62) that are activated independently (by the decoder-driver in an integrated circuit) to create all the digits from 0 to 9. These bars are formed as isolated regions on the front indium tin oxide film. When a voltage is put across a given bar and the large continuous back electrode, the E-field just behind the bar destroys the LC twist in that small region and that segment turns black.

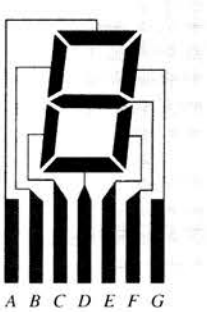


Figure 8.62 A seven-bar electrode array used to display numerals. For example, to form the number 9, a voltage is applied between all of the following segments and the large back electrode, *D*, *E*, *F*, *G*, *A*, and *B*.

*For a proof of this, see B. E. A. Saleh and M. C. Teich, *Fundamentals of Photonics*, p. 228.

Giesecke+Devrient GmbH,
Giesecke+Devrient Currency Technology GmbH,
and Papierfabrik Louisenthal GmbH. - Ex. 1027

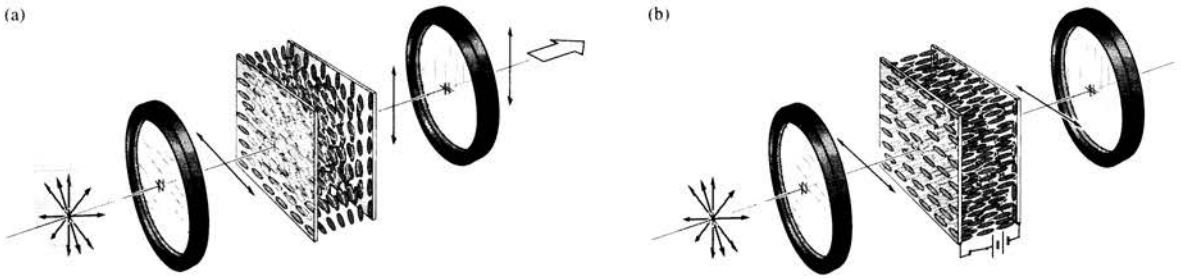
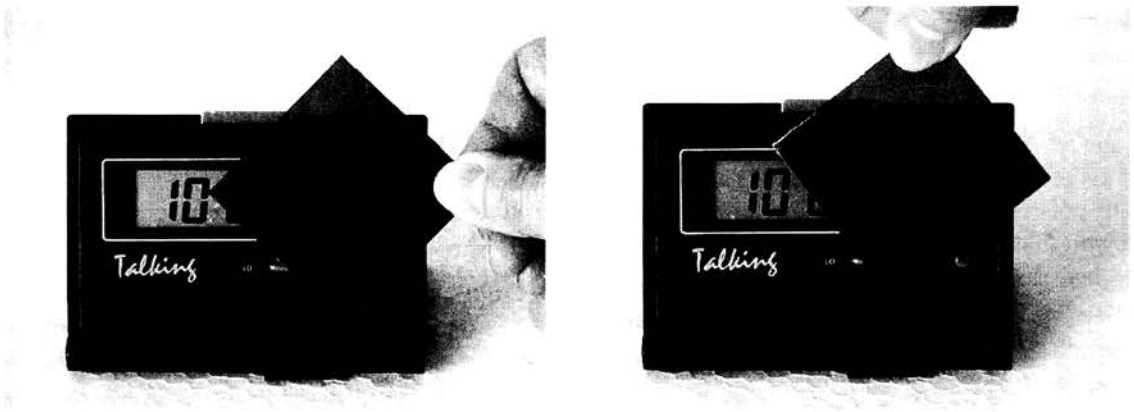


Figure 8.61 (*a*) A twisted nematic cell between crossed linear polarizers. Light polarized vertically emerges from the device. (*b*) When a voltage is applied across the cell it no longer rotates the plane of polarization; light polarized horizontally enters and leaves the LC cell. That light is subsequently absorbed by the second polarizer and no light emerges from the device.



By rotating a linear polarizer in front of a liquid crystal display we can see the numbers appear and disappear. Try it with your calculator. (Photo by E.H.)

8.13 A Mathematical Description of Polarization

Until now we've considered polarized light in terms of the electric field component of the wave. The most general representation was, of course, that of elliptical light. The endpoint of the vector $\vec{\mathbf{E}}$ was envisioned continuously sweeping along the path of an ellipse having a particular shape—the circle and line being special cases. The period over which the ellipse was traversed equaled that of the lightwave (i.e., roughly 10^{-15} s) and was far too short to be detected. In contrast, measurements made in practice are generally averages over comparatively long time intervals.

Clearly, it would be advantageous to formulate an alternative description of polarization in terms of convenient observables, namely, irradiances. Our motives are far more than the ever-present combination of aesthetics and pedagogy. The formalism to be considered has far-reaching significance in

Giesecke+Devrient GmbH,
Giesecke+Devrient Currency Technology GmbH,
and Papierfabrik Louisenthal GmbH. - Ex. 1027

other areas of study, for example, particle physics (the photon is, after all an elementary particle) and Quantum Mechanics. It serves in some respects to link the classical and quantum-mechanical pictures. But even more demanding of our present attention are the considerable practical advantages to be gleaned from this alternative description.

We shall evolve an elegant procedure for predicting the effects of complex systems of polarizing elements on the ultimate state of an emergent wave. The mathematics, written in the compressed form of matrices, will require only the simplest manipulation of those matrices. The complicated logic associated with phase retardations, relative orientations, and so forth, for a tandem series of wave plates and polarizers is almost all built in. One need only select appropriate matrices from a chart and drop them into the mathematical mill.

8.13.1 The Stokes Parameters

The modern representation of polarized light actually had its origins in 1852 in the work of G. G. Stokes. He introduced four quantities that are functions only of observables of the electromagnetic wave and are now known as the **Stokes parameters**.* The polarization state of a beam of light (either natural or totally or partially polarized) can be described in terms of these quantities. We will first define the parameters operationally and then relate them to electromagnetic theory.

Imagine that we have a set of four filters, each of which, under *natural* illumination, will transmit half the incident light, the other half being discarded. The choice is not a unique one, and a number of equivalent possibilities exist. Suppose then that the first filter is simply isotropic, passing all states equally, whereas the second and third are linear polarizers whose transmission axes are horizontal and at $+45°$ (diagonal along the first and third quadrants), respectively. The last filter is a circular polarizer opaque to $\mathscr{L}$-states. Each of these four filters is positioned alone in the path of the beam under investigation, and the transmitted irradiances I_0, I_1, I_2, I_3 are measured with a type of meter that is insensitive to polarization (not all of them are). The operational definition of the Stokes parameters is then given by the relations

$$\mathscr{S}_0 = 2I_0 \tag{8.45a}$$

$$\mathscr{S}_1 = 2I_1 - 2I_0 \tag{8.45b}$$

$$\mathscr{S}_2 = 2I_2 - 2I_0 \tag{8.45c}$$

$$\mathscr{S}_3 = 2I_3 - 2I_0 \tag{8.45d}$$

Notice that $\mathscr{S}_0$ is simply the incident irradiance, and $\mathscr{S}_1$, $\mathscr{S}_2$, and $\mathscr{S}_3$ specify the state of polarization. Thus $\mathscr{S}_1$ reflects a tendency for the polarization to resemble either a horizontal $\mathscr{P}$-state (whereupon $\mathscr{S}_1 > 0$) or a vertical one (in which case $\mathscr{S}_1 < 0$). When the beam displays no preferential orientation with respect to these axes ($\mathscr{S}_1 = 0$), it may be elliptical at $\pm 45°$, circular, or unpolarized. Similarly, $\mathscr{S}_2$ implies a tendency for the light to resemble a $\mathscr{P}$-state oriented in the direction of $+45°$ (when $\mathscr{S}_2 > 0$) or in the direction of $-45°$ (when $\mathscr{S}_2 < 0$) or neither ($\mathscr{S}_2 = 0$). In the same way $\mathscr{S}_3$ reveals a tendency of the beam toward right-handedness ($\mathscr{S}_3 > 0$), left-handedness ($\mathscr{S}_3 < 0$), or neither ($\mathscr{S}_3 = 0$).

Now recall the expressions for quasimonochromatic light,

$$\vec{\mathbf{E}}_x(t) = \hat{\mathbf{i}} E_{0x}(t) \cos\left[(\bar{k}z - \bar{\omega}t) + \varepsilon_x(t)\right] \tag{8.34a}$$

and

$$\vec{\mathbf{E}}_y(t) = \hat{\mathbf{j}} E_{0y}(t) \cos\left[(\bar{k}z - \bar{\omega}t) + \varepsilon_y(t)\right] \tag{8.34b}$$

where $\vec{\mathbf{E}}(t) = \vec{\mathbf{E}}_x(t) + \vec{\mathbf{E}}_y(t)$. Using these in a fairly straightforward way, we can recast the Stokes parameters* as

$$\mathscr{S}_0 = \langle E_{0x}^2 \rangle_T + \langle E_{0y}^2 \rangle_T \tag{8.46a}$$

$$\mathscr{S}_1 = \langle E_{0x}^2 \rangle_T - \langle E_{0y}^2 \rangle_T \tag{8.46b}$$

$$\mathscr{S}_2 = \langle 2E_{0x}E_{0y} \cos \varepsilon \rangle_T \tag{8.46c}$$

$$\mathscr{S}_3 = \langle 2E_{0x}E_{0y} \sin \varepsilon \rangle_T \tag{8.46d}$$

Here $\varepsilon = \varepsilon_y - \varepsilon_x$ and we've dropped the constant $\epsilon_0 c/2$, so

*Much of the material in this section is treated more extensively in Shurcliff's *Polarized Light: Production and Use*, which is something of a classic on the subject. You might also look at M. J. Walker, "Matrix Calculus and the Stokes Parameters of Polarized Radiation," *Am. J. Phys.* **22**, 170 (1954), and W. Bickel and W. Bailey, "Stokes Vectors, Mueller Matrices, and Polarized Scattered Light," *Am. J. Phys.* **53**, 468 (1985).

*For the details, see E. Hecht, "Note on an Operational Definition of the Stokes Parameters," *Am. J. Phys.* **38**, 1156 (1970).

Giesecke+Devrient GmbH,
Giesecke+Devrient Currency Technology GmbH,
and Papierfabrik Louisenthal GmbH. - Ex. 1027

that the parameters are now *proportional* to irradiances. For the hypothetical case of perfectly monochromatic light, $E_{0x}(t)$, $E_{0y}(t)$, and $\varepsilon(t)$ are time-independent, and one need only drop the $\langle\ \rangle$ brackets in Eq. (8.46) to get the applicable Stokes parameters. Interestingly enough, these same results can be obtained by time averaging Eq. (8.14), which is the general equation for elliptical light.*

If the beam is unpolarized, $\langle E_{0x}^2\rangle_T = \langle E_{0y}^2\rangle_T$; neither averages to zero because the amplitude squared is always positive. In that case $\mathcal{S}_0 = \langle E_{0x}^2\rangle_T + \langle E_{0y}^2\rangle_T$, but $\mathcal{S}_1 = \mathcal{S}_2 = \mathcal{S}_3 = 0$. The latter two parameters go to zero, since both $\cos\varepsilon$ and $\sin\varepsilon$ average to zero independently of the amplitudes. It is often convenient to *normalize* the Stokes parameters by dividing each one by the value of $\mathcal{S}_0$. This has the effect of using an incident beam of unit irradiance. The set of parameters ($\mathcal{S}_0$, $\mathcal{S}_1$, $\mathcal{S}_2$, $\mathcal{S}_3$) for *natural light* in the normalized representation is then (1, 0, 0, 0). If the light is horizontally polarized, it has no vertical component, and the normalized parameters are (1, 1, 0, 0). Similarly, for vertically polarized light we have (1, −1, 0, 0). Representations of a few other polarization states are listed in Table 8.5. (The parameters are displayed vertically for reasons to be discussed later.) Notice that for completely polarized light it follows from Eq. (8.46) that

$$\mathcal{S}_0^2 = \mathcal{S}_1^2 + \mathcal{S}_2^2 + \mathcal{S}_3^2 \tag{8.47}$$

Moreover, for partially polarized light it can be shown that the degree of polarization [Eq. (8.29)] is given by

$$V = (\mathcal{S}_1^2 + \mathcal{S}_2^2 + \mathcal{S}_3^2)^{1/2}/\mathcal{S}_0 \tag{8.48}$$

Imagine now that we have two quasimonochromatic waves described by ($\mathcal{S}_0'$, $\mathcal{S}_1'$, $\mathcal{S}_2'$, $\mathcal{S}_3'$) and ($\mathcal{S}_0''$, $\mathcal{S}_1''$, $\mathcal{S}_2''$, $\mathcal{S}_3''$), which are superimposed in some region of space. As long as the waves are *incoherent*, any one of the Stokes parameters of the resultant will be the sum of the corresponding parameters of the constituents (all of which are proportional to irradiance). In other words, the set of parameters describing the resultant is ($\mathcal{S}_0' + \mathcal{S}_0''$, $\mathcal{S}_1' + \mathcal{S}_1''$, $\mathcal{S}_2' + \mathcal{S}_2''$, $\mathcal{S}_3' + \mathcal{S}_3''$). For example, if a unit-flux density vertical $\mathcal{P}$-state (1, −1, 0, 0) is added to an *incoherent* $\mathcal{L}$-state (see Table 8.5) of flux density 2, (2, 0, 0, −2), the composite wave has parameters (3, −1, 0, −2). It is an ellipse of flux density 3, more nearly vertical than horizontal ($\mathcal{S}_1 < 0$), left-handed ($\mathcal{S}_3 < 0$), and having a degree of polarization of $\sqrt{5}/3$.

TABLE 8.5 Stokes and Jones Vectors for Some Polarization States

State of polarization	Stokes vectors	Jones vectors
Horizontal $\mathcal{P}$-state	$\begin{bmatrix}1\\1\\0\\0\end{bmatrix}$	$\begin{bmatrix}1\\0\end{bmatrix}$
Vertical $\mathcal{P}$-state	$\begin{bmatrix}1\\-1\\0\\0\end{bmatrix}$	$\begin{bmatrix}0\\1\end{bmatrix}$
$\mathcal{P}$-state at +45°	$\begin{bmatrix}1\\0\\1\\0\end{bmatrix}$	$\frac{1}{\sqrt{2}}\begin{bmatrix}1\\1\end{bmatrix}$
$\mathcal{P}$-state at −45°	$\begin{bmatrix}1\\0\\-1\\0\end{bmatrix}$	$\frac{1}{\sqrt{2}}\begin{bmatrix}1\\-1\end{bmatrix}$
$\mathcal{R}$-state	$\begin{bmatrix}1\\0\\0\\1\end{bmatrix}$	$\frac{1}{\sqrt{2}}\begin{bmatrix}1\\-i\end{bmatrix}$
$\mathcal{L}$-state	$\begin{bmatrix}1\\0\\0\\-1\end{bmatrix}$	$\frac{1}{\sqrt{2}}\begin{bmatrix}1\\i\end{bmatrix}$

The set of Stokes parameters for a given wave can be envisaged as a *vector*; we have already seen how two such (incoherent) vectors add.* Indeed, it will not be the usual kind of three-dimensional vector, but this sort of representation is widely used in physics to great advantage. More specifically, the parameters ($\mathcal{S}_0$, $\mathcal{S}_1$, $\mathcal{S}_2$, $\mathcal{S}_3$) are arranged in the form of what

*E. Collett, "The Description of Polarization in Classical Physics," *Am. J. Phys.* **36**, 713 (1968).

*The detailed requirements for a collection of objects to form a vector space and themselves be vectors in such a space are discussed in, for example, Davis, *Introduction to Vector Analysis*.

Giesecke+Devrient GmbH,
Giesecke+Devrient Currency Technology GmbH,
and Papierfabrik Louisenthal GmbH. - Ex. 1027

is called a *column vector*,

$$\mathcal{S} = \begin{bmatrix} s_0 \\ s_1 \\ s_2 \\ s_3 \end{bmatrix} \tag{8.49}$$

8.13.2 The Jones Vectors

Another representation of polarized light, which complements that of the Stokes parameters, was invented in 1941 by the American physicist R. Clark Jones. The technique he evolved has the advantages of being applicable to coherent beams and at the same time being extremely concise. Yet unlike the previous formalism, it is *only applicable to polarized waves*. In that case it would seem that the most natural way to represent the beam would be in terms of the electric vector itself. Written in column form, this *Jones vector* is

$$\vec{\mathbf{E}} = \begin{bmatrix} E_x(t) \\ E_y(t) \end{bmatrix} \tag{8.50}$$

where $E_x(t)$ and $E_y(t)$ are the instantaneous scalar components of $\vec{\mathbf{E}}$. Obviously, knowing $\vec{\mathbf{E}}$, we know everything about the polarization state. And if we preserve the phase information, we will be able to handle coherent waves. With this in mind, rewrite Eq. (8.50) in complex form;

$$\tilde{\mathbf{E}} = \begin{bmatrix} E_{0x} e^{i\varphi_x} \\ E_{0y} e^{i\varphi_y} \end{bmatrix} \tag{8.51}$$

where φ_x and φ_y are the appropriate phases. Horizontal and vertical $\mathcal{P}$-states are thus given by

$$\tilde{\mathbf{E}}_h = \begin{bmatrix} E_{0x} e^{i\varphi_x} \\ 0 \end{bmatrix} \quad \text{and} \quad \tilde{\mathbf{E}}_v = \begin{bmatrix} 0 \\ E_{0y} e^{i\varphi_y} \end{bmatrix} \tag{8.52}$$

respectively. The sum of two coherent beams, as with the Stokes vectors, is formed by a sum of the corresponding components. Since $\tilde{\mathbf{E}} = \tilde{\mathbf{E}}_h + \tilde{\mathbf{E}}_v$, when, for example $E_{0x} = E_{0y}$ and $\varphi_x = \varphi_y$, $\tilde{\mathbf{E}}$ is given by

$$\tilde{\mathbf{E}} = \begin{bmatrix} E_{0x} e^{i\varphi_x} \\ E_{0x} e^{i\varphi_y} \end{bmatrix} \tag{8.53}$$

or, after factoring, by

$$\tilde{\mathbf{E}} = E_{0x} e^{i\varphi_x} \begin{bmatrix} 1 \\ 1 \end{bmatrix} \tag{8.54}$$

which is a $\mathcal{P}$-state at $+45°$. This is the case since the amplitudes are equal and the phase difference is zero.

In many applications it is not necessary to know the exact amplitudes and phases. In such instances we can *normalize* the irradiance to unity, thereby forfeiting some information but gaining much simpler expressions. This is done by dividing both elements in the vector by the same scalar (real or complex) quantity, such that the sum of the squares of the components is one. For example, dividing both terms of Eq. (8.53) by $\sqrt{2}\, E_{0x} e^{i\varphi_x}$ leads to

$$\vec{\mathbf{E}}_{45} = \frac{1}{\sqrt{2}} \begin{bmatrix} 1 \\ 1 \end{bmatrix} \tag{8.55}$$

Similarly, in normalized form

$$\vec{\mathbf{E}}_h = \begin{bmatrix} 1 \\ 0 \end{bmatrix} \quad \text{and} \quad \vec{\mathbf{E}}_v = \begin{bmatrix} 0 \\ 1 \end{bmatrix} \tag{8.56}$$

Right-circular light has $E_{0x} = E_{0y}$, and the y-component leads the x-component by 90°. Since we are using the form $(kz - \omega t)$, we will have to add $-\pi/2$ to φ_y, thus

$$\tilde{\mathbf{E}}_{\mathcal{R}} = \begin{bmatrix} E_{0x} e^{i\varphi_x} \\ E_{0x} e^{i(\varphi_x - \pi/2)} \end{bmatrix}$$

Dividing both components by $E_{0x} e^{i\varphi_x}$ yields

$$\begin{bmatrix} 1 \\ e^{-i\pi/2} \end{bmatrix} = \begin{bmatrix} 1 \\ -i \end{bmatrix}$$

Hence the normalized complex Jones vector is*

$$\tilde{\mathbf{E}}_{\mathcal{R}} = \frac{1}{\sqrt{2}} \begin{bmatrix} 1 \\ -i \end{bmatrix} \quad \text{and similarly} \quad \tilde{\mathbf{E}}_{\mathcal{L}} = \frac{1}{\sqrt{2}} \begin{bmatrix} 1 \\ i \end{bmatrix} \tag{8.57}$$

The sum $\tilde{\mathbf{E}}_{\mathcal{R}} + \tilde{\mathbf{E}}_{\mathcal{L}}$ is

$$\frac{1}{\sqrt{2}} \begin{bmatrix} 1+1 \\ -i+i \end{bmatrix} = \frac{2}{\sqrt{2}} \begin{bmatrix} 1 \\ 0 \end{bmatrix}$$

This is a horizontal $\mathcal{P}$-state having an amplitude twice that of either component, a result in agreement with our earlier calculation of Eq. (8.10). The Jones vector for elliptical light can be obtained by the same procedure used to arrive at $\tilde{\mathbf{E}}_{\mathcal{R}}$ and

*Had we used $(\omega t - kz)$ for the phase, the terms in $\tilde{\mathbf{E}}_{\mathcal{R}}$ would have been interchanged. The present notation, although possibly a bit more difficult to keep straight (e.g., $-\pi/2$ for a phase lead), is more often used in modern works. Be wary when consulting references (e.g., Shurcliff).

Giesecke+Devrient GmbH,
Giesecke+Devrient Currency Technology GmbH,
and Papierfabrik Louisenthal GmbH. - Ex. 1027

$\tilde{\mathbf{E}}_{\mathscr{L}}$, where now E_{0x} may not be equal to E_{0y}, and the phase difference need not be 90°. In essence, for vertical and horizontal $\mathscr{E}$-states all we need to do is stretch out the circular form into an ellipse by multiplying either component by a scalar. Thus

$$\frac{1}{\sqrt{5}}\begin{bmatrix} 2 \\ -i \end{bmatrix} \tag{8.58}$$

describes one possible form of horizontal, right-handed, elliptical light.

Two vectors $\vec{\mathbf{A}}$ and $\vec{\mathbf{B}}$ are said to be orthogonal when $\vec{\mathbf{A}}\cdot\vec{\mathbf{B}} = 0$; similarly, two complex vectors are orthogonal when $\tilde{\mathbf{A}}\cdot\tilde{\mathbf{B}}^* = 0$. One refers to two polarization states as being *orthogonal* when their Jones vectors are orthogonal. For example,

$$\tilde{\mathbf{E}}_{\mathscr{R}}\cdot\tilde{\mathbf{E}}^*_{\mathscr{L}} = \tfrac{1}{2}[(1)(1)^* + (-i)(i)^*] = 0$$

or

$$\tilde{\mathbf{E}}_{h}\cdot\tilde{\mathbf{E}}^*_{v} = [(1)(0)^* + (0)(1)^*] = 0$$

where taking the complex conjugates of real numbers obviously leaves them unaltered. Any polarization state will have a corresponding orthogonal state. Notice that

$$\tilde{\mathbf{E}}_{\mathscr{R}}\cdot\tilde{\mathbf{E}}_{\mathscr{R}} = \tilde{\mathbf{E}}_{\mathscr{L}}\cdot\tilde{\mathbf{E}}^*_{\mathscr{L}} = 1$$

and

$$\tilde{\mathbf{E}}_{\mathscr{R}}\cdot\tilde{\mathbf{E}}^*_{\mathscr{L}} = \tilde{\mathbf{E}}_{\mathscr{L}}\cdot\tilde{\mathbf{E}}^*_{\mathscr{R}} = 0$$

Such vectors form an *orthogonal set*, as do $\tilde{\mathbf{E}}_h$ and $\tilde{\mathbf{E}}_v$. As we have seen, any polarization state can be described by a linear combination of the vectors in either one of the orthonormal sets. These same ideas are of considerable importance in Quantum Mechanics, where one deals with orthonormal wavefunctions.

8.13.3 The Jones and Mueller Matrices

Suppose that we have a polarized incident beam represented by its Jones vector $\tilde{\mathbf{E}}_i$, which passes through an optical element, emerging as a new vector $\tilde{\mathbf{E}}_t$ corresponding to the transmitted wave. The optical element has transformed $\tilde{\mathbf{E}}_i$ into $\tilde{\mathbf{E}}_t$, a process that can be described mathematically using a 2×2 matrix. Recall that a matrix is just an array of numbers that has prescribed addition and multiplication operations. Let $\mathscr{A}$ represent the transformation matrix of the optical element in question. Then

$$\tilde{\mathbf{E}}_t = \mathscr{A}\tilde{\mathbf{E}}_i \tag{8.59}$$

where

$$\mathscr{A} = \begin{bmatrix} a_{11} & a_{12} \\ a_{21} & a_{22} \end{bmatrix} \tag{8.60}$$

and the column vectors are to be treated like any other matrices. As a reminder, write Eq. (8.59) as

$$\begin{bmatrix} \tilde{E}_{tx} \\ \tilde{E}_{ty} \end{bmatrix} = \begin{bmatrix} a_{11} & a_{12} \\ a_{21} & a_{22} \end{bmatrix}\begin{bmatrix} \tilde{E}_{ix} \\ \tilde{E}_{iy} \end{bmatrix} \tag{8.61}$$

and, upon expanding,

$$\tilde{E}_{tx} = a_{11}\tilde{E}_{ix} + a_{12}\tilde{E}_{iy}$$

$$\tilde{E}_{ty} = a_{21}\tilde{E}_{ix} + a_{22}\tilde{E}_{iy}$$

Table 8.6 contains a brief listing of Jones matrices for various optical elements. To appreciate how these are used let's examine a few applications. Suppose that $\tilde{\mathbf{E}}_i$ represents a $\mathscr{P}$-state at +45°, which passes through a quarter-wave plate whose fast axis is vertical (i.e., in the y-direction). The polarization state of the emergent wave is found as follows, where we drop the constant-amplitude factors for convenience:

$$\begin{bmatrix} 1 & 0 \\ 0 & -i \end{bmatrix}\begin{bmatrix} 1 \\ 1 \end{bmatrix} = \begin{bmatrix} \tilde{E}_{tx} \\ \tilde{E}_{ty} \end{bmatrix}$$

and thus

$$\tilde{\mathbf{E}}_t = \begin{bmatrix} 1 \\ -i \end{bmatrix}$$

The beam, as you well know, is right-circular. If the wave passes through a series of optical elements represented by the matrices $\mathscr{A}_1, \mathscr{A}_2, \ldots, \mathscr{A}_n$, then

$$\tilde{\mathbf{E}}_t = \mathscr{A}_n \cdots \mathscr{A}_2\mathscr{A}_1\tilde{\mathbf{E}}_t$$

The matrices do not commute; they must be applied in the proper order. The wave leaving the first optical element in the series is $\mathscr{A}_1\tilde{\mathbf{E}}_i$; after passing through the second element, it becomes $\mathscr{A}_2\mathscr{A}_1\tilde{\mathbf{E}}_i$, and so on. To illustrate the process, return to the wave considered above (i.e., a $\mathscr{P}$-state at +45°), but now have it pass through two quarter-wave plates, both with their fast axes vertical. Thus, again discarding the amplitude factors, we have

$$\tilde{\mathbf{E}}_t = \begin{bmatrix} 1 & 0 \\ 0 & -i \end{bmatrix}\begin{bmatrix} 1 & 0 \\ 0 & -i \end{bmatrix}\begin{bmatrix} 1 \\ 1 \end{bmatrix}$$

whereupon

$$\tilde{\mathbf{E}}_t = \begin{bmatrix} 1 & 0 \\ 0 & -i \end{bmatrix}\begin{bmatrix} 1 \\ -i \end{bmatrix}$$

Giesecke+Devrient GmbH,
Giesecke+Devrient Currency Technology GmbH,
and Papierfabrik Louisenthal GmbH. - Ex. 1027

TABLE 8.6 Jones and Mueller matrices.

Linear optical element	Jones matrix	Mueller matrix
Horizontal linear polarizer ↔	$\begin{bmatrix} 1 & 0 \\ 0 & 0 \end{bmatrix}$	$\frac{1}{2}\begin{bmatrix} 1 & 1 & 0 & 0 \\ 1 & 1 & 0 & 0 \\ 0 & 0 & 0 & 0 \\ 0 & 0 & 0 & 0 \end{bmatrix}$
Vertical linear polarizer ↕	$\begin{bmatrix} 0 & 0 \\ 0 & 1 \end{bmatrix}$	$\frac{1}{2}\begin{bmatrix} 1 & -1 & 0 & 0 \\ -1 & 1 & 0 & 0 \\ 0 & 0 & 0 & 0 \\ 0 & 0 & 0 & 0 \end{bmatrix}$
Linear polarizer at +45° ↗	$\frac{1}{2}\begin{bmatrix} 1 & 1 \\ 1 & 1 \end{bmatrix}$	$\frac{1}{2}\begin{bmatrix} 1 & 0 & 1 & 0 \\ 0 & 0 & 0 & 0 \\ 1 & 0 & 1 & 0 \\ 0 & 0 & 0 & 0 \end{bmatrix}$
Linear polarizer at −45° ↘	$\frac{1}{2}\begin{bmatrix} 1 & -1 \\ -1 & 1 \end{bmatrix}$	$\frac{1}{2}\begin{bmatrix} 1 & 0 & -1 & 0 \\ 0 & 0 & 0 & 0 \\ -1 & 0 & 1 & 0 \\ 0 & 0 & 0 & 0 \end{bmatrix}$
Quarter-wave plate, fast axis vertical	$e^{i\pi/4}\begin{bmatrix} 1 & 0 \\ 0 & -i \end{bmatrix}$	$\begin{bmatrix} 1 & 0 & 0 & 0 \\ 0 & 1 & 0 & 0 \\ 0 & 0 & 0 & -1 \\ 0 & 0 & 1 & 0 \end{bmatrix}$
Quarter-wave plate, fast axis horizontal	$e^{i\pi/4}\begin{bmatrix} 1 & 0 \\ 0 & i \end{bmatrix}$	$\begin{bmatrix} 1 & 0 & 0 & 0 \\ 0 & 1 & 0 & 0 \\ 0 & 0 & 0 & 1 \\ 0 & 0 & -1 & 0 \end{bmatrix}$
Homogeneous circular polarizer right ↻	$\frac{1}{2}\begin{bmatrix} 1 & i \\ -i & 1 \end{bmatrix}$	$\frac{1}{2}\begin{bmatrix} 1 & 0 & 0 & 1 \\ 0 & 0 & 0 & 0 \\ 0 & 0 & 0 & 0 \\ 1 & 0 & 0 & 1 \end{bmatrix}$
Homogeneous circular polarizer left ↺	$\frac{1}{2}\begin{bmatrix} 1 & -i \\ i & 1 \end{bmatrix}$	$\frac{1}{2}\begin{bmatrix} 1 & 0 & 0 & -1 \\ 0 & 0 & 0 & 0 \\ 0 & 0 & 0 & 0 \\ -1 & 0 & 0 & 1 \end{bmatrix}$

and finally

$$\tilde{\mathbf{E}}_t = \begin{bmatrix} 1 \\ -1 \end{bmatrix}$$

The transmitted beam is a $\mathscr{P}$-state at −45°, having essentially been flipped through 90° by a half-wave plate. When the same series of optical elements is used to examine various states, it becomes desirable to replace the product $\mathscr{A}_n \cdots \mathscr{A}_2\mathscr{A}_1$ by the single 2×2 *system matrix* obtained by carrying out the multiplication. (The order in which it is calculated should be $\mathscr{A}_2\mathscr{A}_1$, then $\mathscr{A}_3\mathscr{A}_2\mathscr{A}_1$, etc.)

In 1943 Hans Mueller, then a professor of physics at the Massachusetts Institute of Technology, devised a matrix method for dealing with the Stokes vectors. Recall that the Stokes vectors have the attribute of being applicable to both polarized and partially polarized light. The Mueller method shares this quality and thus serves to complement the Jones method. The latter, however, can easily deal with coherent waves, whereas the former cannot. The Mueller, 4×4, matrices are applied in much the same way as are the Jones matrices. There is therefore little need to discuss the method at length; a few simple examples, augmented by Table 8.6, should suffice. Imagine that we pass a unit-irradiance unpolarized wave through a linear horizontal polarizer. The Stokes vector of the emerging wave $\mathcal{S}_t$ is

$$\mathcal{S}_t = \frac{1}{2}\begin{bmatrix} 1 & 1 & 0 & 0 \\ 1 & 1 & 0 & 0 \\ 0 & 0 & 0 & 0 \\ 0 & 0 & 0 & 0 \end{bmatrix}\begin{bmatrix} 1 \\ 0 \\ 0 \\ 0 \end{bmatrix} = \begin{bmatrix} \frac{1}{2} \\ \frac{1}{2} \\ 0 \\ 0 \end{bmatrix}$$

The transmitted wave has an irradiance of $\frac{1}{2}$ (i.e., $\mathcal{S}_0 = \frac{1}{2}$) and is linearly polarized horizontally ($\mathcal{S}_1 > 0$). As another example, suppose we have a partially polarized elliptical wave whose Stokes parameters have been determined to be, say, (4, 2, 0, 3). Its irradiance is 4; it is more nearly horizontal than vertical ($\mathcal{S}_1 > 0$), it is right-handed ($\mathcal{S}_3 > 0$), and it has a degree of polarization of 90%. Since none of the parameters can be larger than $\mathcal{S}_0$, a value of $\mathcal{S}_3 = 3$ is fairly large, indicating that the ellipse resembles a circle. If the wave is now made to traverse a quarter-wave plate with a vertical fast axis, then

$$\mathcal{S}_t = \begin{bmatrix} 1 & 0 & 0 & 0 \\ 0 & 1 & 0 & 0 \\ 0 & 0 & 0 & -1 \\ 0 & 0 & 1 & 0 \end{bmatrix}\begin{bmatrix} 4 \\ 2 \\ 0 \\ 3 \end{bmatrix}$$

Giesecke+Devrient GmbH,
Giesecke+Devrient Currency Technology GmbH,
and Papierfabrik Louisenthal GmbH. - Ex. 1027

and thus

$$\mathcal{S}_t = \begin{bmatrix} 4 \\ 2 \\ -3 \\ 0 \end{bmatrix}$$

The emergent wave has the same irradiance and degree of polarization but is now partially linearly polarized.

We have only touched on a few of the more important aspects of the matrix methods. The full extent of the subject goes far beyond these introductory remarks.*

*One can weave a more elaborate and mathematically satisfying development in terms of something called the coherence matrix. For further, but more advanced, reading, see O'Neill, *Introduction to Statistical Optics*.

PROBLEMS

Complete solutions to all problems—except those with an asterisk—can be found in the back of the book.

8.1 Describe completely the state of polarization of each of the following waves:

(a) $\vec{\mathbf{E}} = \hat{\mathbf{i}}E_0 \cos(kz - \omega t) - \hat{\mathbf{j}}E_0 \cos(kz - \omega t)$

(b) $\vec{\mathbf{E}} = \hat{\mathbf{i}}E_0 \sin 2\pi(z/\lambda - \nu t) - \hat{\mathbf{j}}E_0 \sin 2\pi(z/\lambda - \nu t)$

(c) $\vec{\mathbf{E}} = \hat{\mathbf{i}}E_0 \sin(\omega t - kz) + \hat{\mathbf{j}}E_0 \sin(\omega t - kz - \pi/4)$

(d) $\vec{\mathbf{E}} = \hat{\mathbf{i}}E_0 \cos(\omega t - kz) + \hat{\mathbf{j}}E_0 \cos(\omega t - kz + \pi/2)$.

8.2 Consider the disturbance given by the expression $\vec{\mathbf{E}}(z, t) = [\hat{\mathbf{i}} \cos \omega t + \hat{\mathbf{j}} \cos(\omega t - \pi/2)]E_0 \sin kz$. What kind of wave is it? Draw a rough sketch showing its main features.

8.3 Analytically, show that the superposition of an $\mathscr{R}$- and an $\mathscr{L}$-state having different amplitudes will yield an $\mathscr{E}$-state, as shown in Fig. 8.8. What must ε be to duplicate that figure?

8.4 Write an expression for a $\mathscr{P}$-state lightwave of angular frequency ω and amplitude E_0 propagating along the x-axis with its plane of vibration at an angle of 25° to the xy-plane. The disturbance is zero at $t = 0$ and $x = 0$.

8.5* Write an expression for a $\mathscr{P}$-state lightwave of angular frequency ω and amplitude E_0 propagating along a line in the xy-plane at 45° to the x-axis and having its plane of vibration corresponding to the xy-plane. At $t = 0$, $y = 0$, and $x = 0$ the field is zero.

8.6 Write an expression for an $\mathscr{R}$-state lightwave of frequency ω propagating in the positive x-direction such that at $t = 0$ and $x = 0$ the $\vec{\mathbf{E}}$-field points in the negative z-direction.

8.7* A beam of linearly polarized light with its electric field vertical impinges perpendicularly on an ideal linear polarizer with a vertical transmission axis. If the incoming beam has an irradiance of 200-W/m^2, what is the irradiance of the transmitted beam?

8.8* Given that 300 W/m^2 of light from an ordinary tungsten bulb arrives at an ideal linear polarizer. What is its radiant flux density on emerging?

8.9* A beam of vertically polarized linear light is perpendicularly incident on an ideal linear polarizer. Show that if its transmission axis makes an angle of 60° with the vertical only 25% of the irradiance will be transmitted by the polarizer.

8.10 If light that is initially natural and of flux density I_i passes through two sheets of *HN*-32 whose transmission axes are parallel, what will be the flux density of the emerging beam?

8.11* What will be the irradiance of the emerging beam if the analyzer of the previous problem is rotated 30°?

8.12* The irradiance of a beam of natural light is 400 W/m^2. It impinges on the first of two consecutive ideal linear polarizers whose transmission axes are 40.0° apart. How much light emerges from the two?

8.13* As we saw in Section 8.10, substances such as sugar and insulin are *optically active*; they rotate the plane of polarization in proportion to both the path length and the concentration of the solution. A glass vessel is placed between a pair of crossed *HN*-50 linear polarizers, and 50% of the natural light incident on the first polarizer is transmitted through the second polarizer. By how much did the sugar solution in the cell rotate the light passed by the first polarizer?

8.14* The light from an ordinary flashlight is passed through a linear polarizer with its transmission axis vertical. The resulting beam, having an irradiance of 200 W/m^2, is incident normally on a vertical

Giesecke+Devrient GmbH,
Giesecke+Devrient Currency Technology GmbH,
and Papierfabrik Louisenthal GmbH. - Ex. 1027

HN-50 linear polarizer whose transmission axis is tilted at 30° above the horizontal. How much light is transmitted?

8.15* Linearly polarized light (with an irradiance of 200 W/m^2) aligned with its electric-field vector at +55° from the vertical impinges perpendicularly on an ideal sheet polarizer whose transmission axis is at +10° from the vertical. What fraction of the incoming light emerges?

8.16* Two ideal linear sheet polarizers are arranged with respect to the vertical with their transmission axis at 10° and 60°, respectively. If a linearly polarized beam of light with its electric field at 40° enters the first polarizer, what fraction of its irradiance will emerge?

8.17* Imagine a pair of crossed polarizers with transmission axes vertical and horizontal. The beam emerging from the first polarizer has flux density I_1, and of course no light passes through the analyzer (i.e., $I_2 = 0$). Now insert a perfect linear polarizer (*HN*-50) with its transmission axis at 45° to the vertical between the two elements—compute I_2. Think about the motion of the electrons that are radiating in each polarizer.

8.18* Imagine that you have two identical perfect linear polarizers and a source of natural light. Place them one behind the other and position their transmission axes at 0° and 50°, respectively. Now insert between them a third linear polarizer with its transmission axes at 25°. If 1000 W/m^2 of light is incident, how much will emerge with and without the middle polarizer in place?

8.19* Given that 200 W/m^2 of randomly polarized light is incident normally on a stack of ideal linear polarizers that are positioned one behind the other with the transmission axis of the first vertical, the second at 30°, the third at 60°, and the fourth at 90°. How much light emerges?

8.20* Two *HN*-50 linear polarizers are positioned one behind the other. What angle should their transmission axes make if an incident unpolarized 100-W/m^2 beam is to be reduced to 30.0 W/m^2 on emerging from the pair?

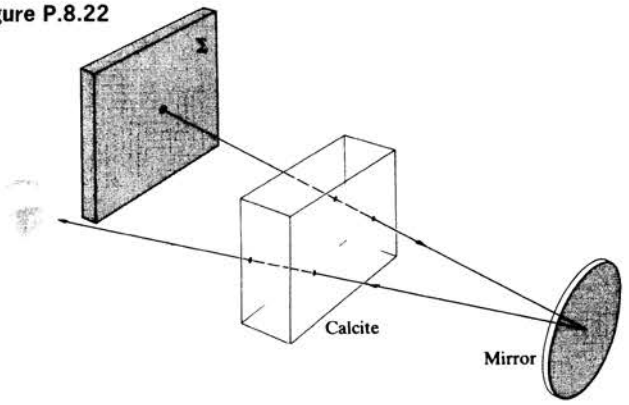
8.21 An ideal polarizer is rotated at a rate ω between a similar pair of stationary crossed polarizers. Show that the emergent flux density will be modulated at four times the rotational frequency. In other words, show that

$$I = \frac{I_1}{8}(1 - \cos 4\omega t)$$

where I_1 is the flux density emerging from the first polarizer and I is the final flux density.

8.22 Figure P.8.22 shows a ray traversing a calcite crystal at nearly normal incidence, bouncing off a mirror, and then going through the crystal again. Will the observer see a double image of the spot on Σ?

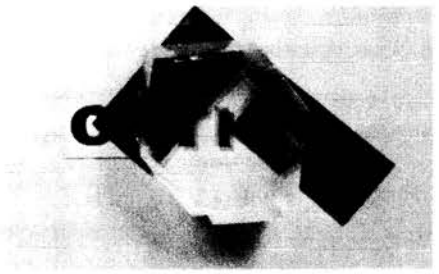
Figure P.8.22



8.23* A pencil mark on a sheet of paper is covered by a calcite crystal. With illumination from above, isn't the light impinging on the paper already polarized, having passed through the crystal? Why then do we see two images? Test your solution by polarizing the light from a flashlight and then reflecting it off a sheet of paper. Try specular reflection off glass; is the reflected light polarized?

8.24 Discuss in detail what you see in Fig. P.8.24. The crystal in the photograph is calcite, and it has a blunt corner at the upper left. The two Polaroids have their transmission axes parallel to their *short* edges.

Figure P.8.24



8.25 The calcite crystal in Fig. P.8.25 is shown in three different orientations. Its blunt corner is on the left in (*a*), the lower left in (*b*), and the bottom in (*c*). The Polaroid's transmission axis is horizontal. Explain each photograph, particularly (*b*).

8.26 In discussing calcite, we pointed out that its large birefringence arises from the fact that the carbonate groups lie in parallel planes

Giesecke+Devrient GmbH,
Giesecke+Devrient Currency Technology GmbH,
and Papierfabrik Louisenthal GmbH. - Ex. 1027

Figure P.8.25a

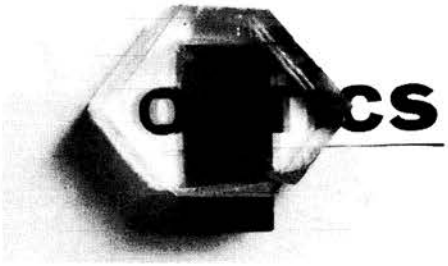


Figure P.8.25b

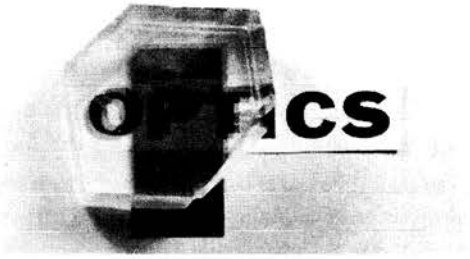


Figure P.8.25c



(normal to the optic axis). Show in a sketch and explain why the polarization of the group will be less when $\vec{\mathbf{E}}$ is perpendicular to the CO_3 plane than when $\vec{\mathbf{E}}$ is parallel to it. What does this mean with respect to $v_\perp$ and $v_\parallel$, that is, the wave's speeds when $\vec{\mathbf{E}}$ is linearly polarized perpendicular or parallel to the optic axis?

8.27* Imagine that we have a transmitter of microwaves that radiates a linearly polarized wave whose $\vec{\mathbf{E}}$-field is known to be parallel to the dipole direction. We wish to reflect as much energy as possible off the surface of a pond (having an index of refraction of 9.0). Find the necessary incident angle and comment on the orientation of the beam.

8.28* At what angle will the reflection of the sky coming off the surface of a pond ($n = 1.33$) completely vanish when seen through a Polaroid filter?

8.29* What is Brewster's angle for reflection of light from the surface of a piece of glass ($n_g = 1.65$) immersed in water ($n_w = 1.33$)?

8.30* A beam of light is reflected off the surface of some unknown liquid, and the light is examined with a linear sheet polarizer. It is found that when the central axis of the polarizer (that is, the perpendicular to the plane of the sheet) is tilted down from the vertical at an angle of 54.30°, the reflected light is completely passed, provided the transmission axis is parallel to the plane of the interface. From this information, compute the index of refraction of the liquid.

8.31* Light reflected from a glass ($n_g = 1.65$) plate immersed in ethyl alcohol ($n_e = 1.36$) is found to be completely linearly polarized. At what angle will the partially polarized beam be transmitted into the plate?

8.32* A beam of natural light is incident on an air–glass interface ($n_{ti} = 1.5$) at 40°. Compute the degree of polarization of the reflected light.

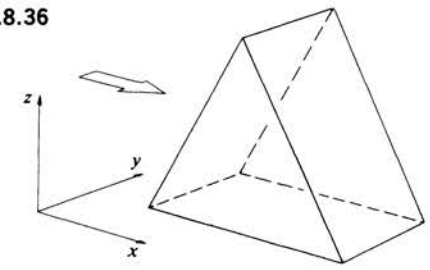
8.33* A beam of natural light incident in air on a glass ($n = 1.5$) interface at 70° is partially reflected. Compute the overall reflectance. How would this compare with the case of incidence at, say, 56.3°? Explain.

8.34 A ray of yellow light is incident on a calcite plate at 50°. The plate is cut so that the optic axis is parallel to the front face and perpendicular to the plane-of-incidence. Find the angular separation between the two emerging rays.

8.35* A beam of light is incident normally on a quartz plate whose optic axis is perpendicular to the beam. If $\lambda_0 = 589.3$ nm, compute the wavelengths of both the ordinary and extraordinary waves. What are their frequencies?

8.36 A beam of light enters a calcite prism from the left, as shown in Fig. P.8.36. There are three possible orientations of the optic axis of particular interest, and these correspond to the x-, y-, and z-directions. Imagine that we have three such prisms. In each case sketch the entering and emerging beams, showing the state of polarization. How can any one of these be used to determine n_o and n_e?

Figure P.8.36



Giesecke+Devrient GmbH,
Giesecke+Devrient Currency Technology GmbH,
and Papierfabrik Louisenthal GmbH. - Ex. 1027

8.37 The electric-field vector of an incident $\mathscr{P}$-state makes an angle of $+30°$ with the horizontal fast axis of a quarter-wave plate. Describe, in detail, the state of polarization of the emergent wave.

8.38 Compute the critical angle for the ordinary ray, that is, the angle for total internal reflection at the calcite–balsam layer of a Nicol prism.

8.39* Draw a quartz Wollaston prism, showing all pertinent rays and their polarization states.

8.40 The prism shown in Fig. P.8.40 is known as a *Rochon polarizer*. Sketch all the pertinent rays, assuming

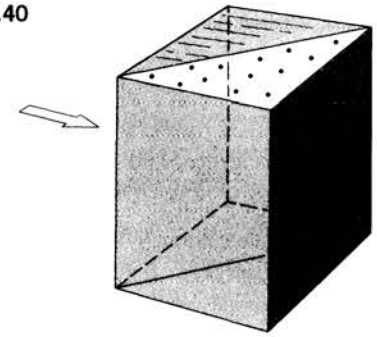
(a) that it is made of calcite.

(b) that it is made of quartz.

(c) Why might such a device be more useful than a dichroic polarizer when functioning with high-flux density laser light?

(d) What valuable feature of the Rochon is lacking in the Wollaston polarizer?

Figure P.8.40



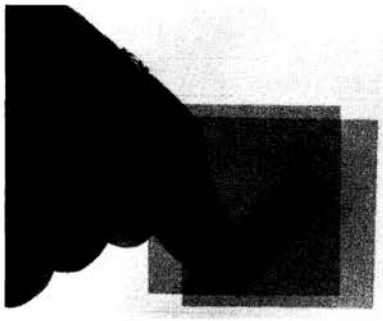
8.41* Take two ideal Polaroids (the first with its axis vertical and the second, horizontal) and insert between them a stack of 10 half-wave plates, the first with its fast axis rotated $\pi/40$ rad from the vertical, and each subsequent one rotated $\pi/40$ rad from the previous one. Determine the ratio of the emerging to incident irradiance, showing your logic clearly.

8.42* Suppose you were given a linear polarizer and a quarter-wave plate. How could you determine which was which, assuming you also had a source of natural light?

8.43* An $\mathscr{L}$-state traverses an eighth-wave plate having a horizontal fast axis. What is its polarization state on emerging?

8.44* Figure P.8.44 shows two Polaroid linear polarizers and between them a microscope slide to which is attached a piece of cellophane tape. Explain what you see.

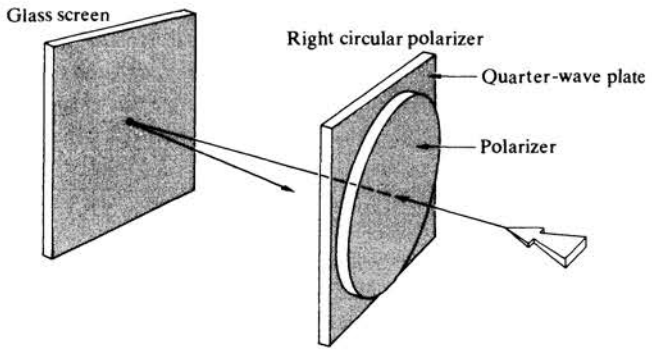
Figure P.8.44



8.45 A Babinet compensator is positioned at 45° between crossed linear polarizers and is being illuminated with sodium light. When a thin sheet of mica (indices 1.599 and 1.594) is placed on the compensator, the black bands all shift by $\frac{1}{4}$ of the space separating them. Compute the retardance of the sheet and its thickness.

8.46 Imagine that we have randomly polarized room light incident almost normally on the glass surface of a radar screen. A portion of it would be specularly reflected back toward the viewer and would thus tend to obscure the display. Suppose now that we cover the screen with a right-circular polarizer, as shown in Fig. P.8.46. Trace the incident and reflected beams, indicating their polarization states. What happens to the reflected beam?

Figure P.8.46



8.47 Is it possible for a beam to consist of two orthogonal incoherent $\mathscr{P}$-states and not be natural light? Explain. How might you arrange to have such a beam?

Giesecke+Devrient GmbH,
Giesecke+Devrient Currency Technology GmbH,
and Papierfabrik Louisenthal GmbH. - Ex. 1027

8.48* The specific rotatory power for sucrose dissolved in water at 20°C ($\lambda_0 = 589.3$ nm) is +66.45° per 10 cm of path traversed through a solution containing 1 g of active substance (sugar) per cm^3 of solution. A vertical $\mathscr{P}$-state (sodium light) enters at one end of a 1-m tube containing 1000 cm^3 of solution, of which 10 g is sucrose. At what orientation will the $\mathscr{P}$-state emerge?

8.49 On examining a piece of stressed photoelastic material between crossed linear polarizers, we would see a set of colored bands (isochromatics) and, superimposed on these, a set of dark bands (isoclinics). How might we remove the isoclinics, leaving only the isochromatics? Explain your solution. Incidentally, the proper arrangement is independent of the orientation of the photoelastic sample.

8.50* Consider a Kerr cell whose plates are separated by a distance d. Let ℓ be the effective length of those plates (slightly different from the actual length because of fringing of the field). Show that

$$\Delta\varphi = 2\pi K \ell V^2/d^2 \qquad [8.41]$$

8.51 Compute the half-wave voltage for a longitudinal Pockels cell made of ADA (ammonium dihydrogen arsenate) at $\lambda_0 \approx 550$ nm, where $r_{63} = 5.5 \times 10^{-12}$ and $n_o = 1.58$.

8.52* The Jones vector for an arbitrary linearly polarized state at an angle θ with respect to the horizontal is

$$\begin{bmatrix} \cos\theta \\ \sin\theta \end{bmatrix}$$

Prove that this matrix is in agreement with the one in Table 8.5 for a $\mathscr{P}$-state at +45°.

8.53 Find a Jones vector $\tilde{\mathbf{E}}_2$ representing a polarization state orthogonal to

$$\tilde{\mathbf{E}}_1 = \begin{bmatrix} 1 \\ -2i \end{bmatrix}$$

Sketch both of these.

8.54* Two incoherent light beams represented by (1, 1, 0, 0) and (3, 0, 0, 3) are superimposed.

(a) Describe in detail the polarization states of each of these.

(b) Determine the resulting Stokes parameters of the combined beam and describe its polarization state.

(c) What is its degree of polarization?

(d) What is the resulting light produced by overlapping the incoherent beams (1, 1, 0, 0) and (1, −1, 0, 0)? Explain.

8.55* Show by direct calculation, using Mueller matrices, that a unit-irradiance beam of natural light passing through a vertical linear polarizer is converted into a vertical $\mathscr{P}$-state. Determine its relative irradiance and degree of polarization.

8.56* Show by direct calculation, using Mueller matrices, that a unit-irradiance beam of natural light passing through a linear polarizer with its transmission axis at +45° is converted into a $\mathscr{P}$-state at +45°. Determine its relative irradiance and degree of polarization.

8.57* Show by direct calculation, using Mueller matrices, that a beam of horizontal $\mathscr{P}$-state light passing through a $\frac{1}{4}\lambda$-plate with its fast axis horizontal emerges unchanged.

8.58* Confirm that the matrix

$$\begin{bmatrix} 1 & 0 & 0 & 0 \\ 0 & 0 & 0 & -1 \\ 0 & 0 & 1 & 0 \\ 0 & 1 & 0 & 0 \end{bmatrix}$$

will serve as a Mueller matrix for a quarter-wave plate with its fast axis at +45°. Shine linear light polarized at 45° through it. What happens? What emerges when a horizontal $\mathscr{P}$-state enters the device?

8.59* The Mueller matrix

$$\begin{bmatrix} 1 & 0 & 0 & 0 \\ 0 & C^2+S^2\cos\Delta\varphi & CS(1-\cos\Delta\varphi) & -S\sin\Delta\varphi \\ 0 & CS(1-\cos\Delta\varphi) & S^2+C^2\cos\Delta\varphi & C\sin\Delta\varphi \\ 0 & S\sin\Delta\varphi & -C\sin\Delta\varphi & \cos\Delta\varphi \end{bmatrix}$$

in which $C = \cos 2\alpha$ and $S = \sin 2\alpha$, represents an arbitrary wave-plate having a retardance $\Delta\varphi$ and a fast axis at an angle α measured with respect to the horizontal. Use it to derive the matrix given in the previous problem.

8.60* Beginning with the Mueller matrix for an arbitrary retarder provided in the previous problem, show that it agrees with the matrix in Table 8.6 for a quarter-wave plate with a vertical fast axis.

8.61 Derive the Mueller matrix for a quarter-wave plate with its fast axis at −45°. Check that this matrix effectively cancels the one in Problem 8.58, so that a beam passing through the two wave plates successively remains unaltered.

8.62* Pass a beam of horizontally polarized linear light through each one of the $\frac{1}{4}\lambda$-plates in the two previous questions and describe

Giesecke+Devrient GmbH,
Giesecke+Devrient Currency Technology GmbH,
and Papierfabrik Louisenthal GmbH. - Ex. 1027

the states of the emerging light. Explain which field component is leading which and how Fig. 8.7 compares with these results.

8.63 Use Table 8.6 to derive a Mueller matrix for a half-wave plate having a vertical fast axis. Utilize your result to convert an $\mathscr{R}$-state into an $\mathscr{L}$-state. Verify that the same wave plate will convert an $\mathscr{L}$- to an $\mathscr{R}$-state. Advancing or retarding the relative phase by $\pi/2$ should have the same effect. Check this by deriving the matrix for a half-wave plate with a horizontal fast axis.

8.64 Construct one possible Mueller matrix for a right-circular polarizer made out of a linear polarizer and a quarter-wave plate. Such a device is obviously an inhomogeneous two-element train and will differ from the *homogeneous* circular polarizer of Table 8.6. Test your matrix to determine that it will convert natural light to an $\mathscr{R}$-state. Show that it will pass $\mathscr{R}$-states, as will the homogeneous matrix. Your matrix should convert $\mathscr{L}$-states incident on the input side to $\mathscr{R}$-states, whereas the homogeneous polarizer will totally absorb them. Verify this.

8.65* If the Pockels cell modulator shown in Fig. 8.57 is illuminated by light of irradiance I_i, it will transmit a beam of irradiance I_t such that

$$I_t = I_i \sin^2(\Delta\varphi/2)$$

Make a plot of I_t/I_i versus applied voltage. What is the significance of the voltage that corresponds to maximum transmission? What is the lowest voltage above zero that will cause I_t to be zero for ADP (λ_0 = 546.1 nm)? How can things be rearranged to yield a maximum value of I_t/I_i for zero voltage? In this new configuration what irradiance results when $V = V_{\lambda/2}$?

8.66 Construct a Jones matrix for an isotropic plate of absorbing material having an amplitude transmission coefficient of t. It might sometimes be desirable to keep track of the phase, since even if $t = 1$, such a plate is still an isotropic phase retarder. What is the Jones matrix for a region of vacuum? What is it for a perfect absorber?

8.67 Construct a Mueller matrix for an isotropic plate of absorbing material having an amplitude transmission coefficient of t. What Mueller matrix will completely depolarize any wave without affecting its irradiance? (It has no physical counterpart.)

8.68 Keeping Eq. (8.29) in mind, write an expression for the randomly polarized flux density component (I_n) of a partially polarized beam in terms of the Stokes parameters. To check your result, add a randomly polarized Stokes vector of flux density 4 to an $\mathscr{R}$-state of flux density 1. Then see if you get $I_n = 4$ for the resultant wave.

8.69* An optical filter can be described by a Jones matrix

$$\begin{bmatrix} \cos\alpha & \sin\alpha \\ -\sin\alpha & \cos\alpha \end{bmatrix}$$

Obtain the form of the emerging light for each of the following incident beams:

(a) A plane polarized beam polarized at angle θ to the horizontal (see Problem 8.52).

(b) A left-circularly polarized beam.

(c) A right-circularly polarized beam.

(d) From the above, identify the filter and explain how it could be constructed.

8.70 An optical filter can be described by a Jones matrix

$$\begin{bmatrix} \cos^2\alpha & \cos\alpha\sin\alpha \\ \cos\alpha\sin\alpha & \sin^2\alpha \end{bmatrix}$$

(a) Obtain the form of the emerging beam when the incident light is plane poloarized at angle θ to the horizontal (see Problem 8.52).

(b) Deduce from the result of part (a) the nature of the filter.

(c) Confirm your deduction above with at least one other test.

8.71* Two linear optical filters have Jones matrices

$$\mathscr{A}_1 = \frac{1}{\sqrt{2}} e^{i\pi/4} \begin{bmatrix} 1 & i \\ i & 1 \end{bmatrix}$$

and

$$\mathscr{A}_2 = \frac{1}{\sqrt{2}} e^{i\pi/4} \begin{bmatrix} 1 & -i \\ -i & 1 \end{bmatrix}.$$

Identify these filters.

8.72* A liquid cell containing an optically active sugar solution has a Jones matix given by

$$\frac{1}{2\sqrt{2}} \begin{bmatrix} 1+\sqrt{3} & -1+\sqrt{3} \\ 1-\sqrt{3} & 1+\sqrt{3} \end{bmatrix}$$

(a) Determine the polarization of the emerging light if the incident beam is a horizontal $\mathscr{P}$-state.

(b) Determine the polarization of the emerging light if the incident beam is a vertical $\mathscr{P}$-state.

(c) Determine the angle of rotation produced by the optically active material.

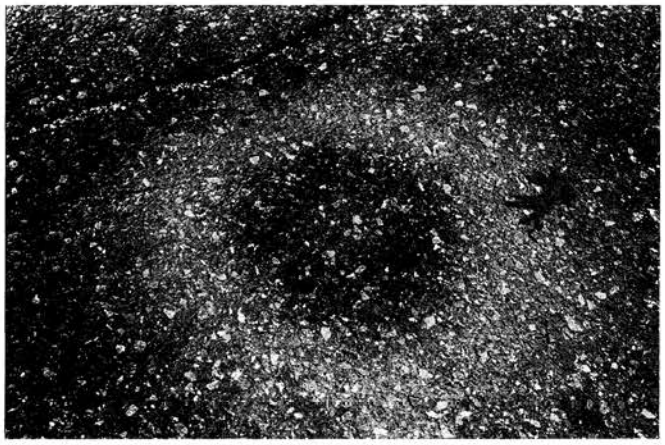
Giesecke+Devrient GmbH,
Giesecke+Devrient Currency Technology GmbH,
and Papierfabrik Louisenthal GmbH. - Ex. 1027

9 Interference

The intricate color patterns shimmering across an oil slick on a wet asphalt pavement (see photo) result from one of the more common manifestations of the phenomenon of interference.* On a macroscopic scale we might consider the related problem of the interaction of surface ripples on a pool of water. Our everyday experience with this kind of situation allows us to envision a complex distribution of disturbances (as shown, e.g., in Fig. 9.1). There might be regions where two (or more) waves have overlapped, partially or even completely canceling each other. Still other regions might exist in the pattern, where the resultant troughs and crests are even more pronounced than those of any of the constituent waves. After being superimposed, the individual waves separate and continue on, completely unaffected by their previous encounter.

Although the subject could be treated from the perspective of QED (p. 139), we'll take a much simpler approach. The wave theory of the electromagnetic nature of light provides a natural basis from which to proceed. Recall that the expression describing the optical disturbance is a second-order, homogeneous, linear, partial, differential equation [Eq. (3.22)]. As we have seen, it therefore obeys the important *Superposition Principle*. Accordingly, the resultant electric-field intensity $\vec{E}$, at a point in space where two or more lightwaves overlap, is equal to the *vector sum* of the individual constituent disturbances. Briefly then, ***optical interference corresponds to the interaction of two or more lightwaves yielding a resultant irradiance that deviates from the sum of the component irradiances.***

*The layer of water on the asphalt allows the oil film to assume the shape of a smooth planar surface. The black asphalt absorbs the transmitted light, preventing back reflection, which would tend to obscure the fringes.



These roughly circular interference fringes are due to an oil film on wet pavement. They are *fringes of equal thickness* (see p. 404) and so don't change when viewed at different angles. Of course, they appear in a rainbow of colors.

Out of the multitude of optical systems that produce interference, we will choose a few of the more important to examine. Interferometric devices will be divided, for the sake of discussion, into two groups: *wavefront splitting* and *amplitude splitting*. In the first instance, portions of the primary wavefront are used either directly as sources to emit secondary waves or in conjunction with optical devices to produce virtual sources of secondary waves. These secondary waves are then brought together, thereupon to interfere. In the case of amplitude splitting, the primary wave itself is divided into two segments, which travel different paths before recombining and interfering.

Giesecke+Devrient GmbH,
Giesecke+Devrient Currency Technology GmbH,
and Papierfabrik Louisenthal GmbH. - Ex. 1027

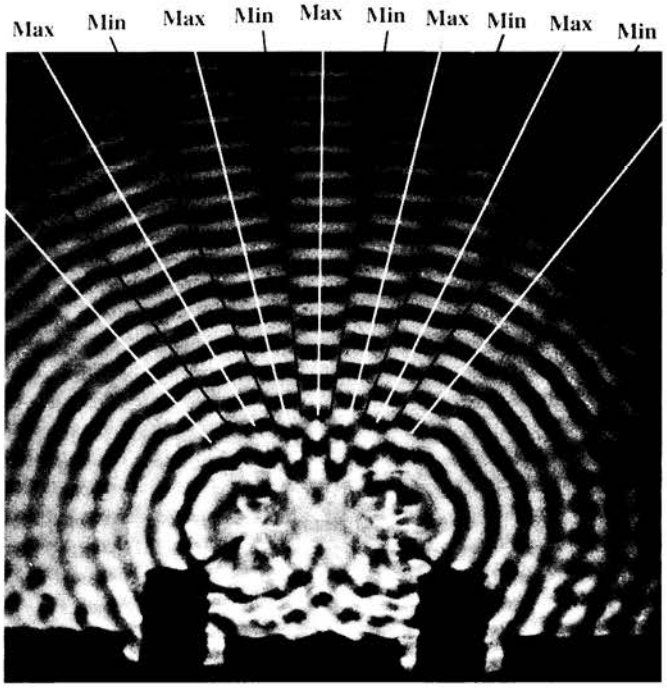


Figure 9.1 Water waves from two in-phase point sources in a ripple tank. In the middle of the pattern the wave peaks (thin bright bands), and troughs (thin black bands) lie within long wedge-shaped areas (maxima) separated by narrow dark regions of calm (minima). Although the nodal lines look straight, they're really hyperbolic. The optical equivalent is the electric field distribution depicted in Fig. 9.3c. (Photo courtesy PSSC *College Physics*, 1968, @ 1965 Educational Development Center, Inc.)

9.1 General Considerations

We have already examined the problem of the superposition of two scalar waves (Section 7.1), and in many respects those results will again be applicable. But light is, of course, a vector phenomenon; the electric and magnetic fields are vector fields. An appreciation of this fact is fundamental to any kind of intuitive understanding of interference. Still, there are many situations in which the particular optical system can be so configured that the vector nature of light is of little practical significance. We will derive the basic interference equations within the context of the vector model, thereafter delineating the conditions under which the scalar treatment is applicable.

In accordance with the Principle of Superposition, the electric field intensity $\vec{\mathbf{E}}$, at a point in space, arising from the separate fields $\vec{\mathbf{E}}_1, \vec{\mathbf{E}}_2, \ldots$ of various contributing sources is given by

$$\vec{\mathbf{E}} = \vec{\mathbf{E}}_1 + \vec{\mathbf{E}}_2 + \cdots \tag{9.1}$$

The optical disturbance, or light field $\vec{\mathbf{E}}$, varies in time at an exceedingly rapid rate, roughly

$$4.3 \times 10^{14}\ \text{Hz} \quad \text{to} \quad 7.5 \times 10^{14}\ \text{Hz}$$

making the actual field an impractical quantity to detect. On the other hand, the irradiance I can be measured directly with a wide variety of sensors (e.g., photocells, bolometers, photographic emulsions, or eyes). The study of interference is therefore best approached by way of the irradiance.

Much of the analysis to follow can be performed without specifying the particular shape of the wavefronts, and the results are therefore quite general (Problem 9.1). For the sake of simplicity, however, consider two point sources, S_1 and S_2, emitting monochromatic waves of the same frequency in a homogeneous medium. Let their separation a be much greater than λ. Locate the point of observation P far enough away from the sources so that at P the wavefronts will be planes (Fig. 9.2). For the moment, consider only linearly polarized waves of the form

$$\vec{\mathbf{E}}_1(\vec{r}, t) = \vec{\mathbf{E}}_{01} \cos(\vec{\mathbf{k}}_1 \cdot \vec{\mathbf{r}} - \omega t + \varepsilon_1) \tag{9.2a}$$

and

$$\vec{\mathbf{E}}_2(\vec{r}, t) = \vec{\mathbf{E}}_{02} \cos(\vec{\mathbf{k}}_2 \cdot \vec{\mathbf{r}} - \omega t + \varepsilon_2) \tag{9.2b}$$

We saw in Chapter 3 that the irradiance at P is given by

$$I = \epsilon v \langle \vec{\mathbf{E}}^2 \rangle_{\mathrm{T}}$$

Inasmuch as we will be concerned only with relative irradiances within the same medium, we will, for the time being at least, simply neglect the constants and set

$$I = \langle \vec{\mathbf{E}}^2 \rangle_{\mathrm{T}}$$

What is meant by $\langle \vec{\mathbf{E}}^2 \rangle_{\mathrm{T}}$ is of course the time average of the magnitude of the electric-field intensity squared, or $\langle \vec{\mathbf{E}} \cdot \vec{\mathbf{E}} \rangle_{\mathrm{T}}$. Accordingly

$$\vec{\mathbf{E}}^2 = \vec{\mathbf{E}} \cdot \vec{\mathbf{E}}$$

where now

$$\vec{\mathbf{E}}^2 = (\vec{\mathbf{E}}_1 + \vec{\mathbf{E}}_2) \cdot (\vec{\mathbf{E}}_1 + \vec{\mathbf{E}}_2)$$

and thus

$$\vec{\mathbf{E}}^2 = \vec{\mathbf{E}}_1^2 + \vec{\mathbf{E}}_2^2 + 2\vec{\mathbf{E}}_1 \cdot \vec{\mathbf{E}}_2 \tag{9.3}$$

Giesecke+Devrient GmbH,
Giesecke+Devrient Currency Technology GmbH,
and Papierfabrik Louisenthal GmbH. - Ex. 1027

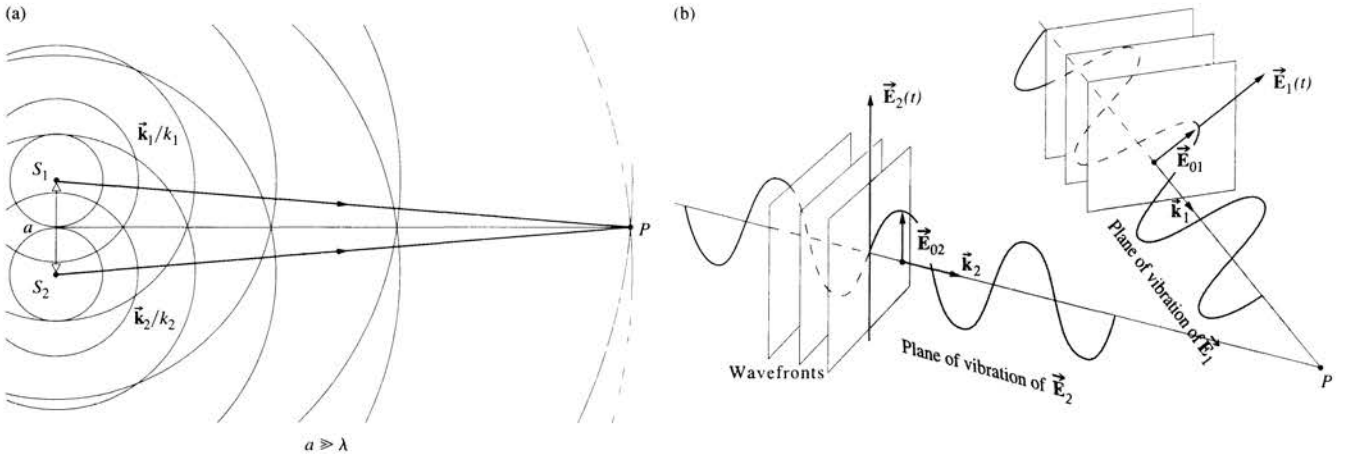


Figure 9.2 Waves from two point sources overlapping in space.

Taking the time average of both sides, we find that the irradiance becomes

$$I = I_1 + I_2 + I_{12} \tag{9.4}$$

provided that

$$I_1 = \langle \vec{E}_1^2 \rangle_T \tag{9.5}$$

$$I_2 = \langle \vec{E}_2^2 \rangle_T \tag{9.6}$$

and

$$I_{12} = 2\langle \vec{E}_1 \cdot \vec{E}_2 \rangle_T \tag{9.7}$$

The latter expression is known as the *interference term*. To evaluate it in this specific instance, we form

$$\vec{E}_1 \cdot \vec{E}_2 = \vec{E}_{01} \cdot \vec{E}_{02} \cos(\vec{k}_1 \cdot \vec{r} - \omega t + \varepsilon_1) \times \cos(\vec{k}_2 \cdot \vec{r} - \omega t + \varepsilon_2) \tag{9.8}$$

or equivalently

$$\vec{E}_1 \cdot \vec{E}_2 =$$

$$\vec{E}_{01} \cdot \vec{E}_{02} [\cos(\vec{k}_1 \cdot \vec{r} + \varepsilon_1) \cos \omega t + \sin(\vec{k}_1 \cdot \vec{r} + \varepsilon_1) \sin \omega t]$$

$$\times [\cos(\vec{k}_2 \cdot \vec{r} + \varepsilon_2) \cos \omega t + \sin(\vec{k}_2 \cdot \vec{r} + \varepsilon_2) \sin \omega t] \tag{9.9}$$

Recall that the time average of some function $f(t)$, taken over an interval T, is

$$\langle f(t) \rangle_T = \frac{1}{T} \int_t^{t+T} f(t')\, dt' \tag{9.10}$$

The period τ of the harmonic functions is $2\pi/\omega$, and for our present concern $T >> \tau$. In that case the $1/T$ coefficient in front of the integral has a dominant effect. After multiplying out and averaging Eq. (9.9) we have

$$\langle \vec{E}_1 \cdot \vec{E}_2 \rangle_T = \tfrac{1}{2} \vec{E}_{01} \cdot \vec{E}_{02} \cos(\vec{k}_1 \cdot \vec{r} + \varepsilon_1 - \vec{k}_2 \cdot \vec{r} - \varepsilon_2)$$

where use was made of the fact (p. 49) that $\langle \cos^2 \omega t \rangle_T = \frac{1}{2}$, $\langle \sin^2 \omega t \rangle_T = \frac{1}{2}$, and $\langle \cos \omega t \sin \omega t \rangle_T = 0$. The interference term is then

$$I_{12} = \vec{E}_{01} \cdot \vec{E}_{02} \cos \delta \tag{9.11}$$

and δ, equal to $(\vec{k}_1 \cdot \vec{r} - \vec{k}_2 \cdot \vec{r} + \varepsilon_1 - \varepsilon_2)$, is the *phase difference* arising from a combined path length and initial phase-angle difference. Notice that if $\vec{E}_{01}$ and $\vec{E}_{02}$ (and therefore $\vec{E}_1$ and $\vec{E}_2$) are perpendicular, $I_{12} = 0$ and $I = I_1 + I_2$. Two such orthogonal $\mathcal{P}$-states will combine to yield an $\mathcal{R}$-, $\mathcal{L}$-, $\mathcal{P}$-, or $\mathcal{E}$-state, but the flux-density distribution will be unaltered.

The most common situation in the work to follow corresponds to $\vec{E}_{01}$ parallel to $\vec{E}_{02}$. In that case, the irradiance reduces to the value found in the scalar treatment of Section 7.1. Under those conditions

$$I_{12} = E_{01} E_{02} \cos \delta$$

This can be written in a more convenient way by noticing that

$$I_1 = \langle \vec{E}_1^2 \rangle_T = \frac{E_{01}^2}{2} \tag{9.12}$$

Giesecke+Devrient GmbH,
Giesecke+Devrient Currency Technology GmbH,
and Papierfabrik Louisenthal GmbH. - Ex. 1027

and $$I_2 = \langle \vec{\mathbf{E}}_2^2 \rangle_T = \frac{E_{02}^2}{2} \tag{9.13}$$

The interference term becomes

$$I_{12} = 2\sqrt{I_1 I_2} \cos \delta$$

whereupon the total irradiance is

$$I = I_1 + I_2 + 2\sqrt{I_1 I_2} \cos \delta \tag{9.14}$$

At various points in space, the resultant irradiance can be greater, less than, or equal to $I_1 + I_2$, depending on the value of I_{12}, that is, depending on δ. A maximum irradiance is obtained when $\cos \delta = 1$, so that

$$I_{\max} = I_1 + I_2 + 2\sqrt{I_1 I_2} \tag{9.15}$$

when $$\delta = 0, \pm 2\pi, \pm 4\pi, \ldots$$

In this case of ***total constructive interference***, the phase difference between the two waves is an integer multiple of 2π, and the disturbances are *in-phase*. When $0 < \cos \delta < 1$ the waves are *out-of-phase*, $I_1 + I_2 < I < I_{\max}$, and the result is *constructive interference*. At $\delta = \pi/2$, $\cos \delta = 0$, the optical disturbances are 90° out-of-phase, and $I = I_1 + I_2$. For $0 > \cos \delta > -1$ we have the condition of *destructive interference*, $I_1 + I_2 > I > I_{\min}$. A minimum irradiance results when the waves are 180° out-of-phase, troughs overlap crests, $\cos \delta = -1$, and

$$I_{\min} = I_1 + I_2 - 2\sqrt{I_1 I_2} \tag{9.16}$$

This occurs when $\delta = \pm\pi, \pm 3\pi, \pm 5\pi, \ldots$, and it is referred to as ***total destructive interference***.

Another somewhat special yet very important case arises when the amplitudes of both waves reaching P in Fig. 9.2 are equal (i.e., $\vec{\mathbf{E}}_{01} = \vec{\mathbf{E}}_{02}$). Since the irradiance contributions from both sources are then equal, let $I_1 = I_2 = I_0$. Equation (9.14) can now be written as

$$I = 2I_0(1 + \cos \delta) = 4I_0 \cos^2 \frac{\delta}{2} \tag{9.17}$$

from which it follows that $I_{\min} = 0$ and $I_{\max} = 4I_0$. For an analysis in terms of the angle between the two beams, see Problem 9.3.

Equation (9.14) holds equally well for the spherical waves emitted by S_1 and S_2. Such waves can be expressed as

$$\vec{\mathbf{E}}_1(r_1, t) = \vec{\mathbf{E}}_{01}(r_1) \exp [i(kr_1 - \omega t + \varepsilon_1)] \tag{9.18a}$$

and $$\vec{\mathbf{E}}_2(r_2, t) = \vec{\mathbf{E}}_{02}(r_2) \exp [i(kr_2 - \omega t + \varepsilon_2)] \tag{9.18b}$$

The terms r_1 and r_2 are the radii of the spherical wavefronts overlapping at P; they specify the distances from the sources to P. In this case

$$\delta = k(r_1 - r_2) + (\varepsilon_1 - \varepsilon_2) \tag{9.19}$$

The flux density in the region surrounding S_1 and S_2 will certainly vary from point to point as $(r_1 - r_2)$ varies. Nonetheless, from the principle of conservation of energy, we expect the spatial average of I to remain constant and equal to the average of $I_1 + I_2$. The space average of I_{12} must therefore be zero, a property verified by Eq. (9.11), since the average of the cosine term is, in fact, zero. (For further discussion of this point, see Problem 9.2.)

Equation (9.17) will be applicable when the separation between S_1 and S_2 is small in comparison with r_1 and r_2 and when the interference region is also small in the same sense. Under these circumstances, $\vec{\mathbf{E}}_{01}$ and $\vec{\mathbf{E}}_{02}$ may be considered independent of position, that is, constant over the small region examined. If the emitting sources are of equal strength, $\vec{\mathbf{E}}_{01} = \vec{\mathbf{E}}_{02}$, $I_1 = I_2 = I_0$ and we have

$$I = 4I_0 \cos^2 \tfrac{1}{2}[k(r_1 - r_2) + (\varepsilon_1 - \varepsilon_2)]$$

Irradiance maxima occur when

$$\delta = 2\pi m$$

provided that $m = 0, \pm 1, \pm 2, \ldots$ Similarly, minima, for which $I = 0$, arise when

$$\delta = \pi m'$$

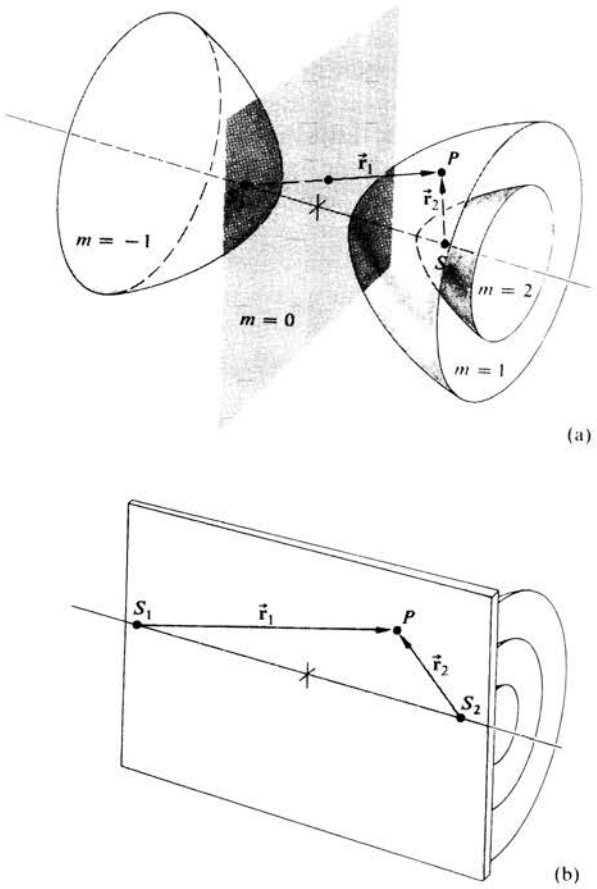
where $m' = \pm 1, \pm 3, \pm 5, \ldots$, or if you like, $m' = 2m + 1$. Using Eq. (9.19) these two expressions for δ can be rewritten such that maximum irradiance occurs when

$$(r_1 - r_2) = [2\pi m + (\varepsilon_2 - \varepsilon_1)]/k \tag{9.20a}$$

and minimum when

$$(r_1 - r_2) = [\pi m' + (\varepsilon_2 - \varepsilon_1)]/k \tag{9.20b}$$

Giesecke+Devrient GmbH,
Giesecke+Devrient Currency Technology GmbH,
and Papierfabrik Louisenthal GmbH. - Ex. 1027



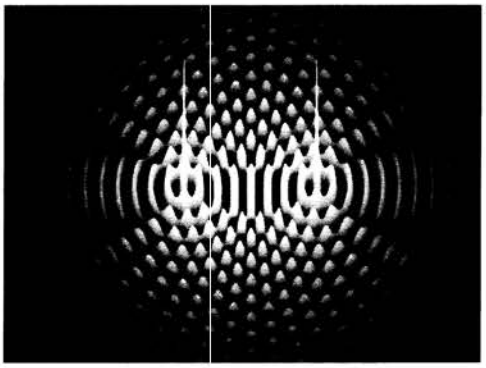


Figure 9.3 (*a*) Hyperboloidal surfaces of maximum irradiance for two point sources. The quantity m is positive where $r_1 > r_2$. (*b*) Here we see how the irradiance maxima are distributed on a plane containing S_1 and S_2. (*c*) The electric-field distribution in the plane shown in part (*b*). The tall peaks, are the point sources S_1 and S_2. Note that the spacing of the sources is different in (*b*) and (*c*). (Photo courtesy, The Optics Project, Mississippi State University.)

Either one of these equations defines a family of surfaces, each of which is a hyperboloid of revolution. The vertices of the hyperboloids are separated by distances equal to the right-hand sides of Eqs. (9.20a) and (9.20b). The foci are located at S_1 and S_2. If the waves are in-phase at the emitter, $\varepsilon_1 - \varepsilon_2 = 0$, and Eqs. (9.20a) and (9.20b) can be simplified to

[maxima] $$(r_1 - r_2) = 2\pi m/k = m\lambda \qquad (9.21a)$$

[minima] $$(r_1 - r_2) = \pi m'/k = \tfrac{1}{2}m'\lambda \qquad (9.21b)$$

for maximum and minimum irradiance, respectively. Figure 9.3*a* shows a few of the surfaces over which there are irradiance maxima. The dark and light zones that would be seen on a screen placed in the region of interference are known as **interference fringes** (Fig. 9.3*b*). Notice that the central bright band, equidistant from the two sources, is the so-called zeroth-order fringe ($m = 0$), which is straddled by the $m' = \pm 1$ minima, and these, in turn, are bounded by the first-order ($m = \pm 1$) maxima, which are straddled by the $m' = \pm 3$ minima, and so forth.

Since the wavelength λ for light is very small, a large number of surfaces corresponding to the lower values of m will exist close to, and on either side of, the plane $m = 0$. A number of fairly straight parallel fringes will therefore appear on a screen placed perpendicular to that ($m = 0$) plane and in the vicinity of it, and for this case the approximation $r_1 \approx r_2$ will hold. If S_1 and S_2 are then displaced normal to the $\overline{S_1S_2}$ line, the fringes will merely be displaced parallel to themselves. *Two narrow slits will generate a large number of exactly overlapping fringes, thereby increasing the irradiance, leaving the central region of the two-point source pattern otherwise essentially unchanged.*

Giesecke+Devrient GmbH,
Giesecke+Devrient Currency Technology GmbH,
and Papierfabrik Louisenthal GmbH. - Ex. 1027

9.2 Conditions for Interference

If two beams are to interfere to produce a stable pattern, they must have very nearly the same frequency. A significant frequency difference would result in a rapidly varying, time-dependent phase difference, which in turn would cause I_{12} to average to zero during the detection interval (see Section 7.1). Still, if the sources both emit white light, the component reds will interfere with reds, and the blues with blues. A great many fairly similar, slightly displaced, overlapping monochromatic patterns will produce one total white-light pattern. It will not be as sharp or as extensive as a quasimonochromatic pattern, but *white light will produce observable interference.*

The clearest patterns exist when the interfering waves have equal or nearly equal amplitudes. The central regions of the dark and light fringes then correspond to complete destructive and constructive interference, respectively, yielding maximum contrast.

For a fringe pattern to be observed, the two sources need not be in-phase with each other. A somewhat shifted but otherwise identical interference pattern will occur if there is some initial phase difference between the sources, as long as it remains constant. Such sources (which may or may not be in step, but are always marching together) are **coherent**.*

9.2.1 Temporal and Spatial Coherence

Remember that because of the granular nature of the emission process, conventional quasimonochromatic sources produce light that is a mix of photon wavetrains. At each illuminated point in space there is a net field that oscillates nicely (through roughly a million cycles) for less than 10 ns or so before it randomly changes phase. This interval over which the lightwave resembles a sinusoid is a measure of its **temporal coherence**. The average time interval during which the lightwave oscillates in a predictable way we have already designated as the coherence time of the radiation. The longer the coherence time, the greater the temporal coherence of the source.

As observed from a fixed point in space, the passing lightwave appears fairly sinusoidal for some number of oscillations between abrupt changes of phase. The corresponding spatial extent over which the lightwave oscillates in a regular, predictable way is the coherence length [Eq. (7.64)]. Once again, it will be convenient to picture the light beam as a progression of well-defined, more or less sinusoidal, wavegroups of average length Δl_c, whose phases are uncorrelated to one another. Bear in mind that ***temporal coherence is a manifestation of spectral purity***. If the light were ideally monochromatic, the wave would be a perfect sinusoid with an infinite coherence length. All real sources fall short of this, and all actually emit a range of frequencies, albeit sometimes quite narrow. For instance, an ordinary laboratory discharge lamp has a coherence length of several millimeters, whereas certain kinds of lasers routinely provide coherence lengths of tens of kilometers.

Figure 9.4 summarizes some of these ideas. In (*a*) the wave, which arises from a point source, is monochromatic and has complete temporal coherence. What happens at P_1' will, a moment later, happen at P_2' and still later at P_3'—all totally predictably. In fact, by watching P_4' we can determine what the wave will be doing at P_1' at any time. Every point on the wave is correlated; its coherence time is unlimited. By contrast, Fig. 9.4*b* shows a point source that changes frequency from moment to moment. Now there's no correlation of the wave at points that are far apart like P_1' and P_4'. The waves lack the total temporal coherence displayed in (*a*), but they're not completely unpredictable; the behavior at points that are close together such as P_2' and P_3' are somewhat correlated. This is an instance of *partial temporal coherence*, a measure of which is the coherence length—the shortest distance over which the disturbance is sinusoidal, that is, the distance over which the phase is predictable.

Notice, in both parts of Fig. 9.4, that the behavior of the waves at points P_1, P_2, and P_3 is completely correlated. Each of the two wave streams arises from a single point source and P_1, P_2, and P_3 lie on the same wavefront in both cases; the disturbance at each of these laterally separated points is in-phase and stays in-phase. Both waves therefore exhibit complete **spatial coherence**. By contrast, suppose the source is broad, that is, composed of many widely spaced point sources (monochromatic ones of period τ), as is Fig. 9.5. If we could take a picture of the wave pattern in Fig. 9.5 every τ seconds, it would be the same; each wavefront would be replaced by an identical one, one wavelength behind it. The disturbances at P_1', P_2', and P_3' are correlated, and the wave is temporally coherent.

Now to insert a little realism; suppose each point source changes phase rapidly and randomly, emitting 10-ns long sinusoidal wavetrains. The waves in Fig. 9.5 would randomly

*Chapter 12 is devoted to the study of coherence, so here we'll merely touch on those aspects that are immediately pertinent.

Giesecke+Devrient GmbH,
Giesecke+Devrient Currency Technology GmbH,
and Papierfabrik Louisenthal GmbH. - Ex. 1027

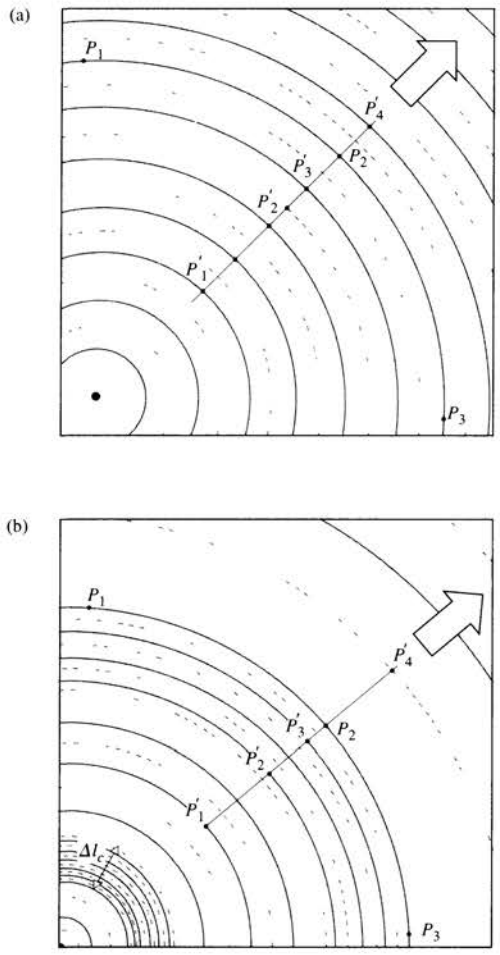


Figure 9.4 Temporal and spatial coherence. (*a*) Here the waves display both forms of coherence perfectly. (*b*) Here there is complete spatial coherence but only partial temporal coherence.

change phase, shifting, combining, and recombining in a frenzied tumult. The disturbances at P'_1, P'_2, and P'_3 would only be correlated for a time less than 10 ns. And the wave field at two, even modestly spaced, lateral points such as P_1 and P_2 would be almost completely uncorrelated depending on the size of the source. The beam from a candle flame or a shaft of sunlight is a multi-frequency mayhem much like this.

Two ordinary sources, two lightbulbs, can be expected to maintain a constant relative phase for a time no greater than Δt_c, so the interference pattern they produce will randomly shift around in space at an exceedingly rapid rate, averaging out and making it quite impractical to observe. Until the advent of the laser, it was a working principle that no two individual sources could ever produce an observable interference pattern. The coherence time of lasers, however, can be appreciable, and interference via independent lasers has been observed and photographed.* The most common means of overcoming this problem with ordinary thermal sources is to make one source serve to produce two coherent secondary sources.

9.2.2 The Fresnel–Arago Laws

In Section 9.1 it was assumed that the two overlapping optical disturbance vectors were linearly polarized and parallel. Nonetheless, the formulas apply as well to more complicated situations; indeed, the treatment is applicable regardless of the polarization state of the waves. To appreciate this, recall that

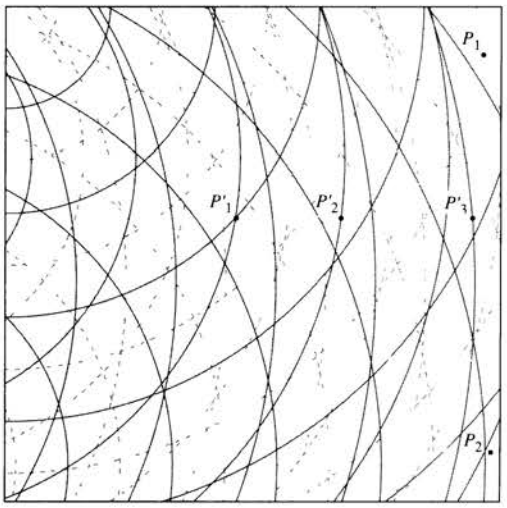


Figure 9.5 With multiple (here four) widely spaced point sources, the resultant wave is still coherent. But if those sources change phase rapidly and randomly, both the spatial and temporal coherence diminish accordingly.

* G. Magyar and L. Mandel, "Interference fringes produced by superposition of two independent maser light beams," *Nature* **198**, 255 (1963). F. Louradour, F. Reynaud, B. Colombeau, and C. Froehly, "Interference fringes between two separate lasers," *Am. J. Phys.* **61**, 242 (1993). L. Basano and P. Ottonello, "Interference fringes from stabilized diode lasers," *Am. J. Phys.* **68**, 245 (2000). E. C. G. Sudarshan and T. Rothman, "The two-slit interferometer reexamined," *Am. J. Phys.* **59**, 592 (1991).

Giesecke+Devrient GmbH,
Giesecke+Devrient Currency Technology GmbH,
and Papierfabrik Louisenthal GmbH. - Ex. 1027

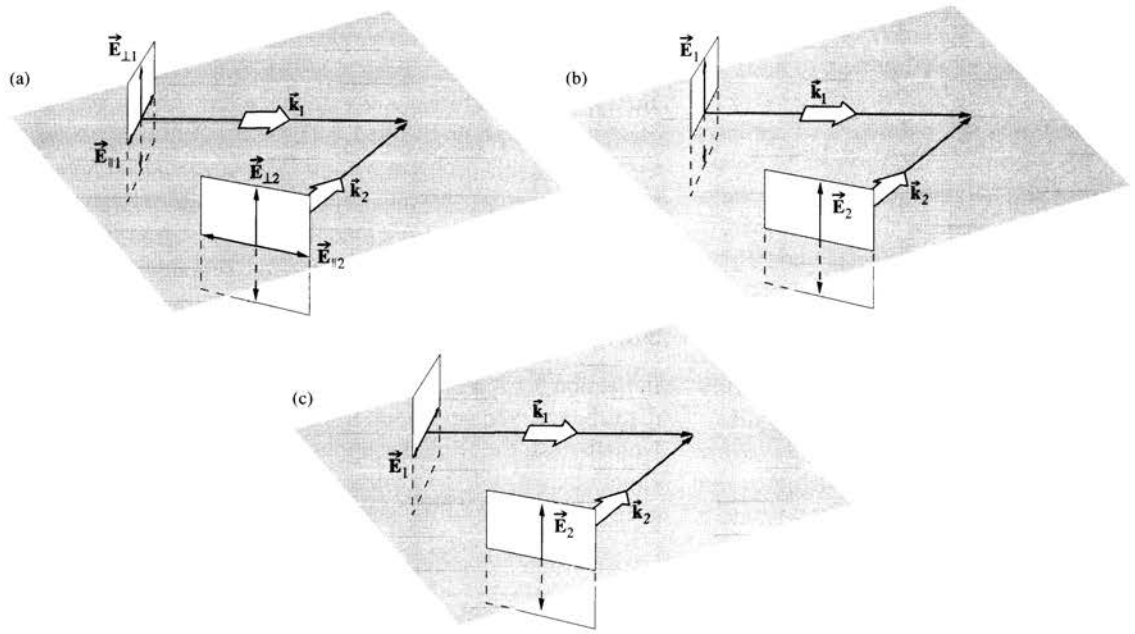


Figure 9.6 Interference of polarized light.

any polarization state can be synthesized out of two orthogonal $\mathcal{P}$-states. For natural light these $\mathcal{P}$-states are mutually incoherent, but that represents no particular difficulty.

Suppose that every wave has its propagation vector in the same plane, so that we can label the constituent orthogonal $\mathcal{P}$-states, with respect to that plane, for example, $\vec{\mathbf{E}}_{\parallel}$ and $\vec{\mathbf{E}}_{\perp}$, which are parallel and perpendicular to the plane, respectively (Fig. 9.6*a*). Thus any plane wave, whether polarized or not, can be written in the form $(\vec{\mathbf{E}}_{\parallel} + \vec{\mathbf{E}}_{\perp})$. Imagine that the waves $(\vec{\mathbf{E}}_{\parallel 1} + \vec{\mathbf{E}}_{\perp 1})$ and $(\vec{\mathbf{E}}_{\parallel 2} + \vec{\mathbf{E}}_{\perp 2})$ emitted from two identical coherent sources superimpose in some region of space. The resulting flux-density distribution will consist of two independent, precisely, overlapping interference patterns $\langle(\vec{\mathbf{E}}_{\parallel 1} + \vec{\mathbf{E}}_{\parallel 2})^2\rangle_T$ and $\langle(\vec{\mathbf{E}}_{\perp 1} + \vec{\mathbf{E}}_{\perp 2})^2\rangle_T$. Therefore, *although we derived the equations of the previous section specifically for linear light, they are applicable to any polarization state, including natural light.*

Notice that even though $\vec{\mathbf{E}}_{\perp 1}$ and $\vec{\mathbf{E}}_{\perp 2}$ are always parallel to each other, $\vec{\mathbf{E}}_{\parallel 1}$ and $\vec{\mathbf{E}}_{\parallel 2}$, which are in the reference plane, need not be. They will be parallel only when the two beams are themselves parallel (i.e., $\vec{\mathbf{k}}_1 = \vec{\mathbf{k}}_2$). The inherent vector nature of the interference process as manifest in the dot-product representation [Eq. (9.11)] of I_{12} cannot be ignored. There are many practical situations in which the beams approach being parallel, and in these cases the scalar theory will do nicely. Even so, (*b*) and (*c*) in Fig. 9.6 are included as an urge to caution. They depict the imminent overlapping of two coherent linearly polarized waves. In Fig. 9.6*b* the optical vectors are parallel, even though the beams aren't, and interference would nonetheless result. In Fig. 9.6*c* the optical vectors are perpendicular, and $I_{12} = 0$, which would be the case here even if the beams were parallel.

Fresnel and Arago made an extensive study of the conditions under which the interference of polarized light occurs, and their conclusions summarize some of the above considerations. The **Fresnel–Arago Laws** are as follows:

1. Two orthogonal, coherent $\mathcal{P}$-states cannot interfere in the sense that $I_{12} = 0$ and no fringes result.
2. Two parallel, coherent $\mathcal{P}$-states will interfere in the same way as will natural light.
3. The two constituent orthogonal $\mathcal{P}$-states of natural light cannot interfere to form a readily observable fringe pattern even if rotated into alignment. This last point is understandable, since these $\mathcal{P}$-states are incoherent.

Giesecke+Devrient GmbH,
Giesecke+Devrient Currency Technology GmbH,
and Papierfabrik Louisenthal GmbH. - Ex. 1027

9.3 Wavefront-splitting Interferometers

The main problem in producing interference is the sources: they must be *coherent*. And yet separate, independent, adequately coherent sources, other than the modern laser, don't exist! That dilemma was first solved two hundred years ago by Thomas Young in his classic double-beam experiment. He brilliantly took a single wavefront, split off from it two coherent portions, and had them interfere.

9.3.1 Young's Experiment

In 1665 Grimaldi described an experiment he had performed to examine the interaction between two beams of light. He admitted sunlight into a dark room through two close-together pinholes in an opaque screen. Like a camera obscura (p. 215), each pinhole cast an image of the Sun on a distant white surface. The idea was to show that where the circles of light overlapped, darkness could result. Although at the time he couldn't possibly understand why, the experiment failed because the primary source, the Sun's disk (which subtends about 32 minutes of arc), was too large and therefore the incident light didn't have the necessary spatial coherence in order to properly simultaneously illuminate the two pinholes. To do that, the Sun would have had to subtend only a few seconds of arc.

A hundred and forty years later, Dr. Thomas Young (guided by the phenomenon of beats, which was understood to be produced by two overlapping sound waves) began his efforts to establish the wave nature of light. He redid Grimaldi's experiment, but this time the sunlight passed through an initial pinhole, which became the primary source (Fig. 9.7). This had the effect of creating a spatially coherent beam that could identically illuminate the two apertures. In this way Young succeeded in producing a system of alternating bight and dark bands—interference fringes. Today, aware of the physics involved, we generally replace the pinholes with narrow slits that let through much more light (Fig. 9.8*a*).

Consider a hypothetical monochromatic plane wave illuminating a long narrow slit. From that primary slit light will be diffracted out at all angles in the forward direction and a cylindrical wave will emerge. Suppose that this wave, in turn, falls on two parallel, narrow, closed spaced slits, S_1 and S_2. This is shown in a three-dimensional view in Fig. 9.8*a*. When symmetry exists, the segments of the primary wavefront arriving at the two slits will be exactly in-phase, and the slits will constitute two coherent secondary sources. We expect that wherever the two waves coming from S_1 and S_2 overlap, interference will occur (provided that the optical path difference is less than the coherence length, $c\,\Delta t_c$).

Figures 9.8*a*, *b*, and *c* correspond to the classic arrangement of **Young's Experiment**, although there are other variations. Nowadays the first screen is usually dispensed with, and plane waves from a laser directly illuminate the aperture screen (Fig. 9.8*f*). In a realistic physical situation, the distance between each of the screens (Σ_a and Σ_o) in Fig. 9.8*c* would be very large in comparison with the distance a between the two slits, several thousand times as much, and all the fringes would be fairly close to the center O of the screen. The optical path difference between the rays along $\overline{S_1P}$ and $\overline{S_2P}$ can be determined, to a good approximation, by dropping a perpendicular from S_2 onto $\overline{S_1P}$. This path difference is given by

$$(\overline{S_1B}) = (\overline{S_1P}) - (\overline{S_2P}) \tag{9.22}$$

or

$$(\overline{S_1B}) = r_1 - r_2$$

Continuing with this approximation (see Problem 9.15), $(r_1 - r_2) = a \sin\theta$ and so

$$r_1 - r_2 \approx a\theta \tag{9.23}$$

since $\theta \approx \sin\theta$. Notice that

$$\theta \approx \frac{y}{s} \tag{9.24}$$

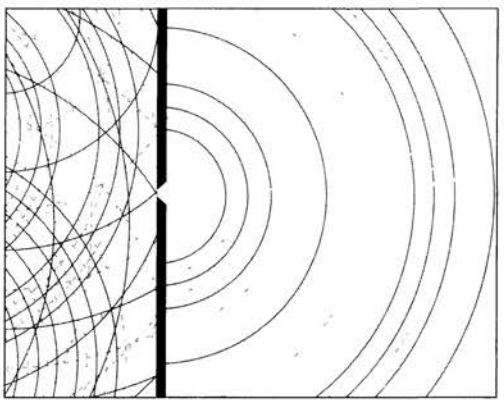
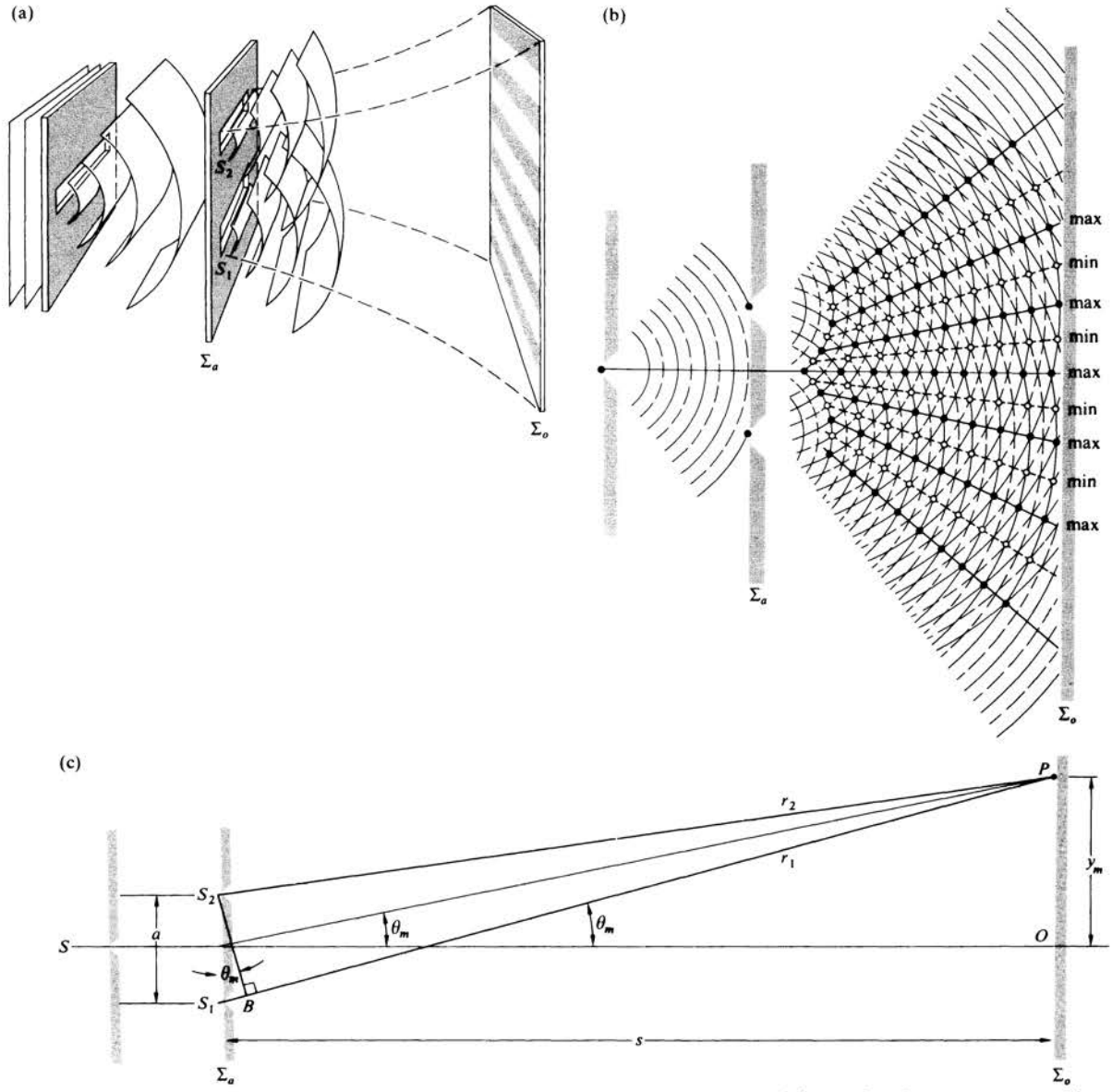


Figure 9.7 The pinhole scatters a wave that is spatially coherent, even though it's not temporally coherent.

Giesecke+Devrient GmbH,
Giesecke+Devrient Currency Technology GmbH,
and Papierfabrik Louisenthal GmbH. - Ex. 1027



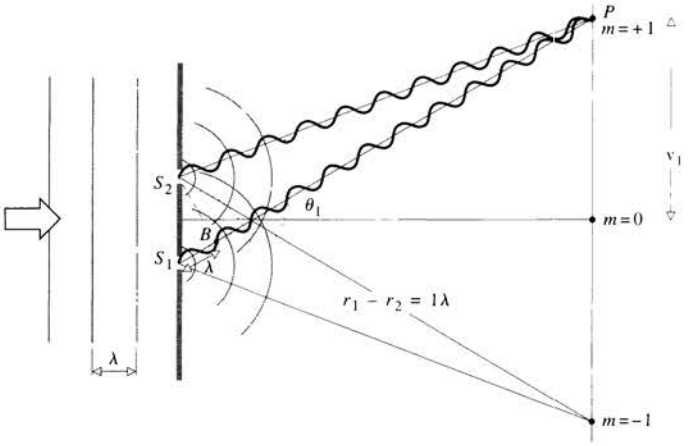
In accordance with Section 9.1, *constructive* interference

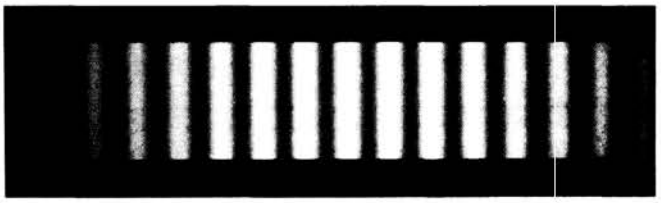
Figure 9.8 Young's Experiment. (*a*) Cylindrical waves superimposed in the region beyond the aperture screen. (*b*) Overlapping waves showing peaks and troughs. The maxima and minima lie along nearly straight hyperbolas. (*c*) The geometry of Young's Experiment. (*d*) A path length difference of one wavelength corresponds to $m = \pm 1$ and the first-order maximum. (*e*) (Photo courtesy M. Cagnet, M. Francon, and J. C. Thierr: *Atlas optischer Erscheinungen*, Berlin–Heidelberg–New York: Springer, 1962.) (*f*) A modern version of Young's Experiment using a photodetector (e.g., a photovoltaic cell or photodiode like the RS 305-462) and an $X - Y$ recorder. The detector rides on a motor-driven slide and scans the interference pattern.

and so $$r_1 - r_2 \approx \frac{a}{s} y \qquad (9.25)$$ will occur when

Giesecke+Devrient GmbH,
Giesecke+Devrient Currency Technology GmbH,
and Papierfabrik Louisenthal GmbH. - Ex. 1027

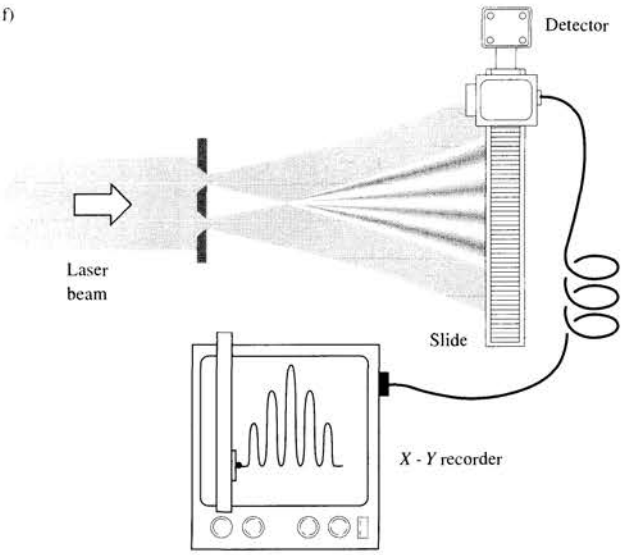
(d)





(e)

(f)



$$r_1 - r_2 = m\lambda \tag{9.26}$$

Thus, from the last two relations we obtain

$$y_m \approx \frac{s}{a} m\lambda \tag{9.27}$$

This gives the position of the mth bright fringe on the screen, if we count the maximum at 0 as the zeroth fringe. The angular position of the fringe is obtained by substituting the last expression into Eq. (9.24); thus

$$\theta_m = \frac{m\lambda}{a} \tag{9.28}$$

This relationship can be obtained directly by inspecting Fig. 9.8*c*. For the mth-order interference maximum, m whole wavelengths should fit within the distance $r_1 - r_2$. Therefore, from the triangle S_1S_2B,

$$a \sin \theta_m = m\lambda \tag{9.29}$$

or $$\theta_m \approx m\lambda/a$$

The spacing of the fringes on the screen can be gotten readily from Eq. (9.27). The difference in the positions of two consecutive maxima is

$$y_{m+1} - y_m \approx \frac{s}{a}(m + 1)\lambda - \frac{s}{a} m\lambda$$

or $$\Delta y \approx \frac{s}{a}\lambda \tag{9.30}$$

Evidently, red fringes are broader than blue ones.

Since this pattern is equivalent to that obtained for two overlapping spherical waves (at least in the $r_1 \approx r_2$ region), we can apply Eq. (9.17). Using the phase difference

$$\delta = k(r_1 - r_2)$$

Eq. (9.17) can be rewritten as

Giesecke+Devrient GmbH,
Giesecke+Devrient Currency Technology GmbH,
and Papierfabrik Louisenthal GmbH. - Ex. 1027

$$I = 4I_0 \cos^2 \frac{k(r_1 - r_2)}{2}$$

provided, of course, that the two beams are coherent and have equal irradiances I_0. With

$$r_1 - r_2 \approx ya/s$$

the resultant irradiance becomes

$$I = 4I_0 \cos^2 \frac{ya\pi}{s\lambda} \tag{9.31}$$

As shown in Fig. 9.9, consecutive maxima are separated by the Δy given in Eq. (9.30). Remember that we effectively assumed that each slit was infinitesimally wide, and so the cosine-squared fringes of Fig. 9.9 are really an unattainable idealization.* The actual pattern, Fig. 9.8*e*, drops off with distance on either side of O because of diffraction.

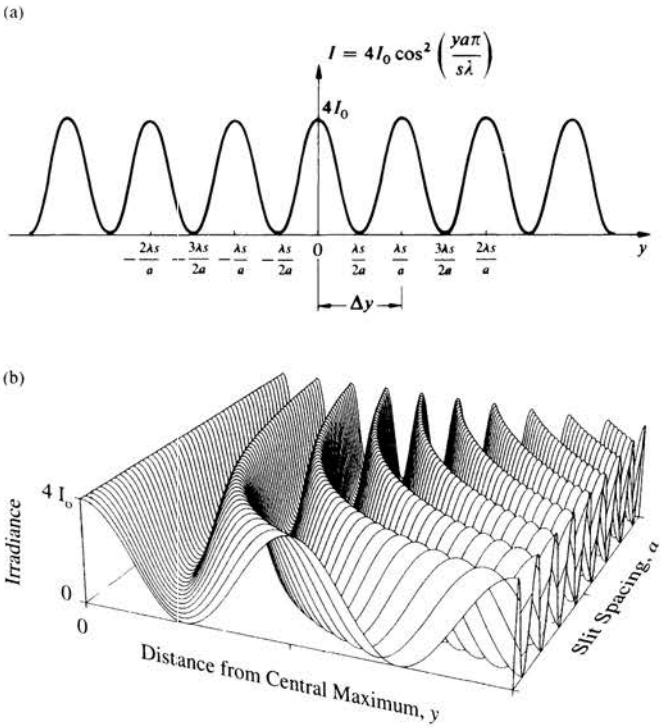


Figure 9.9 (*a*) Idealized irradiance versus distance curve. (*b*) The fringe separation Δy varies inversely with the slit separation, as one might expect from Fourier considerations; remember the inverse nature of spatial intervals and spatial frequency intervals. (Reprinted from "Graphical Representations of Fraunhofer Interference and Diffraction," *Am. J. Phys* **62**, 6 (1994), with permission of A.B. Bartlett, University of Colorado and B. Mechtly, Northeast Missouri State University and the American Association of Physics Teachers.)

The Effects of Finite Coherence Length

As P in Fig. 9.8*c* is taken farther above or below the axis, $\overline{S_1B}$ (which is less than or equal to $\overline{S_1S_2}$) increases. If the primary source has a short coherence length, as the optical path difference increases, identically paired wavegroups will no longer be able to arrive at P exactly together. There will be an increasing amount of overlap in portions of uncorrelated wavegroups, and the contrast of the fringes will degrade. It is possible for Δl_c to be less than $\overline{S_1B}$. In that case, instead of two correlated portions of the same wavegroup arriving at P, only segments of different wavegroups will overlap, and the fringes will vanish.

As depicted in Fig. 9.10*a*, when the path length difference exceeds the coherence length, wavegroup-E_1 from source S_1 arrives at P with wavegroup-D_2 from S_2. There is interference, but it lasts only a short time before the pattern shifts as wavegroup-D_1 begins to overlap wavegroup-C_2, since the relative phases are different. If the coherence length was larger or the path difference smaller, wavegroup-D_1 would more or less interact with its clone wavegroup-D_2, and so on for each pair. The phases would then be correlated, and the interference pattern stable (Fig. 9.10*b*). Since a whitelight source will have a coherence length of less than about three wavelengths, it follows from Eq. (9.27) that only about three fringes will be seen on either side of the central maximum.

Under white light (or with broad bandwidth illumination), all the constituent colors will arrive at $y = 0$ in-phase, having traveled equal distances from each aperture. The zeroth-order fringe will be essentially white, but all other higher order maxima will show a spread of wavelengths, since y_m is a function of λ, according to Eq. (9.27). Thus in white light we can think of the mth maximum as the mth-order band of wavelengths—a notion that will lead directly to the diffraction grating in the next chapter.

The fringe pattern can be observed by punching two small pinholes in a thin card. The holes should be approximately the size of the type symbol for a period on this page, and the separation between their centers about three radii. A street lamp,

*Modifications of this pattern arising as a result of increasing the width of either the primary S or secondary-source slits will be considered in later chapters (10 and 12). In the latter case, fringe contrast will be used as a measure of the degree of coherence (Section 12.1). In the latter, diffraction effects become significant.

Giesecke+Devrient GmbH,
Giesecke+Devrient Currency Technology GmbH,
and Papierfabrik Louisenthal GmbH. - Ex. 1027

car headlight, or traffic signal at night, located a few hundred feet away, will serve as a plane-wave source. The card should be positioned directly in front of and *very close to the eye*. The fringes will appear perpendicular to the line of centers. The pattern is much more readily seen with slits, as discussed in Section 10.2.2, but you should give the pinholes a try.

Microwaves, because of their long wavelength, also offer an easy way to observe double-slit interference. Two slits (e.g., $\lambda/2$ wide by λ long, separated by 2λ) cut in a piece of sheet metal or foil will serve quite well as secondary sources (Fig. 9.11).

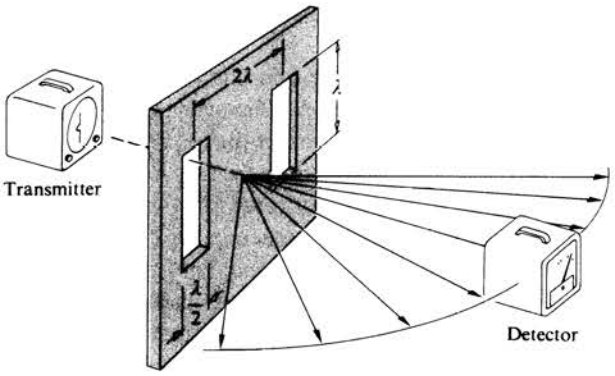


Figure 9.11 A microwave interferometer.

The Fourier Perspective

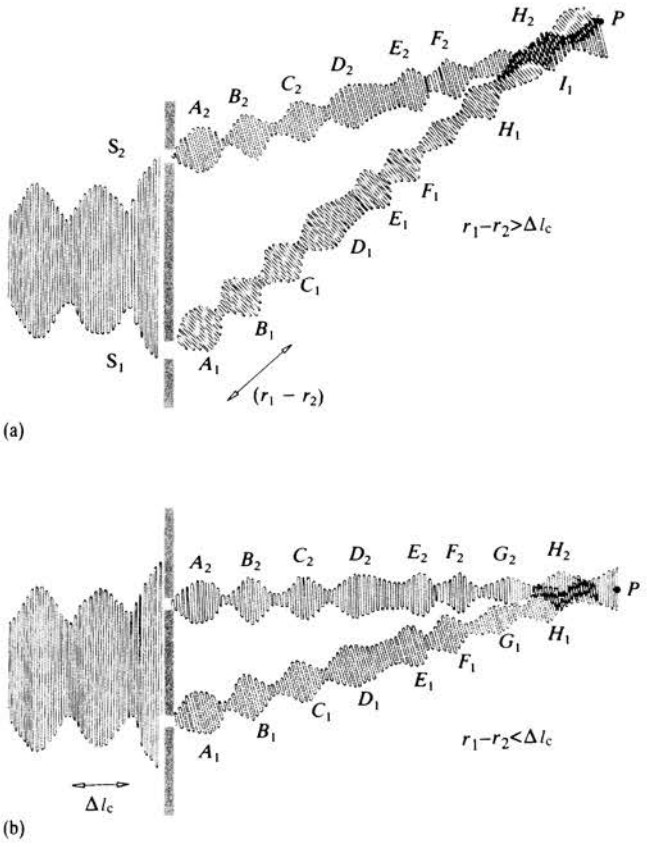


Figure 9.10 A schematic representation of how light, composed of a progression of wavegroups with a coherence length Δl_c, produces interference when (*a*) the path length difference exceeds Δl_c and (*b*) the path length difference is less than Δl_c.

When the plane waves in Fig. 9.8*b* illuminated the first narrow slit, light spilled out (i.e., diffracted) beyond the opaque screen in a form resembling a cylindrical wave; the narrower the slit, the more nearly cylindrical the wave. Beyond the screen the light spread over a very wide range of angles, or equivalently a wide range of spatial frequencies. From a Fourier perspective, this happened because an infinitesimally narrow source (i.e., narrow in space) generates a light field that is infinitely broad (i.e., broad in spatial frequency). The transform of a point source, an ideal one-dimensional signal spike (known as a Dirac delta function, p. 524), is a continuous constant spectrum containing all spatial frequencies, a spherical wave. In the same way, an ideal line source results in a cylindrical wave.

In practice, Young's Experiment usually consists of two in-phase slit sources arranged such that $s >> a$. As a rule, s is so large that the resulting fringe system corresponds to a Fraunhofer diffraction pattern (p. 457). The two very thin slits resemble two line sources, two ideally narrow signal spikes, and the transform of two delta functions is a cosine function—we saw that in Fig. 7.42. To the extent that the slits can be considered infinitesimally narrow, the amplitude of the electric field in the diffraction pattern will be cosinusoidal, and the irradiance distribution will vary as the cosine squared, as in Fig. 9.9.

Several Other Interferometers

The same physical and mathematical considerations applied to Young's Experiment relate directly to a number of other wavefront-splitting interferometers. Most common among

Giesecke+Devrient GmbH,
Giesecke+Devrient Currency Technology GmbH,
and Papierfabrik Louisenthal GmbH. - Ex. 1027

these are Fresnel's double mirror, Fresnel's double prism, and Lloyd's mirror.

Fresnel's double mirror consists of two plane front-silvered mirrors inclined to each other at a very small angle, as shown in Fig. 9.12. One portion of the cylindrical wavefront coming from slit S is reflected from the first mirror, and another portion of the wavefront is reflected from the second mirror. An interference field exists in space in the region where the two reflected waves are superimposed. The images (S_1 and S_2) of the slit S in the two mirrors can be considered as separate coherent sources, placed at a distance a apart. It follows from the Laws of Reflection, as illustrated in Fig. 9.12*a*, that $\overline{SA} = \overline{S_1A}$ and $\overline{SB} = \overline{S_2B}$ so that $\overline{SA} + \overline{AP} = r_1$ and $\overline{SB} + \overline{BP} = r_2$. The optical path length difference between the two rays is then $r_1 - r_2$. The various maxima occur at $r_1 - r_2 = m\lambda$, as they do with Young's Interferometer. Again, the separation of the fringes is given by

$$\Delta y \approx \frac{s}{a}\lambda$$

where s is the distance between the plane of the two virtual sources (S_1, S_2) and the screen. The arrangement in Fig. 9.12 has been deliberately exaggerated to make the geometry somewhat clearer. The angle θ between the mirrors must be quite small if the electric-field vectors for each of the two beams are to be parallel, or nearly so. Let $\vec{\mathbf{E}}_1$ and $\vec{\mathbf{E}}_2$ represent the light-waves emitted from the coherent virtual sources S_1 and S_2. At any instant in time at the point P in space, each of these vectors can be resolved into components, parallel and perpendicular to the plane of the figure. With $\vec{\mathbf{k}}_1$ and $\vec{\mathbf{k}}_2$ parallel to $\overline{AP}$ and $\overline{BP}$, respectively, it should be apparent that the components of $\vec{\mathbf{E}}_1$ and $\vec{\mathbf{E}}_2$ in the plane of the figure will approach being parallel only for small θ. As θ decreases, a decreases and the fringes broaden.

The **Fresnel double prism** or biprism consists of two thin prisms joined at their bases, as shown in Fig. 9.13. A single cylindrical wavefront impinges on both prisms. The top portion of the wavefront is refracted downward, and the lower segment is refracted upward. In the region of superposition, interference occurs. Here, again, two virtual sources S_1 and S_2

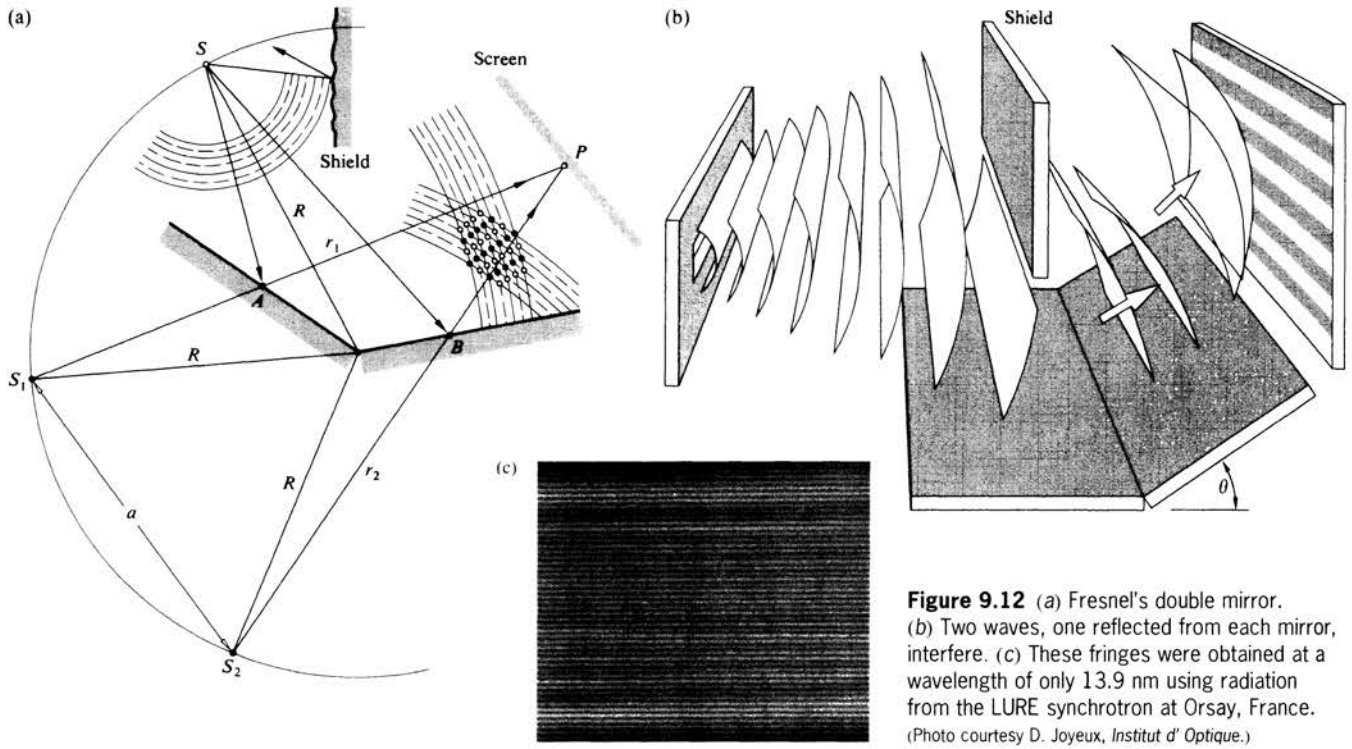
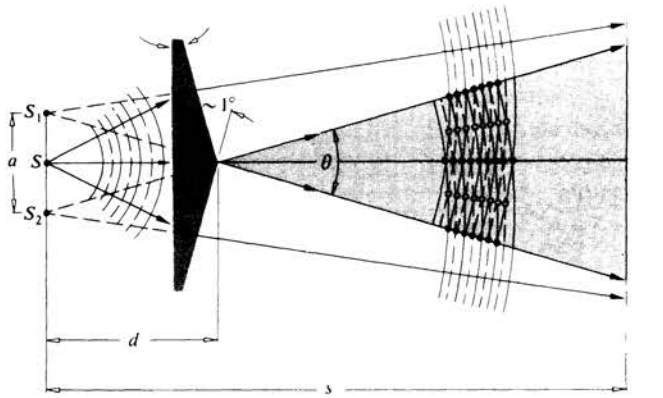
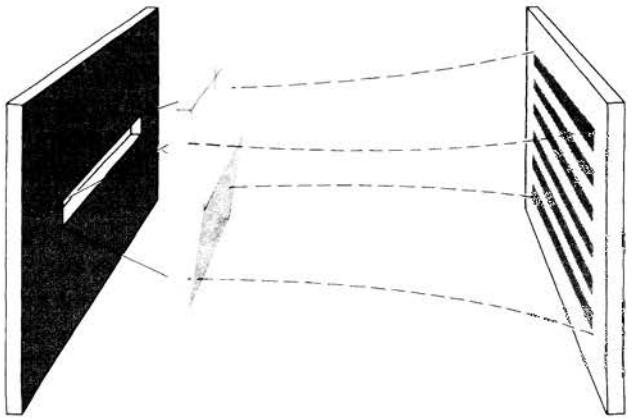


Figure 9.12 (*a*) Fresnel's double mirror. (*b*) Two waves, one reflected from each mirror, interfere. (*c*) These fringes were obtained at a wavelength of only 13.9 nm using radiation from the LURE synchrotron at Orsay, France. (Photo courtesy D. Joyeux, *Institut d' Optique*.)

Giesecke+Devrient GmbH,
Giesecke+Devrient Currency Technology GmbH,
and Papierfabrik Louisenthal GmbH. - Ex. 1027



(a)



(b)



(c)

Figure 9.13 Fresnel's biprism. (*a*) The biprism creates two image sources. (*b*) With a slit source the fringes are bright bands. (*c*) Interference fringes observed with an electron biprism arrangement by G. Möllenstedt. Once again electrons behave like photons. (Photo from *Handbuch der Physik*, edited by S. Flugge, Springer-Verlag, Heidelberg.)

exist, separated by a distance a, which can be expressed in terms of the prism angle α (Problem 9.19), where $s >> a$. The expression for the separation of the fringes is the same as before.

The last wavefront-splitting interferometer that we will consider is **Lloyd's mirror**, shown in Fig. 9.14. It consists of a flat piece of either dielectric or metal that serves as a mirror, from which is reflected a portion of the cylindrical wavefront coming from slit S. Another portion of the wavefront proceeds directly from the slit to the screen. For the separation a, between the two coherent sources, we take the distance between the actual slit and its image S_1 in the mirror. The spacing of the fringes is once again given by $(s/a)\lambda$. The distinguishing feature of this device is that at glancing incidence ($\theta_i = \pi/2$) the reflected beam undergoes a 180° phase shift. (Recall that the amplitude-reflection coefficients are then both equal to -1.) With an additional phase shift of $\pm\pi$,

$$\delta = k(r_1 - r_2) \pm \pi$$

and the irradiance becomes

$$I = 4I_0 \sin^2\left(\frac{\pi a y}{s\lambda}\right)$$

The fringe pattern for Lloyd's mirror is complementary to that of Young's interferometer; the maxima of one pattern exist at values of y that correspond to minima in the other pattern. The top edge of the mirror is equivalent to $y = 0$ and will be the center of a dark fringe rather than a bright one, as in Young's device. The lower half of the pattern will be obstructed by the presence of the mirror itself. Consider what

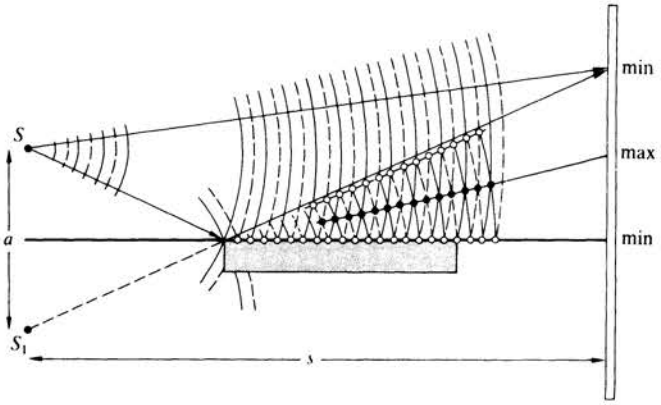


Figure 9.14 Lloyd's mirror.

Giesecke+Devrient GmbH,
Giesecke+Devrient Currency Technology GmbH,
and Papierfabrik Louisenthal GmbH. - Ex. 1027

would happen if a thin sheet of transparent material were placed in the path of the rays traveling directly to the screen. The transparent sheet would have the effect of increasing the number of wavelengths in each direct ray. The entire pattern would accordingly move upward, where the reflected rays would travel a bit farther before interfering. Because of the obvious inherent simplicity of this device, it has been used over a very wide region of the electromagnetic spectrum. The actual reflecting surfaces have ranged from crystals for X-rays, ordinary glass for light, and wire screening for microwaves to a lake or even the Earth's ionosphere for radiowaves.*

All the above interferometers can be demonstrated quite readily either using a laser or, for white light, something a bit more old-fashioned like a discharge lamp or a carbon arc (Fig. 9.15).

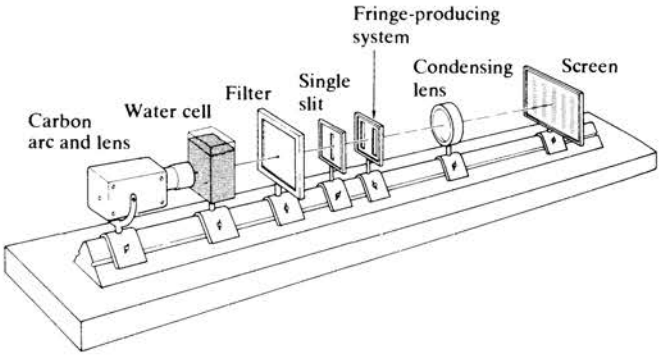


Figure 9.15 Bench setup to study wavefront-splitting arrangements with a carbon arc source.The water cell is needed to keep things cool.

9.4 Amplitude-Splitting Interferometers

Suppose that a lightwave is incident on a half-silvered mirror,† or simply on a sheet of glass. Part of the wave is transmitted and part reflected. Both the transmitted and reflected waves have lower amplitudes than the original one. It can be said figuratively that the amplitude has been "split."

If the two separate waves could be brought together again at a detector, interference would result, as long as the original coherence between the two had not been destroyed. If the path lengths differed by a distance greater than that of the wavegroup (i.e., the coherence length), the portions reunited at the detector would correspond to different wavegroups. No unique phase relationship would exist between them in that case, and the fringe pattern would be unstable to the point of being unobservable. We will get back to these ideas when we consider coherence theory in more detail. For the moment the discussion is restricted, for the most part, to those cases for which the path difference is less than the coherence length.

*For a discussion of the effects of a finite slit width and a finite frequency bandwidth, see R. N. Wolfe and F. C. Eisen, "Irradiance Distribution in a Lloyd Mirror Interference Pattern," *J. Opt. Soc. Am.* **38**, 706 (1948).

†A *half-silvered mirror* is one that is semitransparent, because the metallic coating is too thin to be opaque. You can look through it, and at the same time you can see your reflection in it. *Beamsplitters*, as devices of this kind are called, can also be made of thin stretched plastic films, known as *pellicles*, or even uncoated glass plate.

9.4.1 Dielectric Films—Double-Beam Interference

Interference effects are observable in sheet transparent materials, the thicknesses of which vary over a very broad range, from films less than the length of a lightwave (e.g., for green light λ_0 equals about $\frac{1}{150}$ the thickness of this printed page) to plates several centimeters thick. A layer of material is referred to as a *thin film* for a given wavelength of electromagnetic radiation when its thickness is of the order of that wavelength. Before the early 1940s, interference phenomena associated with thin dielectric films, although well known, had fairly limited practical value. The rather spectacular color displays arising from oil slicks and soap films, however pleasing aesthetically and theoretically, were mainly curiosities.

With the advent of suitable vacuum deposition techniques in the 1930s, precisely controlled coatings could be produced on a commercial scale, and that, in turn, led to a rebirth of interest in dielectric films. During the Second World War, both sides were finding the enemy with a variety of coated optical devices, and by the 1960s multilayered coatings were in widespread use.

Fringes of Equal Inclination

Giesecke+Devrient GmbH,
Giesecke+Devrient Currency Technology GmbH,
and Papierfabrik Louisenthal GmbH. - Ex. 1027

Consider the simple case of a transparent parallel plate of dielectric material having a thickness d (Fig. 9.16). Suppose that the film is nonabsorbing and that the amplitude-reflection coefficients at the interfaces are so low that only the first two reflected beams E_{1r} and E_{2r} (both having undergone only one reflection) need be considered (Fig. 9.17). In practice, the amplitudes of the higher-order reflected beams (E_{3r}, etc.) generally decrease very rapidly, as can be shown for the air–water and air–glass interfaces (Problem 9.25). For the moment, consider S to be a monochromatic point source.

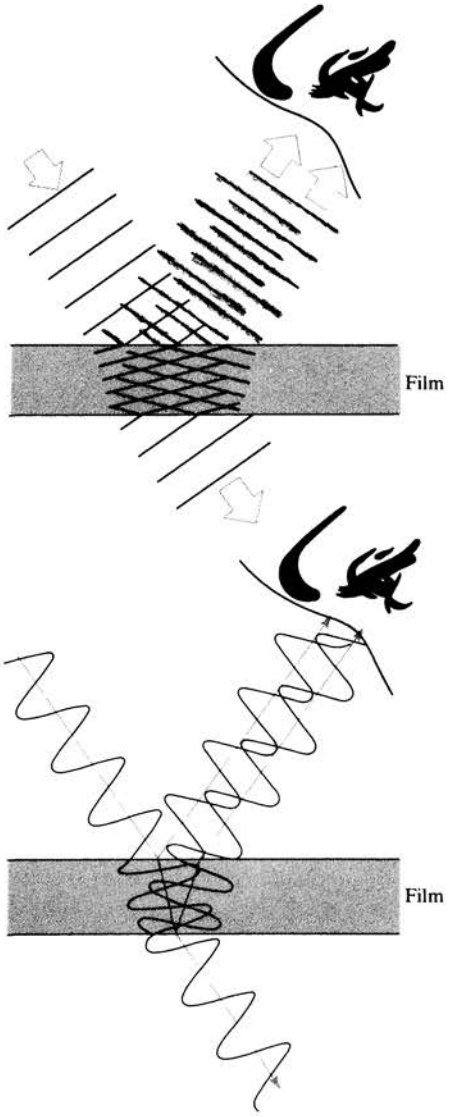


Figure 9.16 The wave and ray representations of thin-film interference. Light reflected from the top and bottom of the film interferes to create a fringe pattern.

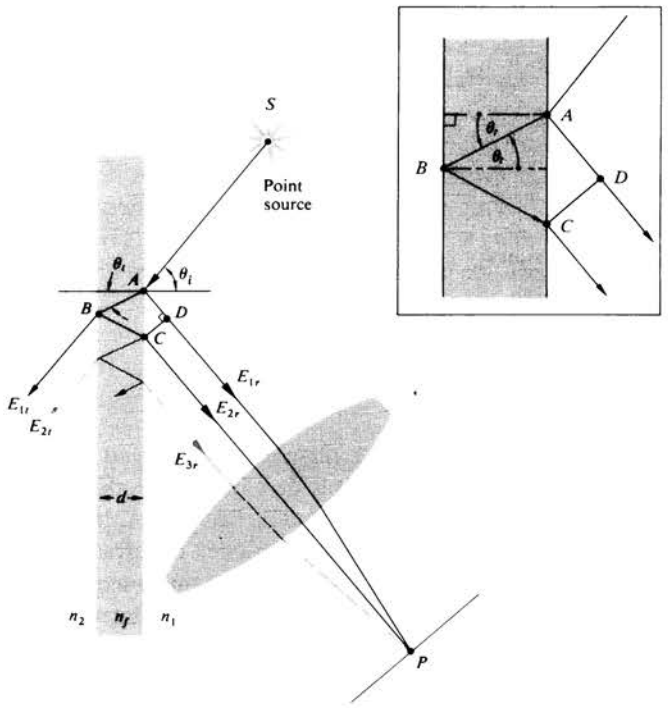


Figure 9.17 Fringes of equal inclination.

The film serves as an amplitude-splitting device, so that E_{1r} and E_{2r} may be considered as arising from two coherent virtual sources lying behind the film; that is, the two images of S formed by reflection at the first and second interfaces. The reflected rays are parallel on leaving the film and can be brought together at a point P on the focal plane of a telescope objective or on the retina of the eye when focused at infinity. From Fig. 9.17, the optical path length difference for the first two reflected beams is given by

$$\Lambda = n_f[(\overline{AB}) + (\overline{BC})] - n_1(\overline{AD})$$

and since $(\overline{AB}) = (\overline{BC}) = d/\cos\theta_t$,

$$\Lambda = \frac{2n_f d}{\cos\theta_t} - n_1(\overline{AD})$$

Now, to find an expression for $(\overline{AD})$, write

Giesecke+Devrient GmbH,
Giesecke+Devrient Currency Technology GmbH,
and Papierfabrik Louisenthal GmbH. - Ex. 1027

$$(\overline{AD}) = (\overline{AC})\sin\,\theta_i$$

Using Snell's Law, this becomes

$$(\overline{AD}) = (\overline{AC})\,\frac{n_f}{n_1}\sin\,\theta_t$$

where

$$(\overline{AC}) = 2d\tan\,\theta_t \tag{9.32}$$

The expression for Λ now becomes

$$\Lambda = \frac{2n_f d}{\cos\,\theta_t}(1-\sin^2\,\theta_t)$$

or finally

$$\Lambda = 2n_f d\cos\,\theta_t \tag{9.33}$$

The corresponding phase difference associated with the optical path length difference is then just the product of the free-space propagation number and Λ, that is, $k_0\Lambda$. If the film is immersed in a single medium, the index of refraction can simply be written as $n_1 = n_2 = n$. Realize that n may be less than n_f, as in the case of a soap film in air, or greater than n_f, as with an air film between two sheets of glass. In either case *there will be an additional phase shift arising from the reflections themselves*. Recall that for incident angles up to about 30°, regardless of the polarization of the incoming light, the two beams, one internally and one externally reflected, will experience a *relative phase shift* of π radians (Fig. 4.44 and Section 4.3). Accordingly,

$$\delta = k_0\Lambda \pm \pi$$

and more explicitly

$$\delta = \frac{4\pi n_f}{\lambda_0}d\cos\,\theta_t \pm \pi \tag{9.34}$$

or

$$\delta = \frac{4\pi d}{\lambda_0}(n_f^2 - n^2\sin^2\,\theta_i)^{1/2} \pm \pi \tag{9.35}$$

The sign of the phase shift is immaterial, so we will choose the negative sign to make the equations a bit simpler. In reflected light an interference maximum, a bright spot, appears at P when $\delta = 2m\pi$—in other words, an even multiple of π. In that case Eq. (9.34) can be rearranged to yield

[maxima]
$$d\cos\,\theta_t = (2m+1)\,\frac{\lambda_f}{4} \tag{9.36}$$

where $m = 0,1,2,\ldots$ and use has been made of the fact that $\lambda_f = \lambda_0/n_f$. This also corresponds to minima in the transmitted light. Interference minima in reflected light (maxima in transmitted light) result when $\delta = (2m \pm 1)\pi$, that is, odd multiples of π. For such cases Eq. (9.34) yields

[minima]
$$d\cos\,\theta_t = 2m\,\frac{\lambda_f}{4} \tag{9.37}$$

The appearance of odd and even multiples of $\lambda_f/4$ in Eqs. (9.36) and (9.37) is significant , as we will see presently. We could, of course, have a situation in which $n_1 > n_f > n_2$ or $n_1 < n_f < n_2$, as with a fluoride film deposited on an optical element of glass immersed in air. The π phase shift would then not be present, and the above equations would simply be modified appropriately.

If the lens used to focus the rays has a small aperture, interference fringes will appear on a small portion of the film. Only the rays leaving the point source that are reflected directly into

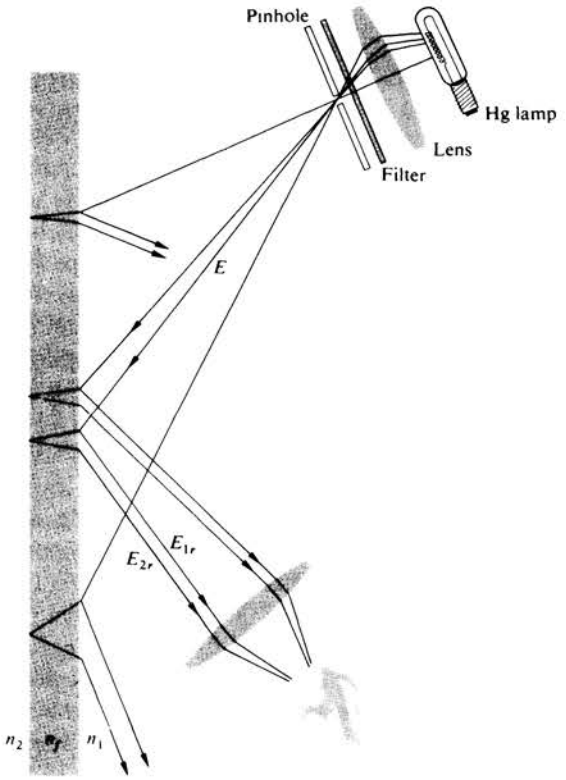


Figure 9.18 Fringes seen on a small portion of the film.

Giesecke+Devrient GmbH,
Giesecke+Devrient Currency Technology GmbH,
and Papierfabrik Louisenthal GmbH. - Ex. 1027

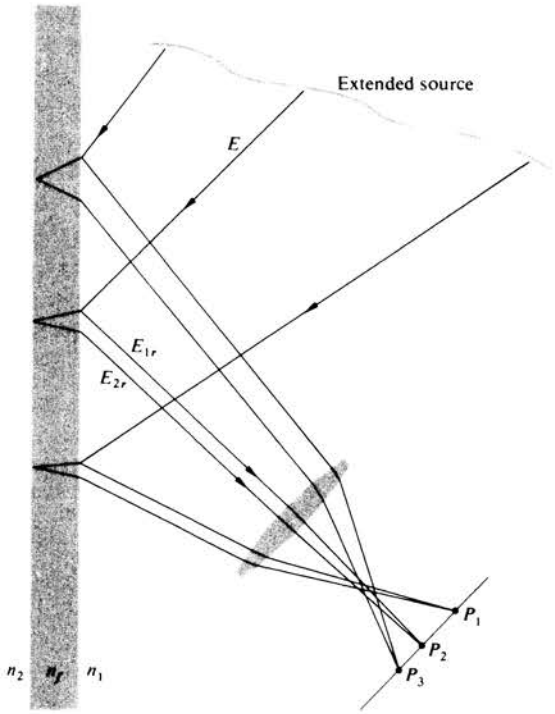


Figure 9.19 Fringes seen on a large region of the film.

the lens will be seen (Fig. 9.18). For an extended source, light will reach the lens from various directions, and the fringe pattern will spread out over a large area of the film (Fig. 9.19).

The angle θ_i or equivalently θ_t, determined by the position of P, will in turn control δ. The fringes appearing at points P_1 and P_2 in Fig. 9.20 are known as **fringes of equal inclination**. (Problem 9.30 discusses some easy ways to see these fringes.) Keep in mind that each source point on the extended source is incoherent with respect to the others. When the image of the extended source is reflected in the surface, it will be seen to be banded with bright and dark fringes. Each of these is an arc of a circle centered on the intersection of a perpendicular dropped from the eye to the film.

As the film becomes thicker, the separation $\overline{AC}$ between E_{1r} and E_{2r} also increases, since

$$\overline{AC} = 2d \tan \theta_t \qquad [9.32]$$

When only one of the two rays is able to enter the pupil of the eye, the interference pattern will disappear. The larger lens of a telescope can then be used to gather in both rays, once again making the pattern visible. The separation can also be reduced by reducing θ_t and therefore θ_i, that is, by viewing the film at nearly normal incidence. The equal-inclination fringes that are seen in this manner for thick plates are known as **Haidinger fringes**, after the Austrian physicist Wilhelm Karl Haidinger (1795–1871). With an extended source, the symmetry of the setup requires that the interference pattern consists of a series of concentric circular bands centered on the perpendicular drawn from the eye to the film (Fig. 9.21). As the observer moves, the interference pattern follows along.

Haidinger fringes can be seen in the ordinary window glass of a store front. Find one with a neon sign in the window and look out at the street, at night, very close to the glowing tube. You'll see circular fringes centered on your eye floating off in the distance.

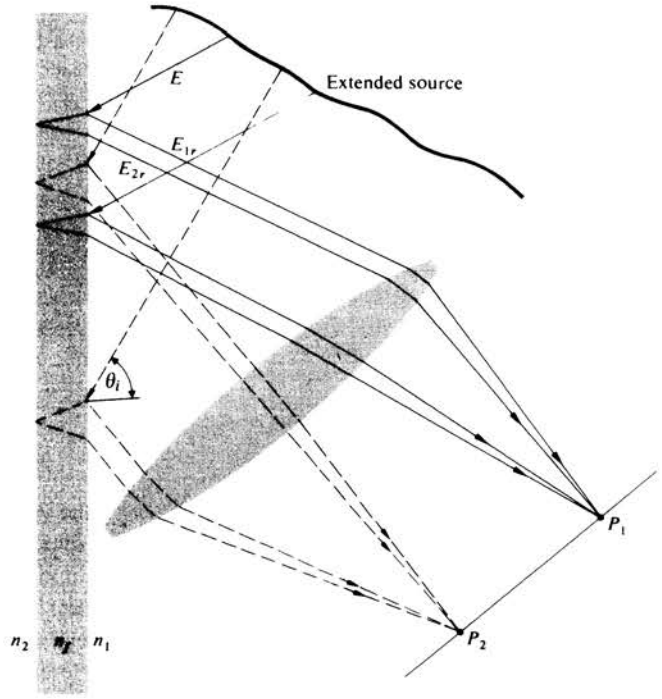


Figure 9.20 All rays inclined at the same angle arrive at the same point.

Giesecke+Devrient GmbH,
Giesecke+Devrient Currency Technology GmbH,
and Papierfabrik Louisenthal GmbH. - Ex. 1027

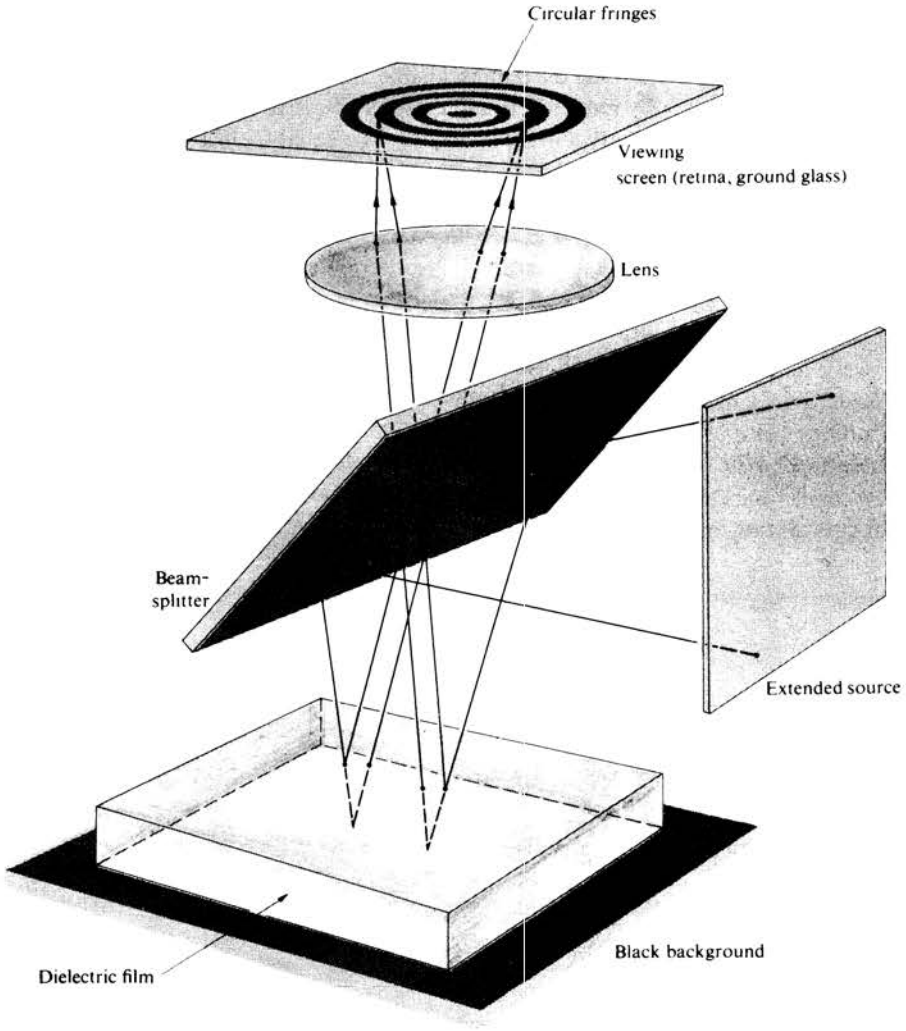


Figure 9.21 Circular Haidinger fringes centered on the lens axis.

Fringes of Equal Thickness

A whole class of interference fringes exists for which the optical thickness, $n_f d$, is the dominant parameter rather than θ_i. These are referred to as **fringes of equal thickness**. Under white-light illumination the iridescence of soap bubbles, oil slicks (a few wavelengths thick), and even oxidized metal surfaces is the result of variations in film thickness. Interference bands of this kind are analogous to the constant-height contour lines of a topographical map. Each fringe is the locus of all points in the film for which the optical thickness is a constant. In general, n_f does not vary, so that the fringes correspond to regions of constant film thickness. As such, they can be quite useful in determining the surface features of optical elements (lenses, prisms, etc.). For example, a surface to be examined may be put into contact with an *optical flat*.* The air in the space between the two generates a thin-film interference pat-

*A surface is said to be optically flat when it deviates by not more than about $\lambda/4$ from a perfect plane. In the past, the best flats were made of clear fused quartz. Now glass-ceramic materials (e.g., CERVIT) having extremely small thermal coefficients of expansion (about one-sixth that of quartz) are available. Individual flats of $\lambda/200$ or a bit better can be made.

Giesecke+Devrient GmbH,
Giesecke+Devrient Currency Technology GmbH,
and Papierfabrik Louisenthal GmbH. - Ex. 1027

tern. If the test surface is flat, a series of straight, equally spaced bands indicates a wedge-shaped air film, usually resulting from dust between the flats. Two pieces of plate glass separated at one end by a strip of paper will form a satisfactory wedge with which to observe these bands.

When viewed at nearly normal incidence in the manner illustrated in Fig. 9.22, the contours arising from a nonuniform film are called **Fizeau fringes**. For a thin wedge of small angle α, the optical path length difference between two reflected rays may be approximated by Eq. (9.33), where d is the thickness at a particular point, that is,

$$d = x\alpha \tag{9.38}$$

For small values of θ_i the condition for an interference maximum becomes

$$(m + \tfrac{1}{2})\lambda_0 = 2n_f d_m$$

or

$$(m + \tfrac{1}{2})\lambda_0 = 2\alpha x_m n_f$$

Since $n_f = \lambda_0/\lambda_f$, x_m may be written as

$$x_m = \left(\frac{m + 1/2}{2\alpha}\right)\lambda_f \tag{9.39}$$

Maxima occur at distances from the apex given by $\lambda_f/4\alpha$, $3\lambda_f/4\alpha$, and so on, and consecutive fringes are separated by a distance Δx, given by

$$\Delta x = \lambda_f/2\alpha \tag{9.40}$$

Notice that the difference in film thickness between adjacent maxima is simply $\lambda_f/2$. Since the beam reflected from the lower surface traverses the film twice ($\theta_i \approx \theta_t \approx 0$), adjacent maxima differ in optical path length by λ_f. Note, too, that the film thickness at the various maxima is given by

$$d_m = (m + \tfrac{1}{2})\frac{\lambda_f}{2} \tag{9.41}$$

which is an odd multiple of a quarter wavelength. Traversing the film twice yields a phase shift of π, which, when added to the shift of π resulting from reflection, puts the two rays back in-phase.

The accompanying photo shows a soap film held vertically so that it settles into a wedge shape under the influence of gravity. When illuminated with white light, the bands are various colors. The black region at the top is a portion where the film is less than $\lambda_f/4$ thick. Twice this, plus an additional shift of $\lambda_f/2$ due to the reflection, is less than a whole wavelength. The reflected rays are therefore out-of-phase. As the thickness decreases still further, the total phase difference approaches π. The irradiance at the observer goes to a mini-

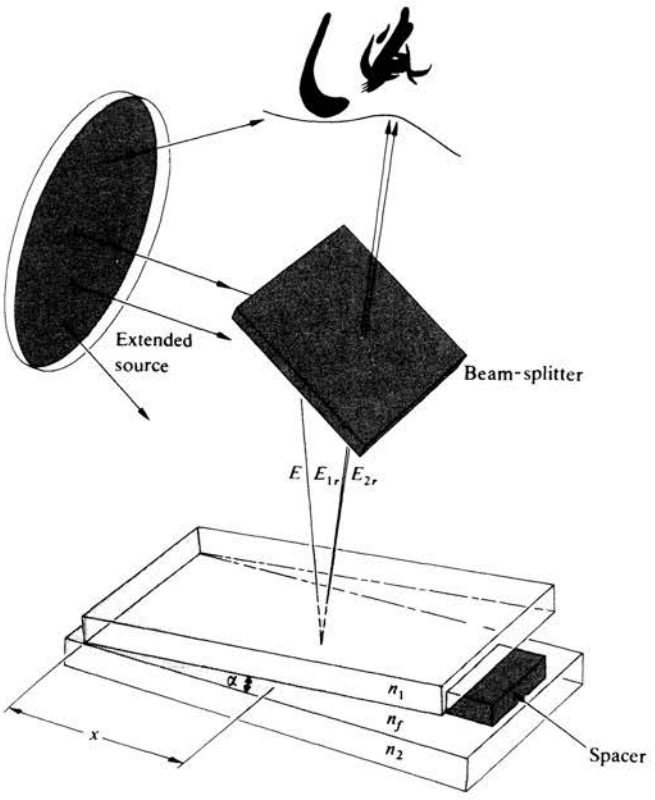
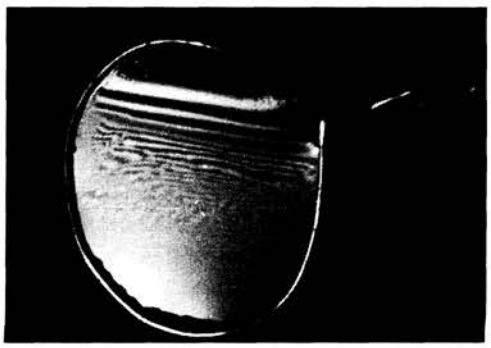


Figure 9.22 Fringes from a wedge-shaped film.



A wedge-shaped film made of liquid dishwashing soap. (Photo by E. H.)

Giesecke+Devrient GmbH,
Giesecke+Devrient Currency Technology GmbH,
and Papierfabrik Louisenthal GmbH. - Ex. 1027



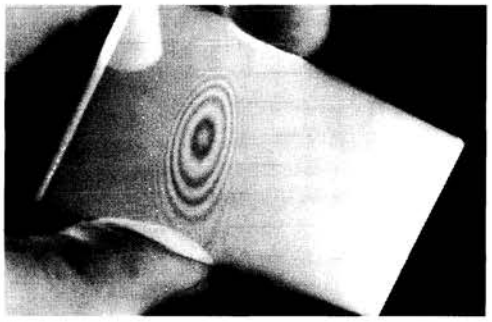
Fringes created by an air film between two microscope slides. (Photo by E. H.)

mum (Eq. 9.16), and the film appears black in reflected light.*

Press two well-cleaned microscope slides together. The enclosed air film will usually not be uniform. In ordinary room light a series of irregular, colored bands (fringes of equal thickness) will be clearly visible across the surface. The thin glass slides distort under pressure, and the fringes move and change accordingly. Tape two slides together with transparent (matt-surfaced) tape. It will scatter light and make the reflected fringes more easily seen.

If the two pieces of glass are forced together at a point, as might be done by pressing on them with a sharp pencil, a series of concentric, nearly circular, fringes is formed about that point. Known as **Newton's rings***, this pattern is more precisely examined with the arrangement of Fig. 9.23. Here a lens is placed on an optical flat and illuminated at normal incidence with quasimonochromatic light. The amount of uniformity in the concentric circular pattern is a measure of the degree of perfection in the shape of the lens. With R as the radius of curvature of the convex lens, the relation between the distance x and the film thickness d is given by

$$x^2 = R^2 - (R - d)^2$$



Newton's rings with two microscope slides. The thin film of air between the slides creates the interference pattern. (Photo by E. H.)

*The relative phase shift of π between internal and external reflection is required if the reflected flux density is to go to zero smoothly, as the film gets thinner and finally disappears.

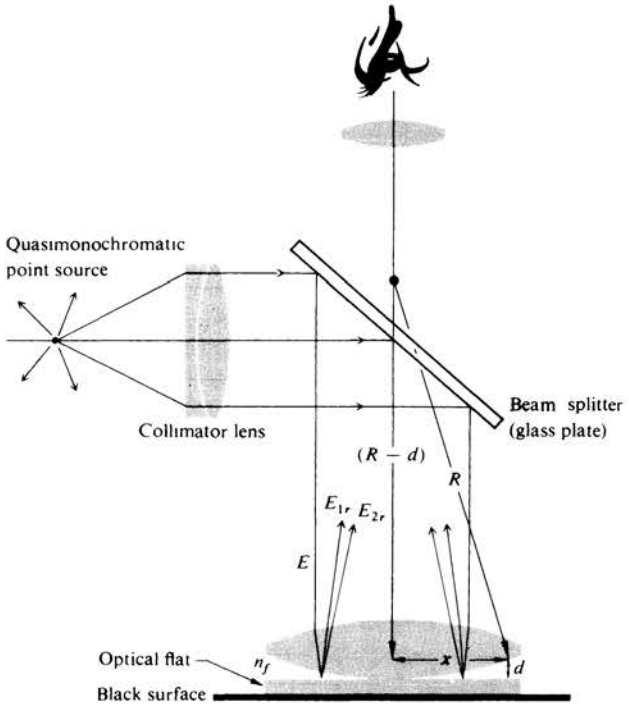


Figure 9.23 A standard setup to observe Newton's rings

*Robert Hooke (1635–1703) and Isaac Newton independently studied a whole range of thin-film phenomena, from soap bubbles to the air film between lenses. Quoting from Newton's *Opticks*:

> I took two Object-glasses, the one a Planoconvex for a fourteen Foot Telescope, and the other a large double Convex for one of about fifty Foot; and upon this, laying the other with its plane side downwards, I pressed them slowly together to make the Colours successfully emerge in the middle of the Circles.

Giesecke+Devrient GmbH,
Giesecke+Devrient Currency Technology GmbH,
and Papierfabrik Louisenthal GmbH. - Ex. 1027



Interference from the thin air film between a convex lens and the flat sheet of glass it rests on. The illumination was quasimonochromatic. These fringes were first studied in depth by Newton and are known as Newton's rings. (Photo by E.H.)

or more simply by

$$x^2 = 2Rd - d^2$$

Since $R >> d$, this becomes

$$x^2 = 2Rd$$

Assume that we need only examine the first two reflected beams E_{1r} and E_{2r}. The mth-order interference maximum will occur in the thin film when its thickness is in accord with the relationship

$$2n_f d_m = (m + \tfrac{1}{2})\lambda_0$$

The radius of the mth bright ring is therefore found by combining the last two expressions to yield

[bright ring] $$x_m = [(m + \tfrac{1}{2})\lambda_f R]^{1/2} \tag{9.42}$$

Similarly, the radius of the mth dark ring is

[dark ring] $$x_m = (m\lambda_f R)^{1/2} \tag{9.43}$$

If the two pieces of glass are in good contact (no dust), the central fringe at that point ($x_0 = 0$) will clearly be a minimum in irradiance, an understandable result since d goes to zero at that point. In transmitted light, the observed pattern will be the complement of the reflected one discussed above, so that the center will now appear bright.

Newton's rings, which are Fizeau fringes, can be distinguished from the circular pattern of Haidinger's fringes by the manner in which the diameters of the rings vary with the order m. The central region in the Haidinger pattern corresponds to the maximum value of m (Problem 9.29), whereas just the opposite applies to Newton's rings.

An optical shop, in the business of making lenses, will have a set of precision spherical test plates or gauges. A designer can specify the surface accuracy of a new lens in terms of the number and regularity of the Newton rings that will be seen with a particular test gauge. The use of test plates in the manufacture of high-quality lenses, however, is giving way to far more sophisticated techniques involving laser interferometers (Section 9.8.2).

9.4.2 Mirrored Interferometers

There are a good number of amplitude-splitting interferometers that utilize arrangements of mirrors and beamsplitters. By far the best known and historically the most important of these is the **Michelson Interferometer**. Its configuration is illustrated in Fig. 9.24. An extended source (e.g., a diffusing ground-glass plate illuminated by a discharge lamp) emits a wave, part of which travels to the right. The beamsplitter at O divides the wave into two, one segment traveling to the right and one up into the background. The two waves are reflected by mirrors M_1 and M_2 and return to the beamsplitter. Part of the wave coming from M_2 passes through the beamsplitter going downward, and part of the wave coming from M_1 is deflected by the beamsplitter toward the detector. The two waves are united, and interference can be expected.

Notice that one beam passes through O three times, whereas the other traverses it only once. Consequently, each beam will pass through equal thicknesses of glass only when a *compensator plate* C is inserted in the arm OM_1. The compensator is an exact duplicate of the beamsplitter, with the exception of any possible silvering or thin film coating on the beamsplitter. It is positioned at an angle of 45°, so that O and C are parallel to each other. With the compensator in place, any optical path difference arises from the actual path difference. In addition,

Giesecke+Devrient GmbH,
Giesecke+Devrient Currency Technology GmbH,
and Papierfabrik Louisenthal GmbH. - Ex. 1027

because of the dispersion of the beamsplitter, the optical path is a function of λ. Accordingly, for quantitative work, the interferometer without the compensator plate can be used only with a quasimonochromatic source. The inclusion of a compensator negates the effect of dispersion, so that even a source with a very broad bandwidth will generate discernible fringes.

To understand how fringes are formed, refer to the construction shown in Fig. 9.25, where the physical components are represented more as mathematical surfaces. An observer at the position of the detector will simultaneously see both mirrors M_1 and M_2 along with the source Σ in the beamsplitter. We can redraw the interferometer as if all the elements were in a straight line. Here M_1' corresponds to the image of mirror M_1 in the beamsplitter, and Σ has been swung over in line with O and M_2. The positions of these elements in the diagram depend on their relative distances from O (e.g., M_1' can be in front of, behind, or coincident with M_2 and can even pass through it). The surfaces Σ_1 and Σ_2 are the images of the source Σ in mirrors M_1 and M_2, respectively. Now consider a single point S on the source emitting light in all directions; let's follow the course of one emerging ray. In actuality a wave from S will be split at O, and its segments will thereafter be reflected by M_1 and M_2. In our schematic diagram we represent this by reflecting the ray off both M_2 and M_1'. To an observer at D, the two reflected rays will appear to have come from the image points S_1 and S_2. [Note that all rays shown in (*a*) and (*b*) of Fig. 9.25 share a common plane-of-incidence.] For all practical purposes, S_1 and S_2 are coherent point sources, and we can anticipate a flux-density distribution obeying Eq. (9.14).

As the figure shows, the optical path difference for these rays is nearly $2d \cos \theta$, which represents a phase difference of $k_0 2d \cos \theta$. There is an additional phase term arising from the fact that the wave traversing the arm OM_2 is internally reflected in the beamsplitter, whereas the OM_1-wave is externally reflected at O. If the beamsplitter is simply an uncoated glass plate, the relative phase shift resulting from the two reflections will be π radians. *Destructive*, rather than constructive, inter-

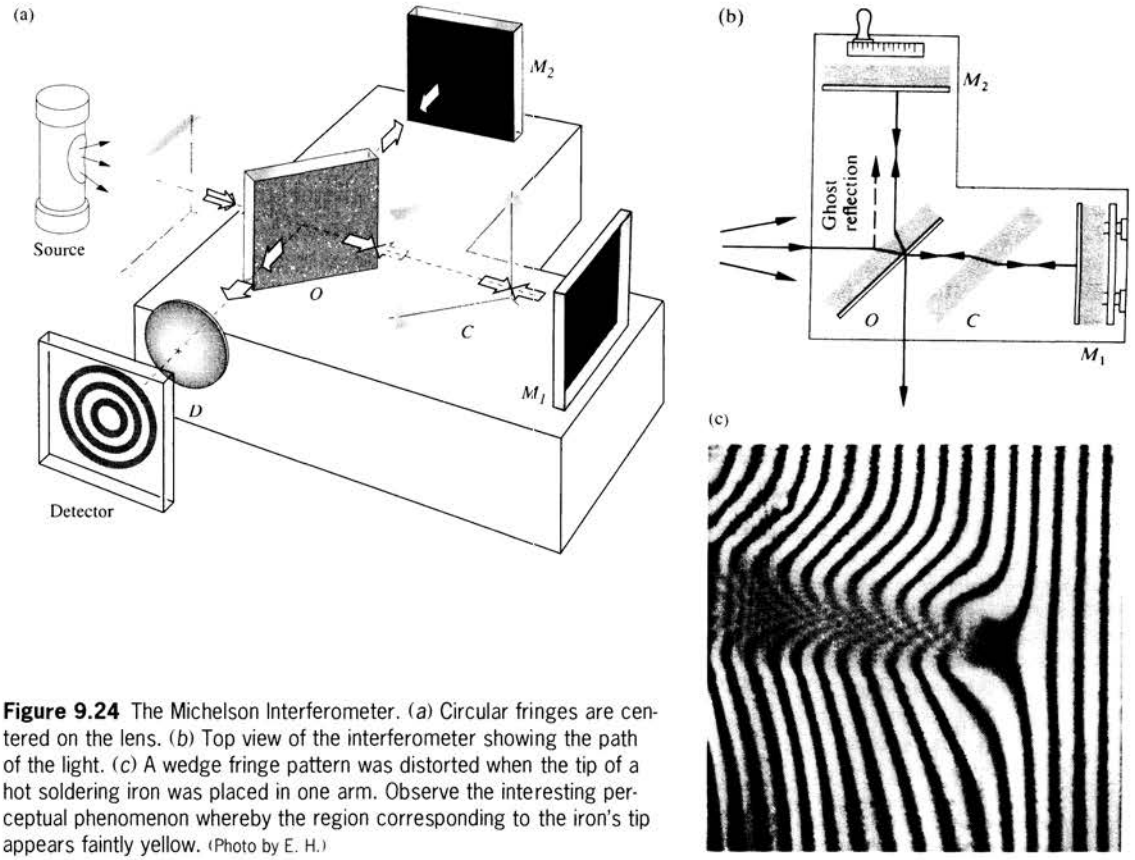
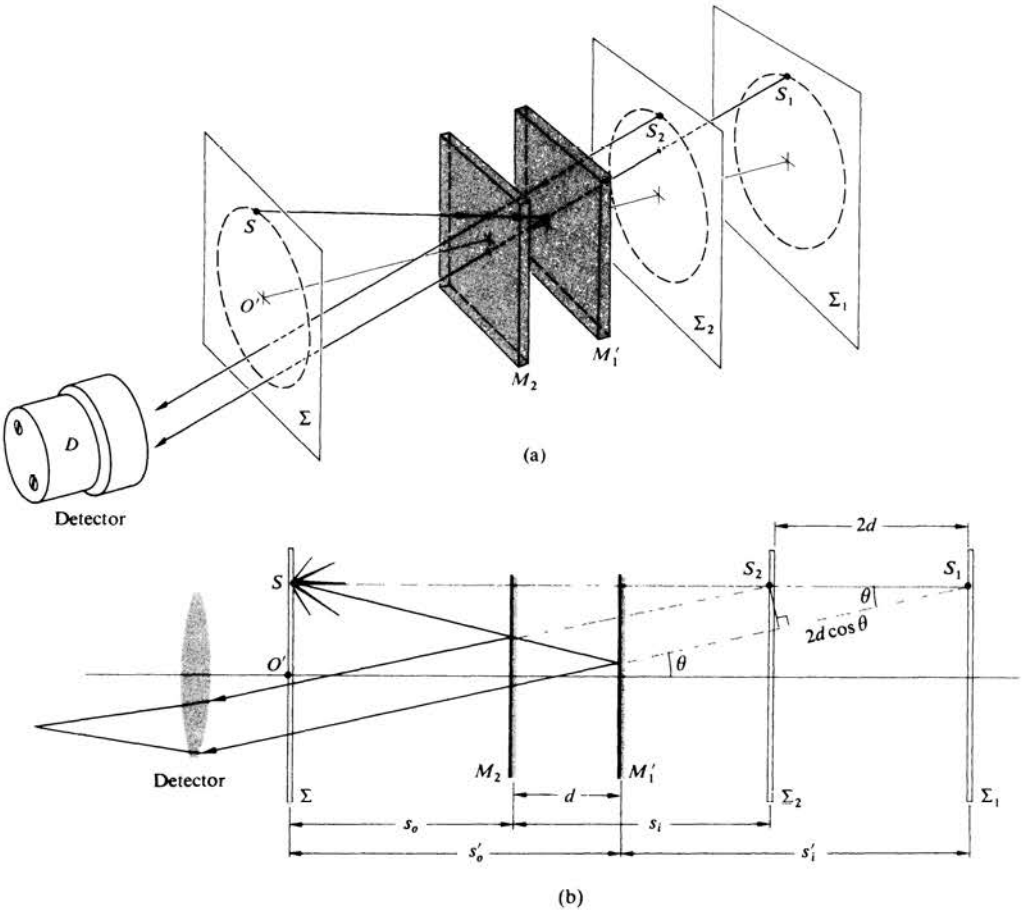


Figure 9.24 The Michelson Interferometer. (*a*) Circular fringes are centered on the lens. (*b*) Top view of the interferometer showing the path of the light. (*c*) A wedge fringe pattern was distorted when the tip of a hot soldering iron was placed in one arm. Observe the interesting perceptual phenomenon whereby the region corresponding to the iron's tip appears faintly yellow. (Photo by E. H.)

Giesecke+Devrient GmbH,
Giesecke+Devrient Currency Technology GmbH,
and Papierfabrik Louisenthal GmbH. - Ex. 1027



(b)

Figure 9.25 A conceptual rearrangement of the Michelson Interferometer.

ference will then exist when

$$2d \cos \theta_m = m\lambda_0 \tag{9.44}$$

where m is an integer. If this condition is fulfilled for the point S, then it will be equally well fulfilled for any point on Σ that lies on the circle of radius $O'S$, where O' is located on the axis of the detector. As illustrated in Fig. 9.26, an observer will see a circular fringe system concentric with the central axis of her eye's lens. Because of the small aperture of the eye, the observer will not be able to see the entire pattern without the use of a large lens near the beamsplitter to collect most of the emergent light.

If we use a source containing a number of frequency components (e.g., a mercury discharge lamp), the dependence of θ_m on λ_0 in Eq. (9.44) requires that each such component generate a fringe system of its own. Note, too, that since $2d \cos \theta_m$ must be less than the coherence length of the source, it follows that laser light will be particularly easy to use in demonstrating the interferometer (see Section 9.5). This point would be made strikingly evident were we to compare the fringes produced by laser light with those generated by "white" light from an ordinary tungsten bulb or a candle. In the latter case, the path difference must be very nearly zero, if we are to see any fringes at all, whereas in the former instance a difference of 10 cm has little noticeable effect.

An interference pattern in quasimonochromatic light typically consists of a large number of alternatively bright and dark rings. A particular ring corresponds to a fixed *order* m. As M_2 is moved toward M_1', d decreases, and according to Eq. (9.44), $\cos \theta_m$ increases while θ_m therefore decreases. The rings shrink toward the center, with the highest-order one disappearing whenever d decreases by $\lambda_0/2$. Each remaining ring broadens as more and more fringes vanish at the center, until only a few fill the whole screen. By the time $d = 0$ has been reached, the central fringe will have spread out, filling the

Giesecke+Devrient GmbH,
Giesecke+Devrient Currency Technology GmbH,
and Papierfabrik Louisenthal GmbH. - Ex. 1027

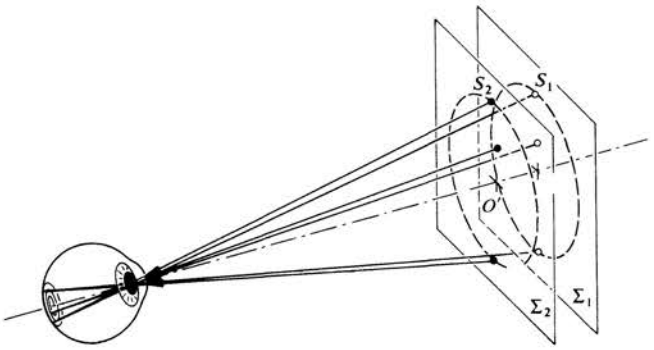


Figure 9.26 Formation of circular fringes.

entire field of view. With a phase shift of π resulting from reflection off the beamsplitter, the whole screen will then be an interference minimum. (Lack of perfection in the optical elements can render this unobservable.) Moving M_2 still farther causes the fringes to reappear at the center and move outward.

Notice that a central dark fringe for which $\theta_m = 0$ in Eq. (9.44) can be represented by

$$2d = m_0\lambda_0 \tag{9.45}$$

(Keep in mind that this is a special case. The central region might correspond to neither a maximum nor a minimum.) Even if d is 10 cm, which is fairly modest in laser light, and $\lambda_0 = 500$ nm, m_0 will be quite large, namely, 400 000. At a fixed value of d, successive dark rings will satisfy the expressions

$$\begin{aligned} 2d\cos\theta_1 &= (m_0 - 1)\lambda_0 \\ 2d\cos\theta_2 &= (m_0 - 2)\lambda_0 \\ &\vdots \\ 2d\cos\theta_p &= (m_0 - p)\lambda_0 \end{aligned} \tag{9.46}$$

The angular position of any ring, for example, the pth ring, is determined by combining Eqs. (9.45) and (9.46) to yield

$$2d(1 - \cos\theta_p) = p\lambda_0 \tag{9.47}$$

Since $\theta_m \equiv \theta_p$, both are just the half-angle subtended at the detector by the particular ring, and since $m = m_0 - p$, Eq. (9.47) is equivalent to Eq. (9.44). The new form is somewhat more convenient, since (using the same example as above) with $d = 10$ cm, the sixth dark ring can be specified by stating that $p = 6$, or in terms of the *order* of the pth ring, that $m = 399\,994$. If θ_p is small,

$$\cos\theta_p = 1 - \frac{\theta_p^2}{2}$$

and Eq. (9.47) yields

$$\theta_p = \left(\frac{p\lambda_0}{d}\right)^{1/2} \tag{9.48}$$

for the angular radius of the pth fringe.

The construction of Fig. 9.25 represents one possible configuration, the one in which we consider only pairs of parallel emerging rays. Since these rays do not actually meet, they cannot form an image without a condensing lens of some sort. Indeed, that lens is most often provided by the observer's eye focused at infinity. The resulting *fringes of equal inclination* (θ_m = constant) located at infinity are also *Haidinger fringes.* A comparison of Figs. 9.25*b* and 9.3*a*, both showing two coherent point sources, suggests that in addition to these (virtual) fringes at infinity, there might also be (real) fringes formed by converging rays. These fringes do in fact exist. Hence, if you illuminate the interferometer with a *broad source* and shield out all extraneous light, you can easily see the projected pattern on a screen in a darkened room (see Section 9.5). The fringes will appear in the space in front of the interferometer (i.e., where the detector is shown), and their size will increase with increasing distance from the beamsplitter. We will consider the (real) fringes arising from point-source illumination a little later on.

When the mirrors of the interferometer are inclined with respect to each other, making a small angle (i.e., when M_1 and M_2 are not quite perpendicular), *Fizeau fringes* are observed. The resultant wedge-shaped air film between M_2 and M_1' creates a pattern of straight parallel fringes. The interfering rays appear to diverge from a point behind the mirrors. The eye would have to focus on this point in order to make these *localized fringes* observable. It can be shown analytically* that by appropriate adjustment of the orientation of the mirrors M_1 and M_2, fringes can be produced that are straight, circular, elliptical, parabolic, or hyperbolic—this holds as well for the real and virtual fringes.

*See, for example, Valasek, *Optics*, p.135.

Giesecke+Devrient GmbH,
Giesecke+Devrient Currency Technology GmbH,
and Papierfabrik Louisenthal GmbH. - Ex. 1027

The Michelson Interferometer can be used to make extremely accurate length measurements. As the moveable mirror is displaced by $\lambda_0/2$, each fringe will move to the position previously occupied by an adjacent fringe. Using a microscope arrangement, one need only count the number of fringes N, or portions thereof, that have moved past a reference point to determine the distance traveled by the mirror Δd, that is,

$$\Delta d = N(\lambda_0/2)$$

Nowadays this can be done fairly easily by electronic means. Michelson used the method to measure the number of wavelengths of the red cadmium line corresponding to the standard meter in Sévres near Paris.*

The Michelson Interferometer can be used along with a few polaroid filters to verify the Fresnel–Arago Laws. A polarizer inserted in each arm will allow the optical path length difference to remain fairly constant, while the vector field directions of the two beams are easily changed.

A microwave Michelson Interferometer can be constructed with sheet-metal mirrors and a chicken-wire beamsplitter. With the detector located at the central fringe, it can easily measure shifts from maxima to minima as one of the mirrors is moved, thereby determining λ. A few sheets of plywood, plastic, or glass inserted in one arm will change the central fringe. Counting the number of fringe shifts yields a value for the index of refraction, and from that we can compute the dielectric constant of the material.

The **Mach–Zehnder Interferometer** is another amplitude-splitting device. As shown in Fig. 9.27, it consists of two beamsplitters and two totally reflecting mirrors. The two waves within the apparatus travel along separate paths. A difference between the optical paths can be introduced by a slight tilt of one of the beamsplitters. Since the two paths are separated, the interferometer is relatively difficult to align. For the same reason, however, the interferometer finds myriad applications. It has even been used, in a somewhat altered yet conceptually similar form, to obtain electron interference fringes.†

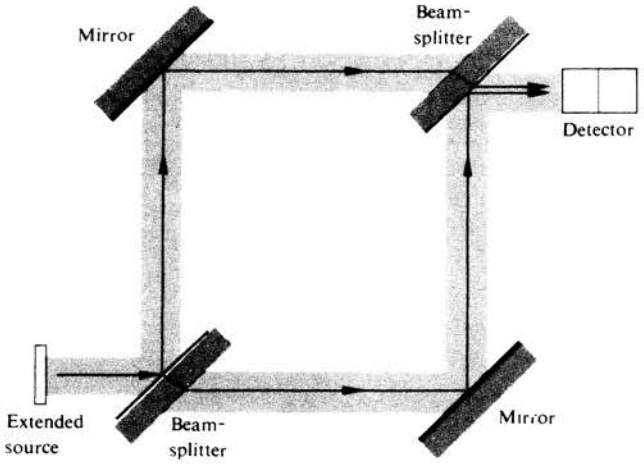
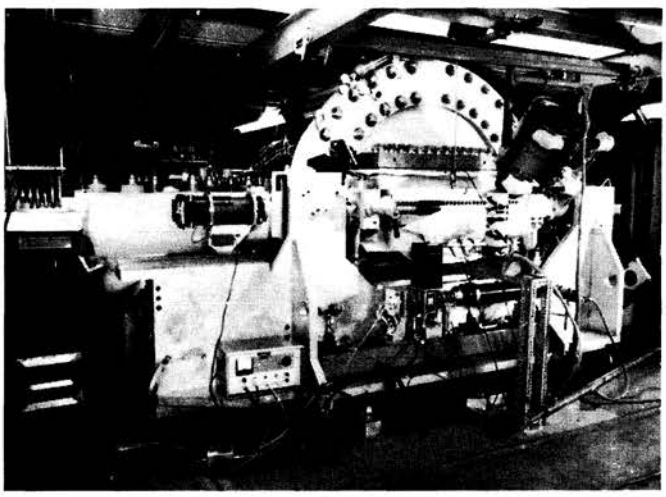


Figure 9.27 The Mach–Zehnder Interferometer.

An object interposed in one beam will alter the optical path length difference, thereby changing the fringe pattern. A common application of the device is to observe the density variations in gas-flow patterns within research chambers (wind tunnels, shock tubes, etc.). One beam passes through the optically flat windows of the test chamber, while the other beam traverses appropriate compensator plates. The beam within the chamber will propagate through regions having a spatially



Scylla IV, an early setup for studying plasma. (Courtesy of University of California, Lawrence Livermore National Laboratory, and the Department of Energy.)

*A discussion of the procedure he used to avoid counting the 3 106 327 fringes directly can be found in Strong, *Concepts of Classical Optics*, p. 238, or Williams, *Applications of Interferometry*, p. 51.

†L. Marton, J. Arol Simpson, and J. A. Suddeth, *Rev. Sci. Instr.* **25**, 1099 (1954), and *Phys. Rev.* **90**, 490 (1953).

Giesecke+Devrient GmbH,
Giesecke+Devrient Currency Technology GmbH,
and Papierfabrik Louisenthal GmbH. - Ex. 1027

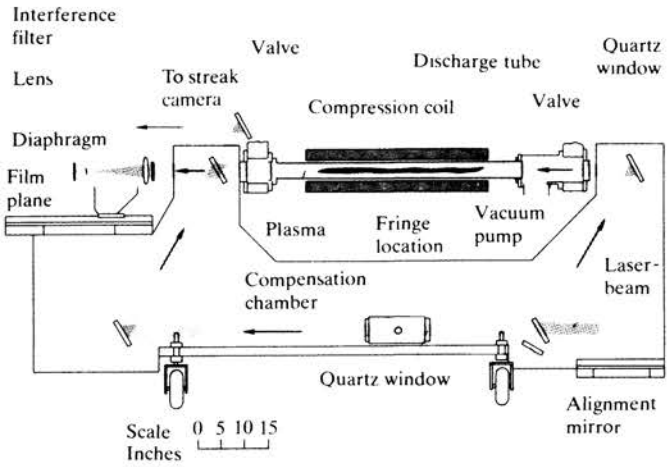
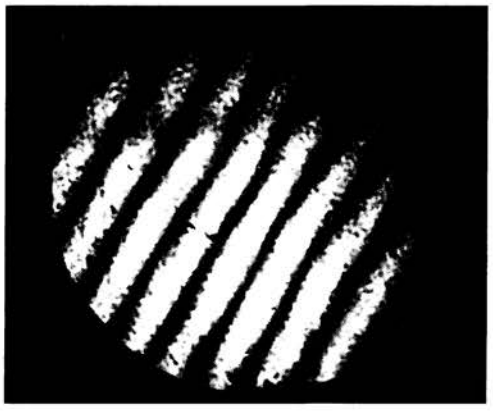


Figure 9.28 Schematic of Scylla IV.

varying index of refraction. The resulting distortions in the wavefront generate the fringe contours. A particularly nice application is shown in Fig. 9.28, which depicts the magnetic compression device known as Scylla IV. It was used to study controlled thermonuclear reactions at the Los Alamos Scientific Laboratory. In this case, the Mach–Zehnder Interferometer appears in the form of a parallelogram. The two ruby laser *interferograms*, as these photographs are called, show the background pattern without a plasma in the tube and the density contours within the plasma during a reaction.

Another amplitude-splitting device, which differs from the previous instrument in many respects, is the **Sagnac Interferometer**. It is very easy to align and quite stable. An interesting application of the device is discussed in the last section of this chapter, where we consider its use as a gyroscope. One form of the Sagnac Interferometer is shown in Fig. 9.29*a* and another in Fig. 9.29*b*; still others are possible. Notice that the main feature of the device is that there are two identical but oppositely directed paths taken by the beams and that both form closed loops before they are united to produce interference. A deliberate slight shift in the orientation of one of the mirrors will produce a path length difference and a resulting fringe pattern. Since the beams are superimposed and therefore inseparable, the interferometer cannot be put to any of the conventional uses. These in general depend on the possibility of imposing variations on only one of the constituent beams.



Interferogram without plasma. (Photo courtesy Los Alamos National Laboratory.)



Interferogram with plasma. (Photo courtesy Los Alamos National Laboratory.)

Real Fringes

Before we examine the creation of real, as opposed to virtual, fringes, let's first consider another amplitude-splitting interferometric device, the **Pohl fringe-producing system**, illustrated in Fig. 9.30. It is simply a thin transparent film illuminated by the light coming from a point source. In this case, the fringes are real and can accordingly be intercepted on a screen placed anywhere in the vicinity of the interferometer without a condensing-lens system. A convenient light source to use is a mercury lamp covered with a shield having a small hole ($\approx \frac{1}{4}$ inch diameter) in it. As a thin film, use a piece of

Giesecke+Devrient GmbH,
Giesecke+Devrient Currency Technology GmbH,
and Papierfabrik Louisenthal GmbH. - Ex. 1027

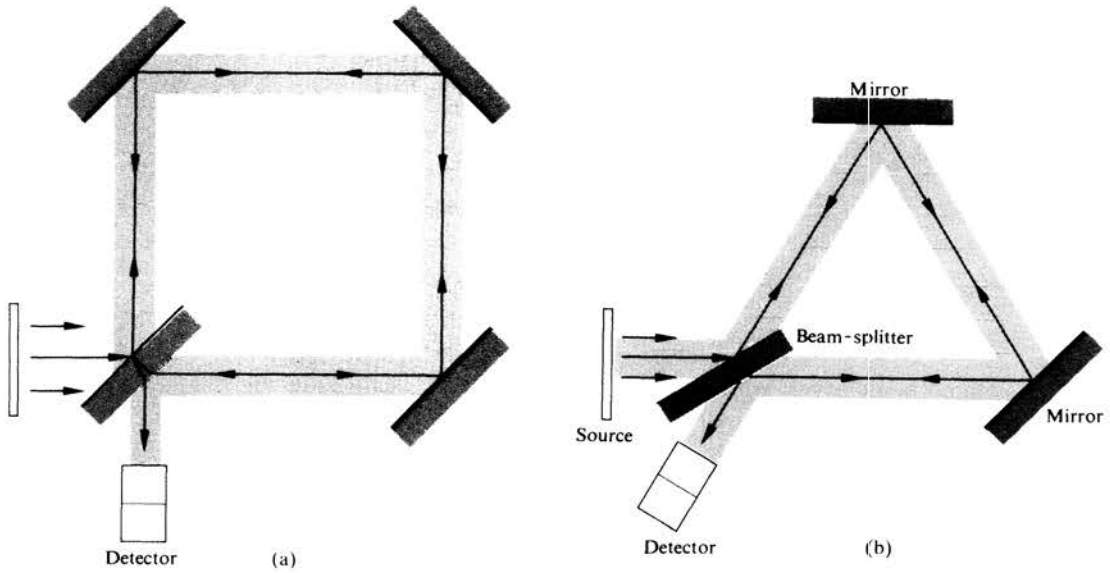


Figure 9.29 (*a*) A Sagnac Interferometer. (*b*) Another variation of the Sagnac Interferometer.

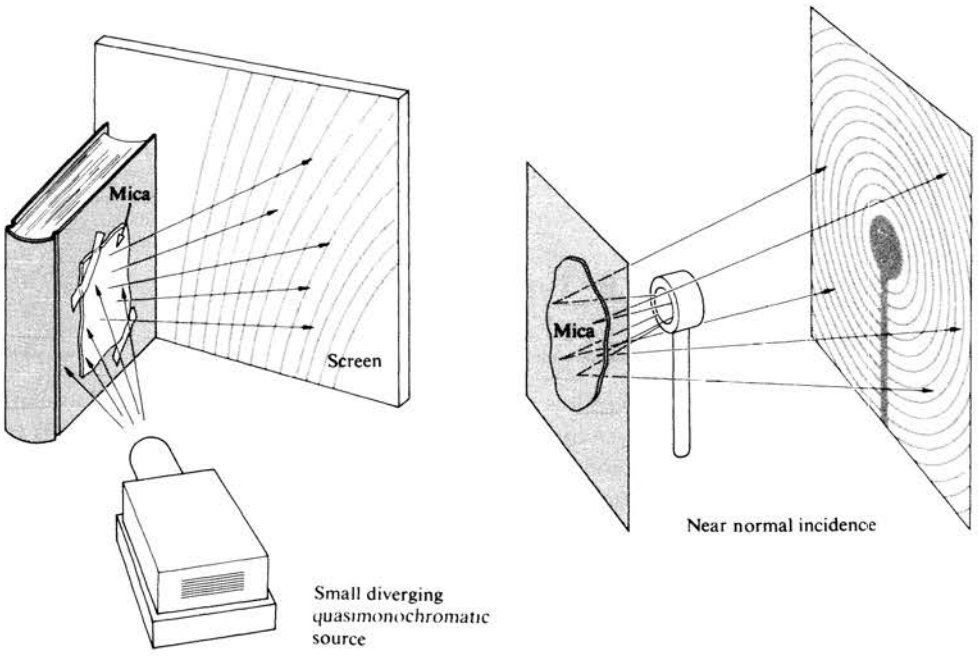


Figure 9.30 The Pohl Interferometer.

Giesecke+Devrient GmbH,
Giesecke+Devrient Currency Technology GmbH,
and Papierfabrik Louisenthal GmbH. - Ex. 1027

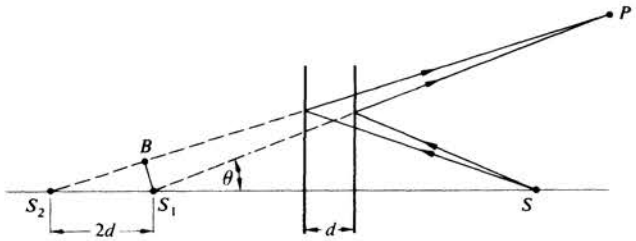


Figure 9.31 Point-source illumination of parallel surfaces.

ordinary mica taped to a dark-colored book cover, which serves as an opaque backing. If you have a laser, its remarkable coherence length and high flux density will allow you to perform this same experiment with almost anything smooth and transparent. Expand the beam to about an inch or two in diameter by passing it through a lens (a focal length of 50 to 100 mm will do). Then just reflect the beam off the surface of a glass plate (e.g., a microscope slide), and the fringes will be evident within the illuminated disk wherever it strikes a screen.

The underlying physical principle involved with point-source illumination for all four of the interferometric devices considered above can be appreciated with the help of a construction, variations of which are shown in Figs. 9.31 and 9.32.* The two vertical lines in Fig. 9.31, or the inclined ones in Fig. 9.32, represent either the positions of the mirrors or the two sides of the thin sheet in the Pohl Interferometer. Let's assume that point P in the surrounding medium is a point at

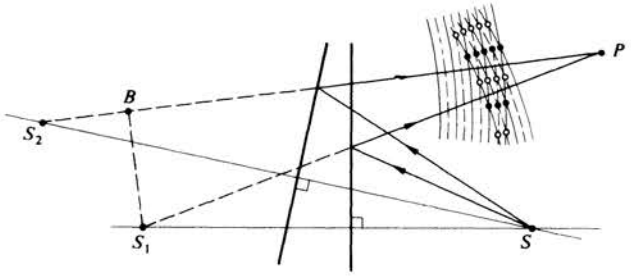
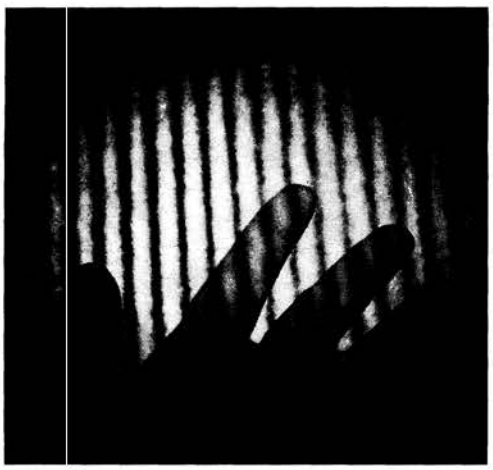


Figure 9.32 Point-source illumination of inclined surfaces.

*A. Zajac, H. Sadowski, and S. Licht, "The Real Fringes in the Sagnac and the Michelson Interferometers," *Am. J. Phys.* **29**, 669 (1961).



Real Michelson fringes using He–Ne laser light. (Photo by E. H.)

which there is constructive interference. A screen placed at that point would intercept this maximum, as well as a whole fringe pattern, without any condensing system. The coherent virtual sources emitting the interfering beams are mirror images S_1 and S_2 of the actual point source S. It should be noted that this kind of real fringe pattern can be observed with both the Michelson and Sagnac Interferometers. If either device is illuminated with an expanded laserbeam, a real fringe pattern will be generated directly by the emerging waves. This is an extremely simple and beautiful demonstration.

9.5 Types and Localization of Interference Fringes

Often it is important to know where the fringes produced in a given interferometric system will be located, since that is the region where we need to focus our detector (eye, camera, telescope). In general, the problem of locating fringes is characteristic of a given interferometer; that is, it has to be solved for each individual device.

Fringes can be classified, first, as either *real* or *virtual* and, second, as either *nonlocalized* or *localized*. Real fringes are those that can be seen on a screen without the use of an additional focusing system. The rays forming these fringes converge to the point of observation, all by themselves. Virtual

Giesecke+Devrient GmbH,
Giesecke+Devrient Currency Technology GmbH,
and Papierfabrik Louisenthal GmbH. - Ex. 1027

fringes cannot be projected onto a screen without a focusing system. In this case the rays obviously do not converge.

Nonlocalized fringes are real and exist everywhere within an extended (three-dimensional) region of space. The pattern is literally nonlocalized, in that it is not restricted to some small region. Young's Experiment, as illustrated in Fig. 9.8, fills the space beyond the secondary sources with a whole array of real fringes. Nonlocalized fringes of this sort are generally produced by small sources, that is, point or line sources, be they real or virtual. In contrast, localized fringes are clearly observable only over a particular surface. The pattern is literally localized, whether near a thin film or at infinity. This type of fringe will always result from the use of extended sources but can be generated with a point source as well.

The Pohl Interferometer (Fig. 9.30) is particularly useful in illustrating these principles, since with a point source it will produce both real nonlocalized and virtual localized fringes. The real nonlocalized fringes (Fig. 9.33, upper half) can be intercepted on a screen almost anywhere in front of the mica film.

For the nonconverging rays, realize that since the aperture of the eye is quite small, it will intercept only those rays that are directed almost exactly at it. For this small pencil of rays, the eye, at a particular position, sees either a bright or dark spot but not much more. To perceive an extended fringe pattern formed by parallel rays of the type shown in the bottom half of Fig. 9.33, a large lens will have to be used to gather in light entering at other orientations. In practice, however, the source is usually somewhat extended, and fringes can generally be seen by looking into the film with the eye focused at infinity. These virtual fringes are localized at infinity and are equivalent to the *equal-inclination fringes* of Section 9.4. Sim-

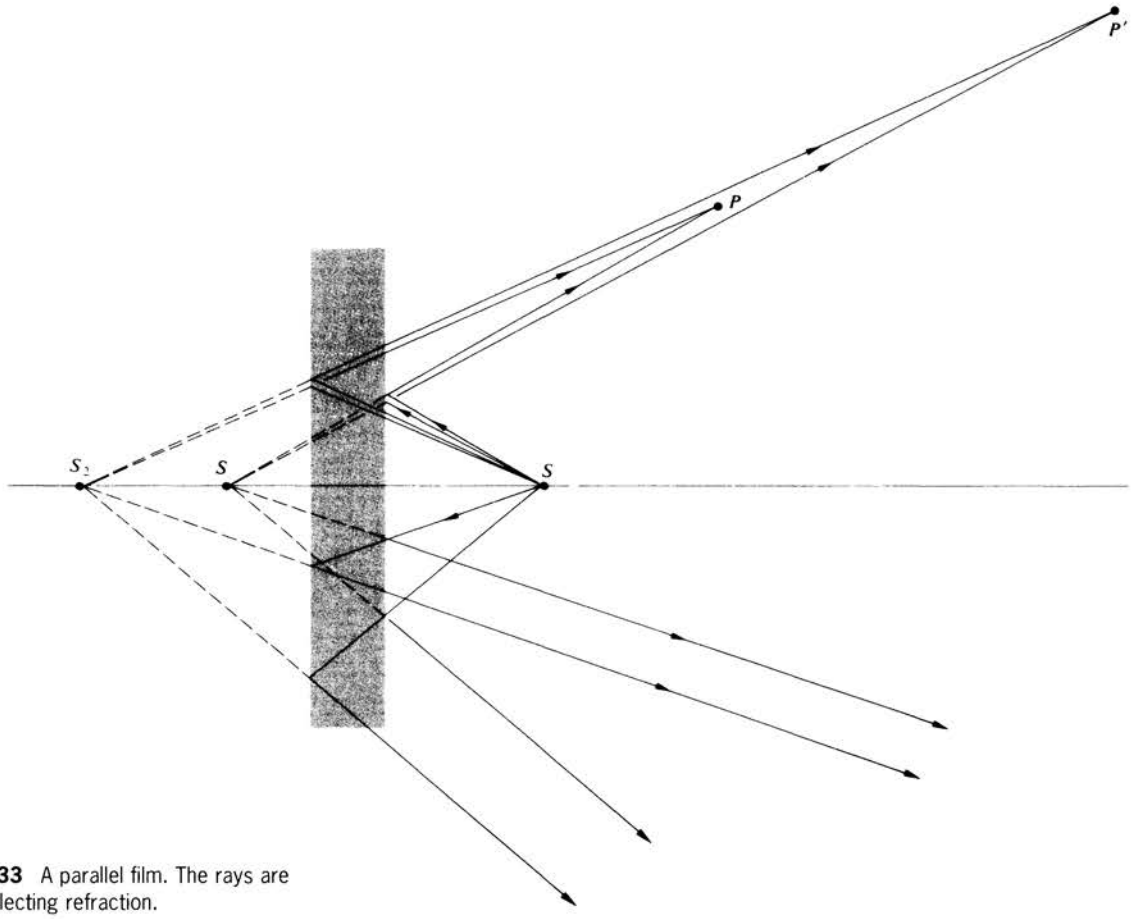


Figure 9.33 A parallel film. The rays are drawn neglecting refraction.

Giesecke+Devrient GmbH,
Giesecke+Devrient Currency Technology GmbH,
and Papierfabrik Louisenthal GmbH. - Ex. 1027

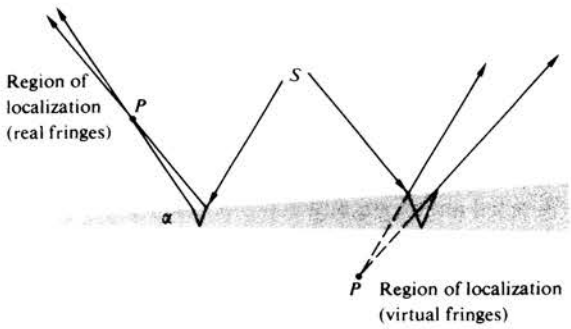


Figure 9.34 Fringes formed by a wedge-shaped film.

ilarly, if the mirrors M_1 and M_2 in the Michelson Interferometer are parallel, the usual circular, virtual, equal-inclination fringes localized at infinity will be seen. We can imagine a thin air film between the surfaces of the mirrors M_2 and M_1' acting to generate these fringes. As with the configuration of Fig. 9.30 for the Pohl device, real nonlocalized fringes will also be present.

The geometry of the fringe pattern seen in reflected light from a transparent wedge of small angle α is shown in Fig. 9.34. The fringe location P will be determined by the direction of incidence of the incoming light. Newton's rings have this same kind of localization, as do the Michelson, Sagnac, and other interferometers for which the equivalent interference system consists of two reflecting planes inclined slightly to each other. The wedge setup of the Mach–Zehnder Interferometer is distinctive in that by rotating the mirrors, one can localize the resulting virtual fringes on any plane within the region generally occupied by the test chamber (Fig. 9.35).

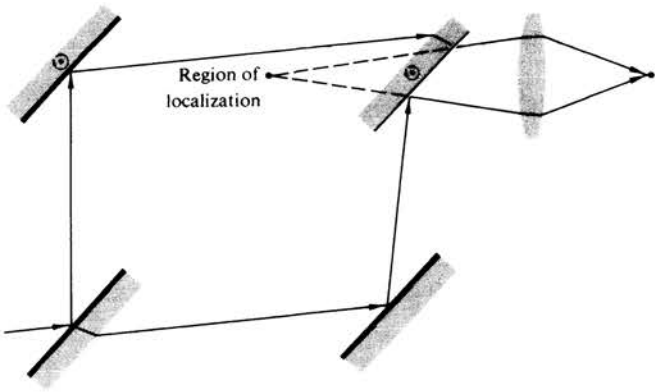


Figure 9.35 Fringes in the Mach–Zehnder Interferometer.

9.6 Multiple Beam Interference

Thus far we have examined a number of situations in which two coherent beams are combined under diverse conditions to produce interference patterns. There are, however, circumstances under which a much larger number of mutually coherent waves are made to interfere. In fact, whenever the amplitude-reflection coefficients, the r's, for the parallel plate illustrated in Fig. 9.17 are not small, as was previously the case, the higher-order reflected waves $\vec{\mathbf{E}}_{3r}$, $\vec{\mathbf{E}}_{4r}$,... become quite significant. A glass plate, slightly silvered on both sides so that the r's approach unity, will generate a large number of multiply internally reflected rays. For the moment, we will consider only situations in which the film, substrate, and surrounding medium are transparent dielectrics. This avoids the more complicated phase changes resulting from metal-coated surfaces.

To begin the analysis as simply as possible, let the film be nonabsorbing and let $n_1 = n_2$. The notation will be in accord with that of Section 4.10; the amplitude-transmission coefficients are represented by t, the fraction of the amplitude of a wave transmitted on entering into the film, and t', the fraction transmitted when a wave leaves the film. The rays are actually lines drawn perpendicular to the wavefronts and therefore are also perpendicular to the optical fields $\vec{\mathbf{E}}_{1r}$, $\vec{\mathbf{E}}_{2r}$, and so forth. Since the rays will remain nearly parallel, the scalar theory will suffice as long as we are careful to account for any possible phase shifts.

As shown in Fig. 9.36, the scalar amplitudes of the reflected waves $\vec{\mathbf{E}}_{1r}$, $\vec{\mathbf{E}}_{2r}$, $\vec{\mathbf{E}}_{3r}$,..., are respectively $E_0 r$, $E_0 t r' t'$, $E_0 t r'^3 t'$,..., where E_0 is the amplitude of the initial incoming wave and $r = -r'$ via Eq. (4.89). The minus sign indicates a phase shift, which we will consider later. Similarly, the transmitted waves $\vec{\mathbf{E}}_{1t}$, $\vec{\mathbf{E}}_{2t}$, $\vec{\mathbf{E}}_{3t}$,... will have amplitudes $E_0 t t'$, $E_0 t r'^2 t'$, $E_0 t r'^4 t'$,.... Consider the set of parallel reflected rays. Each ray bears a fixed phase relationship to all the other reflected rays. The phase differences arise from a combination of optical path length differences and phase shifts occurring at the various reflections. Nonetheless, the waves are mutually

Giesecke+Devrient GmbH,
Giesecke+Devrient Currency Technology GmbH,
and Papierfabrik Louisenthal GmbH. - Ex. 1027

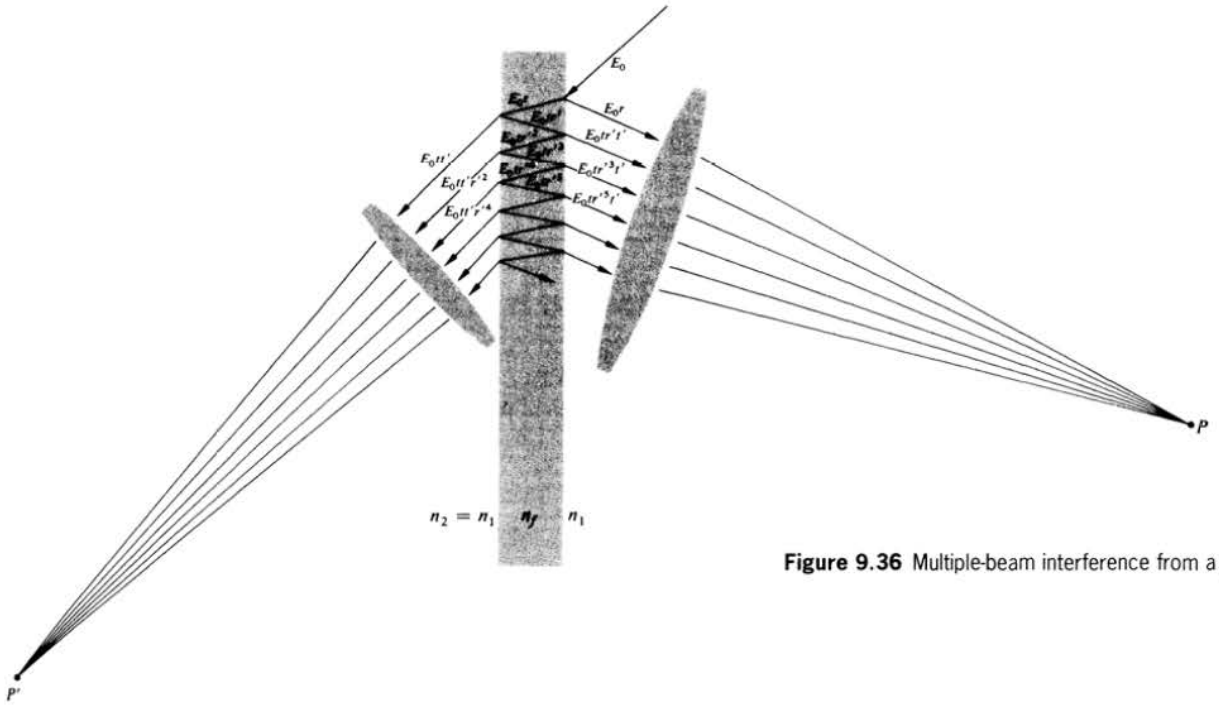


Figure 9.36 Multiple-beam interference from a parallel film.

coherent, and if they are collected and brought to focus at a point P by a lens, they will all interfere. The resultant irradiance expression has a particularly simple form for two special cases.

The difference in optical path length between adjacent rays is given by

$$\Lambda = 2n_f d \cos \theta_t \qquad [9.33]$$

All the waves except for the first, $\vec{\mathbf{E}}_{1r}$, undergo an odd number of reflections *within* the film. It follows from Fig. 4.44 that at each internal reflection the component of the field parallel to the plane-of-incidence changes phase by either 0 or π, depending on the internal incident angle $\theta_i < \theta_c$. The component of the field perpendicular to the plane-of-incidence suffers no change in-phase on internal reflection when $\theta_i < \theta_c$. Clearly then, no relative change in-phase among these waves results from an odd number of such reflections (Fig. 9.37). As the *first special case*, if $\Lambda = m\lambda$, the second, third, fourth, and successive waves will all be in-phase at P. The wave $\vec{\mathbf{E}}_{1r}$, however, because of its reflection at the top surface of the film, will be out-of-phase by 180° with respect to all the other waves. The

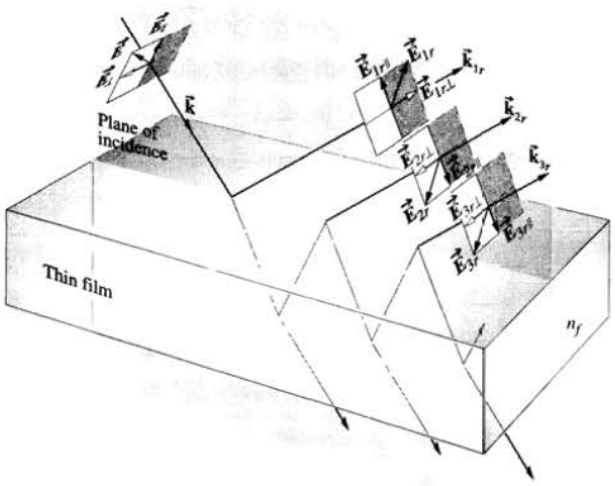


Figure 9.37 Phase shifts arising purely from the reflections (internal $\theta_i < \theta_p'$).

Giesecke+Devrient GmbH,
Giesecke+Devrient Currency Technology GmbH,
and Papierfabrik Louisenthal GmbH. - Ex. 1027

phase shift is embodied in the fact that $r = -r'$ and r' occurs only in odd powers. The sum of the scalar amplitudes, that is, the total *reflected amplitude* at point P, is then

$$E_{0r} = E_0 r - (E_0 trt' + E_0 tr^3 t' + E_0 tr^5 t' + \cdots)$$

or

$$E_{0r} = E_0 r - E_0 trt'(1 + r^2 + r^4 + \cdots)$$

where since $\Lambda = m\lambda$, we've just replaced r' by $-r$. The geometric series in parentheses converges to the finite sum $1/(1 - r^2)$ as long as $r^2 < 1$, so that

$$E_{0r} = E_0 r - \frac{E_0 trt'}{(1 - r^2)} \tag{9.49}$$

It was shown in Section 4.10, when we considered Stokes's treatment of the principle of reversibility (Eq. 4.86), that $tt' = 1 - r^2$, and it follows that

$$E_{0r} = 0$$

Thus when $\Lambda = m\lambda$ the second, third, fourth, and successive waves exactly cancel the first reflected wave, as shown in Fig. 9.38. In this case no light is reflected; all the incoming energy is transmitted. The *second special case* arises when $\Lambda = (m + \frac{1}{2})\lambda$. Now the first and second rays are in-phase, and all other adjacent waves are $\lambda/2$ out-of-phase; that is, the second is out-of-phase with the third, the third is out-of-phase with the fourth, and so on. The resultant *scalar amplitude* is then

$$E_{0r} = E_0 r + E_0 trt' - E_0 tr^3 t' + E_0 tr^5 t' - \cdots$$

or

$$E_{0r} = E_0 r + E_0 rtt'(1 - r^2 + r^4 - \cdots)$$

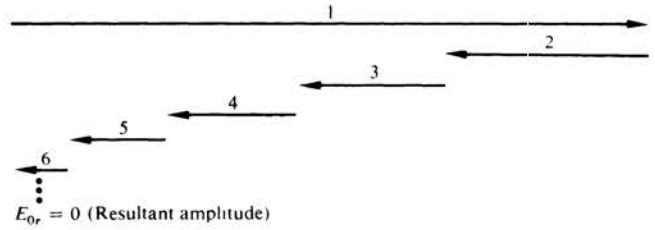


Figure 9.38 Phasor diagram.

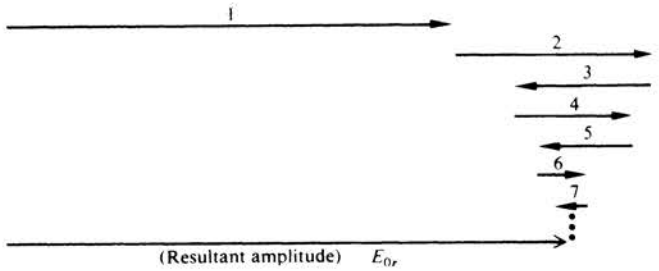


Figure 9.39 Phasor diagram.

The series in parentheses is equal to $1/(1 + r^2)$, in which case

$$E_{0r} = E_0 r\left[1 + \frac{tt'}{(1 + r^2)}\right]$$

Again, $tt' = 1 - r^2$; therefore, as illustrated in Fig. 9.39,

$$E_{0r} = \frac{2r}{(1 + r^2)} E_0$$

Since this particular arrangement results in the addition of the first and second waves, which have relatively large amplitudes, it should yield a large reflected flux density. The irradiance is proportional to $E_{0r}^2/2$, so from Eq. (3.44)

$$I_r = \frac{4r^2}{(1 + r^2)^2}\left(\frac{E_0^2}{2}\right) \tag{9.50}$$

That this is in fact the maximum, $(I_r)_{\max}$, will be shown later.

We will now consider the problem of multiple-beam interference in a more general fashion, making use of the complex representation. Again let $n_1 = n_2$, thereby avoiding the need to introduce different reflection and transmission coefficients at each interface. The optical fields at point P are given by

$$\tilde{E}_{1r} = E_0 re^{i\omega t}$$
$$\tilde{E}_{2r} = E_0 tr't'e^{i(\omega t - \delta)}$$
$$\tilde{E}_{3r} = E_0 tr'^3 t' e^{i(\omega t - 2\delta)}$$
$$\vdots$$
$$\tilde{E}_{Nr} = E_0 tr'^{(2N-3)} t' e^{i[\omega t - (N-1)\delta]}$$

where $E_0 e^{i\omega t}$ is the incident wave.

Giesecke+Devrient GmbH,
Giesecke+Devrient Currency Technology GmbH,
and Papierfabrik Louisenthal GmbH. - Ex. 1027

The terms $\delta, 2\delta, \ldots, (N-1)\delta$ are the contributions to the phase arising from an optical path length difference between adjacent rays ($\delta = k_0\Lambda$). There is an additional phase contribution arising from the optical distance traversed in reaching point P, but this is common to each ray and has been omitted. The relative phase shift undergone by the first ray as a result of the reflection is embodied in the quantity r'. The resultant *reflected scalar wave* is then

$$\tilde{E}_r = \tilde{E}_{1r} + \tilde{E}_{2r} + \tilde{E}_{3r} + \cdots + \tilde{E}_{Nr}$$

or upon substitution (Fig. 9.40)

$$\tilde{E}_r = E_0 r e^{i\omega t} + E_0 t r' t' e^{i(\omega t - \delta)} + \cdots + E_0 t r'^{(2N-3)} t' \times e^{i[\omega t - (N-1)\delta]}$$

This can be rewritten as

$$\tilde{E}_r = E_0 e^{i\omega t}\{r + r' t t' e^{-i\delta}[1 + (r'^2 e^{-i\delta}) + (r'^2 e^{-i\delta})^2 + \cdots + (r'^2 e^{-i\delta})^{N-2}]\}$$

If $|r'^2 e^{-i\delta}| < 1$, and if the number of terms in the series approaches infinity, the series converges. The resultant wave becomes

$$\tilde{E}_r = E_0 e^{i\omega t}\left[r + \frac{r' t t' e^{-i\delta}}{1 - r'^2 e^{-i\delta}}\right] \tag{9.51}$$

In the case of zero absorption, no energy being taken out of the waves, we can use the relations $r = -r'$ and $tt' = 1 - r^2$ to rewrite Eq. (9.51) as

$$\tilde{E}_r = E_0 e^{i\omega t}\left[\frac{r(1 - e^{-i\delta})}{1 - r^2 e^{-i\delta}}\right]$$

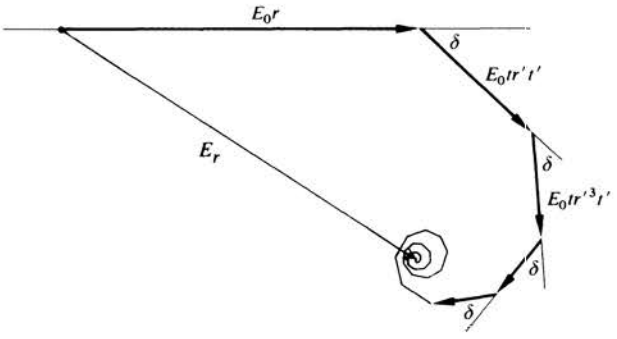


Figure 9.40 Phasor diagram.

The reflected flux density at P is then $I_r = \tilde{E}_r \tilde{E}_r^*/2$, that is,

$$I_r = \frac{E_0^2 r^2 (1 - e^{-i\delta})(1 - e^{+i\delta})}{2(1 - r^2 e^{-i\delta})(1 - r^2 e^{+i\delta})}$$

which can be transformed into

$$I_r = I_i \frac{2r^2(1 - \cos\delta)}{(1 + r^4) - 2r^2 \cos\delta} \tag{9.52}$$

The symbol $I_i = E_0^2/2$ represents the incident flux density, since, of course, E_0 was the amplitude of the incident wave. Similarly, the amplitudes of the transmitted waves given by

$$\begin{aligned}
\tilde{E}_{1t} &= E_0 t t' e^{i\omega t} \\
\tilde{E}_{2t} &= E_0 t t' r'^2 e^{i(\omega t - \delta)} \\
\tilde{E}_{3t} &= E_0 t t' r'^4 e^{i(\omega t - 2\delta)} \\
&\vdots \\
\tilde{E}_{Nt} &= E_0 t t' r'^{2(N-1)} e^{i[\omega - (N-1)\delta]}
\end{aligned}$$

can be added to yield

$$\tilde{E}_t = E_0 e^{i\omega t}\left[\frac{tt'}{1 - r^2 e^{-i\delta}}\right] \tag{9.53}$$

(Because we are interested in the irradiance, a common factor of $e^{-i\delta/2}$, arising from the transmission through the film, was omitted. It contributes to the fact that there is a phase difference of $\pi/2$ between the reflected and transmitted waves, but that is of no concern here.)

Multiplying Eq. (9.53) by its complex conjugate yields (Problem 9.39) the irradiance of the transmitted beam

$$I_t = \frac{I_i (tt')^2}{(1 + r^4) - 2r^2 \cos\delta} \tag{9.54}$$

Using the trigonometric identity $\cos\delta = 1 - 2\sin^2(\delta/2)$, Eqs. (9.52) and (9.54) become

$$I_r = I_i \frac{[2r/(1 - r^2)]^2 \sin^2(\delta/2)}{1 + [2r/(1 - r^2)]^2 \sin^2(\delta/2)} \tag{9.55}$$

and

$$I_t = I_i \frac{1}{1 + [2r/(1 - r^2)]^2 \sin^2(\delta/2)} \tag{9.56}$$

where energy is not absorbed, that is, $tt' + r^2 = 1$. If indeed

Giesecke+Devrient GmbH,
Giesecke+Devrient Currency Technology GmbH,
and Papierfabrik Louisenthal GmbH. - Ex. 1027

none of the incident energy is absorbed, the flux density of the incoming wave should exactly equal the sum of the flux density reflected off the film and the total transmitted flux density emerging from the film. It follows from Eqs. (9.55) and (9.56) that this is indeed the case, namely,

$$I_i = I_r + I_t \tag{9.57}$$

This will not be true, however, if the dielectric film is coated with a thin layer of semitransparent metal. Surface currents induced in the metal will dissipate a portion of the incident electromagnetic energy.

Consider the transmitted waves as described by Eq. (9.54). A maximum will exist when the denominator is as small as possible, that is, when $\cos \delta = 1$, in which case $\delta = 2\pi m$ and

$$(I_t)_{\max} = I_i$$

Under these conditions, Eq. (9.52) indicates that

$$(I_r)_{\min} = 0$$

as we would expect from Eq. (9.57). Again, from Eq. (9.54) it is clear that a minimum transmitted flux density will exist when the denominator is a maximum, that is, when $\cos \delta = -1$. In that case $\delta = (2m + 1)\pi$ and

$$(I_t)_{\min} = I_i \frac{(1 - r^2)^2}{(1 + r^2)^2} \tag{9.58}$$

The corresponding maximum in the reflected flux density is

$$(I_r)_{\max} = I_i \frac{4r^2}{(1 + r^2)^2} \tag{9.59}$$

Notice that the constant-inclination fringe pattern has its maxima when $\delta = (2m + 1)\pi$ or

$$\frac{4\pi n_f}{\lambda_0} d \cos \theta_t = (2m + 1)\pi$$

which is the same as the result we arrived at previously, in Eq. (9.36), by using only the first two reflected waves. Note, too, that Eq. (9.59) verifies that Eq. (9.50) was indeed a maximum.

The form of Eqs. (9.55) and (9.56) suggests that we introduce a new quantity, the ***coefficient of finesse*** F, such that

$$F \equiv \left(\frac{2r}{1 - r^2}\right)^2 \tag{9.60}$$

whereupon these equations can be written as

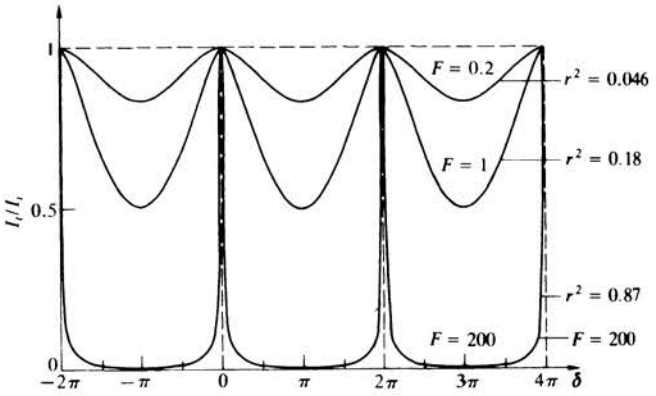


Figure 9.41 Airy function.

$$\frac{I_r}{I_i} = \frac{F \sin^2 (\delta/2)}{1 + F \sin^2(\delta/2)} \tag{9.61}$$

and

$$\frac{I_t}{I_i} = \frac{1}{1 + F \sin^2(\delta/2)} \tag{9.62}$$

The term $[1 + F \sin^2 (\delta/2)]^{-1} \equiv \mathscr{A}(\theta)$ is known as the **Airy function**. It represents the transmitted flux-density distribution and is plotted in Fig. 9.41. The complementary function $[1 - \mathscr{A}(\theta)]$, that is, Eq. (9.61), is plotted as well, in Fig. 9.42. When $\delta/2 = m\pi$, the Airy function is equal to unity for all values of F and therefore r. When r approaches 1, the transmitted flux density is very small, except within the sharp spikes centered about the points $\delta/2 = m\pi$. Multiple-beam interference has resulted in a redistribution of the energy density in comparison to the sinusoidal two-beam pattern (of

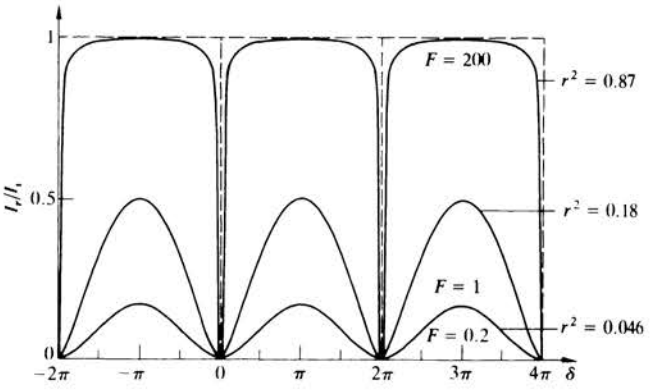


Figure 9.42 One minus the Airy function.

Giesecke+Devrient GmbH,
Giesecke+Devrient Currency Technology GmbH,
and Papierfabrik Louisenthal GmbH. - Ex. 1027

which the curves corresponding to a small reflectance are reminiscent). This effect will be further demonstrated when we consider the diffraction grating. At that time we will see this same peaking effect, resulting from an increased number of coherent sources contributing to the interference pattern. Remember that the Airy function is, in fact, a function of θ_t or θ_i by way of its dependence on δ, which follows from Eqs. (9.34) and (9.35), ergo the notation $\mathscr{A}(\theta)$. Each spike in the flux-density curve corresponds to a particular δ and therefore a particular θ_i. For a plane-parallel plate, the fringes, in transmitted light, will consist of a series of narrow bright rings on an almost completely dark background. In reflected light, the fringes will be narrow and dark on an almost uniformly bright background.

Constant-thickness fringes can also be made sharp and narrow by applying a light silver coating to the relevant reflecting surfaces to produce multiple-beam interference.

9.6.1 The Fabry–Perot Interferometer

The multiple-beam interferometer, first constructed by Charles Fabry and Alfred Perot in the late 1800s, is of considerable contemporary interest. Besides being a spectroscopic device of extremely high resolving power, it serves as the basic laser resonant cavity. In principle, the device consists of two plane, parallel, highly reflecting surfaces separated by some distance d. This is the simplest configuration, and as we shall see, other forms are also widely in use. In practice, two semisilvered or aluminized glass optical flats form the reflecting boundary surfaces. The enclosed air gap generally ranges from several millimeters to several centimeters when the apparatus is used interferometrically, and often to considerably greater lengths when it serves as a laser resonant cavity. If the gap can be mechanically varied by moving one of the mirrors, it's referred to as an interferometer. When the mirrors are held fixed and adjusted for parallelism by screwing down on some sort of spacer (invar or quartz is commonly used), it's said to be an **etalon** (although it is still an interferometer in the broad sense). If the two surfaces of a single quartz plate are appropriately polished and silvered, it too will serve as an etalon; the gap need not be air. The unsilvered sides of the plates are often made to have a slight wedge shape (a few minutes of arc) to reduce the interference pattern arising from reflections off these sides.

The etalon in Fig. 9.43 is shown illuminated by a broad source, which might be a mercury arc or a He–Ne laserbeam spread out in diameter to several centimeters. This can be done rather nicely by sending the beam into the back end of a telescope focused at infinity. The light can then be made diffuse by passing it through a sheet of ground glass. Only one ray emitted from some point S_1 on the source is traced through the etalon. Entering by way of the partially silvered plate, it is multiply reflected within the gap. The transmitted rays are collected by a lens and brought to a focus on a screen, where they interfere to form either a bright or dark spot. Consider this particular plane-of-incidence, which contains all the reflected rays. Any other ray emitted from a different point S_2, parallel to the original ray and in that plane-of-incidence, will form a spot at the same point P on the screen. As we shall see, the discussion of the previous section is again applicable, so that Eq. (9.54) determines the transmitted flux density I_t.

The multiple waves generated in the cavity, arriving at P from either S_1 or S_2, are coherent among themselves. But the rays arising from S_1 are completely incoherent with respect to those from S_2, so that there is no sustained mutual interference. The contribution to the irradiance I_t at P is just the sum of the two irradiance contributions.

All the rays incident on the gap at a given angle will result in a single circular fringe of uniform irradiance (Fig. 9.44). With a broad diffuse source, the interference bands will be narrow concentric rings, corresponding to the multiple-beam transmission pattern.

The fringe system can be observed visually by looking directly into the etalon, while focusing at infinity. The job of the focusing lens, which is no longer needed, is done by the eye. At large values of d, the rings will be close together, and a telescope might be needed to magnify the pattern. A relatively inexpensive monocular will serve the same purpose and will allow for photographing the fringes localized at infinity.

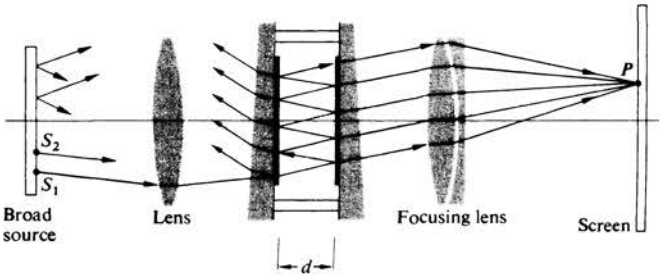


Figure 9.43 Fabry–Perot etalon.

Giesecke+Devrient GmbH,
Giesecke+Devrient Currency Technology GmbH,
and Papierfabrik Louisenthal GmbH. - Ex. 1027

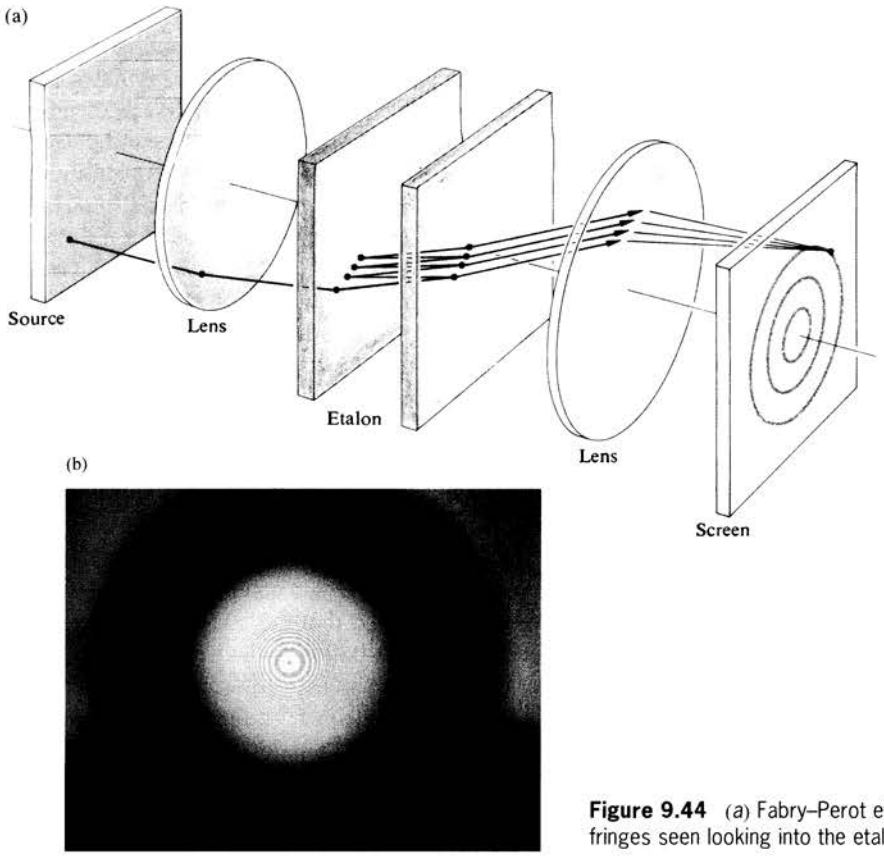


Figure 9.44 (*a*) Fabry–Perot etalon. (*b*) The axially symmetric fringes seen looking into the etalon. (Photo by E. H.)

As might be expected from the considerations of Section 9.5, it is possible to produce real nonlocalized fringes using a bright point source.

The partially transparent metal films that are often used to increase the reflectance ($R = r^2$) will absorb a fraction A of the flux density; this fraction is referred to as the ***absorptance***.

The expression

$$tt' + r^2 = 1$$

or

$$T + R = 1 \qquad [4.60]$$

where T is the transmittance, must now be rewritten as

$$T + R + A = 1 \qquad (9.63)$$

One further complication introduced by the metallic films is an additional phase shift $\phi(\theta_i)$, which can differ from either zero or π. The phase difference between two successively transmitted waves is then

$$\delta = \frac{4\pi n_f}{\lambda_0} d \cos \theta_t + 2\phi \qquad (9.64)$$

For the present conditions, θ_i is small and ϕ may be considered to be constant. In general, d is so large, and λ_0 so small, that ϕ can be neglected. We can now express Eq. (9.54) as

$$\frac{I_t}{I_i} = \frac{T^2}{1 + R^2 - 2R \cos \delta}$$

or equivalently

$$\frac{I_t}{I_i} = \left(\frac{T}{1 - R}\right)^2 \frac{1}{1 + [4R/(1 - R)^2] \sin^2(\delta/2)} \qquad (9.65)$$

Making use of Eq. (9.63) and the definition of the Airy function, we obtain

$$\frac{I_t}{I_i} = \left[1 - \frac{A}{(1 - R)}\right]^2 \mathcal{A}(\theta) \qquad (9.66)$$

Giesecke+Devrient GmbH,
Giesecke+Devrient Currency Technology GmbH,
and Papierfabrik Louisenthal GmbH. - Ex. 1027

as compared with the equation for zero absorption

$$\frac{I_t}{I_i} = \mathscr{A}(\theta) \qquad [9.62]$$

Inasmuch as the absorbed portion A is never zero, the transmitted flux-density maxima $(I_t)_{\max}$ will always be somewhat less than I_i. [Recall that for $(I_t)_{\max}$, $\mathscr{A}(\theta) = 1$.]

Accordingly, the *peak transmission* is defined as $(I_t/I_i)_{\max}$:

$$\frac{(I_t)_{\max}}{I_i} = \left[1 - \frac{A}{(1-R)}\right]^2 \qquad (9.67)$$

A silver film 50 nm thick would be approaching its maximum value of R (e.g., about 0.94), while T and A might be, respectively, 0.01 and 0.05. In this case, the peak transmission will be down to $\frac{1}{36}$. The relative irradiance of the fringe pattern will still be determined by the Airy function, since

$$\frac{I_t}{(I_t)_{\max}} = \mathscr{A}(\theta) \qquad (9.68)$$

A measure of the sharpness of the fringes, that is, how rapidly the irradiance drops off on either side of the maximum, is given by the half-width γ. Shown in Fig. 9.45, γ is the width of the peak, in radians, when $I_t = (I_t)_{\max}/2$.

Peaks in the transmission occur at specific values of the phase difference $\delta_{\max} = 2\pi m$. Accordingly, the irradiance will drop to half its maximum value [i.e., $\mathscr{A}(\theta) = \frac{1}{2}$] whenever $\delta = \delta_{\max} \pm \delta_{1/2}$. Inasmuch as

$$\mathscr{A}(\theta) = [1 + F \sin^2(\delta/2)]^{-1}$$

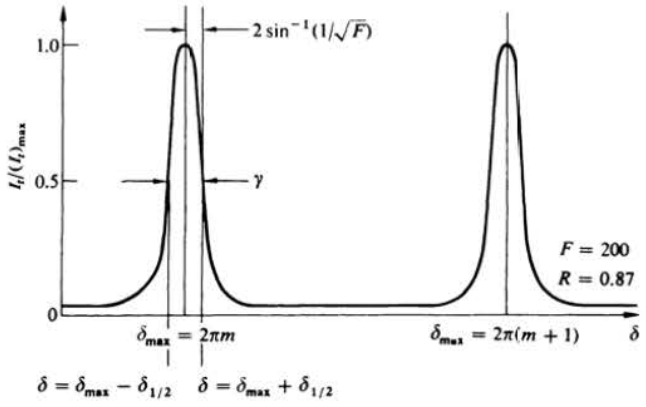


Figure 9.45 Fabry–Perot fringes.

then when

$$[1 + F \sin^2(\delta_{1/2}/2)]^{-1} = \tfrac{1}{2}$$

it follows that

$$\delta_{1/2} = 2 \sin^{-1}(1/\sqrt{F})$$

Since F is generally rather large, $\sin^{-1}(1/\sqrt{F}) \approx 1/\sqrt{F}$, and therefore the half-width, $\gamma = 2\delta_{1/2}$, becomes

$$\gamma = 4/\sqrt{F} \qquad (9.69)$$

Recall that $F = 4R/(1-R)^2$, so that the larger R is, the sharper the transmission peaks will be.

Another quantity of particular interest is the ratio of the separation of adjacent maxima to the half-width. Known as the **finesse**, $\mathscr{F} \equiv 2\pi/\gamma$ or, from Eq. (9.69),

$$\mathscr{F} = \frac{\pi\sqrt{F}}{2} \qquad (9.70)$$

Over the visible spectrum, the finesse of most ordinary Fabry–Perot instruments is about 30. The physical limitation on $\mathscr{F}$ is set by deviations in the mirrors from plane parallelism. Keep in mind that as the finesse increases, the half-width decreases, but so too does the peak transmission. Incidentally, a finesse of about 1000 is attainable with curved-mirror systems using dielectric thin-film coatings.*

Fabry–Perot Spectroscopy

The Fabry–Perot Interferometer is frequently used to examine the detailed structure of spectral lines. We will not attempt a complete treatment of interference spectroscopy, but rather will define the relevant terminology, briefly outlining appropriate derivations.†

*The paper "Multiple Beam Interferometry," by H. D. Polster, *Appl. Opt.* **8**, 522 (1969), should be of interest. Also look at "The Optical Computer," E. Abraham, C. Seaton, and S. Smith, *Sci. Am.* (Feb. 1983), p. 85, for a discussion of the use of the Fabry–Perot Interferometer as an optical transistor.

†A more complete treatment can be found in Born and Wolf, *Principles of Optics*, and in W. E. Williams, *Applications of Interferometry*, to name only two.

Giesecke+Devrient GmbH,
Giesecke+Devrient Currency Technology GmbH,
and Papierfabrik Louisenthal GmbH. - Ex. 1027

As we have seen, a hypothetical, purely monochromatic lightwave generates a particular circular fringe system. But δ is a function of λ_0, so that if the source were made up of two such monochromatic components, two superimposed ring systems would result. When the individual fringes partially overlap, a certain amount of ambiguity exists in deciding when the two systems are individually discernible, that is, when they are said to be *resolved*. Lord Rayleigh's* criterion for resolving two equal-irradiance overlapping slit images is well accepted, even if somewhat arbitrarily in the present application. Its use, however, will allow a comparison with prism or grating instruments. The essential feature of this criterion is that the fringes are *just resolvable* when the combined irradiance of both fringes at the center, or saddle point, of the resultant broad fringe is 8 π^2 times the maximum irradiance. This simply means that one would see a broad bright fringe with a grey central region. To be a bit more analytic about it, examine Fig. 9.46, keeping in mind the previous derivation of the half-width. Consider the case in which the two constituent fringes have equal irradiances, $(I_a)_{\max} = (I_b)_{\max}$. The peaks in the resultant, occurring at $\delta = \delta_a$ and $\delta = \delta_b$, will have equal irradiances,

$$(I_t)_{\max} = (I_a)_{\max} + I' \tag{9.71}$$

At the saddle point, the irradiance $(8/\pi^2)(I_t)_{\max}$ is the sum of the two constituent irradiances, so that, recalling Eq. (9.68),

$$(8/\pi^2)\frac{(I_t)_{\max}}{(I_a)_{\max}} = [\mathscr{A}(\theta)]_{\delta=\delta_a+\Delta\delta/2} + [\mathscr{A}(\theta)]_{\delta=\delta_b+\Delta\delta/2} \tag{9.72}$$

Using $(I_t)_{\max}$ given by Eq. (9.71), along with the fact that

$$\frac{I'}{(I_a)_{\max}} = [\mathscr{A}(\theta)]_{\delta=\delta_a+\Delta\delta}$$

we can solve Eq. (9.72) for $\Delta\delta$. For large values of F,

$$(\Delta\delta) \approx \frac{4.2}{\sqrt{F}} \tag{9.73}$$

This then represents the smallest phase increment, $(\Delta\delta)_{\min}$, separating two resolvable fringes. It can be related to equivalent minimum increments in wavelength $(\Delta\lambda_0)_{\min}$, frequency $(\Delta\nu)_{\min}$, and wave number $(\Delta k)_{\min}$. From Eq. (9.64), for $\delta = 2\pi m$, we have

$$m\lambda_0 = 2n_f d\cos\theta_t + \frac{\phi\lambda_0}{\pi} \tag{9.74}$$

Dropping the term $\phi\lambda_0/\pi$, which is clearly negligible, and then differentiating, yields

$$m(\Delta\lambda_0) + \lambda_0(\Delta m) = 0$$

or

$$\frac{\lambda_0}{(\Delta\lambda_0)} = -\frac{m}{(\Delta m)}$$

The minus will be omitted, since it means only that the order increases when λ_0 decreases. When δ changes by 2π, m changes by 1,

$$\frac{2\pi}{(\Delta\delta)} = \frac{1}{(\Delta m)}$$

and thus

$$\frac{\lambda_0}{(\Delta\lambda_0)} = \frac{2\pi m}{(\Delta\delta)} \tag{9.75}$$

The ratio of λ_0 to the least resolvable wavelength difference, $(\Delta\lambda_0)_{\min}$, is known as the ***chromatic resolving power*** $\mathscr{R}$ of any spectroscope. At nearly normal incidence

$$\mathscr{R} \equiv \frac{\lambda_0}{(\Delta\lambda_0)_{\min}} \approx \mathscr{F}\frac{2n_f d}{\lambda_0} \tag{9.76}$$

or

$$\mathscr{R} \approx \mathscr{F}m$$

For a wavelength of 500 nm, $n_f d = 10$ mm, and $R = 90\%$, the

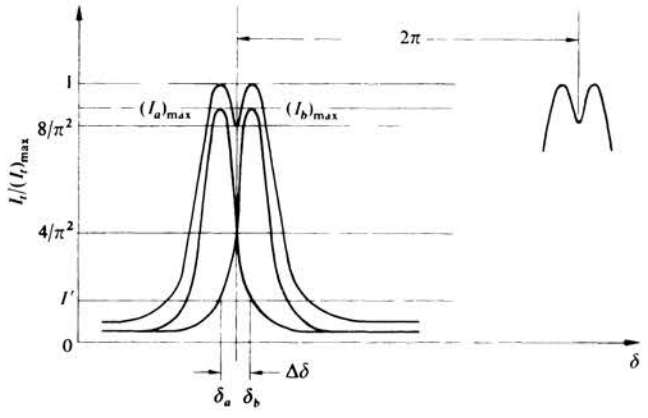


Figure 9.46 Overlapping fringes.

*The criterion will be reconsidered with respect to diffraction in the next chapter (see Fig. 10.26).

Giesecke+Devrient GmbH,
Giesecke+Devrient Currency Technology GmbH,
and Papierfabrik Louisenthal GmbH. - Ex. 1027

resolving power is well over a million, a range achieved by the finest diffraction gratings. It follows as well, in this example, that $(\Delta\lambda_0)_{\min}$ is less than a millionth of λ_0. In terms of frequency, the ***minimum resolvable bandwidth*** is

$$(\Delta\nu)_{\min} = \frac{c}{\mathcal{F}2n_f d} \tag{9.77}$$

inasmuch as $|\Delta\nu| = |c\Delta\lambda_0/\lambda_0^2|$.

As the two components present in the source become increasingly different in wavelength, the peaks shown overlapping in Fig. 9.46 separate. As the wavelength difference increases, the mth-order fringe for one wavelength λ_0 will approach the $(m + 1)$th-order for the other wavelength $(\lambda_0 - \Delta\lambda_0)$. The particular wavelength difference at which overlapping takes place, $(\Delta\lambda_0)_{\text{fsr}}$, is known as the ***free spectral range***. From Eq. (9.75), a change in δ of 2π corresponds to $(\Delta\lambda_0)_{\text{fsr}} = \lambda_0/m$, or at near normal incidence,

$$(\Delta\lambda_0)_{\text{fsr}} \approx \lambda_0^2/2n_f d \tag{9.78}$$

and similarly

$$(\Delta\nu)_{\text{fsr}} \approx c/2n_f d \tag{9.79}$$

Continuing with the above example (i.e., $\lambda_0 = 500$ nm and $n_f d = 10$ mm), $(\Delta\lambda_0)_{\text{fsr}} = 0.0125$ nm. If we attempt to increase the resolving power by merely increasing d, the free spectral range will decrease, bringing with it the resulting confusion from the overlapping of orders. What is needed is that $(\Delta\lambda_0)_{\min}$ *be as small as possible and* $(\Delta\lambda_0)_{\text{fsr}}$ *be as large as possible*. But lo and behold,

$$\frac{(\Delta\lambda_0)_{\text{fsr}}}{(\Delta\lambda_0)_{\min}} = \mathcal{F} \tag{9.80}$$

This result should not be too surprising in view of the original definition of $\mathcal{F}$.

Both the applications and configurations of the Fabry–Perot Interferometer are numerous indeed. Etalons have been arranged in series with other etalons, as well as with grating and prism spectroscopes, and multilayer dielectric films have been used to replace the metallic mirror coatings.

Scanning techniques are now widely in use. These take advantage of the superior linearity of photoelectric detectors over photographic plates, to obtain more reliable flux-density measurements. The basic setup for *central-spot scanning* is illustrated in Fig. 9.47. Scanning is accomplished by varying δ, by changing n_f or d rather than $\cos\theta_t$. In some arrangements, n_f is smoothly varied by altering the air pressure within the etalon. Alternatively, mechanical vibration of one mirror with a displacement of $\lambda_0/2$ will be enough to scan the free spectral range, corresponding as it does to $\Delta\delta = 2\pi$. A popular technique for accomplishing this utilizes a piezoelectric mirror mount. This kind of material will change its length, and therefore d, as a voltage is applied to it. The voltage profile determines the mirror motion.

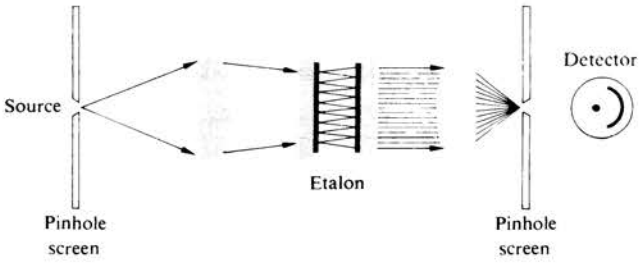


Figure 9.47 Central spot scanning.

Instead of photographically recording irradiance over a large region in space, at a single point in time, this method records irradiance over a large region in time, at a single point in space.

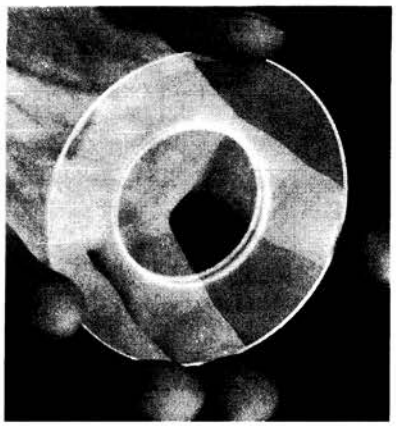
The actual configuration of the etalon itself has also undergone some significant variations. Pierre Connes in 1956 first described the *spherical-mirror Fabry–Perot Interferometer*. Since then, curved-mirror systems have become prominent as laser cavities and are also finding increasing use as spectrum analyzers.

9.7 Applications of Single and Multilayer Films

The optical uses to which coatings of thin dielectric films have been put in recent times are many indeed. Coatings to eliminate unwanted reflections off a diversity of surfaces, from showcase glass to high-quality camera lenses, are now commonplace (see photo on page 426). Multilayer, nonabsorbing beamsplitters and *dichroic* mirrors (color-selective beamsplitters that transmit and reflect particular wavelengths) can be purchased commercially.

Figure 9.48 is a segmented diagram illustrating the use of a *cold mirror* in combination with a *heat reflector* to channel infrared radiation to the rear of a motion-picture projector. The intense unwanted infrared radiation emitted by the source is

Giesecke+Devrient GmbH,
Giesecke+Devrient Currency Technology GmbH,
and Papierfabrik Louisenthal GmbH. - Ex. 1027



This glass disk has an antireflection coating in the shape of a circle applied to the central region of both its sides. (Photo by E. H.)

removed from the beam to avoid heating problems at the photographic film. The top half of Fig. 9.48 is an ordinary back-silvered mirror shown for comparison. Solar cells, which are one of the prime power-supply systems for space vehicles, and even the astronauts' helmets and visors, are shielded with similar heat control coverings.

Multilayer broad and narrow band-pass filters that transmit only over a specific spectral range can be made to span the region from infrared to ultraviolet. In the visible, for example, they play an important part in splitting up the image in color television cameras, and in the infrared they're used in missile guidance systems, CO_2 lasers, and satellite horizon sensors. The applications of thin-film devices are manifold, as are their

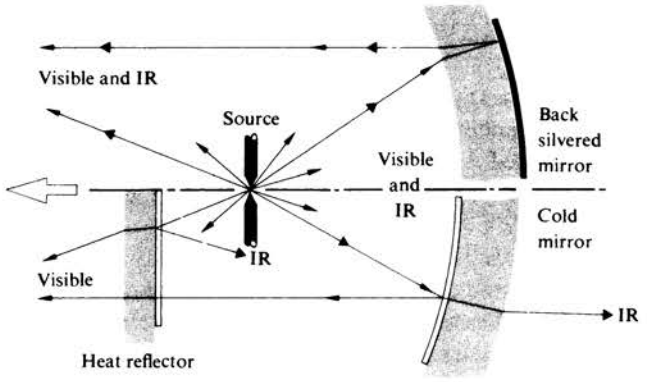


Figure 9.48 A composite drawing showing an ordinary system in the top half and a coated one in the bottom.

structures, which extend from the simplest single coatings to intricate arrangements of one hundred or more layers.

The treatment of multilayer film theory used here will deal with the *total* electric and magnetic fields and their boundary conditions in the various regions. This is a far more practical approach for many-layered systems than is the multiple-wave technique used earlier.*

9.7.1 Mathematical Treatment

Consider the linearly polarized wave shown in Fig. 9.49, impinging on a thin dielectric film between two semi-infinite transparent media. In practice, this might correspond to a dielectric layer a fraction of a wavelength thick, deposited on

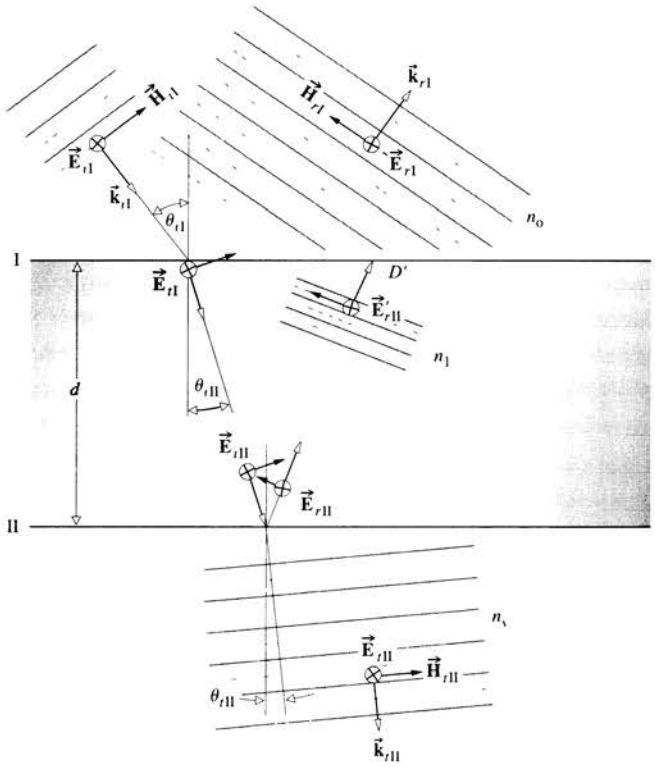


Figure 9.49 Fields at the boundaries.

*For a very readable nonmathematical discussion, see P. Baumeister and G. Pincus, "Optical Interference Coatings," *Sci. Amer.* **223**, 59 (December 1970).

Giesecke+Devrient GmbH,
Giesecke+Devrient Currency Technology GmbH,
and Papierfabrik Louisenthal GmbH. - Ex. 1027

the surface of a lens, a mirror, or a prism. One point must be made clear at the outset: each wave $E_{r\text{I}}$, $E'_{r\text{II}}$, $E_{r\text{II}}$, and so forth, represents the resultant of all possible waves traveling in that direction, at that point in the medium. The summation process is therefore built in. As discussed in Section 4.6.2, the boundary conditions require that the tangential components of both the electric ($\vec{\mathbf{E}}$) and magnetic ($\vec{\mathbf{H}} = \vec{\mathbf{B}}/\mu$) fields be continuous across the boundaries (i.e., equal on both sides). At boundary I

$$E_{\text{I}} = E_{i\text{I}} + E_{r\text{I}} = E_{t\text{I}} + E'_{r\text{II}} \tag{9.81}$$

and

$$H_{\text{I}} = \sqrt{\frac{\epsilon_0}{\mu_0}}(E_{i\text{I}} - E_{r\text{I}})n_0 \cos\theta_{i\text{I}}$$

$$H_{\text{I}} = \sqrt{\frac{\epsilon_0}{\mu_0}}(E_{t\text{I}} - E'_{r\text{II}})n_1 \cos\theta_{i\text{II}} \tag{9.82}$$

where use is made of the fact that $\vec{\mathbf{E}}$ and $\vec{\mathbf{H}}$ in nonmagnetic media are related through the index of refraction and the unit propagation vector:

$$\vec{\mathbf{H}} = \sqrt{\frac{\epsilon_0}{\mu_0}}\, n\hat{\mathbf{k}} \times \vec{\mathbf{E}}$$

At boundary II

$$E_{\text{II}} = E_{i\text{II}} + E_{r\text{II}} = E_{t\text{II}} \tag{9.83}$$

and

$$H_{\text{II}} = \sqrt{\frac{\epsilon_0}{\mu_0}}(E_{i\text{II}} - E_{r\text{II}})n_1 \cos\theta_{i\text{II}}$$

$$H_{\text{II}} = \sqrt{\frac{\epsilon_0}{\mu_0}}E_{t\text{II}}n_s \cos\theta_{t\text{II}} \tag{9.84}$$

the substrate having an index n_s. In accord with Eq. (9.33), a wave that traverses the film once undergoes a shift in-phase of $k_0(2n_1 d \cos\theta_{i\text{II}})/2$, which will be denoted by $k_0 h$, so that

$$E_{i\text{II}} = E_{t\text{I}}e^{-ik_0h} \tag{9.85}$$

and

$$E_{r\text{II}} = E'_{r\text{II}}e^{+ik_0h} \tag{9.86}$$

Equations (9.83) and (9.84) can now be written as

$$E_{\text{II}} = E_{t\text{I}}e^{-ik_0h} + E'_{r\text{II}}e^{+ik_0h} \tag{9.87}$$

and

$$H_{\text{II}} = (E_{t\text{I}}e^{-ik_0h} - E'_{r\text{II}}e^{+ik_0h})\sqrt{\frac{\epsilon_0}{\mu_0}}n_1 \cos\theta_{t\text{II}} \tag{9.88}$$

These last two equations can be solved for $E_{t\text{I}}$ and $E'_{r\text{II}}$, which when substituted into Eqs. (9.81) and (9.82) yield

$$E_{\text{I}} = E_{\text{II}} \cos k_0h + H_{\text{II}}(i \sin k_0h)/\Upsilon_1 \tag{9.89}$$

and

$$H_{\text{I}} = E_{\text{II}}\Upsilon_1 i \sin k_0h + H_{\text{II}} \cos k_0h \tag{9.90}$$

where

$$\Upsilon_1 \equiv \sqrt{\frac{\epsilon_0}{\mu_0}}n_1 \cos\theta_{i\text{II}}$$

When $\vec{\mathbf{E}}$ is in the plane-of-incidence, the above calculations result in similar equations, provided that now

$$\Upsilon_1 \equiv \sqrt{\frac{\epsilon_0}{\mu_0}}n_1/\cos\theta_{i\text{II}}$$

In matrix notation, the above linear relations take the form

$$\begin{bmatrix} E_{\text{I}} \\ H_{\text{I}} \end{bmatrix} = \begin{bmatrix} \cos k_0h & (i \sin k_0h)/\Upsilon_1 \\ \Upsilon_1 i \sin k_0h & \cos k_0h \end{bmatrix}\begin{bmatrix} E_{\text{II}} \\ H_{\text{II}} \end{bmatrix} \tag{9.91}$$

or

$$\begin{bmatrix} E_{\text{I}} \\ H_{\text{I}} \end{bmatrix} = \mathcal{M}_1\begin{bmatrix} E_{\text{II}} \\ H_{\text{II}} \end{bmatrix} \tag{9.92}$$

The *characteristic matrix* $\mathcal{M}_1$ relates the fields at the two adjacent boundaries. It follows, therefore, that if two overlaying films are deposited on the substrate, there will be three boundaries or interfaces, and now

$$\begin{bmatrix} E_{\text{II}} \\ H_{\text{II}} \end{bmatrix} = \mathcal{M}_{\text{II}}\begin{bmatrix} E_{\text{III}} \\ H_{\text{III}} \end{bmatrix} \tag{9.93}$$

Multiplying both sides of this expression by $\mathcal{M}_1$, we obtain

$$\begin{bmatrix} E_{\text{I}} \\ H_{\text{I}} \end{bmatrix} = \mathcal{M}_1\mathcal{M}_{\text{II}}\begin{bmatrix} E_{\text{III}} \\ H_{\text{III}} \end{bmatrix} \tag{9.94}$$

In general, if p is the number of layers, each with a particular value of n and h, then the first and the last boundaries are related by

$$\begin{bmatrix} E_{\text{I}} \\ H_{\text{I}} \end{bmatrix} = \mathcal{M}_1\mathcal{M}_{\text{II}} \cdots \mathcal{M}_p\begin{bmatrix} E_{(p+1)} \\ H_{(p+1)} \end{bmatrix} \tag{9.95}$$

The characteristic matrix of the entire system is the resultant of the product (in the proper sequence) of the individual 2×2 matrices, that is,

$$\mathcal{M} = \mathcal{M}_1\mathcal{M}_{\text{II}} \cdots \mathcal{M}_p = \begin{bmatrix} m_{11} & m_{12} \\ m_{21} & m_{22} \end{bmatrix} \tag{9.96}$$

To see how all this fits together, we will derive expressions for the amplitude coefficients of reflection and transmission using the above scheme. By reformulating Eq. (9.92) in terms of the boundary conditions [(9.81), (9.82), and (9.84)] and

Giesecke+Devrient GmbH,
Giesecke+Devrient Currency Technology GmbH,
and Papierfabrik Louisenthal GmbH. - Ex. 1027

setting

$$\mathrm{Y}_0 = \sqrt{\frac{\epsilon_0}{\mu_0}}\, n_0 \cos\theta_{i\mathrm{I}}$$

and

$$\mathrm{Y}_s = \sqrt{\frac{\epsilon_0}{\mu_0}}\, n_s \cos\theta_{t\mathrm{II}}$$

we obtain

$$\begin{bmatrix} (E_{i\mathrm{I}} + E_{r\mathrm{I}}) \\ (E_{i\mathrm{I}} - E_{r\mathrm{I}})\mathrm{Y}_0 \end{bmatrix} = \mathcal{M}_1 \begin{bmatrix} E_{t\mathrm{II}} \\ E_{t\mathrm{II}}\mathrm{Y}_s \end{bmatrix}$$

When the matrices are expanded, the last relation becomes

$$1 + r = m_{11}t + m_{12}\mathrm{Y}_s t$$

and

$$(1 - r)\mathrm{Y}_0 = m_{21}t + m_{22}\mathrm{Y}_s t$$

inasmuch as

$$r = E_{r\mathrm{I}}/E_{i\mathrm{I}} \quad \text{and} \quad t = E_{t\mathrm{II}}/E_{i\mathrm{I}}$$

Consequently,

$$r = \frac{\mathrm{Y}_0 m_{11} + \mathrm{Y}_0\mathrm{Y}_s m_{12} - m_{21} - \mathrm{Y}_s m_{22}}{\mathrm{Y}_0 m_{11} + \mathrm{Y}_0\mathrm{Y}_s m_{12} + m_{21} + \mathrm{Y}_s m_{22}} \tag{9.97}$$

and

$$t = \frac{2\mathrm{Y}_0}{\mathrm{Y}_0 m_{11} + \mathrm{Y}_0\mathrm{Y}_s m_{12} + m_{21} + \mathrm{Y}_s m_{22}} \tag{9.98}$$

To find either r or t for any configuration of films, we need only compute the characteristic matrices for each film, multiply them, and then substitute the resulting matrix elements into the above equations.

9.7.2 Antireflection Coatings

Now consider the extremely important case of normal incidence, that is,

$$\theta_{i\mathrm{I}} = \theta_{i\mathrm{II}} = \theta_{t\mathrm{II}} = 0$$

which in addition to being the simplest, is also quite frequently approximated in practical situations. If we put a subscript on r to indicate the number of layers present, the reflection coefficient for a single film becomes

$$r_1 = \frac{n_1(n_0 - n_s)\cos k_0 h + i(n_0 n_s - n_1^2)\sin k_0 h}{n_1(n_0 + n_s)\cos k_0 h + i(n_0 n_s + n_1^2)\sin k_0 h} \tag{9.99}$$

Multiplying r_1 by its complex conjugate leads to the reflectance

$$R_1 = \frac{n_1^2(n_0 - n_s)^2\cos^2 k_0 h + (n_0 n_s - n_1^2)^2 \sin^2 k_0 h}{n_1^2(n_0 + n_s)^2\cos^2 k_0 h + (n_0 n_s + n_1^2)^2 \sin^2 k_0 h} \tag{9.100}$$

This formula becomes particularly simple when $k_0 h = \frac{1}{2}\pi$, which is equivalent to saying that the optical thickness h of the film is an odd multiple of $\frac{1}{4}\lambda_0$. In this case $d = \frac{1}{4}\lambda_f$, and

$$R_1 = \frac{(n_0 n_s - n_1^2)^2}{(n_0 n_s + n_1^2)^2} \tag{9.101}$$

which, quite remarkably, will equal zero when

$$n_1^2 = n_0 n_s \tag{9.102}$$

Generally, d is chosen so that h equals $\frac{1}{4}\lambda_0$ in the yellow-green portion of the visible spectrum, where the eye is most sensitive. Cryolite ($n = 1.35$), a sodium aluminum fluoride compound, and magnesium fluoride ($n = 1.38$) are common low-index films. Since MgF_2 is by far the more durable, it is used more frequently. On a glass substrate, ($n_s \approx 1.5$), both these films have indices that are still somewhat too large to satisfy Eq. (9.102). Nonetheless, a single $\frac{1}{4}\lambda_0$ layer of MgF_2 will reduce the reflectance of glass from about 4% to a bit more than 1%, over the visible spectrum. It is now common practice to apply antireflection coatings to the elements of optical instruments. On camera lenses, such coatings produce a decrease in the haziness caused by stray internally scattered light, as well as a marked increase in image brightness. At wavelengths on either side of the central yellow-green region, R increases and the lens surface will appear blue-red in reflected light.

For a double-layer, quarter-wavelength antireflection coating,

$$\mathcal{M} = \mathcal{M}_{\mathrm{I}}\mathcal{M}_{\mathrm{II}}$$

or more specifically

$$\mathcal{M} = \begin{bmatrix} 0 & i/\mathrm{Y}_1 \\ i\mathrm{Y}_1 & 0 \end{bmatrix}\begin{bmatrix} 0 & i/\mathrm{Y}_2 \\ i\mathrm{Y}_2 & 0 \end{bmatrix} \tag{9.103}$$

At normal incidence this becomes

$$\mathcal{M} = \begin{bmatrix} -n_2/n_1 & 0 \\ 0 & -n_1/n_2 \end{bmatrix} \tag{9.104}$$

Giesecke+Devrient GmbH,
Giesecke+Devrient Currency Technology GmbH,
and Papierfabrik Louisenthal GmbH. - Ex. 1027

Substituting the appropriate matrix elements into Eq. (9.97) yields r_2, which, when squared, leads to the reflectance

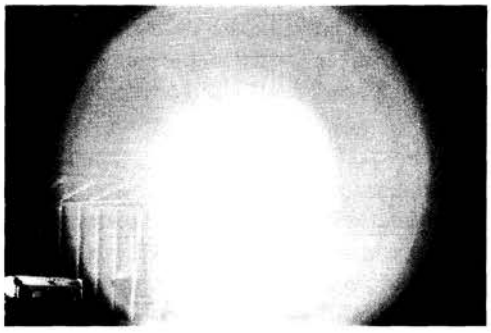
$$R_2 = \left[\frac{n_2^2 n_0 - n_s n_1^2}{n_2^2 n_0 + n_s n_1^2}\right]^2 \tag{9.105}$$

For R_2 to be exactly zero at a particular wavelength, we need

$$\left(\frac{n_2}{n_1}\right)^2 = \frac{n_s}{n_0} \tag{9.106}$$

This kind of film is referred to as a *double-quarter*, *single-minimum* coating. When n_1 and n_2 are as small as possible, the reflectance will have its single broadest minimum equal to zero at the chosen frequency. It should be clear from Eq. (9.106) that $n_2 > n_1$; accordingly, it is now common practice to designate a (glass)–(high index)–(low index)–(air) system as $gHLa$. Zirconium dioxide ($n = 2.1$), titanium dioxide ($n = 2.40$), and zinc sulfide ($n = 2.32$) are commonly used for H-layers, and magnesium fluoride ($n = 1.38$) and cerium fluoride ($n = 1.63$) often serve as L-layers.

Other double- and triple-layer schemes can be designed to satisfy specific requirements for spectral response, incident angle, cost, and so on. The accompanying photo is a scene photographed through a 15-element zoom lens, with a 150-W lamp pointing directly into the camera. The lens elements were covered with a single layer of MgF_2. When a triple-layer antireflection coating is used (see photo), the improved contrast and glare reduction are apparent.



Lens elements coated with a single layer of MgF_2. (Photo courtesy Optical Coating Laboratory, Inc. Santa Rosa, CA.)



Lens elements coated with a multilayer film structure. (Photo courtesy Optical Coating Laboratory, Inc., Santa Rosa, CA.)

9.7.3 Multilayer Periodic Systems

The simplest kind of periodic system is the *quarter-wave stack*, which is made up of a number of quarter-wave layers. The periodic structure of alternately high- and low-index materials, illustrated in Fig. 9.50, is designated by

$$g(HL)^3a$$

Figure 9.51 illustrates the general form of a portion of the spectral reflectance for a few multilayer filters. The width of

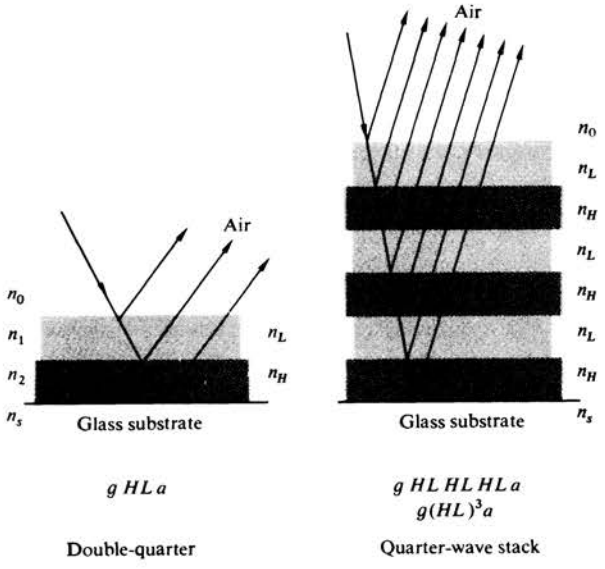


Figure 9.50 A periodic structure. Refraction has been omitted for simplicity.

Giesecke+Devrient GmbH,
Giesecke+Devrient Currency Technology GmbH,
and Papierfabrik Louisenthal GmbH. - Ex. 1027

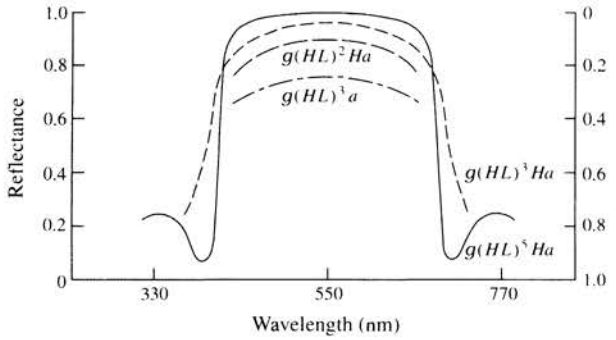


Figure 9.51 Reflectance and transmittance for several periodic structures.

the high-reflectance central zone increases with increasing values of the index ratio n_H/n_L, and its height increases with the number of layers. Note that the maximum reflectance of a periodic structure such as $g(HL)^m a$ can be increased further by adding another H-layer, so that it has the form $g(HL)^m Ha$. Mirror surfaces with very high reflectance can be produced using this arrangement.

The small peak on the short-wavelength side of the central zone can be decreased by adding an eighth-wave low-index film to both ends of the stack, in which case the whole arrangement will be denoted by

$$g(0.5L)(HL)^m H(0.5L)a$$

This has the effect of increasing the short-wavelength high-frequency transmittance and is therefore known as a *high-pass filter*. Similarly, the structure

$$g(0.5H)L(HL)^m(0.5H)a$$

merely corresponds to the case in which the end H-layers are $\lambda_0/8$ thick. It has a higher transmittance at the long-wavelength, low-frequency range and serves as a *low-pass filter*.

At nonnormal incidence, up to about 30°, there is quite frequently little degradation in the response of thin-film coatings. In general, the effect of increasing the incident angle is a shift in the whole reflectance curve down to slightly shorter wavelengths. This kind of behavior is evidenced by several naturally occurring periodic structures, for example, peacock and hummingbird feathers, butterfly wings, and the backs of several varieties of beetles.

The last multilayer system to be considered is the *interference*, or more precisely the *Fabry–Perot filter*. If the separation between the plates of an etalon is of the order of λ, the transmission peaks will be widely separated in wavelength. It will then be possible to block all the peaks but one by using absorbing filters of colored glass or gelatin. The transmitted light corresponds to a single sharp peak, and the etalon serves as a narrow band-pass filter. Such devices can be fabricated by depositing a semitransparent metal film onto a glass support, followed by a MgF_2 spacer and another metal coating.

All-dielectric, essentially nonabsorbing Fabry–Perot filters have an analogous structure, two possible examples of which are

$$g\ HLH\ LL\ HLH\ a$$

and

$$g\ HLHL\ HH\ LHLH\ a$$

The characteristic matrix for the first of these is

$$\mathcal{M} = \mathcal{M}_H\mathcal{M}_L\mathcal{M}_H\mathcal{M}_L\mathcal{M}_L\mathcal{M}_H\mathcal{M}_L\mathcal{M}_H$$

but from Eq. (9.104)

$$\mathcal{M}_L\mathcal{M}_L = \begin{bmatrix} -1 & 0 \\ 0 & -1 \end{bmatrix}$$

or

$$\mathcal{M}_L\mathcal{M}_L = -\mathcal{I}$$

where $\mathcal{I}$ is the unity or identity matrix. The central double layer, corresponding to the Fabry–Perot cavity, is a half-wavelength thick ($d = \frac{1}{2}\lambda_f$). It therefore has no effect on the reflectance *at the particular wavelength under consideration.* Thus, it is said to be an absentee layer, and as a consequence,

$$\mathcal{M} = -\mathcal{M}_H\mathcal{M}_L\mathcal{M}_H\mathcal{M}_H\mathcal{M}_L\mathcal{M}_H$$

The same conditions prevail over and over again at the center and will finally result in

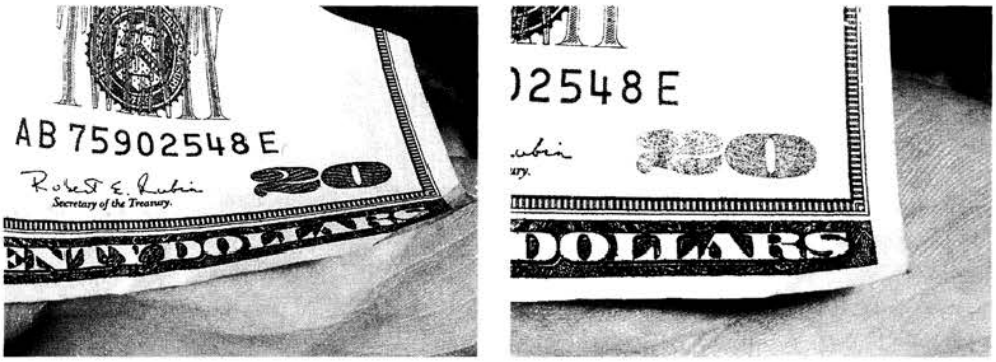
$$\mathcal{M} = \begin{bmatrix} 1 & 0 \\ 0 & 1 \end{bmatrix}$$

At the special frequency for which the filter was designed, r at normal incidence, according to Eq. (9.97), reduces to

$$r = \frac{n_0 - n_s}{n_0 + n_s}$$

the value for the uncoated substrate. In particular, for glass ($n_s = 1.5$), in air ($n_0 = 1$) the theoretical peak transmission is

Giesecke+Devrient GmbH,
Giesecke+Devrient Currency Technology GmbH,
and Papierfabrik Louisenthal GmbH. - Ex. 1027



In Fig. 9.16 the optical path length difference depends on λ (i.e., the color of the light) and on the viewing angle. In a similar way the ink used to print the denominations on U.S. currency now contains structured particles that produce interference colors. The ink is infused with tiny flakes all oriented in the same direction. Each flake is a multilayered interference filter. Here the number 20 changes from black to green as the viewing angle changes.

96% (neglecting reflections from the back surface of the substrate, as well as losses in both the blocking filter and the films themselves).

9.8 Applications of Interferometry

There have been many physical applications of the principles of interferometry. Some of these are only of historical or pedagogical significance, whereas others are now being used extensively. The advent of the laser and the resultant availability of highly coherent quasimonochromatic light have made it particularly easy to create new interferometer configurations.

9.8.1 Scattered-Light Interference

Probably the earliest recorded study of interference fringes arising from scattered light is to be found in Sir Isaac Newton's *Optiks* (1704, Book Two, Part IV). Our present interest in this phenomenon is twofold. First, it provides an extremely easy way to see some rather beautiful colored interference fringes. Second, it is the basis for a remarkably simple and highly useful interferometer.

To see the fringes, lightly rub a thin layer of ordinary talcum powder onto the surface of any common back-silvered mirror (dew will do as well). Neither the thickness nor the uniformity of the coating is particularly important. The use of a bright point source, however, is crucial. A satisfactory source can be made by taping a heavy piece of cardboard having a hole about $\frac{1}{4}$ inch in diameter over a good flashlight. Initially, stand back from the mirror about 3 or 4 feet; the fringes will be too fine and closely spaced to see if you stand much nearer. Hold the flashlight alongside your cheek and illuminate the mirror so that you can see the brightest reflection of the bulb in it. The fringes will then be clearly seen as a number of alternately bright and dark bands.

In Fig. 9.52 two coherent rays leaving the point source are shown arriving at point P after traveling different routes. One ray is reflected from the mirror and then scattered by a single transparent talcum grain toward P. The second ray is first scattered downward by the grain, after which it crosses the mirror

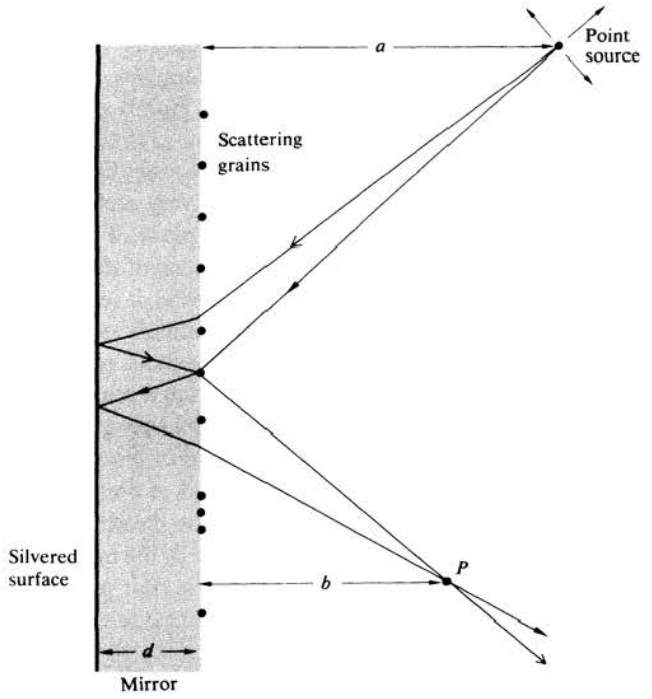


Figure 9.52 Interference of scattered light.

Giesecke+Devrient GmbH,
Giesecke+Devrient Currency Technology GmbH,
and Papierfabrik Louisenthal GmbH. - Ex. 1027